UNIVERSITY OF ALBERTA

THE ARREST OF DELAYED HYDRIDE CRACKING IN ZR-2.5%NB ALLOYS AT ELEVATED TEMPERATURES

BY

©

GANG LIN

A THESIS SUBMITTED TO THE FACULTY OF GRADUATE STUDIES
AND RESEACH IN PARTICTIAL FULFILMENT OF THE
REQUIREMENTS
FOR THE DEGREE OF

DOCTOR OF PHILOSOPHY

IN

MATERIALS ENGINEERING

DEPARTMENT OF CHEMICAL AND MATERIALS ENGINEERING

EDMONTON, ALBERTA

SPRING 1999

National Library
of Canada

Acquisitions and
Bibliographic Services

395 Wellington Street
Ottawa ON K1A 0N4
Canada

Bibliothèque nationale
du Canada

Acquisitions et
services bibliographiques

395, rue Wellington
Ottawa ON K1A 0N4
Canada

Your file Votre référence

Our file Notre référence

The author has granted a non-exclusive licence allowing the National Library of Canada to reproduce, loan, distribute or sell copies of this thesis in microform, paper or electronic formats.

The author retains ownership of the copyright in this thesis. Neither the thesis nor substantial extracts from it may be printed or otherwise reproduced without the author's permission.

L'auteur a accordé une licence non exclusive permettant à la Bibliothèque nationale du Canada de reproduire, prêter, distribuer ou vendre des copies de cette thèse sous la forme de microfiche/film, de reproduction sur papier ou sur format électronique.

L'auteur conserve la propriété du droit d'auteur qui protège cette thèse. Ni la thèse ni des extraits substantiels de celle-ci ne doivent être imprimés ou autrement reproduits sans son autorisation.

0-612-39560-X

Canada

University of Alberta

Library Release Form

Name of Author:	Gang Lin
Title of Thesis:	The Arrest of Delayed Hydride Cracking in Zr-2.5%Nb Alloys at Elevated Temperatures
Degree:	Doctor of Philosophy
Year of this degree Granted:	1999

Permission is hereby granted to the University of Alberta Library to reproduce single copies of this thesis and to lend or sell such copies for private, scholarly, or scientific research purposes only.

The author reserves all other publication and other rights in association with the copyright in the thesis, and except as hereinbefore provided, neither the thesis nor any substantial portion thereof may be printed or otherwise reproduced in any material form whatever without the author's prior written permission.

843 Ryan Place
Edmonton, Alberta
Canada, T6R 2N1

Dec. 23, 1998

University of Alberta

Faculty of Graduate Studies and Research

The undersigned certify that they have read, and recommend to the Faculty of Graduate Studies and Research for acceptance, a thesis entitled The Arrest of Delayed Hydride Cracking in Zr-2.5%Nb Alloys at Elevated Temperatures submitted by Gang Lin in partial fulfillment of the requirements for the degree of Doctor of Philosophy in Materials Engineering.

Reg Eadie
Dr. R.L. Eadie (Supervisor)

Dr. F. Ellyin

Dongyang Li
Dr. D. Li

Qi Liu
Dr. Q. Liu

B M Patchett
Dr. B.M. Patchett

Qi Liu
for Dr. S.-Q. Shi (External)

Dec. 22, 1998

Abstract

The cracking arrest phenomenon in Zr-2.5%Nb at high temperature, which has been reported but not understood, has been studied. The values of the cracking arrest temperature (T_{CAT}) under various testing conditions have been determined. The cracking arrest phenomenon has been found to be caused by the inability of the crack tip hydrides to fracture. The possible cause of this inability to crack has been explored based on the experimental results from cracking tests and metallographic and fractographic analysis of fractured specimens. The correlation between the cracking arrest phenomena and other related phenomena, such as the existence of a critical stress intensity factor for initiation of DHC and an incubation period, has been discussed. By taking advantage of the fact that crack tip hydrides form and remain uncracked, a semi-quantitative, three dimensional description of crack tip hydrides has been made, which is believed to be extremely valuable for understanding the initiation of the DHC process in Zr-2.5%Nb.

Acknowledgments

I am indebted to the following individuals without whom the completion of this project could not have been possible:

Dr. R.L. Eadie, my supervisor, for his suggestion on this interesting topic, his scientific guidance and his continuous support throughout the process of this project;

Dr. F. Ellyin, Dr. D. Li, Dr. Q. Liu, Dr. B.M. Patchett, Dr. S.-Q. Shi and Dr. M.L. Wayman for their time and valuable advice;

Dr. M.T. Jovanovic, Dr. Skrzypek, M. Anderson, P. Poruks, J. Doesburg, D. Reynold, D. Yan and X. Chen for their assistance and remarks;

T. Barker, B. Konzuk, B. Smith, R. Stefaniuk and H. Skrzypek for their technical support.

Especially, I wish to express my gratitude to my wife, Y. Ma, for her encouragement, understanding and assistance while I was working on this project.

Table of Contents

Chapter 1 Research Topic Selection..1

Chapter 2 Background Information..6

2.1 Zirconium and Its Application in the Nuclear Industry 6

2.2 Theory of Delayed Hydride Cracking.. 11

2.2.1 Overview 11

2.2.2 Hydrogen Content and Distribution.. 14

2.2.3 Zirconium Hydrides 17

2.2.3.1 Zirconium Hydrides and Their Properties 17

2.2.3.2 Hydride Orientation and Morphology 18

2.2.3.3 Fracture Criteria of Crack Tip Hydrides........................ 21

2.2.4 Stress and Stress Distribution.. 26

2.2.4.1 General Description of Stress Distribution at Crack Tips 26

2.2.4.2 Stress Re-distribution due to Hydrogen Diffusion
and Hydride Formation.. 28

2.2.5 Factors Affecting the DHC Behavior of Zr-2.5%Nb 32

2.2.5.1 Matrix Hydrogen Content 32

2.2.5.2 Stress Intensity Factor.. 33

2.2.5.3 Temperature... 34

2.2.5.4 Matrix Strength of Zr-2.5%Nb 35

2.2.5.5 Matrix Microstructure.. 37

2.2.6 The Behavior of Zr-2.5%Nb 39

2.2.6.1 Temperature Related Behavior 40

2.2.6.1.1 Temperature Dependence of Cracking Velocity 40

2.2.6.1.2 Temperature Variation (Thermal Cycling) Effect of DHC Behavior 42

2.2.6.1.3 Existence of a T_{DAT} (Direction of Approaching Temperature) 45

2.2.6.2 Loading Related Behaviors (Existence of a K_{IH}) 46

2.2.6.3 Time Related Behaviors (Existence of an Incubation Time) 47

2.2.6.4 Existence of Fracture Surface Striations 48

2.2.6.5 Existence of a T_{CAT} (Cracking Arrest Temperature) 49

2.3 Cracking Monitoring Techniques 51

Chapter 3 Experimental 68

3.1 Testing Material and Specimen Preparation 68

3.2 Cracking Tests 71

3.2.1 Loading Arrangement and Calculations of Applied Loads 71

3.2.2 Temperature Measurements and Control 73

3.2.3 Measurement of Potential Drop (PD) 73

3.2.4 Measurement of Acoustic Emission (AE) 76

3.2.5 Measurement of Crack Advance 76

3.2.6 DHC Velocity (DHCV) Measurement using Combined AE and PD 77

3.3 Metallographic Analysis 82

3.3.1 Optical Microscope 82

3.3.2 Scanning Electron Microscope (SEM) 83

3.3.3 Specimen Preparation 83

3.4 Fractographic Analysis 85
3.5 Other Testing Methods 86
    3.5.1 Vickers Hardness Measurement 86
    3.5.2 Hydrogen Content Analysis 86

Chapter 4 Experimental Result 98
4.1 Results from Pre-analysis 101
    4.1.1 Hydrogen Content 101
    4.1.2 Amount of Cold Work and Matrix Hardness 101
    4.1.3 Bulk Hydrides Morphology 103
    4.1.4 Matrix Grain Structure 105
4.2 Results from Cracking Tests 106
    4.2.1 Determination of Cracking Arrest Temperature (T_{CAT}) and Its Affecting Parameters 106
        4.2.1.1 T_{CAT} on As-manufactured Specimens at $K=17$ MPa√m 107
        4.2.1.2 T_{CAT} on Additionally Cold Worked Specimens at $K=17$ MPa√m 107
        4.2.1.3 T_{CAT} under Different Testing Conditions 108
        4.2.1.4 Reversibility of Cracking Arrest Phenomenon 108
    4.2.2 Determination of Temperature Dependence of DHC Velocity (DHCV) 109
        4.2.2.1 DHCV at Test Temperature Close to but below T_{CAT} 109
        4.2.2.2 DHCV Distributions with Test Temperature 110

4.3 Results from Metallographic Analysis 112
4.3.1 Existence of Re-oriented Crack Tip Hydrides at T_{CAT} 112
4.3.2 Morphology of Re-oriented Crack Tip Hydrides Formed at T_{CAT} 113
4.3.2.1 Observations of Crack Tip Hydrides on Axial-circumferential Planes 114
4.3.2.1.1 Crack Tip Hydrides on As-manufactured Specimens 114
4.3.2.1.2 Effect of Additional Cold Working 115
4.3.2.1.3 Crack tip Areas at Test Temperatures below T_{CAT} 116
4.3.2.2 Observations of Crack Tip Hydrides on Circumferential-radial Planes 116
4.4 Results from Fractographic Analysis 120

Chapter 5 Discussion 204
5.1 About The Cracking Arrest Phenomenon 204
5.1.1 Summary of Experimental Evidence about the Cracking Arrest Phenomenon 204
5.1.2 Indications of the Experimental Evidence 207
5.1.3 The Effect of Test Temperature, Diffusible Hydrogen and Stress Intensity Factor on DHC Initiation 209
5.1.4 The Causes of Cracking Arrest Phenomenon at High Temperatures 213
5.1.5 Estimation of Temperature Range for T_{CAT} Existence 222
5.1.6 Critical Stress Intensity Factor (K_{IH}) and Critical Test Temperature for DHC T_{CAT} 228

5.1.7 Incubation Phenomenon and Cracking Arrest Phenomenon 231

5.1.8 A Possible Existence of an Absolute Cracking Arrest Temperature ($T_{CAT}^{ABSOLUTE}$) 232

5.2 About Crack Tip Hydride Morphology and Fracture Initiation Criteria 234

5.3 About DHC Process and The Parameters Affecting It 244

Chapter 6 Conclusions 277

Chapter 7 References.......279

List of Tables

Chapter 4 Experimental Results

Table 4-1 Initial conditions of tested specimens including their amount of additional cold work and hydrogen concentration 189

Table 4-2 Measured T_{CAT} values for as-manufactured specimens (peak temperature =340°C, K =17 MPa√m).. 190

Table 4-3 Measured T_{CAT} values for as-manufactured and additionally cold worked specimens (peak temperature =360°C, K =17 MPa√m).. 191

Table 4-4a Measured T_{CAT} values on as-manufactured specimens under various stress intensity factors (peak temperature =370°C).............. 192

Table 4-4b Measured T_{CAT} values on 20% additionally cold worked specimens under various stress intensity factors (H%=160μ/μg, peak temperature =370°C) 193

Table 4-4c Measured T_{CAT} values on 40% additionally cold worked specimens under various stress intensity factors (H%=160μ/μg, peak temperature =370°C) 194

Table 4-4d Measured T_{CAT} values on 60% additionally cold worked specimens under various stress intensity factors (H%=160μ/μg, peak temperature =370°C) 195

Table 4-5 DHCV in nm/s for as-manufactured specimens under K=17MPa√m (H%=160 μg/g).. 196

Table 4-6 DHCV in nm/s for 40% additionally cold worked specimens under K=17 MPa√m (H%=160 μg/g) 197
Table 4-7 Comparison between T_{CAT} and $T_{DHCVSTOP}$ 198
Table 4-8 Measurement results of hydride thickness 199
Table 4-9 Dimensions of hydride cluster and individual hydrides obtained on the specimens with and without additional cold work 202
Table 4-10 Roughness measurement results....................203

Chapter 5 Discussion

Table 5-1 The effect of cold work on the preferred orientation of basal plane of hexagonal zirconium in three directions [75]....................275
Table 5-2 Comparison of calculated T_P and measured T_{CAT} values 276

List of Figures

Chapter 2 Background Information

Figure 2-1 Simplified diagram of a *CANDU* reactor [9] 54

Figure 2-2 Simplified diagram of a *CANDU* reactor fuel channel [9] 55

Figure 2-3 Effect of roll extension on the residual circumferential stresses in the pressure tube at a rolled joint [16] 56

Figure 2-4 Hydrogen solubility curves for precipitation and dissolution 57

Figure 2-5 Cross-section of fracture surface [30] 58

Figure 2-6 Comparison of theoretical K_{IH} with experimental data [31] 59

Figure 2-7 Stress zones near crack tip [23] 60

Figure 2-8 Crack tip stress distribution [34] 61

Figure 2-9 Distribution of stress component normal to the crack plane due to hydride expansion [36] 62

Figure 2-10 Effect of different hydride length on the normal stress distribution [36] 63

Figure 2-11 Hydride shape distribution based on hydrostatic stress criterion [37] 64

Figure 2-12 Schematic diagram of the dependence of Delayed Hydride Cracking Velocity (DHCV) on stress intensity factor [38] 65

Figure 2-13 The effect of cooling rate and maximum temperature on the total hydrogen Level, $C_{H(tot)}$, at the peak stress location during temperature cycles of a Zr-2.5%Nb specimen containing 60 μg/g hydrogen and a notch of depth 0.8 mm and tip radius of 0.2 mm under net section stress 300 MPa [46]....66

Figure 2-14 Temperature profile and acoustic emission rate indicating T_{CAT} [6]....67

Chapter 3 Experimental

Figure 3-1 All the steps the specimens have experienced prior to cracking tests....87

Figure 3-2 Schematic illustration of specimens' preparation done in this lab....88

Figure 3-3 Dimensions of specimens....89

Figure 3-4 Schematic diagram of experimental rig for cracking tests....90

Figure 3-5 Schematic diagram showing positions of the current leads, potential drop (PD) measuring leads and the thermocouple....91

Figure 3-6 Potential drop (PD) measurement system....92

Figure 3-7 Schematic diagram showing the method of measuring crack advance....93

Figure 3-8 Measurement result of AE and PD at 280°C with a peak temperature of 320°C....94

Figure 3-9 Measurement result of AE and PD at 260°C with a peak temperature of 320°C....95

Figure 3-10 Measurement result of AE and PD at 170°C with a peak temperature of 320°C....96

Figure 3-11 Measurement result of AE and PD at 200°C with a peak temperature of 320°C and loading only at the test temperature........97

Chapter 4 Experimental Results

Figure 4-1 Effect of additional cold work on Vickers hardness of Zr-2.5%Nb, measured on the axial-circumferential plans with a 10 Kg load........123
Figure 4-2 Correlation between tensile strength and Vickers hardness of Zr-2.5%Nb [73]........124
Figure 4-3 The effect of additional cold work on the room temperature tensile strength of Zr-2.5%Nb [74]........125
Figure 4-4 Matrix hydride morphology........126
Figure 4-5 Schematic illustration correlating structural features in a cold worked Zr-2.5%Nb pressure tube with a compact specimen [28]........130
Figure 4-6 SEM micrograph of matrix material........131
Figure 4-7 Typical AE measurement result for Determining Cracking Arrest Temperature (T_{CAT})........139
Figure 4-8 AE measurements at T_{CAT} (305°C) and at the temperature just below T_{CAT} (300°C) (H% =160 μg/g, K=17 MPa√m)........140
Figure 4-9a DHCV versus test temperature (0% additional CW, H%=160 μg/g, peak temperature = 320°C, K=17 MPa√m)........141
Figure 4-9b DHCV (log) versus test temperature (0% additional CW, H%=160 μg/g, peak temperature = 320°C, K=17 MPa√m)........142

Figure 4-10a DHCV versus test temperature (0% additional CW, H%=160 μg/g, peak temperature = 370°C, K=17 MPa√m) 143

Figure 4-10b DHCV (log) versus test temperature (0% additional CW, H%=160 μg/g, peak temperature = 370°C, K=17 MPa√m) 144

Figure 4-11a DHCV versus test temperature (40% additional CW, H%=160 μg/g, peak temperature = 320°C, K=17 MPa√m) 145

Figure 4-11b DHCV (log) versus test temperature (40% additional CW, H%=160 μg/g, peak temperature = 320°C, K=17 MPa√m) 146

Figure 4-12a DHCV versus test temperature (40% additional CW, H%=160 μg/g, peak temperature = 370°C, K=17 MPa√m) 147

Figure 4-12b DHCV (log) versus test temperature (40% additional CW, H%=160 μg/g, peak temperature = 370°C, K=17 MPa√m) 148

Figure 4-13 Summary of DHCV on as-manufactured (0%CW) specimens for different peak temperatures (H%=160 μg/g, K=17 MPa√m) 149

Figure 4-14 Summary of DHCV on additionally cold worked (40%CW) specimens for different peak temperatures (H%=160 μg/g, K=17 MPa√m) 150

Figure 4-15 Measured DHCV on as-manufactured (0% CW) and additionally cold worked (40%CW) specimens under the same testing conditions (H%=160 μg/g, peak temperature=320°C, K=17 MPa√m) 151

Figure 4-16 Measured DHCV on as-manufactured (0% CW) and additionally cold worked (40%CW) specimens under the same testing conditions (H%=160 μg/g, peak temperature=370°C, K=17 MPa√m) 152

Figure 4-17 Summary of measured DHCV on as-manufactured specimens (peak temperature = 360°C, K=17 MPa√m) [73].......153

Figure 4-18 Summary of measured DHCV on 40% additionally cold worked specimens (peak temperature = 360°C, K=17 MPa√m) [73].......154

Figure 4-19 SEM micrograph (BSE image) of crack tip hydride image on axial-circumferential plane (0% additional CW).......155

Figure 4-20 Axial-circumferential crack tip hydride image obtained in repeated tests on the same specimen used for obtaining Figure 4-19 (0% additional CW).......156

Figure 4-21 Axial-circumferential crack tip hydride image obtained on specimens with different amounts of additional cold work.......157

Figure 4-22 Hydride thickness versus location.......160

Figure 4-23 SEM micrograph (BSE image) of crack tip area at test temperatures below T_{CAT} on circumferential-radial plane.......161

Figure 4-24a Axial-circumferential crack tip hydride obtained after the first polish (0% additional CW).......162

Figure 4-24b Axial-circumferential crack tip hydride obtained after the second polish (0% additional CW).......163

Figure 4-24c Axial-circumferential crack tip hydride obtained after the third polish (0% additional CW).......164

Figure 4-25 SEM micrograph (BSE image) of crack tip hydrides on circumferential-radial plane (0% additional CW).......165

Figure 4-26 Schematic illustration of crack front.......166

Figure 4-27 SEM micrograph (BSE image) of crack tip hydrides on circumferential-radial plane (0% additional CW).......167

Figure 4-28 SEM micrograph (BSE image) of crack tip hydrides on circumferential-radial plane (40% additional CW) 168
Figure 4-29 SEM micrograph (BSE image) of crack tip hydrides on circumferential-radial plane (0% additional CW) 169
Figure 4-30 SEM micrograph (BSE image) of crack tip hydrides on circumferential-radial plane (0% additional CW) 170
Figure 4-31 SEM micrograph (BSE image) of crack tip hydrides on circumferential-radial plane (0% additional CW) 171
Figure 4-32 SEM micrograph (BSE image) of crack tip hydrides on circumferential-radial plane (0% additional CW) 173
Figure 4-33 SEM micrograph (BSE image) of crack tip hydrides on circumferential-radial plane (0% additional CW) 175
Figure 4-34 SEM micrograph (BSE image) of crack tip hydrides on circumferential-radial plane (0% additional CW) 177
Figure 4-35 Cross-section of a fractured surface [30] 179
Figure 4-36 SEM micrograph (BSE image) of crack tip hydrides on circumferential-radial plane (0% additional CW) 180
Figure 4-37 Measurement result of roughness according to the definition given by Luo in [30] 182
Figure 4-38 A typical "fish-scale" pattern observed on fractured surface.........183
Figure 4-39 A typical "fish-scale" pattern observed on fractured surfaces under high magnification 184
Figure 4-40 SEM and digitized images of striations on fractured surfaces.......185
Figure 4-41 An example of image analysis on striation pattern 186
Figure 4-42 The area fractions of crack tip hydrides versus test temperature 187
Figure 4-43 Striation ridge width versus test temperature 188

Chapter 5 Discussion

Figure 5-1 Effect of temperature on striation spacing [77] 247

Figure 5-2 Change in crack tip stress due to growth of hydride elastic-perfectly plastic, σ_y = 550 MPa, E= 80 GPa [78]..........................248

Figure 5-3 Increments of hydride growth reducing hydrostatic stress [37].....249

Figure 5-4 Temperature dependence of hydrogen concentration factor β 250

Figure 5-5 Effect of matrix strength values on calculating hydrogen concentration factor β 251

Figure 5-6 Graphical calculation of the highest possible temperature for hydride precipitation (T_p) with a peak temperature of 340°C.........252

Figure 5-7 Effect of matrix strength values on calculating the highest possible temperature for hydride precipitation (T_p) with a peak temperature of 340°C...253

Figure 5-8 Graphical calculation of the highest possible temperature for hydride precipitation (T_p) with a peak temperature of 360°C.........254

Figure 5-9 Graphical calculation of the highest possible temperature for hydride precipitation (T_p) with a peak temperature of 370°C.........255

Figure 5-10 Effect of σ_y and C_H^d values on calculating the highest possible temperature for hydride precipitation (T_p).......................256

Figure 5-11 Effect of C_H^P values on calculating the highest possible temperature for hydride precipitation (T_p)....................................257

Figure 5-12 The two temperature dependent hydrogen concentration curves from the two C_H^P curves given by Shi [31]........................258

Figure 5-13 Calculated temperature range for the highest possible temperature for hydride precipitation (T_p) with a peak temperature of 360°C...259

Figure 5-14 Temperature dependence of measured K_{IH} values [31] 260
Figure 5-15 Effect of applied stress intensity factor on cracking activity indicated by accumulated AE signals 261
Figure 5-16 Combination of measured K_{IH} and calculated "K_{IH}" from measured T_{CAT} values 262
Figure 5-17 Effect of peak temperature on measured T_{CAT} values 263
Figure 5-18 SEM image of fractured surface showing a nested structure 264
Figure 5-19 Schematic illustration of a "disk-like" ("cornflake-like") crack tip hydride configuration 265
Figure 5-20 Schematic illustration of development of crack tip hydride "disks" ("cornflakes") configuration and its development.............266
Figure 5-21 Suggested hydride morphologies based on a "disk-like" model....267
Figure 5-22 Schematic illustration of a "stripe-like" crack tip hydride configuration and its development..268
Figure 5-23 Schematic illustration of a uniform "stripe-like" crack tip hydride configuration and its development 269
Figure 5-24 Suggested hydride morphologies based on a "strip-like" model ...270
Figure 5-25 Schematic illustration of a "platelet-like" crack tip hydride configuration and its development..271
Figure 5-26 Suggested hydride morphologies based on a "platelet-like" model...272
Figure 5-27 Schematic illustration of a featured surface produced by a "platelet-like" crack tip hydride configuration 273
Figure 5-28 A three dimensional presentation of critical conditions for DHC fracture initiation 274

List of Symbols and Terminology

Greek

α	alpha phase, zirconium, hexagonal close packed structure
β	beta phase, zirconium or niobium, body centered cubic structure
β	hydrogen concentration factor
γ-hydride	gamma zirconium hydride (ZrH)
δ-hydride	delta zirconium hydride ($ZrH_{1.6}$)
$\varepsilon_{\perp}$	vertical elastic deformation
ν	Poisson's ratio
Θ_{DHC}	imaginary physical quantity describing the cracking initiation condition
σ	stress
σ_{22}	stress component normal to the crack plane
σ_{local}	local stress
σ_f^h	stress needed for hydride fracture
σ_{eff}^a	effective applied stress at hydride
σ^h	stress created by hydride formation
σ_{XX}	peak stress in X-direction
σ_y, σ_o	yield stress
σ_{YY}	peak stress in Y-direction
σ_{ZZ}	peak stress in Z-direction
τ	effective thickness
$\mu_{H,o}$	chemical potential of hydrogen at zero stress
$\mu_{H,p}$	chemical potential of hydrogen

Nomenclature & Abbreviations

AE	acoustic emission
BCC	Body Centered Cubic
BSE	Back-scattered Electron
CANDU	**Canada Deuterium Uranium**
CW	cold working
D_2O	heavy water, deuterium
DHC	Delayed Hydride Cracking
DHCV	Delayed Hydride Cracking Velocity
EDM	electrospark discharge machining
HCC	hydride continuity coefficient
HCC^*	hydride continuity coefficient on the fracture surface
HIDC	Hydrogen-Induced Delayed Cracking
MTS	Material Testing System
NGS	Nuclear Generating Station
PWH	Pressured Heavy Water
PD	potential drop
SEM	Scanning Electron Microscope

Symbols

a	crack extension measured from specimen fracture surface
C_H	hydrogen concentration
C_H^d	dissolution solubility
C_H^p	precipitation solubility
$C_{H(tot)}$	total hydrogen level
C_{local}	local hydrogen level
C_{MAX}	increased hydrogen level in solution at crack tip
C_o	matrix hydrogen level in solution
C_{yi}	circumferential distance between the *ith* and the (i+1)*th* hydride
D, D_H	diffusion coefficient of hydrogen
E	Young's Modulus
$E_{hydride}$	hydride fracture energy
E_{matrix}	matrix fracture energy
E_{total}	total fracture energy per unit area of hydrided material
f, f_a	area fraction of hydrides at crack tip
$f_{hydride}$	area fraction of hydrides at crack initiation
f_{matrix}	area fraction of matrix at crack initiation
J_H	hydrogen flux
G_c	surface energy
G_{finite}	general elasto-plastic energy
G_h	hydride fracture energy
G_m	matrix fracture energy in tension
G_s	matrix fracture energy in shearing
K_{IC}	critical stress intensity factor
K_{IC}^{Zr}	crack initiation threshold for a zirconium alloy containing no hydride

K_{IH}	critical stress intensity factor
K_{IH}^{exp}	experimentally observed K_{IH}
p	average principal stress
r_y	plastic zone size at crack tip
R	surface roughness
R	gas constant
t	time
t_{incub}	incubation time
t_{iso}	isothermal cracking time
t_{noniso}	non-isothermal cracking time
t	thickness
t_o	effective specimen's thickness
T	temperature, °C or K
T_{CAT}	Cracking Arrest Temperature
$T_{CAT}^{ABSOLUTE}$	Absolute Cracking Arrest Temperature
T_{DAT}	Direction of Approaching Temperature
$T_{DHCVMAX}$	test temperature at which DHCV reaches its maximum value
$T_{DHCVSTOP}$	test temperature at which DHCV reaches zero
T_P	the highest possible temperature for hydride precipitation
TSS	terminal solid solubility
TSSd	terminal solid solubility for dissolution
TSSp	terminal solid solubility for precipitation
V_H	partial molar volume of hydrogen dissolved in zirconium lattice
w_i	width of the i*th* hydride

Chapter 1 Research Topic Selection

Delayed hydride cracking (DHC) has been recognized as an important failure mechanism for zirconium alloys used in the nuclear industry. Following the pressure tube failures in the *CANDU*[1] (**CAN**ada **D**euterium **U**ranium) reactors, a great amount of work has been performed in an attempt to explain the phenomenon [1-5]. Generally speaking, the DHC process involves the following steps which are repeated: diffusion of hydrogen along a stress gradient to the crack tip region, formation of hydrides at the crack tip because of a build-up of hydrogen and cracking of those hydrides when the local fracture toughness is reduced to the level of the applied stress intensity factor. Since it involves three different phenomena - stress induced diffusion, phase transformation and fracture - the DHC process is a complicated one and there are still a number of questions remaining unanswered. Among those unsolved problems, the cracking arrest at high temperatures has been selected for this study, because it is directly related to the cracking criterion, a very important fundamental problem in DHC, and, at the same time, quite suitable as a research project.

Studying the cracking arrest phenomenon in DHC has both theoretical and practical significance, since it contributes to a better understanding of fracture processes via DHC and to the establishment of a cracking arrest methodology for nuclear reactor pressure tubing materials. The existence of a cracking arrest temperature, or T_{CAT}, on Zr-2.5%Nb has been reported by Smith and Eadie in 1988 [6]. They found, based on their DHCV (Delayed Hydride Cracking Velocity) study using acoustic emission, that there is a temperature above which cracking ceases even if the mechanism of hydride precipitation still exists. They also noticed that after the cracking has stopped, if the temperature is lowered below T_{CAT}, in a range where cracking has previously been documented, the cracking will recommence. What these findings imply is that at temperatures above T_{CAT}, a certain condition has been reached where crack propagation becomes unfavorable despite the existence of ample hydrogen and the cracking cessation at T_{CAT} seems to be reversible.

---

[1] *CANDU* is a trademark of AECL, Ottawa, Ontario, Canada

Compared to other phenomena in DHC, T_{CAT} is new and unexplored. As a matter of fact, the Smith and Eadie paper is the only one to deal directly with this phenomenon. Until the time when this study began, little was known about T_{CAT} except its existence. It was strongly believed, however, that further exploration of this phenomenon would be beneficial because of the following reasons.

First of all, there was a strong desire to understand the cause of cracking cessation at T_{CAT}. From its basic principle, DHC will stop when crack tip hydrides do not form or they form but do not crack. What is then the case at T_{CAT}? Is it because hydrides can not be formed at the crack tip due to, say, the fact that hydrogen does not diffuse to crack tip or hydride precipitation has become not possible anymore? Or does cracking stop as a consequence of the fact that the crack tip hydrides still form but do not crack? Knowing the exact reason for T_{CAT} would improve our knowledge about the DHC behaviour at high temperatures.

Secondly, the existence of T_{CAT} seemed to challenge the idea of using terminal solid solubility for precipitation (TSSp) at the flaw tip as the upper limit for DHC. The highest possible temperature for DHC has been generally thought to be determined by the hydrogen solvus or TSS simply due to the fact that the presence of hydride is essential. The existence of T_{CAT}, however, implies that, using TSSp as the upper limit for DHC might be conservative. In other words, as a crack initiation condition, the TSSp might be necessary but not sufficient, since DHC can stop despite the presence of ample hydrogen. Studying this phenomenon will, therefore, bring us a better understanding about the basic requirements of DHC.

Thirdly, the existence of T_{CAT} itself is a clear indication of the temperature influence on DHC behavior, since this phenomenon shows that cracking can cease solely due to temperature increases. Through T_{CAT} study, more detailed information about how the temperature can affect DHC will be obtained.

Fourthly, since T_{CAT} seems to represent a critical condition in terms of crack initiation, all parameters which are found to have effects on T_{CAT} values should be considered being decisive for crack initiation. These parameters could include all the material properties, which are directly or indirectly temperature dependent, or, the external factors such as applied K_I, which change the crack tip stress states.

Fifthly, it is certainly interesting to see if the observed independency of T_{CAT} from the solvus temperature is conditional. In other words, whether there exists an absolute cracking arrest temperature for Zr-2.5%Nb alloy, a $T_{CAT}^{ABSOLUTE}$, above which DHC will not occur no matter how much hydrogen is available. This $T_{CAT}^{ABSOLUTE}$ will then give a temperature range, beyond which Zr-2.5%Nb alloy becomes immune to the DHC problem.

In addition to these five original objectives, a sixth one has been developed during the course of this study after the author had realized that T_{CAT} actually occurs with crack tip hydrides formed but uncracked. By taking advantage of the fact that crack tip hydrides form and remain uncracked at T_{CAT}, valuable information about crack tip hydrides has been obtained. Since it is directly related to crack initiation, the hydride morphology is an essential point for controlling the DHC processes. More and more, the importance of crack tip hydride morphology has been brought up in literature [7-8] because it has been realized that the oversimplified picture of a single hydride lying at the crack tip should be replaced by a more realistic crack tip hydride configuration. The knowledge about the crack tip hydride is, however, disappointedly limited, which prohibits further developments of DHC process modeling and quantitative fracture criteria of crack tip hydrides.

In summary, the objective of this work is to explore the cessation of cracking at high temperatures. The existence of T_{CAT} had been experimentally found but its mechanism was not known at the time when this project was started. In this study, the T_{CAT} values have been measured under various conditions and the affecting parameters on T_{CAT} values investigated. A more detailed description of T_{CAT}, its range, its controlling factors and cause, has been made available through this project. Valuable information about crack tip hydrides, semi-quantitative and three dimensional, has also been obtained. Although the description of crack tip hydrides is a byproduct of this project since it was not an original objective, it is at least as important as the exploration of cracking arrest phenomenon itself. Crack tip hydride morphology is a key point in understanding DHC behaviour but they have never been studied in such an intensive way. Some other fracture initiation related DHC phenomena, such as the existence of K_{IH} and incubation period, have also been explored in conjunction with the study of T_{CAT}, the similarities and differences between them have been summarized. The results acquired in this study are considered to be useful in understanding crack tip hydride formation and fracture initiation processes. Although it is unlikely that DHC can be eliminated totally in Zr-2.5%Nb alloys, it should be possible to control this process better. This goal can be achieved only by constantly improving our knowledge about the process through continuous studies and this project is part of the effort.

Chapter 2 Background Information

2.1 Zirconium and Its Application in the Nuclear Industry

The alloy of zirconium with 2.5 weight percent niobium (Zr-2.5%Nb) is the alloy used in pressure tubes in *CANDU* (CANada Deuterium Uranium) nuclear reactors. The *CANDU* nuclear reactor is recognized worldwide as one of the most successful electricity generating systems ever developed. In conventional electricity generating stations, combustion of coal, oil or natural gas is used to boil water into steam, which turns a turbine to drive a generator. In nuclear power plants, the fission of uranium-235 is used as the source of heat [9]. At the heart of the *CANDU* system is a unique reactor core. This core consists of a large vessel, the calandria, containing heavy water moderator which is penetrated by about four hundreds horizontal fuel channels, Figure 2-1. Each channel consists of two end fittings and a pressure tube into which twelve or thirteen fuel bundles containing natural uranium are placed, Figure 2-2. Operating at a pressure of about 10 MPa, the heavy water coolant (D_2O) of the primary heat transport system flows through the pressure tubes and over the fuel, increasing in temperature from about 250°C at the inlet to about 300°C at the outlet end. This environment dictates that pressure tube material must meet stringent requirements for strength, corrosion resistance and response to radiation. Zirconium, owing to its combination of good mechanical properties, excellent corrosion resistance and low neutron absorption cross-section, has been selected as the structural material for nuclear reactors. Low neutron absorption cross-section means a lower fraction of neutrons will be absorbed by the material. The fewer the number of neutrons absorbed, the greater the number of neutrons will be available to produce fission of the fuel, and, therefore, the easier it is to maintain the chain reaction. Although important to all nuclear reactors, neutron economy is vital to the *CANDU* system because of the choice of natural uranium fuel, which is mostly uranium-238 with only a small fraction (about 0.7%) of the fissionable isotope uranium-235.

There are four reactor grade zirconium based alloys, namely Zircaloy-2, Zircaloy-4, Zr-2.5%Nb and the less common Zr-2.5%Nb-0.5%Cu alloy. The Zircaloys are Zr-based alloys with 1.5 wt% tin, while, as its name implies, Zr-2.5%Nb is alloyed with niobium. The earliest *CANDU* pressure tubes were Zircaloy-2 and later all *CANDU* reactor tubes have been constructed with zirconium-niobium alloy. Compared with Zircaloys, Zr-2.5%Nb is stronger and more resistant to creep deformation. This increased strength means that thinner walled tubes (about 20% thinner) can be used with a significant saving in the thermal neutrons and thus better neutron economy. It has subsequently been discovered that the Zr-2.5%Nb alloy is also more corrosion resistant in nuclear reactor operating environment and picks up far smaller quantities of hydrogen and its isotopes [10]. However, Zr-2.5%Nb has experienced the problem of coolant leakage from the primary heat transport [11-12].

The first observed failure in Zr-2.5%Nb occurred in an experimental fuel sheath assembly [13]. The thin-walled tubular sheath was closed at each end by a welded end cap. The residual stresses from welding concentrated at the sharp angle between the weld upset and the sheath were sufficiently high to cause failure at room temperature. Hydride precipitation at the crack tip was found by metallurgical examinations. In 1974 and 1975, several pressure tubes made from

Zr-2.5%Nb were found to be leaking in Units 3 & 4 of the Pickering Nuclear Generating Station (NGS) [14-15]. DHC cracks had initiated on the inside surface of the pressure tubes near the rolled-joint connections to the end fittings and propagated in the radial-axial plane of the tube. Over-extension of the forming tool during fabrication of the joints caused high tensile residual circumferential stresses in the regions where cracks were observed. Figure 2-3. Metallurgical examination of shallow cracks adjacent to the through-wall cracks, which caused the detected leakage, once again revealed hydride precipitation at the crack tip. In total, 74 of 780 pressure tubes were found to contain cracks. The dimensions of the cracks ranged between 15 and 20 mm in length and from less than 0.5 mm up to through-wall in thickness. Studies initiated following the leakage concluded that all the leakages were associated with high residual stresses [16] and this conclusion was consistent with the findings of Weinstein and Holtz about ten years earlier [11]. It was also believed that increased matrix yield strength due to neutron irradiation would affect the DHC process.

In 1982, leakage was once again detected in the fuel channels of a *CANDU* reactor, this time at the Bruce NGS Unit 2 reactor [4]. The fuel channels of this reactor were installed prior to the discovery of the cracks in the Pickering reactors. To minimize the potential for cracking initiation in the rolled-joint connections due to high residual stresses from over-extended rollers, these units were stress-relieved prior to being commissioned for service. However, the time between forming the rolled joints and the stress relieving treatment seemed to have already permitted cracks to initiate in each of the X14 and A14 fuel channel pressure tubes, which later led to the detected leakage. A third fuel channel, J11, was also found to be leaking in the rolled-joint region.

In 1986, a single pressure tube ruptured at room temperature in the Bruce NGS Unit 2 reactor while the reactor was shut down. The extensive failure analysis [17] found that a 3.8 metre long crack had resulted from the rupture of N06 pressure tube, which contained a manufacturing flaw. The flaw, a shallow-angle planar lamination at one end of the pressure tube, had preferentially corroded and cracked along its plane during reactor operation. The stress necessary to initiate cracking was achieved by a combination of the operating circumferential stress, the residual stress from rolled-joint forming and the localized stress concentration associated with the lamination. Unlike previously examined fractures which had single-point origins, the manufacturing flaw provided multiple cracking initiation sites. Several cracks initiated in the same plane of the tube and grew simultaneously, eventually forming one long crack.

The above mentioned service failures resulted in an extensive research program investigating the cause of these leakages. The problem was determined to be caused by delayed hydride cracking (DHC) [1]. The direct cause of leakage was associated with the corrosion process which increased the hydrogen content of the pressure tubes and the high residual stresses in the tubes near the rolled-joint regions [15]. The rolling procedure was designed to plastically deform pressure tube material into grooves in the stainless steel end fittings in order to provide a pressure seal. However, due to over-extended rolling, i.e. the rolls extended too far into the tubes during rolling, residual stresses of approximately three times the expected values were introduced. This stress, in combination with ordinary operating stresses of the reactors, produced a stress gradient of sufficient magnitude to initiate cracking. When the reactors were cooled under pressure, re-oriented radial hydrides formed in the highly stressed regions. As a consequence of the formation of these re-oriented hydrides, cracking initiated and propagated through the wall thickness causing leaks. Based on these research results, a new rolling procedure had been developed and followed for all the pressure tubes after the Bruce NGS units. All the tubes are also stress relieved. Thus, no further cracking from these sources should occur in *CANDU* reactors. However, the phenomenon of DHC is not fully understood and numerous phenomena remain unexplained. Despite the improved knowledge of DHC, further investigation is still needed to answer all the questions on the nuclear-related delayed cracking problems.

2.2 Theory of Delayed Hydride Cracking

2.2.1 Overview

Hydrogen can damage a wide variety of materials and the resultant deterioration can take different forms, including

- blisters - accumulation of gaseous hydrogen in a local area below the metal surface;
- hydrogen embrittlement - lack of ductility; or
- hydride induced delayed cracking - metal failure involving the formation of a hydride phase near the tip of existing flaws.

The deteriorating effect of hydrogen in steels is probably the most well known example for hydrogen related damage. Other common engineering metals such as zinc (Zn), copper (Cu), nickel (Ni) and chromium (Cr) also exhibit reduced mechanical properties due to the presence of hydrogen. Another group of less common engineering metals including titanium (Ti), vanadium (V), zirconium (Zr) and niobium (Nb), suffers failure caused by the formation of brittle hydrides [18]. Since the embrittlement caused by these hydrides occurs in a time-delayed mode, this type of hydrogen related deterioration has been termed Hydrogen-Induced Delayed Cracking (HIDC) or Delayed Hydride Cracking (DHC). The acronym of DHC will be used throughout this thesis.

DHC is a multi-step, diffusion controlled crack propagation process caused by hydride formation and fracture. In this process, hydrogen atoms diffuse to highly stressed regions such as near existing crack tips. The driving force for the diffusion is the lowered local chemical potential. As a result of this diffusion process, the concentration of diffusible hydrogen, i.e. hydrogen in solution, at these regions increases. As soon as the local hydrogen level exceeds the solid solubility limit, hydrides will form and grow as long as the driving force for diffusion remains. When these crack tip hydrides reach a critical condition, fracture of these hydrides will occur. The crack propagates by repeating this hydrogen diffusion, hydride formation and fracture process at the new crack tip.

Although being important for nuclear reactor safety and economy, a full understanding of this cracking process is not easily achievable because the process involves the following three distinct phenomena:

- diffusion - the migration of hydrogen into stressed region such as crack tips;
- phase transformation - the hydride formation at crack tips when the hydrogen solubility is exceeded; and
- fracture, which refers to the breakup of these crack tip hydrides when certain fracture criteria are satisfied.

Firstly a thorough understanding of each of these three phenomena requires both intensive experimental work and theoretical description of the process. Secondly, the fact that these three phenomena are not isolated but inter-dependent makes the study of this process more sophisticated. As a consequence of hydrogen diffusion, which is caused by the uneven stress distribution, hydrides will form at the tips of existing cracks. The formation of these hydrides will, in turn, cause the crack tip stress re-distribution and, inevitably, influence the hydrogen diffusion process. Fracture of hydrides will also modify the crack tip stress distribution and affect the hydrogen diffusion process.

The DHC process can be studied either macroscopically or microscopically. The macroscopic study of the process deals with the DHC properties that can be averaged. One example of macroscopic DHC study is the crack velocity measurement which is the result of dividing the total crack advance by the time frame during which the crack advance has occurred. Since the crack velocity is an averaged quantity, no attention needs to be made towards the details about how cracking actually advances. Microscopic study of DHC, on the other hand, investigates the properties which can not be averaged. One example in this category is the precipitation and growth of the crack tip hydrides. For microscopic studies, it is absolutely critical that all the physical details of how a process develops be known clearly. Due to its high degree of complexity, the work done on DHC so far has been mainly macroscopic in nature. Logically, the theoretical models developed based on these works are only successful in explaining some of the "averageable" behaviors such as cracking velocity [19]. Not yet incorporated by these models are the microscopic characteristics of DHC such as cracking initiation criteria of crack tip hydrides, which requires detailed experimental measurements to provide physical descriptions of the cracking initiation process occurring at the crack tip. Due to basic differences in approaching the problem, many of the assumptions, which form the basis for macroscopic studies, can not be adopted for microscopic analysis. For instance, one of the assumptions used in macroscopic modeling of the DHC process is that the process proceeds continuously. For macroscopic studies, this assumption is perfectly acceptable, since the results are averaged numbers anyway. From the microscopic point of view, however, this assumption is not correct because all the experimental evidence, including intermittent acoustic emissions [20], discrete potential drop changes [7] and fracture surface striations [8], confirm that DHC is an intermittent not a continuous process. Macroscopic studies usually started before microscopic studies due to limited knowledge about the process. With the improvement of knowledge, DHC study now starts to move into the microscopic stage. In the past few years, study areas such as hydride cracking criteria and K_{IH} analysis become more and more active. For the success of these studies, analysis has to be done in a microscopic way. The topic of this work - the cessation of DHC at elevated temperatures - is also microscopic in nature.

2.2.2 Hydrogen Content and Distribution

One of the fundamental requirements for DHC to occur is that the material must contain sufficient hydrogen to exceed the solubility limit at the temperature of interest.

The initial hydrogen content in zirconium pressure tubes is low, estimated to be approximately 15 μg/g [21], in older tubes and much lower in newer tubes. With total hydrogen at this level, all hydrogen remains in solution and the material is not susceptible to DHC except at low temperature. Over time, however, the hydrogen content of these tubes increases due to a slow corrosion process by which hydrogen (deuterium)[1] migrates into the metal. It is believed that up to 50 μg/g of hydrogen can be absorbed by pressure tubes over a period of 30 years [22]. As the result of this corrosion process, these tubes gradually become susceptible to DHC even up to the operating temperature of the reactor because the hydrogen content may eventually exceed the solubility limit.

There are two solvi in Zr-2.5%Nb alloys, one during the process of cooling (precipitation) and another during the process of heating (dissolution). The precipitation solvus is higher because of the strain energy to accommodate precipitation. The dissolution solubility, C_H^d, and the precipitation solubility, C_H^p, are given (in μg/g) as [23]:

---

[1] In this paper, hydrogen and deuterium are considered to be indistingueshable in their influence on DHC behavior.

$$C_H^d = 6.86 \times 10^4 \exp\{-4061/T\} \qquad (2.1)$$

$$C_H^p = 4.11 \times 10^4 \exp\{-3368/T\} \qquad (2.2)$$

Because of the existence of these two solubilities, for any given sample containing a certain percentage of hydrogen, the amount of hydrogen present in solution can vary dramatically, depending on whether the temperature has been approached by cooling or by heating. The effect of the thermal history on the hydrogen content in solution can be visualized by the use of an example, see Figure 2-4. For a zirconium sample with, say, 160 μg/g hydrogen in total, its hydrogen level can be about 58 μg/g if this sample has been heated to 300°C. But the same sample can also have as high as 115 μg/g hydrogen in solution if it has been heated to 370°C and then cooled to 300°C. In other words, the amount of hydrogen in solution is highly path dependent, and the thermal history of the sample must be known to accurately predict this quantity.

The analysis of hydrogen in zirconium is further complicated by the fact that the local hydrogen level can be different from the average content in pressure tubes. This is due to stress induced diffusion. It has been observed that hydrogen, present as an interstitial solute, migrates to highly stressed regions if the parts are loaded under tension. The result of this stress-induced diffusion is a local accumulation of hydrogen in regions such as at crack tips. More discussion about the stress distribution will be given in section 2.2.4. The susceptibility of material to DHC depends more on the distribution of hydrogen than on its average volume fraction because it is the local hydrogen level which decides if hydrides can be formed or not. Thus, the hydrogen accumulation due to non-uniform stress distribution inside samples has to be considered in studying the DHC process.

For a sample with a pre-existing crack under a tensile stress, the effective tensile stress at the crack tip is higher than in other regions. This effect of raised stress in local regions because of the sample's geometry is termed the stress concentration. Due to its influence on hydrogen distribution, the stress distribution analysis is important for DHC study. If the total hydrogen concentration is so low, that even an increased local level of hydrogen is still not sufficient for hydride precipitation, then the material is not susceptible to DHC. But as soon as the local hydrogen level in highly stressed regions is high enough to form hydrides, the material becomes susceptible to DHC even though the average volume fraction of hydrogen may still be below the solubility. This increased local hydrogen content can occur because of an elevated hydrostatic tension near the crack tips.

The stress-induced migration of diffusible hydrogen is caused by changes of chemical potential under the stress field. The chemical potential of a mobile species H, $\mu_{H,p}$, in a stressed solid is given by

$$\mu_{H,p} = \mu_{H,o} - pV_H \qquad (2.3)$$

where $\mu_{H,o}$ is the chemical potential at zero stress,

p is the average principal stress which is positive if tensile, and

V_H is the partial molar volume of hydrogen dissolved in the zirconium lattice.

The chemical potential is, however, also dependent on the concentration of the hydrogen, C_H, and can be calculated by:

$$\mu_H = \mu_o + RT \ln C_H \qquad (2.4)$$

Combining equations 2.3 and 2.4, we have:

$$\mu_{H,p} = \mu'_{H,o} + RT \ln C_H - pV_H \qquad (2.5)$$

That is, the concentration and the stress vary the chemical potential simultaneously. According to equation 2.5 the higher a tensile stress is, the lower the $\mu_{H,p}$ will be if C_H remains constant. In other words, the effect of increased hydrostatic tension can be balanced by locally increasing the value of C_H [24] and diffusion occurs to even out any gradient in chemical potential.

2.2.3 Zirconium Hydrides

2.2.3.1 Zirconium Hydrides and Their Properties

After hydrogen has been concentrated in highly stressed areas, near a crack tip for instance, hydrides will be formed locally if the build-up of hydrogen exceeds the solid solubility. The hydride formed in zirconium alloys can be either:

- γ-hydride (ZrH), face centered tetragonal and formed on fast cooling particularly at lower temperature, or
- δ-hydride ($ZrH_{1.6}$), face centered cubic and formed on slow cooling.

Once these hydrides form, the behavior of the alloy will be greatly affected by the properties of these hydrides. The determination of the mechanical properties of zirconium hydrides has proven to be very difficult. The major problems are the inherent brittleness of the hydride and the difficulty in obtaining relatively large crack-free test specimens [25]. It is estimated that the fracture toughness of δ-hydride is about 1 MPa√m at 20°C and about 3 MPa√m at 300°C [26]. In comparison, Zr-2.5%Nb matrix displays a fracture toughness of at least 40 MPa√m at room temperature and greater than 100 MPa√m at about 300°C [27]. To the author's best knowledge, no reports on the mechanical property differences between the γ-hydrides and δ-hydrides have ever been published.

2.2.3.2 Hydride Orientation and Morphology

Not all the hydrides formed in Zr-Nb alloys can cause DHC. Depending on their morphology (size, shape, position, distribution and orientation with respect to any residual or applied stresses), the ambient temperature and the stress level, these hydrides may or may not crack.

In nuclear reactor pressure tubes, two types of hydride orientations can be found, namely circumferential-axial and radial-axial. Radial-axial hydrides can provide a ready crack path under a circumferential stress. Fortunately, the cold-drawing techniques for the fabrication of pressure tubes produce a matrix with a strong tendency to form circumferential-axially oriented hydrides. However, hydrides which precipitate while the tubes are under stress, e.g. reactor cooled under pressure, will have their normals in the circumferential direction and these radial-axially oriented hydrides make pressure tubes susceptible to DHC. The degree of hydride re-orientation varies with parameters such as peak temperature, matrix texture and applied stress levels. In this thesis, these radial-axially oriented hydrides will be referred to as "radial" or "re-oriented" hydrides.

For these "radial" or "re-oriented" hydrides, whether they will fracture or not is then determined by their morphology. It is widely agreed that these re-oriented hydrides have to reach a critical dimension before they crack. It is not clear though what this critical dimension is. Until very recently, only the hydride dimension along the crack advance direction, the axial direction, has been considered as decisive and a one dimensional threshold value, termed as "critical length", has been used to describe the critical dimension. Using a single, one dimensional quantity to define the cracking initiation condition reflects the concept that the crack tip hydrides have been assumed to form as a single piece ahead of crack tips. This concept has been found to be inaccurate or greatly simplified [21, 28-29]. Instead of using a mono-hydride-platelet model, a more acceptable analysis about crack hydrides should be based on a multi-hydride-platelet model. Confirmed by recent metallographic observations, crack tip hydrides are discontinuous along both the radial and axial directions. These hydrides are also found to form on different planes in front of crack tips. Obviously, instead of only a single parameter (the "critical length"), a set of parameters should be used to characterize the crack tip hydrides and these parameters should contain at least the length, width and thickness of the hydrides as well as their spacing in the three directions. The "length" refers to the dimension of each individual hydride platelet along the axial direction; the "width" the dimension of each individual hydride platelet along the radial direction and the "thickness" the dimension of each hydride platelet along the circumferential direction. The "spacing" refers to the distance between two adjacent hydride platelets along one of the three directions mentioned above. Almost for sure, the dimensions of the hydride "cluster" have to be considered too, since it is not clear yet if it is the dimension of the individual hydride platelet or the overall dimension of the hydride cluster which dictates the cracking initiation.

In 1993, Luo developed a quantitative model correlating cracking initiation toughness with crack tip hydrides. In his model he has treated the crack tip hydrides as a cluster of hydride platelets [30]. By applying this model, Luo has calculated the cracking initiation toughness for given conditions. In developing his model, Luo has suggested the use of a hydride continuity coefficient (HCC) and a roughness measure (R) to describe hydride structures along both the radial and circumferential directions. According to Luo, the first parameter, the HCC, reflects the horizontal distance between hydrides in the radial direction. It is thus the measurement of the continuity of the hydrides in the radial direction and is related to the hydride density on the fracture surface, a key factor in the cracking initiation process. The hydride continuity coefficient on the fracture surface, HCC^*, can be expressed by the equation:

$$HCC^* = \frac{\sum_{i=1}^{n} w_i}{t_o} \tag{2.6}$$

where W_i is the width of the *ith* hydride and t_o the effective specimen width. This HCC^* can be measured on the cross-section of the fractured surface.

The second parameter, the roughness R, measures the average vertical distance between two neighboring hydrides along the circumferential direction. This parameter considers the fact that not all the hydride platelets are formed on the same radial-axial plane and is designed to reflect the change in cracking resistance associated with shearing of the matrix between the neighboring hydrides. Thus, the roughness is expressed as the shearing length per unit specimen width as shown in equation 2.7 and Figure 2.5.

$$R = \frac{\sum_{i=1}^{n} c_{yi}}{t_o} \tag{2.7}$$

where C_{yi} is the circumferential distance between the *ith* and the (i+1)*th* hydride.

2.2.3.3 Fracture Criteria of Crack Tip Hydrides

Fracture of the "re-oriented" crack tip hydrides is the cause of DHC. Despite its importance, an applicable cracking criterion for these radial-axial hydrides is not yet available. Developing a quantitative cracking criterion is challenging because it depends on factors such as hydrogen content, thermal history, material geometry, matrix microstructure and impurity level. It requires a precise quantitative description of crack tip stress distribution and the interactions between crack tip stress field, hydride precipitation, its growth and fracture. It also relies on accurate experimental measurements of crack tip hydride morphology and all the possible affecting parameters.

Although difficult, attempts have been made to develop a fracture criterion which is theoretically sound and practically applicable. In the literature dealing with this topic, two recent papers are outlined below. The first paper was published in 1994 by Shi and Puls [31]. In this paper, the authors have derived a model for DHC initiation for a sharp crack tip in zirconium alloys. The basic idea of their work is the existence of a critical threshold stress for hydride fracture. Hence, when the local stress at some point inside a hydride, σ_{local}, is larger than the stress needed for hydride fracture, σ_f^h, i.e.:

$$\sigma_{local} \geq \sigma_f^h \tag{2.8}$$

a cracking initiates in the hydride. With some further simplifications, equation 2.8 has been transformed to:

$$\sigma_{eff}^a + \sigma^h \geq \sigma_f^h \tag{2.9}$$

where σ_{eff}^a is the effective applied stress at hydride (tensile) and σ^h the stress created by hydride formation process (compressive). By analyzing σ_{eff}^a, σ^h and σ_f^h individually, a quantitative equation for cracking initiation has been given in terms of K_{IH} ,which is the critical stress intensity factor for the process. For a mono-hydride-platelet model, the equation is:

$$(K_{IH})^2 = \frac{E^2 \epsilon_{\perp} t}{8\pi(1-\nu^2)^2\left(\frac{1}{1-2\nu} - \frac{\sigma_f^h}{\sigma_y}\right)} \tag{2.10}$$

with t being the thickness of the hydride platelet. Under the stated assumptions, the expression in equation 2.10 shows that K_{IH} decreases with increases in yield stress (σ_y), with other factors remaining constant. Thus the yield stress of the matrix is an important variable in controlling K_{IH}. Any factor which makes σ_y decrease, an increase in temperature for instance, will increase the value of K_{IH}. In other words, the cracking condition will be affected by temperature through its effect on σ_y. From equation 2.10 we can see that the value of K_{IH} is also sensitive to t, the thickness of the hydride platelet. The accurate measurement of the t value is therefore critical for calculating K_{IH}. Any parameter which favors the precipitation of a thicker hydride would raise the value of K_{IH}. The higher the K_{IH} is, the more difficult is the cracking initiation.

Although showing a correct trend for its dependence on temperature, the K_{IH} values calculated from equation 2.10 (the dotted lines) are considerably lower than the experimentally observed K_{IH}^{exp} (the symbols) for Zr-2.5%Nb, see Figure 2-6.

The discrepancy is believed to come from the simplifications and assumptions adopted during the derivation of equation 2.10 and the mono-hydride-platelet model applied. Using a multi-hydride platelet model, which is closer to the reality, should bring better results. There are at least two improvements which can be made to increase the predicted value of K_{IH} towards that of the K_{IH}^{exp}. Both improvements are associated with a more careful description of the crack tip hydride morphology. The first improvement can come from considering the fact that crack tip hydrides are actually formed on different radial-axial planes. Therefore, instead of a thickness (t), an effective thickness (τ) should be used to include the effect of multi-layered hydrides at the front of the crack tip. In the simplest case, this τ could be the sum of the thicknesses of each layer, i.e. $\tau = \sum t_i$, if the t_i's values are available. The second improvement can be made by taking the incomplete coverage of hydrides into account. This can be done by introducing a weighting factor, f, which is the area fraction of hydride coverage in front of the crack tip. Accordingly, this would give [31]

$$K_{IH} = f\, K_{IH}^{s} + (1-f)\, K_{IC}^{Zr} \qquad (2.11)$$

where K_{IC}^{Zr} is the cracking initiation threshold for a zirconium alloy containing virtually no hydride, and K_{IH}^{s} is the K_{IH} derived in equation 2.10 based a the mono-hydride-platelet model. Although it can improve the predicted accuracy, the adoption of multi-hydride platelet model makes the evaluation of K_{IH} more dependent on the crack tip hydride morphology. The Shi-Puls model also implies an inevitability of dealing with a number of material properties, whose measurements can be quite difficult.

The second paper dealing with fracture criterion was published in 1995 in which Zheng and his co-authors have approached the problem from a different perspective [32]. Instead of analyzing the fracture stress, they have proposed a fracture criterion based on the principle of energy balance. Assuming a finite length of crack advance, which is reasonable due to the discrete nature of hydride cracking, and a crack extension being equal to the length of the inclusion, they have started their analysis from a fundamental equation based on the thermodynamic energies involved:

$$G_{finite} = (\Delta W - \Delta U)/\Delta A \qquad (2.12)$$

where ΔW is the mechanical work done by external loads during the finite crack extension under constant load, ΔU is the change in total energy which includes both elastic and plastic energy terms, and ΔA is the area formed after the crack extension. The G_{finite} is the general elasto-plastic energy released over a finite crack extension. Cracking will occur when

$$G_{finite} = G_c \qquad (2.13)$$

Although defined by Zheng *et al* as the "surface energy" of the material to be fractured, G_c actually also includes the plastic work related to fracture and it reflects the combined effect of both hydride and zirconium matrix on the fracture process. For the situation of a small length of cracking initiation at the edge of a flat plane with a relatively large width, the energy release rate over finite length can be expressed as:

$$G_c = K_I^2 (1 - \nu^2)/2E \qquad (2.14)$$

with E and ν being Young's Modulus and Poisson's ratio respectively. This relationship suggests that the specific energy available for fracturing a hydride is proportional to the square root of the hydride length, since $K_I \propto \sqrt{a}$.

Zheng's paper has also suggested an empirical relationship correlating fracture energy with crack tip hydride structure. If G_i is the fracture energy per unit area of hydrided materials, then:

$$G_i = f_a G_h + (1 - f_a) G_m + RG_s \qquad (2.15)$$

where f_a is the area fraction of hydrides at cracking initiation,

G_h is the hydride fracture energy,

G_m is the matrix fracture energy in tension,

G_s is the matrix fracture energy in shearing, and

R is the surface roughness.

While G_h, G_m and G_s are material constants, f_a and R describe the hydride structure and have to be experimentally measured. Again, a number of material constants are involved and the crack tip hydride morphology has to be analyzed before any evaluation of crack advance can be made. It is interesting to point out the f_a in equation 2.15 is virtually the same as the f in equation 2.11. Although being needed in the both models, neither reliable experimental values nor theoretical equations for calculating f (f_a) is available.

2.2.4 Stress and Stress Distribution

2.2.4.1 General Description of Stress Distribution at Crack Tips

The stress level and its distribution in pressure tubes are one of the fundamental parameters for determining the probability and rate of DHC which may occur. The importance of stress and its distribution stems from its two-fold influence on the process: affecting both the hydrogen migration and the hydride fracture, as discussed in section 2.2.2 and 2.2.3. Service failures of zirconium alloys consistently point to the presence of high tensile stress, see section 2.1. In pressure tubes, the applied stress resulting from normal operation and anticipated abnormal or transient pressures is, generally speaking, not high enough to cause DHC. However, DHC can initiate and propagate when the applied stress is combined with other stresses, such as the high residual stresses associated with improper roll-joining procedures.

The stresses near a crack tip produce four distinct zones as schematically shown in Figure 2-7 [23]. The first one, closest to the crack tip, is known as the process zone and extends 2δ from the tip, with δ being the crack tip opening displacement.

It is believed that the stresses in this processes zone are somewhat limited due to crack tip blunting, although the stresses and strain in this zone are not fully understood because of non-proportional loading and very large strains. The second zone is a plastic annulus beyond the process zone, where the Hutchinson-Rice-Rosengren (HRR) solution is valid. Outside the plastic annulus is the third zone called the plastic zone. In this plastic zone the HRR solution is not valid since the elastic strains are not negligible compared to the plastic strains, but yet there is a significant plastic strain. The fourth and the farthest zone from the crack tip is the region in which linear elastic fracture mechanics are valid. Among these four zones, the plastic zone has drawn a lot of attention in cracking criterion studies since its dimension is believed may be somehow related to the critical length of the crack tip hydrides. The shape of the plastic zone is given by [23]:

$$r_y\,(\theta) = \frac{K_I^2}{4\pi\sigma_{ys}^2}\left\{(1-2\nu)^2(1+\cos\theta)+\frac{3}{2}\sin^2\theta\right\} \tag{2.16}$$

It has been suggested that the stress at the crack tip is elevated due to through thickness constraint [19]. In their paper, Dutton and Puls suggested that the peak stress close to the crack tip be given as:

$$\sigma_{YY} = 3.0\sigma_y \tag{2.17}$$

$$\sigma_{XX} = 1.8\sigma_y \tag{2.18}$$

$$\sigma_{ZZ} = 2.4\sigma_y \tag{2.19}$$

where σ_y is the uniaxial yield stress, y is the normal to cracking plane, x the cracking direction and z the radial direction. The peak hydrostatic stress is equal to

$2.4\sigma_y$. McMeeking [33] later adjusted this value to $2.7\sigma_y$ which is later re-adjusted to be $2.71\sigma_y$ based on a modification for cold working [34]. The importance of this conclusion is that a higher stress level exists at the crack tips and therefore the local hydrogen level in these locations is increased in order to minimize the chemical potential, see equation 2.5 in section 2.2.2. Equations 2-17, 2-18 & 2-19 are also important in understanding the temperature effects on DHC behavior. Since the peak stress at the crack tips is directly proportional to the matrix yield strength, any changes in yield stress will cause peak strength variations. Such yield strength changes can be caused by temperature changes, irradiation and cold working, see section 2.2.5.4 for details.

2.2.4.2 Stress Re-distribution due to Hydrogen Diffusion and Hydride Formation

As discussed earlier, hydrogen flux and hydride formation/fracture are affected by the stress field around the crack tips. It is important to point out that the hydrogen diffusion and hydride formation processes will cause modification of the existing stress field and induce a redistribution of local stresses. This effect of hydrogen diffusion and hydride formation on the stress field comes from the dilation accompanying the processes.

Since the partial molar volume of hydrogen in zirconium is positive, being 1.67×10^{-6} m^3/mol according to MacEwan *et al.* [35] and 1.7×10^{-6} m^3/mol according to Eadie *et al.* [24], the hydrogen atom has a positive volume effect on zirconium-niobium alloy matrix. This difference in molar volumes of pure zirconium and zirconium containing hydrogen results in a volume expansion when the hydrogen content increases. The higher the hydrogen content is, the larger is the dilation. During the stress-induced diffusion, a hydrogen concentration gradient is built up in the opposite direction of the hydrostatic stress gradient. This will cause a relaxation of local tensile stress, which decreases the driving force for hydrogen diffusing along the stress gradient. Compared with hydrogen diffusion, hydride formation has a larger impact on stress field due to the accumulation of a much larger number of hydrogen atoms (≈16000 μg/g) in the matrix in order to form hydride. The volume of the hydride phase is estimated to be about 17% greater than that of the metal matrix it replaces. The result of this volume difference is a dilation of volume when hydrogen in solution transforms into hydride. Eadie and Ellyin [34] have proposed an approach to establish a qualitative description of the stress changes caused by hydride precipitation. They have suggested that there is a region of dilation in the plastic zone mentioned in the previous section due to hydride precipitation. They have simulated this dilation by adding a tensile stress ahead of the crack tip, as illustrated in Figure 2-8. Another paper on the effect of hydride expansion on the elasto-plastic stress field near a crack tip has been published by Ellyin and Wu in 1994 [36]. In this paper, a center cracked panel subjected to a uniformly distributed tensile load perpendicular to the crack plane is chosen because this type of loading condition is a close representation of a pressure tube with a tensile stress applied in the transverse direction of the tube due to the internal pressure. The hydride expansion is simulated by imposing an appropriate displacement perpendicular to the crack plane. Based on their results, both the thickness and length of a hydride platelet affect the crack tip stress distribution. The distribution of the normal stress component along the crack plane following hydride expansion is shown in Figure 2-9 [36]. A clear influence of hydride expansion (hydride thickness change) can be seen because both the magnitude of the stress over the entire hydride platelet (the stress in the region of $X_1/(K_I^2/\sigma_o^2) = 0.00$ and 0.04) and the value of the peak stress in front of the crack (the stress at $X_1/(K_I^2/\sigma_o^2)$ » 0.004) decrease with increased hydride expansion. Figure 2-9 also indicates that the maximum tensile stress will be shifted to the front end of the hydride platelet $(X_1/(K_I^2/\sigma_o^2) > 0.04)$ when a hydride platelet forms. As a consequence of this shift of peak stress, hydrogen will migrate to this location and hydride will grow along the crack plane away from the crack tip. Figure 2-10 [36] illustrates the distributions of normal stress for three different hydride lengths. A general trend is that the precipitation of a crack tip radial hydride will decrease the crack tip stress as well as the magnitude of stress over the entire hydride platelet. The growth of a precipitated hydride platelet, however, will cause an increase in the stress at the crack tip as well as over the hydride platelet from the lowered values. This re-modified stress distribution will affect both the hydrogen flux to crack tip regions and hydride fracture in these regions, making the analysis of both processes more complicated. In 1995, Metzger and Sauve analyzed the interaction of hydride precipitation with local stress field by using a stepwise coupled diffusion/stress analysis. The fact that the diffusion in DHC process is stress induced implies that hydride(s) should form at the locations where the stress peaks are. As soon as a piece of hydride precipitates, the volumetric expansion of the hydride(s) will modify the initial stress field and lower the hydrostatic stress acting on the hydride(s). Subsequent hydrogen diffusion and hydride precipitation will be affected by this modified stress field. Metzger and Sauve believe that this interaction between an existing crack tip hydride and the local stress field needs to be integrated into the modeling of the DHC process [37]. Metzger and Sauve also believe that the shape of the radial hydride platelet is a critical factor in accounting for the effect of its expansion on the stress field [37]. As a matter of fact, such an effect has already been implied by Ellyin and Wu because they have shown that a slight shape change to the hydride end will drastically affect the local stress distribution [36].

The basic steps involved in Metzger-Sauve model are:

- obtain stress distribution by elastic-plastic stress analysis of flaw geometry;
- assume radial hydride forms at the stress peak of hydrostatic stress, as dictated by diffusion driving force;
- for an increment in hydride growth, introduce a corresponding transformation strain increment and obtain a new elastic-plastic stress distribution;
- this updated stress field is fed back to the modeling process to analyze the further growth of the existing hydride.

The key result in Metzger-Sauve model is that the hydride growth always tends to flatten the hydrostatic stress peak and the interaction between the existing hydride and the stress field dictates both the actual stress distribution and the shape of the precipitated hydride. The shape of a crack tip hydride should be such that the local stress field is equalized as much as possible over the entire hydride length. Finite element analyses based on Metzger-Sauve model suggest that a linear wedge is a good approximate of the radial hydride and an increase in hydride length is accompanied by an increase in hydride thickness, as shown in Figure 2-11 [37]. The consequence of the growth of such a wedged hydride is that the stress peak decreases in magnitude and spreads farther ahead of the crack. Similarly to Figure 2-10, Figure 2-11[2] suggests that the hydride growth will be on the crack plane, with the difference that the stress distribution given by Figure 2-11 being monotonic and containing no compressive region. The predicated hydride shape was shown to agree with some observed hydride shapes.

---

[2] The fact that Figure 2-10 uses σ_{22}/σ_o and Figure 2-11 uses hydrostatic stress does not affect the validity of a qualitative comparison of the two models.

2.2.5 Factors Affecting the DHC Behavior of Zr-2.5%Nb

2.2.5.1 Matrix Hydrogen Content

A minimum hydrogen content is required for DHC to occur, since hydride precipitates are absolutely essential, as mentioned in section 2.2.1. In other words, for DHC to occur, the precipitation solvus must be exceeded, at least locally. In situations where the matrix hydrogen content is too low to reach the solubility limit, all hydrogen remains in solution and the material is not susceptible to DHC because no hydrides can be formed. In the cases of *CANDU* reactor pressure tubes, DHC did not and could not occur during reactor operation at the initial stage of operation simply because of the low initial hydrogen level. However, the tubes gradually became susceptible to DHC at higher temperatures when they absorb hydrogen during service by reacting with the coolant water during corrosion. As the matrix hydrogen content increases up to the precipitation solvus at any temperature, DHC velocity increases. Since only a certain amount of hydrogen goes into solution at a given temperature and hydrogen as matrix hydride away from the cracking plane has no effect on the DHC process, further increases in matrix hydrogen content has little effect on the DHC velocity at that temperature [38-39].

2.2.5.2 Stress Intensity Factor

The magnitude of the force causing a crack to propagate is described by using a stress intensity factor (K). A stress intensity factor is a function of the applied load, the geometry of the parts and the length of the existing crack. Stress intensity factors have the units of MPa√m and for the condition of a crack opening stress the notation of K_I is used.

The effect of stress intensity factor, K_I, on DHC behavior can be summarized by saying:

- there is a nonlinear relationship between cracking velocities and K_I, and
- there exists a limiting value of K_I below which cracks will not propagate from a pre-existing notch.

Known as K_{IH}, the lowest value of K_I with which DHC occurs, is reported as about 5 MPa√m [38]. As the stress intensity factor increases near K_{IH}, so does the DHC velocity (DHCV). The DHCV dependence on K_{IH} can be schematically shown as in Figure 2-12. The curve can be divided into three stages. In Stage I, where K_I is very close to K_{IH}, DHCV is very sensitive to variations in K_I. The detailed explanation for this rapid change of DHCV is still not available. In stage II, DHCV remains almost unaffected with varying K_I. This is because the peak hydrostatic stress at the crack tip is determined by the yield strength of the matrix and is approximately equal to $2.7\sigma_y$ [40] as discussed in section 2.2.4.1, regardless of K_I. In stage III, the cracking velocity increases sharply with any small increases of K_I and the material fails by fast fracture. More discussion on K_{IH} will be given in section 2.2.6.2.

2.2.5.3 Temperature

The effect of temperature on DHC is multifold and complex. As mentioned in section 2.2.1, the DHC process involves three distinct processes: hydrogen diffusion, hydride formation and hydride fracture. All of these three processes are temperature dependent in nature.

The temperature dependence of the diffusion process can be described by using a general diffusion equation:

$$J_H = -(D_H C_H/RT)\nabla\mu_H \qquad (2.20)$$

where J_H is the hydrogen flux,
D_H is the diffusion coefficient of hydrogen in α-zirconium,
C_H is the hydrogen concentration in solution,
R is the gas constant,
T is the temperature, and
μ_H is the hydrogen chemical potential driving the diffusion.

Indicated clearly by equation 2.20 is a dependence of hydrogen flux (J_H) on temperature (T). (Also the hydrogen concentration in solution, C_H, depends on temperature history as previously discussed.) The effect of temperature on the diffusion process in DHC is complicated by the fact that the diffusion process is not a concentration-driven migration process but a stress induced one. Because it affects the matrix strength of the matrix and, therefore, the stress distribution, the temperature change will modify the stress field, which inevitably has influence on the DHC process. Temperature changes also affect the hydride formation process because they will change the solubility limit of hydrogen. The higher the temperature, the greater the quantity of hydrogen which is needed to produce hydride precipitation. Also the hydride fracture is not insensitive to temperature changes. The temperature influence on hydride fracture process has been confirmed by experimental results but a satisfactory explanation is not yet available. As a matter of fact, among the three phenomena involved in DHC, the fracture process is the least understood one. People know that crack tip hydrides will fracture when they reach a critical condition but people still do not know what this critical condition is. Nor can they predict in detail how temperature change will affect the critical condition for cracking initiation. The existence of T_{CAT}, which is the topic of this work, indicates clearly a temperature effect on the cracking process, either on the crack initiation or on the crack propagation. The exact mechanism of this phenomenon was, however, not clear to the point when this work was started.

2.2.5.4 Matrix Strength of Zr-2.5%Nb

The mechanical properties of Zr-Nb matrix, such as the yield strength, are important for the DHC process because they affect the process by altering the stress field around crack tip. While in service, the matrix strength of Zr-2.5%Nb pressure tube can be affected by both operating temperature and neutron irradiation.

The higher the temperature, the softer are the pressure tubes. That is the yield strength of the tubes decreases with increasing operating temperatures. A widely accepted equation for estimating the yield strength of unirradiated pressure tube materials in the circumferential direction at a given temperature is given by

$$\sigma_y = 1088 - 1.02T \qquad (2.21)$$

where T is temperature in Kelvin and σ_y is yield strength in MPa [31].

The matrix strength level is also affected by the neutron irradiation experienced by the pressure tubes. The result of the irradiation is an increased yield strength and decreased ductility. The unique design of the *CANDU* reactors in which the pressure containing surfaces are actually in the neutron flux zone of the reactor generates some interesting effects. One such effect is the manner in which the yield strength of the zirconium alloy tubes increases with exposure to the high energy neutron fluence produced by the on-going nuclear reaction. Sagat *et al.* [40] have reported results of experiments in which Zr-2.5%Nb material had been exposed to neutron fluxes in the rage of $1.6X10^{17}$ to $1.8X10^{18}$ N/m^2s to cumulative fluences of 10^{23} to 10^{26} N/m^2. A five-fold increase in DHCV has been observed after irradiation. This significant increase in DHCV is believed to be related to the increased material yield strength after irradiation hardening via dislocation multiplication. In the laboratory environment, where the effect of irradiation needs to be investigated, the irradiation induced “hardening” can be simulated by cold working the specimens. The increase in strength is in the right direction but in other respect the processes are distinct.

2.2.5.5 Matrix Microstructure

The microstructure of Zr-2.5%Nb consists of a matrix of α-Zirconium grains surrounded by a continuous grain boundary film of β-zirconium, the latter is a BCC phase containing approximately 20% niobium. The diffusion coefficient for hydrogen (D_H) in β-Zirconium is nearly two orders of magnitudes higher than that in α-Zirconium at temperature near 100°C. The average crack velocity of heat-treated specimens, whose β-phase decomposed into individual precipitates, is about five times lower than that of "as-manufactured" specimen, which has continuous β-phase layers. This change in cracking velocity is the result of the microstructure changes, which alter the diffusion rate of hydrogen and decrease the strength [41].

That the precipitation of hydride platelets in Zr-2.5%Nb alloy is also dependent on the microstructure of alloys is the main topic of the Perovic and Weatherly paper [42]. Since formation of hydride begins with nucleation, the nucleation behavior of hydrides must be considered in light of the difficulties of accommodating the volume and shear strains associated with precipitation. A second consideration is the non-uniform distribution of hydrogen in solid solution before precipitation. As hydrogen dissolves in solid solution, it dilates the zirconium lattice, thus it will be attracted to any defect or interface where the dilation can be partially or wholly accommodated. In other words, the nucleation behaviour is determined by the site in the microstructure where the most effective relief of the strain associated with precipitation can be achieved.

The microstructure of Zr-Nb alloys is sensitive to heat treatment. The β_{Zr} phase, for example, is unstable and can decompose according to the reactions:

$$\beta_{Zr} \rightarrow \omega + \beta_r \qquad \text{(at temperatures} < 450^{\circ}\text{C)} \quad (2.22)$$

or, $$\beta_{Zr} \rightarrow \alpha + \beta_{Nb} + \beta_r \rightarrow \alpha + \beta_{Nb} \qquad \text{(at temperatures} > 450^{\circ}\text{C)} \quad (2.23)$$

Since heat treatments will change the α-β structure, it will, in turn, affect the precipitation of the hydride [42]. From this fact, it is clear that to understand DHC behavior of a given specimen its thermal history has to be known. The fabrication procedures for *CANDU-PHW* pressure tubes, from which our specimens come, have been reported by Cheadle *et al.* [22]. The susceptibility of a pressure tube to DHC depends, at least partly, on the parameters used in the tube manufacturing process. For example the step of stress relief at 400°C [22] could cause β-phase decomposition, which inevitably influences the crack velocity since it changes the diffusion rate of hydrogen.

2.2.6 The DHC Behavior of Zr-2.5%Nb

Since the occurrence of DHC is the consequence of three distinct yet inter-related processes: hydrogen diffusion, hydride formation and hydride cracking, there are a number of prerequisites which have to be satisfied before these processes can take place. These basic necessities for DHC are reflected in the following experimentally observed behaviors. It is based on this experimentally observed DHC behavior that various theories have been developed with the purpose of understanding the mechanism of the process. So far, the suggested explanations of the observed DHC behavior range from being "successful" to being "acceptable" to being "ambiguous". The difficulties in fully understanding DHC mechanism come partially from the high complexity of the process, but partially also from the lack of precise experimental measurements. The best example for the importance of experimental results is about the crack tip hydride morphology. Although its importance is well recognized, very little systematical experimental work has been carried out to actually examine the crack tip hydrides. The lack of a precise description of crack tip hydrides forced people to build up theoretical model based on the assumption of crack tip hydrides being through-thickness and single-pieced, which, of course, can not give satisfactory explanation to DHC behavior. In this section, some of the DHC behavior, especially that to which the topic of this work is closely related, will be presented.

2.2.6.1 Temperature Related Behavior

As introduced in the previous sections, temperature has a profound and multifold effect on DHC behavior. Experimentally observed temperature related DHC behavior include

- temperature dependence of crack velocity,
- temperature variation (thermal cycling) effect on DHC behavior,
- existence of a T_{DAT} (Direction of Approaching Temperature), and
- existence of a T_{CAT} (Cracking Arrest Temperature).

All this temperature related behavior will be introduced here in this section except for the existence of a T_{CAT} which will be discussed separately in section 2.2.6.5 simply because T_{CAT} is the topic of this work.

2.2.6.1.1 Temperature Dependence of Cracking Velocity

The temperature dependence of DHC velocity (DHCV) has been studied intensively by many researchers [8, 41, 43-45]. There are two temperature-related parameters which affect DHCV. The first one is the test temperature at which DHCV is measured. The second parameter is the peak temperature prior to reaching a test temperature in the cases when there is sufficient hydrogen to reach the dissolution solvus at the peak temperature.

For a specimen with a certain amount of hydrogen, depending on the temperature at which DHCV is measured, different results will be obtained. According to Simpson, for instance, DHC velocities can be calculated by using [45]

$$\text{DHCV (m/sec)} = 6.86\text{x}10^{-1} \exp(-71500/RT) \qquad (2.24)$$

where T is the test temperature in Kelvin and R is the gas constant. This assumes that the test temperature is approached from at least 50°C above.

The peak temperature also affects the DHCV since it dictates the amount of diffusible hydrogen at a test temperature under the condition that the matrix hydrogen is sufficient. A peak temperature refers to the highest temperature reached prior to a specimen reaching a test temperature. When a test temperature is approached from above, i.e. by cooling from a temperature higher than the test temperature, a higher level of diffusible hydrogen can be reached in the specimen because more matrix hydride will be dissolved during heating, provided enough matrix hydrides are present in the specimen. When the difference between the peak temperature and test temperature is large enough, a saturation condition for the diffusible hydrogen can be created at the test temperature, which promotes easier hydride formation. The observed DHCV under a given condition is the consequence of a combination of peak and test temperatures. Up to the limit where hydrogen in solution at the peak temperature equals to the precipitation solvus at the test temperature (about 60K), the larger the difference between peak temperature and test temperature is, the faster hydrides can precipitate due to the increased amount of the diffusible hydrogen available at the test temperature. For a fixed peak temperature, lowering the test temperature will increase the difference between the peak and the test temperature. But at the same time, lowering test temperatures makes the hydrogen diffusion rate decrease which slows down the process. A higher test temperature results in higher diffusion rate but the driving force will diminish when the peak temperature and test temperature get too close to each other. Obviously, the maximum DHCV can only be obtained by having an optimum combination of peak temperature and test temperatures. For any given peak temperature, there is one test temperature, $T_{DHCVMAX}$, at which DHCV reaches its maximum value. Below this $T_{DHCVMAX}$ DHCV decreases with decreasing test temperature due to decreased hydrogen diffusion rates. Above this $T_{DHCVMAX}$, further increase in test temperature makes DHCV drop, eventually reaching zero when the test temperature and peak temperature are too close to each other. The rapid drop in DHCV after the $T_{DHCVMAX}$ is surpassed has to do with the decreased supply of diffusible hydrogen associated with increasing test temperature. The equation 2.24 is valid only for the temperature range in which DHCV increases with increasing test temperature as explained in 2.2.6.1.3.

2.2.6.1.2 Temperature Variation (Thermal Cycling) Effect on DHC Behavior

Besides test temperature and peak temperature, temperature variation also affects DHC behaviour. This effect of temperature variation, or thermal cycling between two different temperatures, comes from the fact that temperature variations influence the local hydrogen. According to Eadie *et al.*, every temperature variation or thermal cycling "pumps" more hydrogen into the highly stressed regions such as crack tips and this "pumping" effect is termed the "ratchetting effect" [46].

There are altogether three different types of ratchetting: pure ratchetting, cooldown ratchetting and hydride formation ratchetting and all of these three types of ratchetting can be understood by going through the following example. Assuming a notched specimen with 60 µg/g of hydrogen is loaded under tension and thermally cycled between room temperature (25°C), 295°C and 250°C. The 25°C is the start point of the thermal cycle, the 295°C is the peak temperature and the 250°C is the test temperature. Simple calculations will show how the regional hydrogen level will be affected by simply thermally cycling the specimen between these three temperatures. For a specimen with uniform hydrogen level of 60 μg/g, when it is heated to 295°C, it has a diffusible hydrogen level of 52.4 μg/g which is the dissolution solvus at a temperature of 295°C. When cooled to 250°C from 295°C, the specimen will still have a diffusible hydrogen level of 52.4 μg/g because a minimum of 65.6 μg/g is required to form any hydride at 250°C. The diffusible hydrogen level is, however, not everywhere the same throughout the whole specimen but higher at notch tips due to the stress concentration effect mentioned in section 2.2.4.1. With a stress concentration at the notch tip sufficient to cause an increase in hydrogen level by a factor of 1.3, the local diffusible hydrogen level can be as high as 65 μg/g at notch tips, just slightly lower than the precipitation solvus of 65.6 μg/g for 250°C. Upon cooling this specimen to room temperature, all the hydrogen contained in the specimen will transform to hydride but slightly more hydride will form at the notch tip region since the hydrogen level was higher at the location. That is, as the consequence of one thermal cycling, the total hydrogen level at the notch tips has increased from 60 μg/g to 65 μg/g. When the specimen is re-heated to 295°C at the beginning of the second thermal cycle, 52.4 μg/g of hydrogen goes into solution and 12.6 μg/g hydrogen stays as undissolved hydride because 65 μg/g minus 52.4 μg/g gives 12.6 μg/g. Despite this increased local total hydrogen level, the stress concentration still needs to be balanced by increasing local diffusible hydrogen to be 65.6 μg/g at the notch tip to reach local equilibrium. When the specimen is quenched to room temperature at the end of second thermal cycle and reheated to 295°C for the third time, the total hydrogen level at the notch tip will be about 77 μg/g. In this manner, the ratchetting effect of thermal cycling keeps increasing the hydrogen level at the notch tips, as indicated in Figure 2-13a. In a thermal cycle, the hydrogen accumulation occurs throughout the whole process. The "ratchetting" at constant temperature is called "pure ratchetting" while the hydrogen accumulation during cooldown is termed as "cooldown ratchetting". For a thermal cycle with a instantaneous cooling, the accumulation during cooling can be ignored and only the pure ratchetting needs to be considered. More realistically, however, because the cooling will never be instantaneous, the process is actually a combination of pure ratchetting and cooldown ratchetting. The driving force for cooldown ratchetting is the same as the one for pure ratchetting: the hydrogen level at the notch tip has to be always 1.3 times higher. The slower the cooling rate, the longer the cooling lasts, the more hydrogen will be accumulated during this period of time. By reducing the cooling rate from "very rapid" to 1 K/min., the additional increase in hydrogen during the cooldown becomes noticeable. If the cooling rate is further decreased to 0.5 K/min., the cooldown ratchetting is even more effective as shown by Figures 2-13b) & c).

The third type of ratchetting, known as "hydride formation ratchetting", is associated with the highest temperature reached in thermal cycling (i.e. the peak temperature). Consider a similar thermal cycle as previously discussed with only the peak temperatures changed from 295°C to 300°C. The increased peak temperature will cause the hydrogen concentration at the notch tips to increase, as shown in Figure 2-13b). Since hydride forms before the "equilibrium" hydrogen concentration can be reached, the hydrogen keeps migrating into notch tips forming hydrides during the entire hold at 250°C and the local hydrogen concentration can reach as high as 3000 μg/g, instead of being only 240 μg/g, see Figure 2-13b). This drastic change is caused by the formation of hydride. Under this circumstance local equilibrium will not be achieved until pure hydride is formed, which needs about 16000 μg/g, causing hydrogen to keep pouring into the highly stressed regions. Among these three ratchetting effects, the most significant one is the hydride formation ratchet, followed by the cooldown ratchet and then by the pure ratchet [46].

2.2.6.1.3 Existence of a T_{DAT} (Direction of Approaching Temperature)

The relationship presented by equation 2.24 in section 2.2.6.1.1 is only valid when the test temperature is approached from above. As mentioned earlier, the rate of hydride cracking is affected by the degree of hydrogen "supersaturation". When a test temperature is approached from above, i.e. by cooling, a "supersaturation" is created. Under this condition, the DHCV shows an Arrhenius dependence on test temperature. When a test temperature is approached from below, i.e. by heating, on the other hand, no hydrogen "supersaturation" is created and cracking either progresses at much lower rates or even stops entirely. This dependence of cracking activity on the direction of approaching test temperature was first reported by Ambler [45]. The temperature, termed T_{DAT} (Direction of Approach to Temperature), above which this effect of approaching direction occurs, is normally about 150°C. At temperatures above $T_{DAT,}$ difficulty in starting cracking has been reported unless the temperature is approached from above. For the cases where the temperature is approached from below, the crack velocity is much lower and less predictable. Clearly indicated by this phenomenon is the importance of diffusible hydrogen level in the DHC process. The amount of diffusible hydrogen has to be large enough to overcome the elastic and plastic deformation associated with hydride formation. Although it has been used for designing a reactor shutdown maneuver, a full understanding of the T_{DAT} still needs to be achieved.

2.2.6.2 Loading Related Behaviors (Existence of a K_{IH})

Loading condition is another important factor in DHC process. There is a minimum stress intensity factor value below which DHC will simply not occur. This threshold value for stress intensity factor in DHC process is termed as K_{IH} was discussed in 2.2.5.2, which is a measure of the material's susceptibility to DHC. The lower the K_{IH} value is, the more susceptible this material is to DHC. Two characteristics of K_{IH} are interesting enough to be mentioned here. The first one is that, although DHC is caused by fracture of crack tip hydride platelets, the experimentally measured K_{IH} is significantly higher than the fracture toughness of zirconium hydride, with the latter being about 2 MPa√m [26] and the former approximately 6 MPa√m [38]. This discrepancy between the stress intensity factors indicates involvement of the matrix in the fracture process, which has been confirmed by fractographic studies, see section 2.2.6.4 for more discussion. The other interesting observation about K_{IH} is its dependence on temperature. Although it used to be considered temperature independent, K_{IH} is now believed to be a function of test temperature [47]. Analysis of all the test results on K_{IH} show an increased K_{IH} at higher temperature. This temperature dependence of K_{IH} clearly suggests the condition for DHC to occur is a combined consequence of temperature and loading conditions. Shek and Seahra have reported a K_{IH}-dependence on hydrogen "supersaturation". Their results show that K_{IH} values increase with decrease in hydrogen "supersaturation" at 230-250°C [48]. Hydrogen "supersaturation" is the amount of hydrogen in solution in excess of TSSd (dissolution) concentration, which is controlled by the difference between the peak temperature and the test temperature. Shek and Seahra believe that this observed effect of hydrogen "supersaturation" on K_{IH} can be explained with the interaction of radial hydride growth and crack tip stress discussed in 2.2.4.2.

2.2.6.3 Time Related Behavior (Existence of an Incubation Time)

The characteristic delay between establishing the conditions for DHC and initiation of cracking is called the incubation time. Early studies on incubation times, such as the work from Coleman and Ambler, have shown a dependence of incubation time on test temperature and loading conditions [20, 38, 55]. Recent studies by Shalabi and Meneley have confirmed Coleman and Ambler's observations of:

- shorter incubation time with higher test temperature, and
- longer incubation time at lower applied stress intensity factors and when the test temperature has been approached by heating rather than by cooling [21, 49].

Considering incubation time as a direct indication of the ease with which DHC initiates, one can see the importance of the three factors - loading condition, test temperature and direction of approaching test temperature - on the length of incubation time. As mentioned in the previous sections, these three factors also play important roles in DHCV. This similarity, however, should not conceal the difference between the studies of DHCV and incubation time, the former being about the crack propagation while the latter the crack initiation. Compared with crack propagation, crack initiation requires higher driving force to overcome the "inertia". Experimental results indicate that the stress intensity factors required to start a crack are higher than the stress intensity factors needed to keep the crack growing. Cracking tests also show that incubation exists only prior to the very first crack "jump" when a cracking process starts but not prior to the "jumps" after the first cracking advance event. The word "jump" here refers to any individual crack progress step in intermittent DHC propagation. Each of these progress steps consists of hydrogen diffusion, hydride formation and their fracture. The very first "jump" for the crack front is definitely different from all the following "jumps" in that this first one is the initiation of the crack while the following "jumps" are crack propagation. A certain combination of stress intensity factor, test temperature and "supersaturation" can keep cracking progressing but may not be good enough to cause a cracking process to start. All the cracking initiation studies are efforts trying to understand under what kind of condition(s) cracking can initiate and the study of incubation time under various conditions should provide valuable hints.

2.2.6.4 Existence of Fracture Surface Striations

The intermittent nature of DHC propagation has been mentioned several times in the previous sections. One more experimental observation which supports the conclusion that DHC is an intermittent process is the existence of fracture surfaces striation. When inspected by the unaided eye, DHC fracture surfaces appear to be flat, indicating the fracture is brittle in nature. When examined under a Scanning Electron Microscope (SEM) however, narrow bands of ductile tearing can be observed between cleavage fractured regions. These bands are normally oriented perpendicular to the direction of crack propagation and are termed "striations" [7-8]. In addition to indicating the intermittent nature of DHC, the presence of the alternate brittle and ductile fractured regions is also a direct indication of matrix involvement in the DHC process, which agrees with the experimentally observed discrepancy between the measured K_{IH} and the K_{IH} of hydrides. It is believed that the cleavage fractured regions are the fractured hydrides and the ductile regions torn during fracture process are the matrix materials [32]. The existence of striations can, at least qualitatively, explain the discrepancy between the measured K_{IH} and the K_{IH} of hydrides as mentioned in section 2.2.3.3. Furthermore, since striations are caused by crack tip hydride fracture, the size and pattern of these striations left on the fractured surfaces should be the direct traces of the fractured crack tip hydrides. It has been reasoned that the distance between striations, or the "striation spacing", represents the critical length for the crack tip hydrides to fracture. Experimentally, it has been found that striation spacing increases when the test temperature increases and when the applied K_I approaches K_{IH}. These two observations seem to be in agreement with the observed relationship that fracture initiation becomes more difficult when the test temperature increases and when the applied K_{IH} decreases.

2.2.6.5 Existence of a T_{CAT} (Cracking Arrest Temperature)

Compared with all the phenomena discussed earlier, the existence of a T_{CAT} is the least explored one. The existence of a T_{CAT} has been reported for the first time in 1988 by Smith and Eadie [6]. As a matter of fact, Smith and Eadie's paper is the only literature which deals directly with this phenomenon. Figure 2-14 illustrates this cracking arrest phenomenon based on the acoustic emission rate, as well as the thermal cycles necessary to obtain cracking [6].

At lower temperatures, acoustic emission rates, which are directly proportional to cracking velocities, increase steadily when the temperature goes up. But above a certain point, the acoustic emission rate will drop to zero if the temperature is further increased. This cracking cessation occurs despite the presence of ample hydrogen. It has also been found that cracking will sometimes recommence with little delay if the temperature is lowered back to a temperature below T_{CAT} at which cracking had previously been documented. The value of T_{CAT} has been determined to be in the range of 320°C for specimens with about 110 μg/g hydrogen under K_I equaling 17 MPa√m. The mechanism of T_{CAT} is unknown.

2.3 Cracking Monitoring Techniques

Measurement of fracture behavior is important in studying all cracking phenomenon including DHC. As a matter of fact, it is based on the experimentally observed intermittent crack advance, the DHC process in Zr-2.5%Nb alloy is recognized as a series of repeated fracture events and, therefore, is intermittent in nature [20, 43, 51-53]. The crack measuring techniques can be divided into two groups: cracking initiation detection and cracking advance monitoring. Having an appropriate cracking detection and monitoring capability is crucial for this work since this work deals with both fracture initiation and propagation and is experimental in nature. Without reliable, qualitative and quantitative fracture measurements, no study on cracking cessation can be carried out. The techniques used in this work are acoustic emission (AE) and potential drop (PD).

Among all the measurement techniques used in cracking process monitoring, acoustic emission (AE) and potential drop (PD) are the two most widely used [54-55]. Acoustic emission occurs as the result of the release of elastic strain energy which accompanies fracture, therefore the AE technique can be used in crack phenomena study. An acoustic emission measuring apparatus consists of an acoustic piezoelectric transducer which translates the minute mechanical vibrations caused by cracking activities into electrical signals which can be recorded. AE tests can be carried out either qualitatively or quantitatively. Crack initiation detection is a typical example of qualitative AE measurement while cracking velocity measurement requires quantitative AE evaluation capabilities. Of qualitative and quantitative AE measurements, the later is less reliable due to the complex nature of AE and the limited understanding of the details about AE signal generation and propagation [56-61]. The large spread of AE data which causes difficulties in quantitative crack advance evaluation is also due to the dependence of AE signals on the measuring conditions such as the property and shape of the objects being studied, the threshold value selected, the type of transducer used, the position of the transducer and its distance to AE sources, etc. Although a tendency towards more AE counts per unit area fractured at higher temperature exists, the values of AE counts per unit crack extension change from specimen to specimen and a reliable description of the relationship between temperature and AE counts per unit crack extension is lacking.

Compared with AE, PD brings more reliable results in monitoring crack advance, at least when the test temperatures are constant [62-66]. In order to measure the PD, a constant electrical current is applied across the sample and the microvolt variation is recorded. Under conditions of changing temperatures, crack measurement using PD becomes more complicated because of the interfering effect of temperature. Variation of temperature affects the resistivity, $\rho(T)$, of the specimen's material which, in turn, brings changes in electrical potential not caused by crack length. The measured potential value is therefore not just a function of the crack growth, but depends on the crack growth and temperature changes.

From the above discussion it is implied that AE is good in crack initiation detection but not reliable in quantitative crack advance evaluation. PD, on the other hand, is better in cracking advance monitoring but only when the test temperature variation is minimum. PD performs also less satisfactorily in crack initiation detection. To meet the requirement of this work, AE and PD are used in combination with each other to make use of their advantages and minimize their inherent disadvantages. A detailed description of using AE and PD jointly in crack advance evaluation is given in a published paper by Lin *et al.* [67].

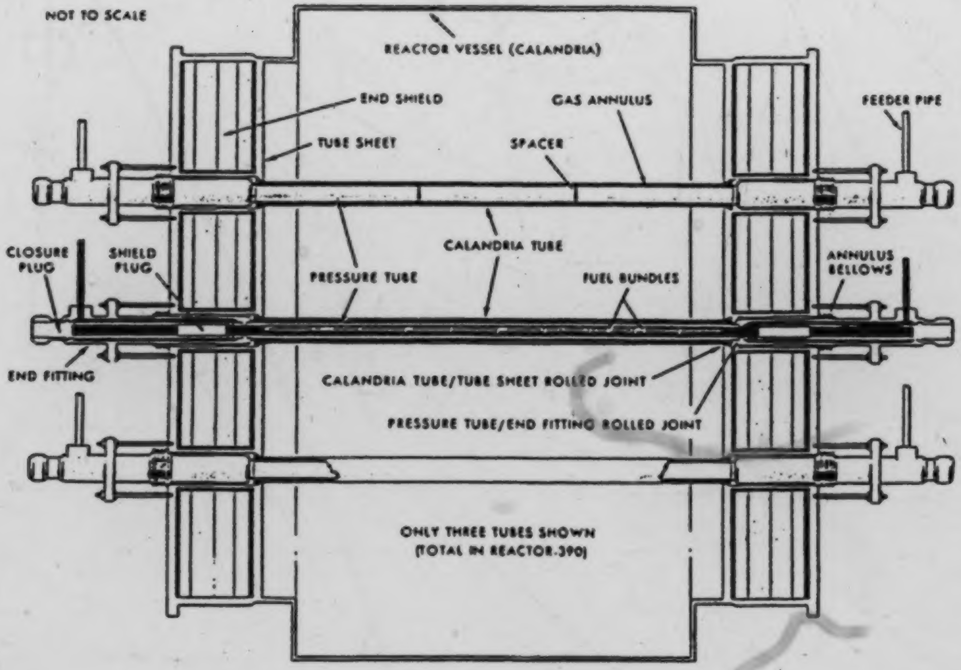
NOT TO SCALE
REACTOR VESSEL (CALANDRIA)
END SHIELD
GAS ANNULUS
FEEDER PIPE
TUBE SHEET
SPACER
CLOSURE PLUG
SHIELD PLUG
CALANDRIA TUBE
ANNULUS BELLOWS
PRESSURE TUBE
FUEL BUNDLES
END FITTING
CALANDRIA TUBE/TUBE SHEET ROLLED JOINT
PRESSURE TUBE/END FITTING ROLLED JOINT
ONLY THREE TUBES SHOWN
(TOTAL IN REACTOR-390)

Figure 2-1 Simplified diagram of a *CANDU* reactor [9]

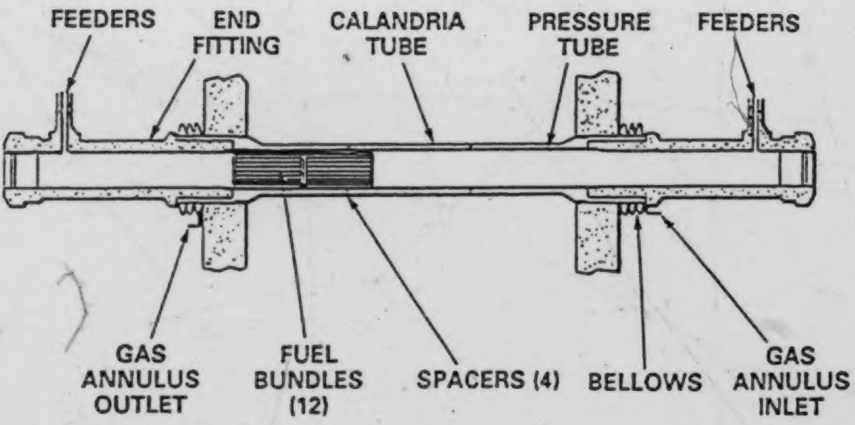
FEEDERS
END FITTING
CALANDRIA TUBE
PRESSURE TUBE
FEEDERS
GAS ANNULUS OUTLET
FUEL BUNDLES (12)
SPACERS (4)
BELLOWS
GAS ANNULUS INLET

Figure 2-2 Simplified diagram of a *CANDU* reactor fuel channel [9]

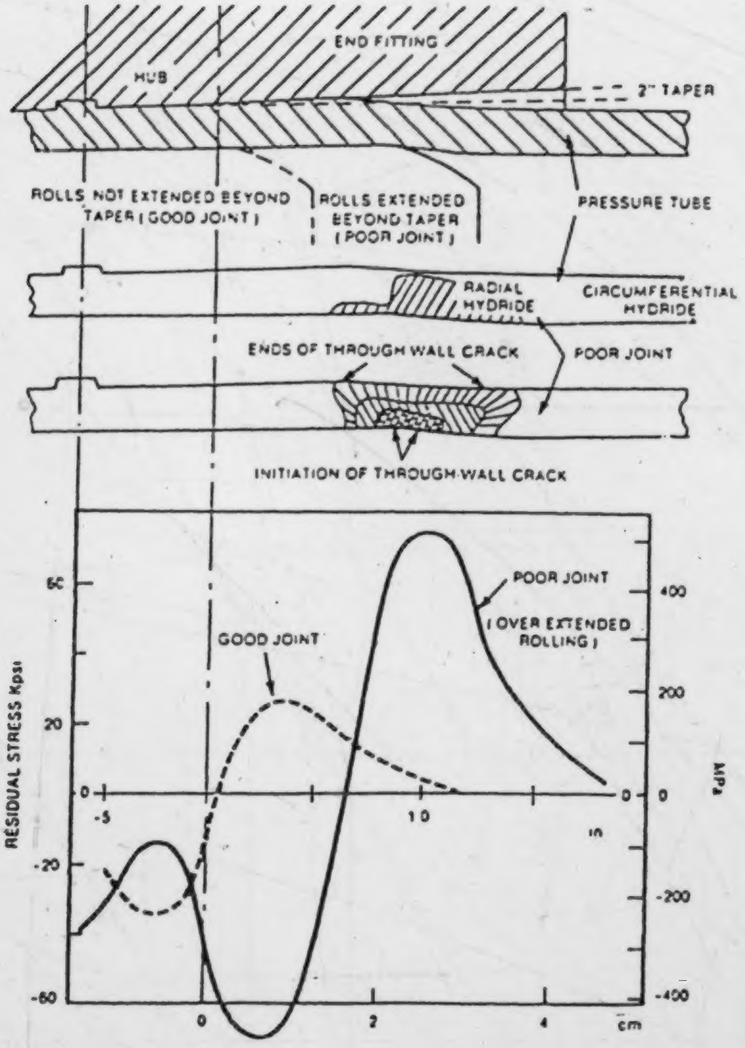
END FITTING
HUB
2" TAPER
ROLLS NOT EXTENDED BEYOND TAPER (GOOD JOINT)
ROLLS EXTENDED BEYOND TAPER (POOR JOINT)
PRESSURE TUBE
RADIAL HYDRIDE
CIRCUMFERENTIAL HYDRIDE
ENDS OF THROUGH WALL CRACK
POOR JOINT
INITIATION OF THROUGH-WALL CRACK
RESIDUAL STRESS Kpsi
MPa
POOR JOINT (OVER EXTENDED ROLLING)
GOOD JOINT
60
20
0
-20
-60
400
200
0
-200
-400
-.5
0
1.0
in
0
2
4
cm

Figure 2-3 Effect of roll extension on the residual circumferential stresses in the pressure tube at a rolled joint [16]

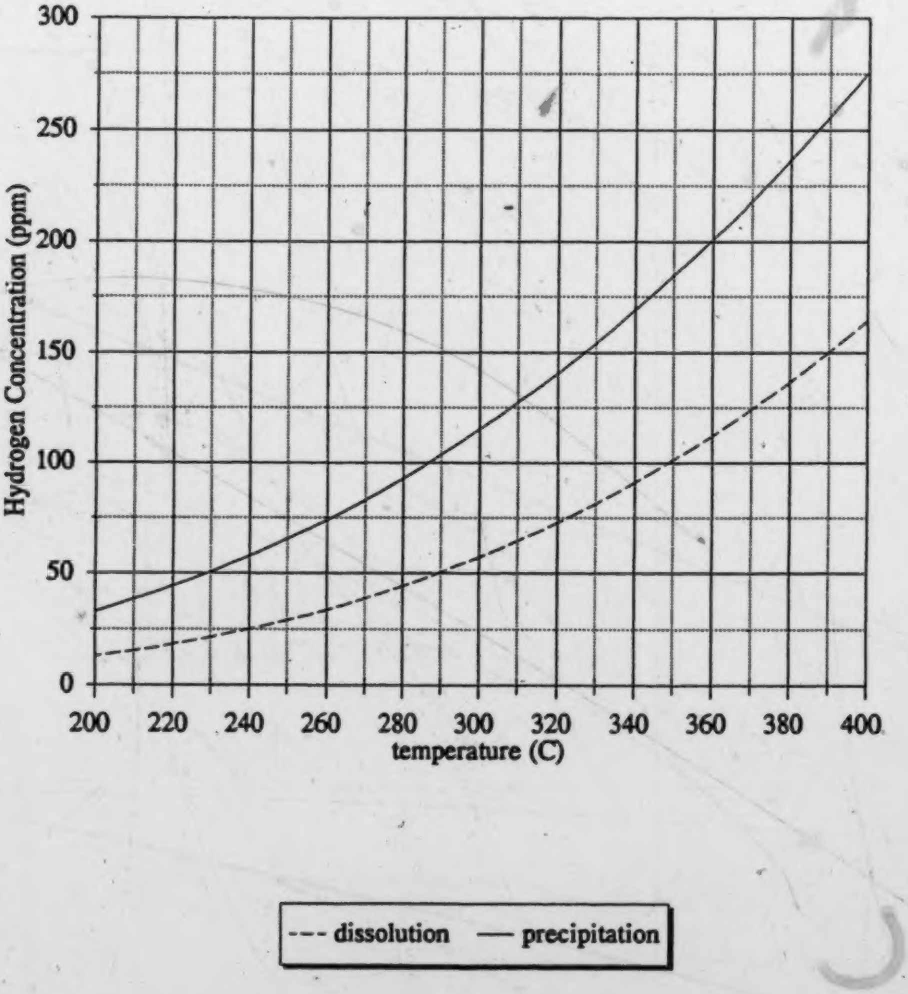

Figure 2-4 Hydrogen solubility curves for precipitation and dissolution

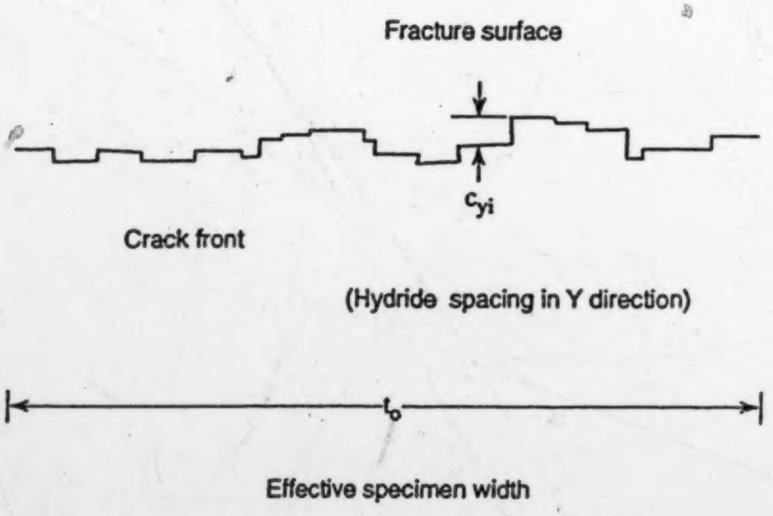
Fracture surface
c_{yi}
Crack front
(Hydride spacing in Y direction)
t_o
Effective specimen width

Figure 2-5 Cross-section of fracture surface [30]

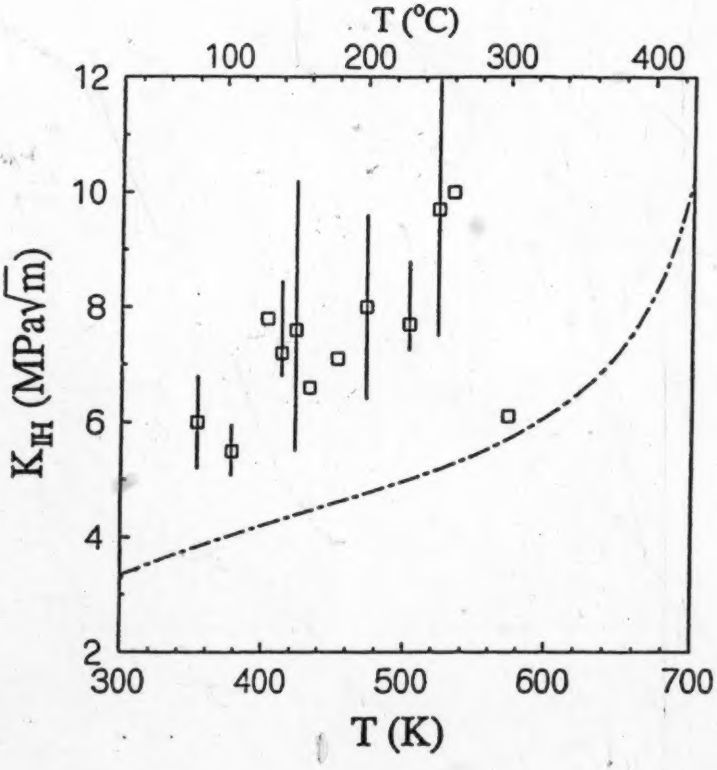

Figure 2-6 Comparison of theoretical K_{IH} with experimental data [31]

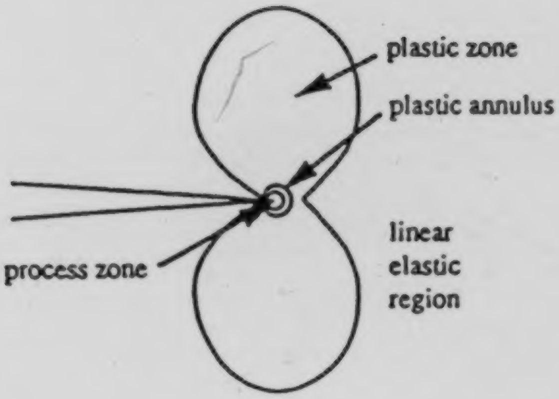
plastic zone
plastic annulus
linear
elastic
region
process zone

Figure 2-7 Stress zones near crack tip [23]

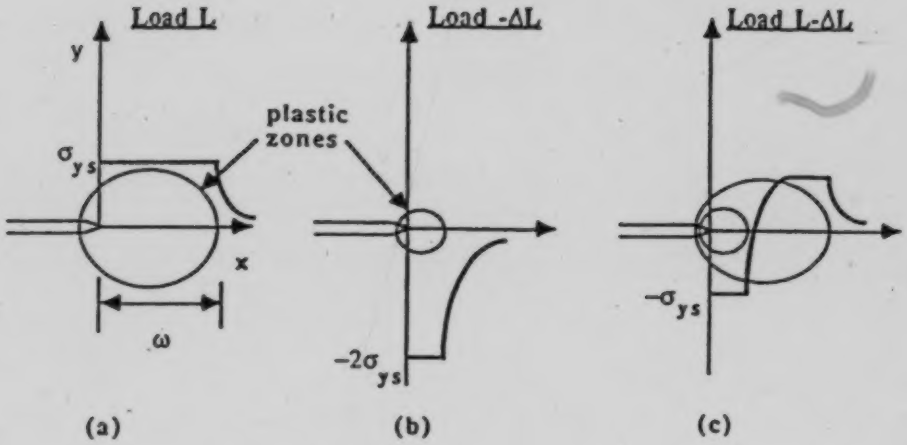
Load L
y
σ_{ys}
x
ω
(a)
Load -ΔL
plastic zones
$-2\sigma_{ys}$
(b)
Load L-ΔL
$-\sigma_{ys}$
(c)

Figure 2-8 Crack tip stress distribution [34]

a) Stresses for the applied Load L

b) Stresses for the reversed Load ΔL

c) Stresses for superposition

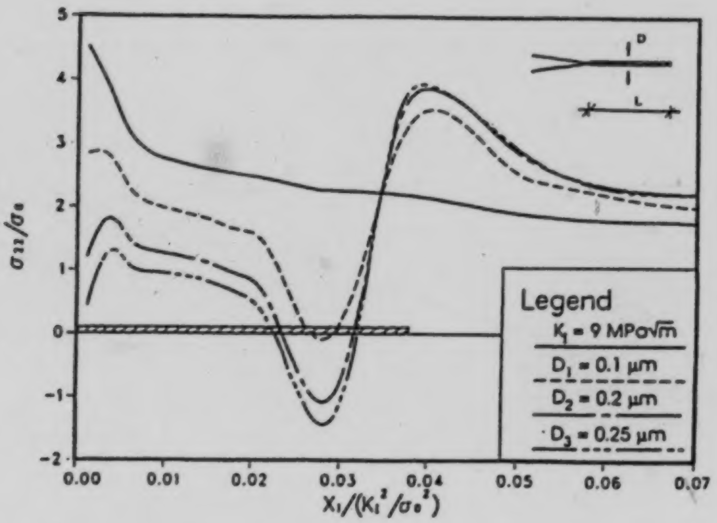

Figure 2-9 Distribution of stress component normal to the crack plane due to hydride expansion (Length of hydride platelet L=10μm, X_1=0 denotes the crack tip.) [36]

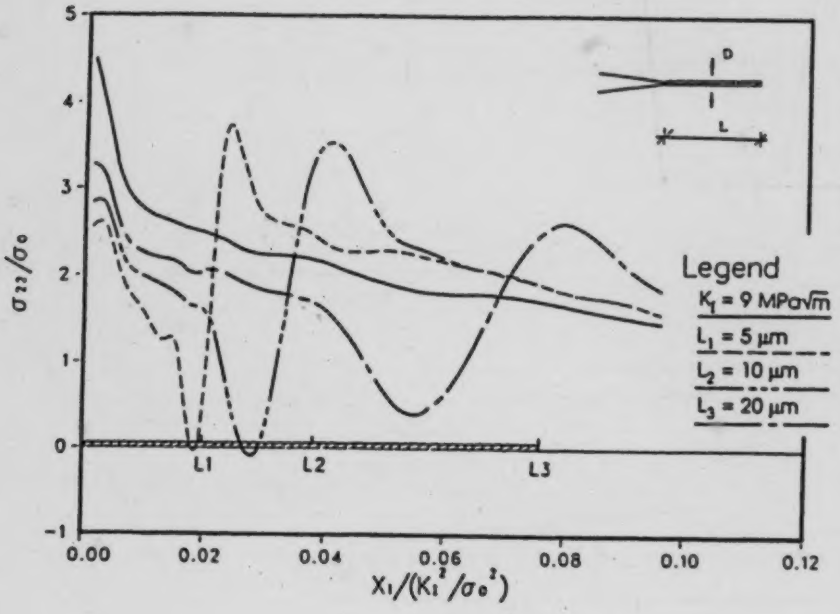

Figure 2-10 Effect of different hydride length on the normal stress distribution (Expansion of hydride platelet D=0.1μm for all three cases.) [36]

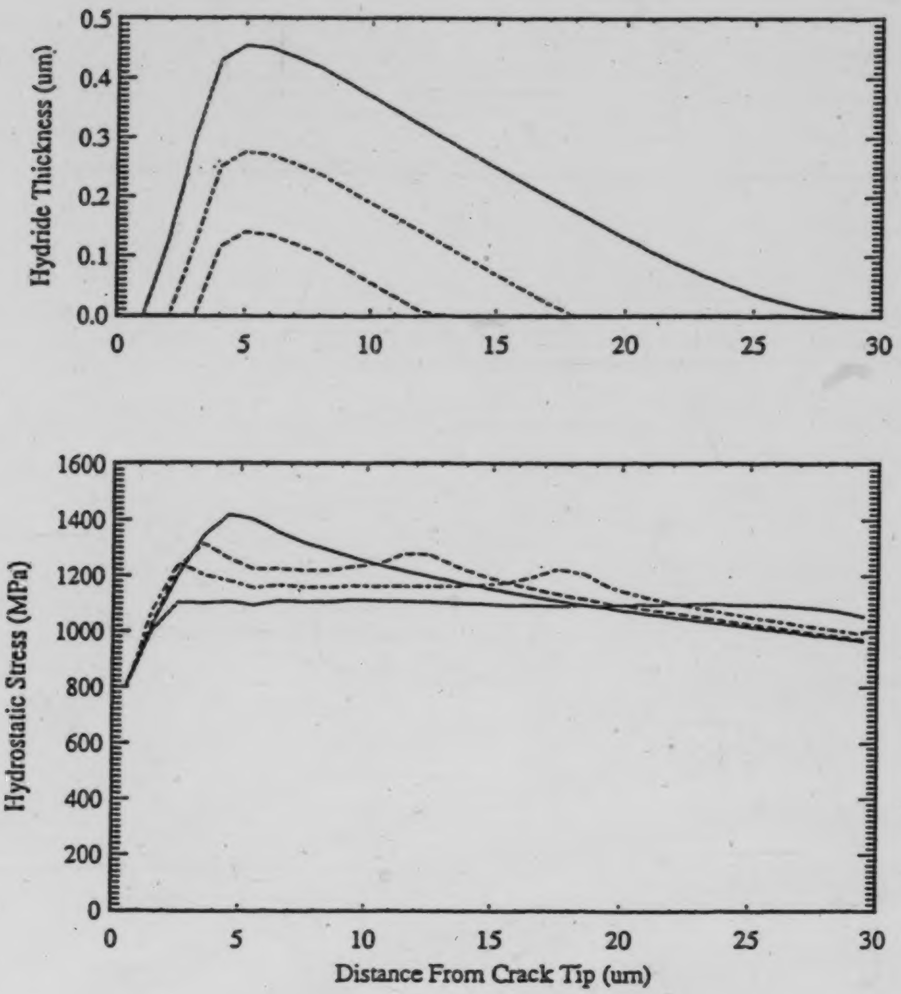

Figure 2-11 Hydride shape distribution based on hydrostatic stress criterion [37]

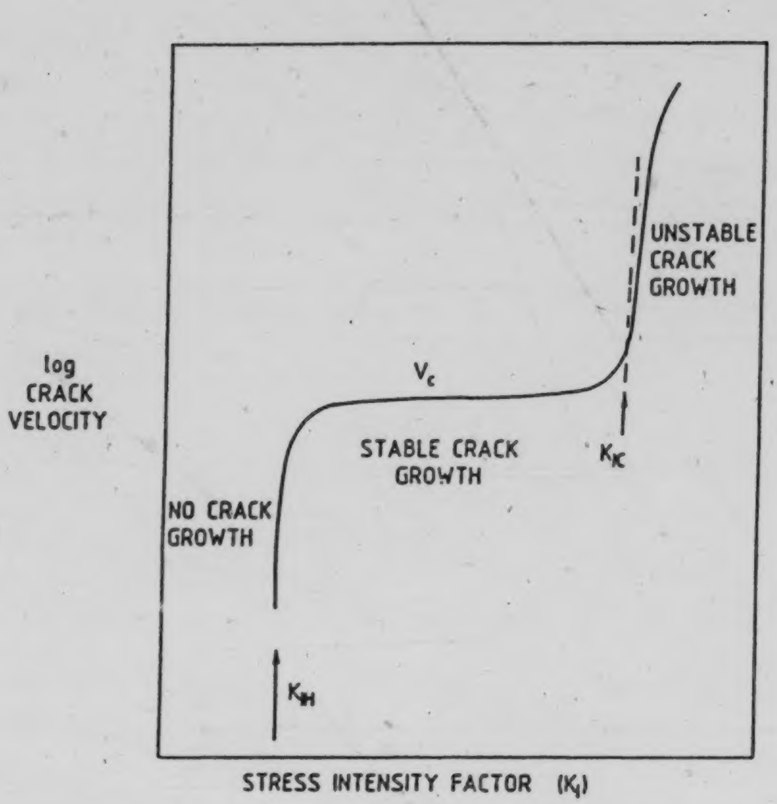

Figure 2-12 Schematic diagram of the dependence of Delayed Hydride Cracking Velocity (DHCV) on stress intensity factor [38]

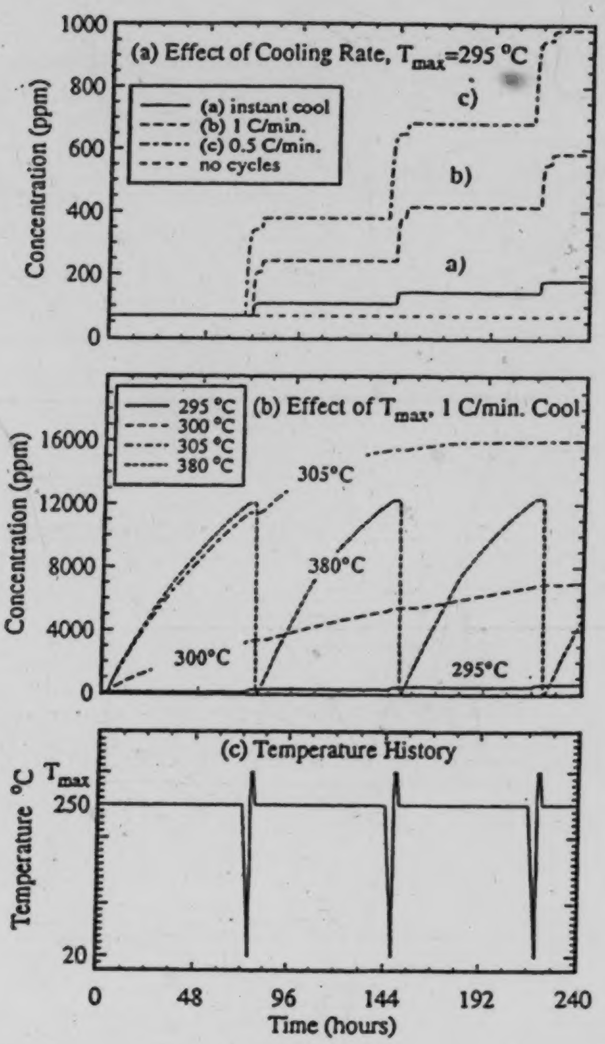

Figure 2-13 The effect of cooling rate and maximum temperature on the total hydrogen level, $C_{H(tot)}$, at the peak stress location during temperature cycles of a Zr-2.5%Nb specimen containing 60 µg/g hydrogen and a notch of depth 0.8 mm and tip radius of 0.2 mm under net section stress 300 MPa [46]

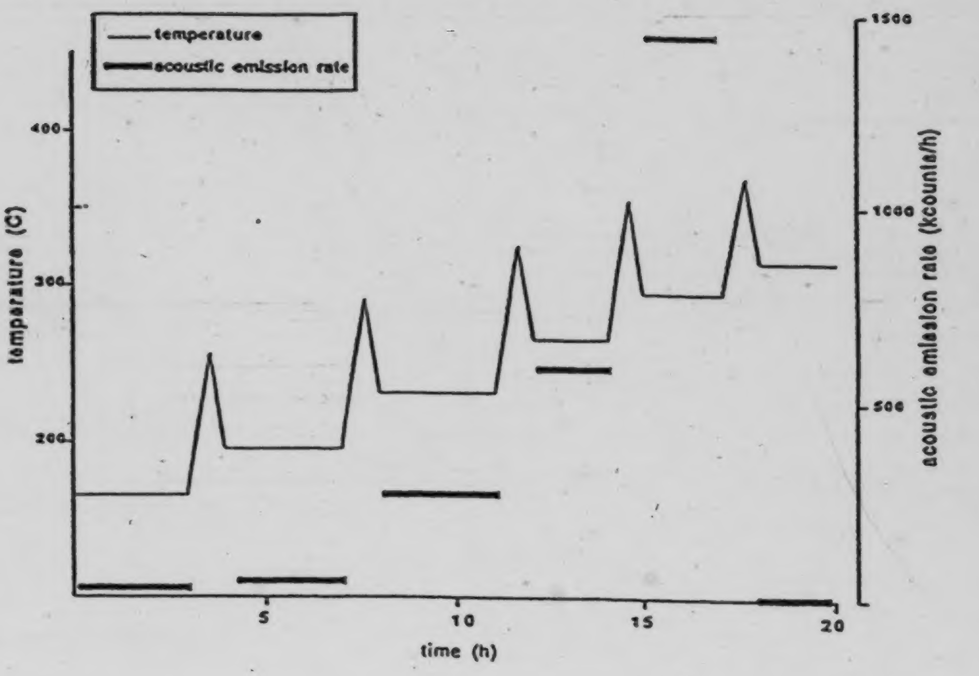

Figure 2-14 Temperature profile and acoustic emission rate indicating T_{CAT} [6]

Chapter 3 Experimental

3.1 Testing Material and Specimen Preparation

In order to make the results directly applicable to operating reactors, all the specimens used in this study were prepared from Zr-2.5%Nb pressure tubes manufactured for use in *CANDU-PHW* (**CAN**ada **D**euterium **U**ranium-**P**ressurized **H**eavy **W**ater) nuclear reactors. A typical pressure tube is 6.1 meters (20 feet) in length, 103 millimeters (4.07 inches) in diameter and 4 millimeters (0.160 inch) in wall-thickness [22]. Figure 3-1 shows all the steps the specimens have experienced prior to the cracking tests and Figure 3-2 schematically highlights the steps performed in this lab. As is shown in Figure 3-2, pieces cut from pressure tubes were flattened by reverse bending. There was no thickness change for the sections of pressure tube which were flattened by reverse bending and this condition was termed as "as-manufactured". Some of the flattened sections were then additionally cold rolled in the axial direction to simulate the increase in strength caused by irradiation hardening during service. This cold-rolled condition was termed as "additionally cold-worked". The amounts of additional cold working ranged from 10% to 60%, according to their thickness reductions. All the additionally cold worked specimens were stress relieved at 325°C for 24 hours.

The specimens were then electrolytically hydrided to have a hydride layer formed on their surfaces. The hydriding process took place inside a beaker containing 5%

H_2SO_4 solution with the specimens being cathodes (electric positive) [68]. The current intensity was about 100-150 mA/cm^2. The hydriding temperature was approximately 90°C and a typical hydriding process lasted about 24 hours.

The specimen hydriding was followed by a diffusion anneal to allow hydrogen to diffuse into the specimens. The temperature of annealing was decided by the hydrogen level required, being 400°C for 160 μg/g for instance. The time needed for sufficient hydrogen diffusion could be estimated by using the equation

$$x = (D_H t)^{1/2} \qquad (3.1)$$

where D_H is the diffusion coefficient,
t is the diffusion time, and
x is the diffusion distance.

The actual diffusion time, t, used, however, was always much longer than the estimated value based on equation 3.1 to ensure a complete homogenization of hydrogen. The diffusion coefficient D_H was a function of the temperature and could be expressed as [24]:

$$D_H\,(\mathrm{m^2/s}) = 4.1\mathrm{X}10^{-7} \exp\{-4618.72/T(K)\} \qquad (3.2)$$

After having gone through the procedures mentioned above, the sections of pressure tube had enhanced hydrogen levels, enough to meet the requirements of cracking tests. The hydrogen levels reported were the expected value from diffusion annealing temperature. Some subsequent hydrogen analyses were performed to check the actual hydrogen content, see section 4.1.1 for the hydrogen analysis results. These hydrided pressure tubes were then cut into the shape of either compact toughness or tapered double cantilever beam (constant K) specimens using electrospark discharge machining (EDM). The dimensions of the two kinds of specimen are given in Figure 3-3. While the compact toughness specimens were mainly used for crack tip hydride morphology study, the constant K specimens were used for cracking velocity measurements because, within a certain range of crack length, the possible effect of changing stress intensity factor caused by the increasing crack length could be eliminated [69].

The last step of specimen preparation was fatigue pre-cracking on a Material Testing System (MTS), model 810. The purpose of the fatigue pre-cracking was to produce a uniformly deep crack with a sharp tip extending from the notch. To eliminate a possible effect of this fatigue pre-cracking on the following cracking tests, care was taken during the pre-cracking operations to avoid exceeding the values of stress intensity factor (K_I) applied later for cracking tests. For instance, for specimens prepared for cracking tests at $K = 17$ MPa√m, the stress intensity factor applied during pre-fatigue was usually less than 10 MPa√m when the pre-cracking finished.

3.2 Cracking Tests

The purpose of the cracking tests was to determine the T_{CAT} values under various conditions and to measure cracking velocities at selected test temperatures. For T_{CAT} studies, those specimens, which had been kept at T_{CAT} for more than 24 hours with no cracking observed were then metallographically analyzed looking particularly for crack tip hydrides and their morphology. Some of the surface of the cracked specimens was subsequently fractographically studied for fracture features such as striations.

The experimental rig used for the cracking tests is schematically shown in Figure 3-4. The rig consists of an insulated electric furnace, a programmable temperature controller, a loading system capable of carrying adjustable loads in order to vary the applied stress intensity factor and systems for crack monitoring through AE and PD measurements. All the data collected during the cracking tests were recorded and stored using a computer-based data acquisition system.

3.2.1 Loading Arrangement and Calculations of Applied Loads

The load was applied to the specimens by dead weight through a pin and clevis arrangement. The arm ratio of the loading side to the specimen side was ten to one. The calculations of the necessary loading to get a certain stress intensity factor were different for compact toughness specimens and tapered double cantilever beam (constant K) specimens.

For compact toughness specimens, the stress intensity factor applied changes with the crack advance. Other parameters affecting on the stress intensity factor include the specimen thickness, B, and w, which is 17 millimeters as shown in Figure 3-3. The relationship for the stress intensity factor, K_I, and other parameters is:

$$K_I = f(a/w) \times P/B \times \sqrt{w} \qquad (3.3)$$

with f(a/w) being a function of specimen's geometry and P being the applied load. Since a large number of compact toughness specimens have been used in this project, a *FORTRAN* program has been developed for calculating the actual applied K_I values based on the applied load and the crack length. The applied load has been re-adjusted before every cracking test to ensure the stress intensity factor applied is correct.

For constant K specimens, determinations of applied K_I values are simple because the applied stress intensity factors are independent of the crack length when the ratio of (a/W) is between 0.22 and 0.55. Since W is equal to 35 millimeters in our case, see Figure 3-3b, the stress intensity factor does not change as long as the crack length is between 7.7 millimeters and 19.25 millimeters. Within this range, the equation for K, in $MPa\sqrt{m}$, calculation is [69]:

$$K = 0.0581\ (P/B) \qquad (3.4)$$

where P is the applied load in Newton, and
B is the thickness of the specimen in millimeters.

The specimens used in the work are considered to be in the plane strain condition because the thickness of the specimens is larger than $2.5(K/\sigma_y)^2$.

3.2.2 Temperature Measurements and Control

Temperatures were measured by means of a Chromel-Alumel thermocouple (K-type). The thermocouple was welded to the specimen for accurate measurement. The readings of the thermocouple were calibrated by using a Wahl Thermocouple Calibration Standard C-65.

A temperature controller (Eurotherm) was programmed to give the desired temperature-time profiles. A typical temperature-time profile for cracking tests consisted of heating with a constant rate to a peak temperature, holding at the peak temperature for 1 hour, cooling with a constant rate to a test temperature and holding at the test temperature. The heating rate for all the tests was 5 K/min. and the cooling rates were mostly 2 K/min. The holding time at test temperatures was either 24 hours if no cracking was observed or up to the point when cracking started. With all its parameters correctly set, the temperature controller provided a satisfactory temperature profile and stopped overshooting and overcooling within 1 K.

3.2.3 Measurement of Potential Drop (PD)

The basic requirements for PD measurement are a source of constant electrical current and the means to measure microvolt changes in potential drop across the specimen. To minimize its heating effects, the electrical current went through the specimens not constantly but only when measurements were taken. The measurement system for PD consisted of four main components: a DC current power supplier (HP6263B), an I/O system to the computer (Mini-16), a MOSFET bridge-switch and a computer (IBM-PC/XT).

The power supply was set to provide a constant current of 8 A with a maximum voltage compliance of 5 V to prevent damage to the MOSFET bridge-switch in case of a malfunction. The current return leg of the measuring circuit had a 500 μΩ shunt resistor inserted into it to allow direct measurement of the applied current via a mV signal. This current reading was taken immediately before each set of specimen potential readings to compensate for any drift of the power supply output as well as to compensate for phase shift errors due to the power supply ripple frequency.

The 8 A measuring current was applied to the MOSFET bridge-switch which, under control of the computer program, switched the current through the test rig for the measuring intervals. Between measurements the MOSFET bridge-switch bypassed the circuit containing the specimen and allowed the current to continue to flow through half of the bridge with minimal interruption in order to increase the stability of the measuring current supply and reduce electrical heating effects in the test specimen.

The current was delivered to the specimens by heavy gauge copper wires connected to lugs machined from nickel and screwed to the specimen. Gold-coated surfaces were used to reduce the effect of oxidation between the machined contact and the specimen at elevated temperatures. The copper wires were silver-soldered to machined contacts. The potential measurement leads were alumel wires spot-welded to the specimen near the mouth of the crack. They were attached on opposite sides of the specimen above and below the crack, see Figure 3-5.

The procedure used to obtain a potential drop measurement was as follow:

- A clock interrupt, whose period had been specified during rig setup, e.g. every 5 minutes, started the testing process.
- The power supply output current was measured while the bridge-switch was still in the "bypass" mode by reading the voltage from the return leg current shunt.
- The bridge-switch was then directed to switch the measuring current through the specimen, first in the "normal" direction, see Figure 3-6.
- A delay of 50 ms was used to allow the current to settle after being switched.
- Altogether ten voltage readings were taken from the specimen at a 60-readings per second rate, only the six readings in the middle were stored in an array.
- The bridge-switch was redirected into "bypass" mode for 100 ms.
- The measuring current was then directed through the specimen again, but this time in the opposite direction.
- Step e) was repeated and the result was stored in another array.
- The bridge-switch was directed into the "bypass" mode again until the nest next scheduled reading.
- The average of the absolute values of the "normal" and "reverse" measurements were used as the potential measurement for this interval and this mean value, together with the corresponding time and the AE count number, were stored in a computer.

3.2.4 Measurement of Acoustic Emission (AE)

The measurement system for AE consisted of a Dunegan-Endevco type of acoustic emission panel (Series 3000) using a 0.1-0.3 MHz filter, a piezoelectric transducer (Model D150M), a 40 dB pre-amplifier and a transducer (S9204). The lower rod of the loading arrangement was used as a wave guide and the piezoelectric transducer was fixed at the end of the lower rod. High temperature vacuum grease was used as a couplant between the transducer and the wave guide rod to ensure a good contact. The wave guide rod was made of stainless steel of 8 mm in diameter and 250 mm in length. This arrangement was found to give equivalent results to more elaborate wave guide techniques and was very convenient to implement.

AE signals can be processed in many ways and the most common one is the so called "ringdown" counting. The AE counts obtained by this method correspond to the number of times the AE signals exceed a pre-set threshold value. In this study, the time interval for AE collection was usually 2 minutes and the obtained AE signals were, therefore, the accumulated AE counts within that time period.

3.2.5 Measurement of Crack Advance

Direct measurement on the fractured surface is the most reliable way to determine crack advance. In our lab, recognition of fracture bands is made easier by using a technique called “heat tinting”. Heat tinting means heating the samples to a high temperature, usually the peak temperature used for crack testing, and holding them there for an hour with a minimum load of about 200 grams which is approximately equivalent to $K_I = 0.03$ MPa$\sqrt{m}$. By heat tinting, an oxide layer of different thicknesses is left on the fractured surface and a typical one is shown in Figure 3-

7a. Due to the thickness change in the oxide layer, a group of bands, which corresponds to a series of crack advances, can be identified. The widths of these bands represent the crack advance distances along the axial direction. Since those bands are rarely uniformly rectangular, the mean value of seven width measurements is usually taken as the average crack advance, as shown in Figure 3-7b. By this means, an absolute value of crack advance is obtained and cracking velocities can be calculated. See the next section for detailed discussion about crack velocity calculation under various conditions.

3.2.6 DHC Velocity (DHCV) Measurement using Combined AE and PD

For setting up a profile of cracking velocities versus temperature, as shown in section 4.2.2, isothermal cracking velocities have to be measured at different test temperatures. Measuring isothermal cracking velocities are sometimes easy but not always. The difficulties come from the fact the cracking can be a mixture of isothermal and non-isothermal cracking activities or isothermal cracking with an incubation period. In those cases, the accuracy in cracking velocity measurement depends directly on how precisely the isothermal portion can be defined. Being aware of the uncertainty in quantitatively evaluating crack extension by using either AE or PD, we have combined these two techniques to measure cracking extension. Because of their sensitivity and event-related response, AE signals were informative about when cracking occurred. In most cases a sudden slope change of accumulated AE counts indicated either a start or an end of cracking. After direct measurements of crack advance from post-fracture surfaces, decisions were made, by analyzing AE and PD records, if there had been significant non-isothermal cracking taken place. In the cases when crack advance was not a pure isothermal one but a mixture of isothermal and non-isothermal cracking activities, a value of

$(PD_3-PD_2)/(PD_3-PD_1)$ were used to estimate the ratio of the isothermal portion to the non-isothermal one, see Figure 3-10. For situations when cracking started after the test temperature had been reached, the incubation periods were determined and excluded in cracking rate calculations. Examples given below will show how AE/PD measurements was used in conjunction with post-fracture analysis in determining the isothermal cracking velocities at various test temperatures.

Cracking activities can start when a test temperature was reached. They could also occur before the test temperature was reached or sometime after. Depending on when cracking started, situations encountered in cracking velocity measurements were divided into four categories:

- pure isothermal cracking only (category I)
- isothermal cracking with insignificant portion of non-isothermal cracking (category II)
- isothermal cracking with significant portions of non-isothermal cracking (category III)
- pure isothermal cracking but with incubation period (category IV)

The handling of these four different situations is illustrated via four examples. The four test temperatures are 280°C, 260°C, 200°C and 170°C. For the specimen used, which contains 160 μg/g hydrogen, 280°C is approximately the cracking start temperature when cooled from a peak temperature of 320°C. Therefore, only for the cracking tests carried out at 280°C the total time kept at test temperature can be taken as the isothermal cracking time. In all other cases, corrections have to be made either to exclude the crack extension occurred before the test temperature is reached or to exclude the incubation time from the total cracking time used for velocity calculation.

The simplest case is the one carried out at 280°C, shown in Figure 3-8. AE signals indicate that the cracking has started at about 282°C, only 2°C above the test temperature. Therefore, the whole time the specimen was kept at 280°C can be taken as isothermal cracking time. Isothermal cracking velocity in this case, Category I, is simply calculated by:

$$DHCV = a / t_{iso} \qquad (3.5)$$

where a is the crack extension measured from fractured surface, and

t_{iso} is the isothermal cracking time.

More sophisticated is the isothermal cracking velocity measurements in the Categories II and III, in which cracking has started during cooling. The DHCV measurement at 260°C, shown in Figure 3-9, represents the Category II. In Figure 3-9, cracking has started at 286°C, 26°C higher than the test temperature. The crack extension measured from the fracture surface is, therefore, not 100% isothermal, although the non-isothermal portion is quite small. For cases like this, crack length measured from specimen surface has still been used as crack extension but the cracking time has been modified by adding the non-isothermal cracking time to the total cracking time at the test temperature. By doing this, the non-isothermal cracking occurred between 286°C and 260°C has been actually considered as isothermal. Due to the fact that the non-isothermal cracking period is short, the difference in cracking velocities between the non-isothermal portion and the isothermal portion is minor. Thus, the consequent calculation error is believed to be negligible. The formula for the cracking velocity calculation in this cases is :

$$DHCV = a / (t_{noniso} + t_{iso}) \quad (3.6)$$

where a is the crack extension measured from specimen fracture surface,

t_{noniso} is the non-isothermal cracking time, and

t_{iso} is the isothermal cracking time.

The Category III is presented in Figure 3-10. In this case the difference between the test temperature of 170°C and 279°C, where cracking has started, is 109°C and the cracking advance during this time is significant. In such cases, instead of correcting the cracking time, we have modified the crack extension measured from the fractured surface by multiplying it with a ratio of $(PD_3-PD_2)/(PD_3-PD_1)$ so that the fracture advance caused by non-isothermal cracking is excluded. The formula for calculation is then changed to:

$$DHCV = \gamma a / t_{iso} \quad (3.7)$$

where a is the total crack extension measured from specimen surface,

t_{iso} is the isothermal cracking time, and

γ is the ratio of the isothermal cracking to the total cracking, calculated by $(PD_3-PD_2)/(PD_3-PD_1)$.

The last category, Category IV, refers to the cases when cracking starts after the isothermal temperature has been reached, as shown in Figure 3-11. Under this circumstance, the correction is about excluding incubation period from the total cracking time. In these cases AE signals are helpful in determining when cracking has started. The calculation formula can be presented as:

$$\mathrm{DHCV} = a / (t_{iso} - t_{incub}) \tag{3.8}$$

where a is the crack extension measured from fractured surface,

t_{iso} is the total isothermal time, and

t_{incub} is the incubation time.

The combined application of AE and PD in cracking monitoring used in this thesis is unique since no similar work have ever been published. It has been found that combining these two techniques can, to a degree, make up for their individual deficiencies and produce more accurate and reliable results in cracking monitoring. Because of the "event-dependence" of AE and the "state-dependence" of PD, both the sensitivity and stability required in DHC process monitoring can be obtained when the two techniques are used in conjunction. By following the procedures suggested above, isothermal cracking velocities can be measured accurately with minimum concerns over the possible interfere of non-isothermal cracking activities. All the DHCV results reported in section 4.2.2 have been obtained by using this combined AE/PD technique.

3.3 Metallographic Analysis

Metallographic analyses were performed before and after cracking tests. The analyses on specimens prior to cracking tests were designed to determine the bulk hydride morphology. The bulk hydrides were the "original", not “re-oriented” hydrides, which lay mainly on the axial-circumferential planes. The bulk hydrides were analyzed on both axial-radial and circumferential-radial planes. In addition to the bulk hydride morphology, the matrix grain structure and β-phase morphology were also studied prior to cracking tests. The metallographic analysis after the cracking tests were aimed mainly at crack tip hydrides, termed “radial hydrides” because they were re-oriented from the axial-circumferential to the axial-radial planes. These metallographic analyses were performed on the specimens held at T_{CAT} for at least 24 hours and on both axial-circumferential and circumferential-radial planes. Furthermore, metallographic features such as crack surface roughness, see section 2.2.3.2 for its definition, were also measured. For the metallographic studies, optical microscopes and electron microscopes were used. A key issue in metallographic study was the specimen preparation, by which the phase(s) of interest was (were) made visible.

3.3.1. Optical Microscope

The optical microscope used for crack tip hydride analysis was a Carl Zeiss, model H-PL-Pol. The light microscope was equipped with a Hitachi-VK-C350 color video camera and a Sony multiscan video printer, model UP-930, so that video prints of the images could be made.

3.3.2 Scanning Electron Microscope (SEM)

Most of the metallographic studies were performed on a Hitachi S-2700 SEM equipped with image analysis functions. Applications of SEM in studying hydride morphology have been described in the literature [70] and have proved to be advantageous compared to optical microscopes. First of all, the SEM offered a larger range of magnification, including far higher magnifications than are possible in optical microscope. The useful magnifications for metallographic study ranged from 400 up to 4000 times. Secondly, by using SEM it was possible to have the compositional (atomic number) contrast using back scattered electron (BSE) imaging. The hydride phase had a lower mean atomic number than the metallic (zirconium) phase and thus provided a good contrast to the matrix under BSE imaging mode.

3.3.3 Specimen Preparation

The specimen preparations for optical microscope analysis and SEM analysis were slightly different. While the preparation for optical microscope analysis consisted of regular grinding and polishing, an additional attack polishing was usually performed on specimens for SEM analysis.

For optical microscopy, the specimens were ground to 600 grit and polished with 6 μm diamond paste. The resulting surfaces were somewhat mirror-like but were always with small scratches. After this preparation, the hydrides looked brighter than matrix in the light microscope. An additional attack polishing, described by Kiely [71], was found to be beneficial in terms of removing most of the scratches and revealing more details about hydrides under SEM. Attack polishing was actually an additional polishing with abrasive Cr_2O_3 ashes and a small amount of diluted hydrofluoric acid (1 ml of 48% HF in 200 ml of distilled water). The Cr_2O_3 ashes for attack polishing were produced by igniting ammonium dichromate [71]. After attack polishing the specimen surfaces were shining and free of scratches. Hydrides appeared darker compared with the surrounding matrix in the BSE imaging mode.

3.4 Fractographic Analysis

Post-fracture analysis can reveal a lot of useful information about cracking procedures and fracture properties. The fracture features studied in this work included striations, matrix ligaments and hydride coverage. Compared to metallographic studies, specimens needed little preparation for fractographic analysis. In inter-striation distance measurements, in addition to optical microscope and SEM, a Zeiss Stereomicroscope SR had been also used for low magnification measurements. In matrix ligaments and hydride coverage studies, a piece of software written by Link Analytical for image analysis was used. By selecting a threshold value, images of fractured surfaces were transformed into black and white patterns by using the Single Image Phase Analysis (IPA) function. Based on the principle of point counting, estimations of the ratio of black to white, corresponding to matrix and hydrides respectively, were given. It was also easier to measure the width of the ligaments on the resulting black and white patterns. However, these measurements should be considered only as semi-quantitative because the selection of threshold values was somewhat subjective.

3.5 Other Testing Methods

3.5.1 Vickers Hardness Measurement

Vickers hardness tests was performed on the specimens which have experienced different amounts of additional cold working to estimate their matrix strength. The hardness testing were made on an Amsler material testing machine made by Otto Wolpert-Werke GmbH in Germany. The loading used in hardness testing was 10 kilograms.

3.5.2 Hydrogen Content Analysis

Hydrogen content analysis is not possible in our lab. Some of the specimens were sent to the Department of Metallurgy and Materials Science, University of Toronto for subsequent vacuum extraction analysis of average hydrogen level in the hydrided specimens.

Double-Arc-Melted Ingot
⇩
Ultrasonic Inspection
⇩
Forge to Bar
⇩
Machine Hollow Billets
⇩
Ultrasonic Inspection
⇩
Clad Billets in Steel and Copper
⇩
Preheat Billets to 847°C and Extrude into a Tube
⇩
Dissolve the Copper and Steel Clading
⇩
Sand Blast Inside, Grinde Outside
⇩
Cold Draw 12 to 15%
⇩
Sand Blast Inside and Grind Outside
⇩
Cold Draw 12 to 15%
⇩
Hydrostatic Test
⇩
Hone Inside, Grinde Outside
⇩
Ultrasonic Inspection
⇩
Stress Relieve in an Autoclave for 24 h at 400°C
⇩
Straighten, Correct Ovality
⇩
Ultrasonic Inspection

- -

⇩
Straightening (rolling)
⇩
Stress-relief Annealing for 24 h at 400°C
⇩
Electrolytically Hydriding
⇩
Diffusion Heat Treatment for 48 h at about 390°C
⇩
Electrospark Discharge Machining into Compact Tension/Constant-K specimens
⇩
Pre-fatigue

Figure 3-1 All the steps the specimens have experienced prior to cracking tests

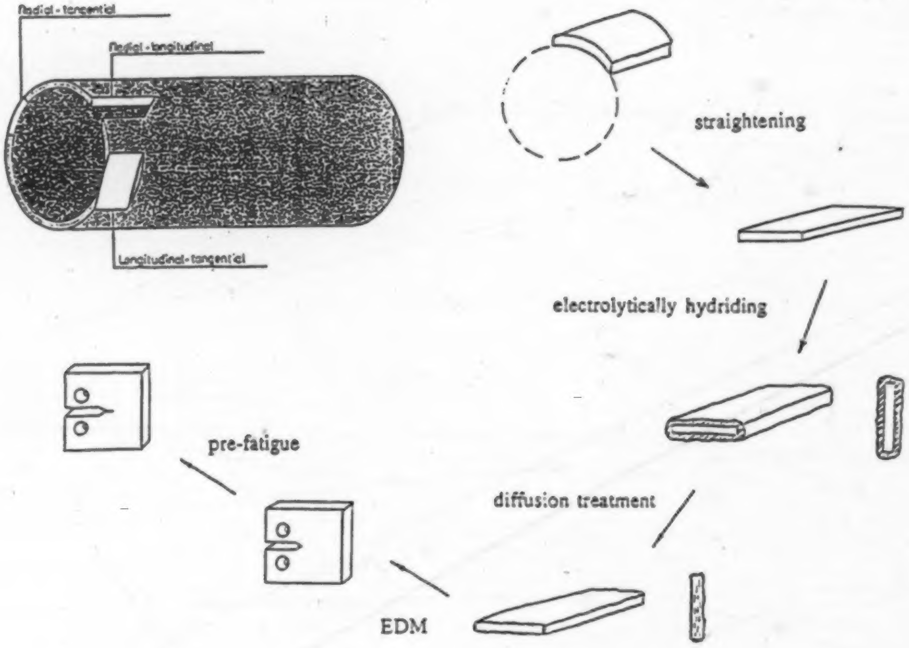
Radial - tangential
Radial - longitudinal
Longitudinal - tangential
straightening
electrolytically hydriding
diffusion treatment
EDM
pre-fatigue

Figure 3-2 Schematic illustration of specimens' preparation done in this lab

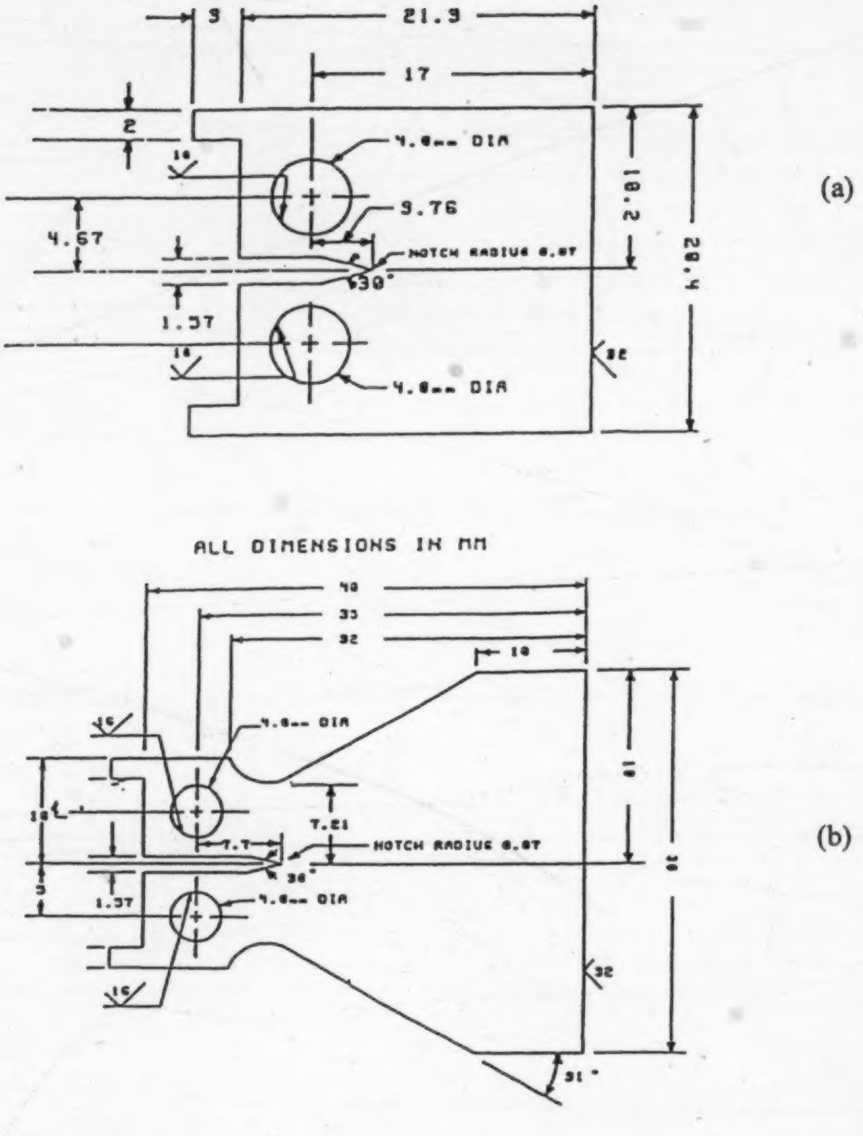
3
21.3
17
2
4.8mm DIA
3.76
NOTCH RADIUS 0.07
30°
4.67
1.37
18.2
28.4
32
(a)
ALL DIMENSIONS IN MM
40
33
32
10
4.8mm DIA
7.21
7.7
NOTCH RADIUS 0.07
30°
1.37
17
38
31°
32
(b)

Figure 3-3 Dimension of specimens

a) dimensions of compact toughness specimen

b) dimensions of tapered double cantilever beam (constant K) specimen

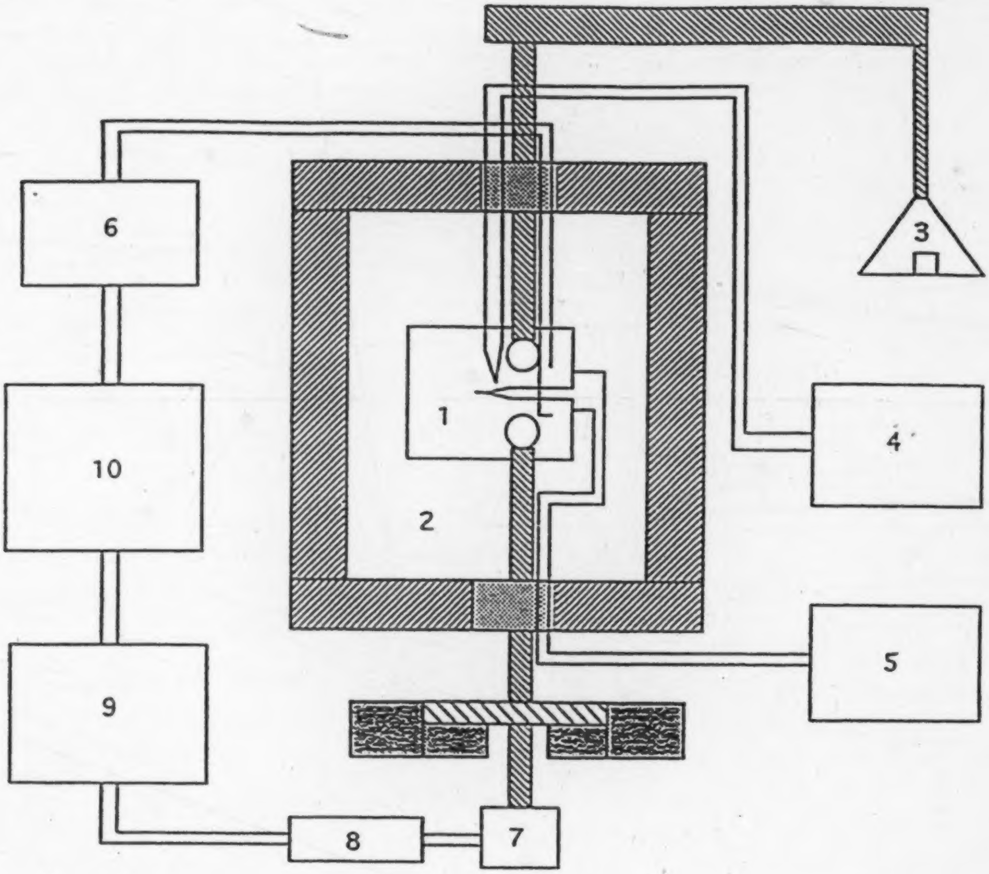

Figure 3-4 Schematic diagram of experimental rig for cracking tests
1. specimen; 2. furnace; 3. loading system;
4. temperature controller; 5. D.C. constant power for DC;
6. PD rig; 7. AE transducer; 8. AE preamplifier;
9. AE rig; 10 computer for data requisition

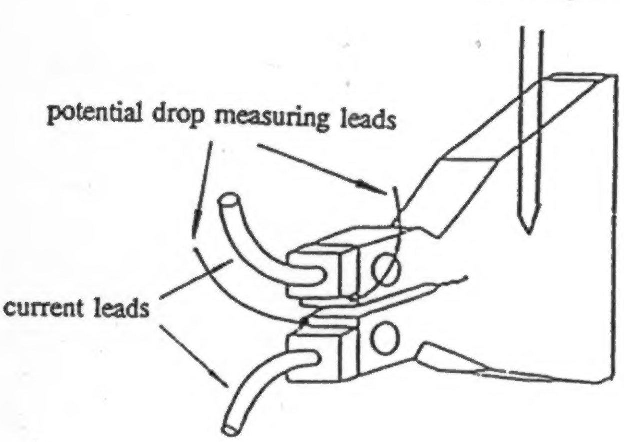
thermocouple
potential drop measuring leads
current leads

Figure 3-5 Schematic diagram showing positions of the current leads, potential drop (PD) measuring leads and the thermocouple

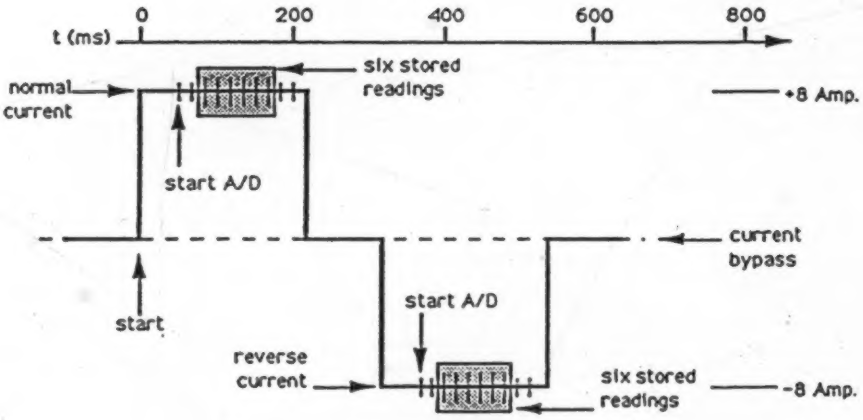
t (ms)
0
200
400
600
800
normal current
six stored readings
+8 Amp.
start A/D
current bypass
start
start A/D
reverse current
six stored readings
-8 Amp.

Figure 3-6 Potential drop (PD) measurement system

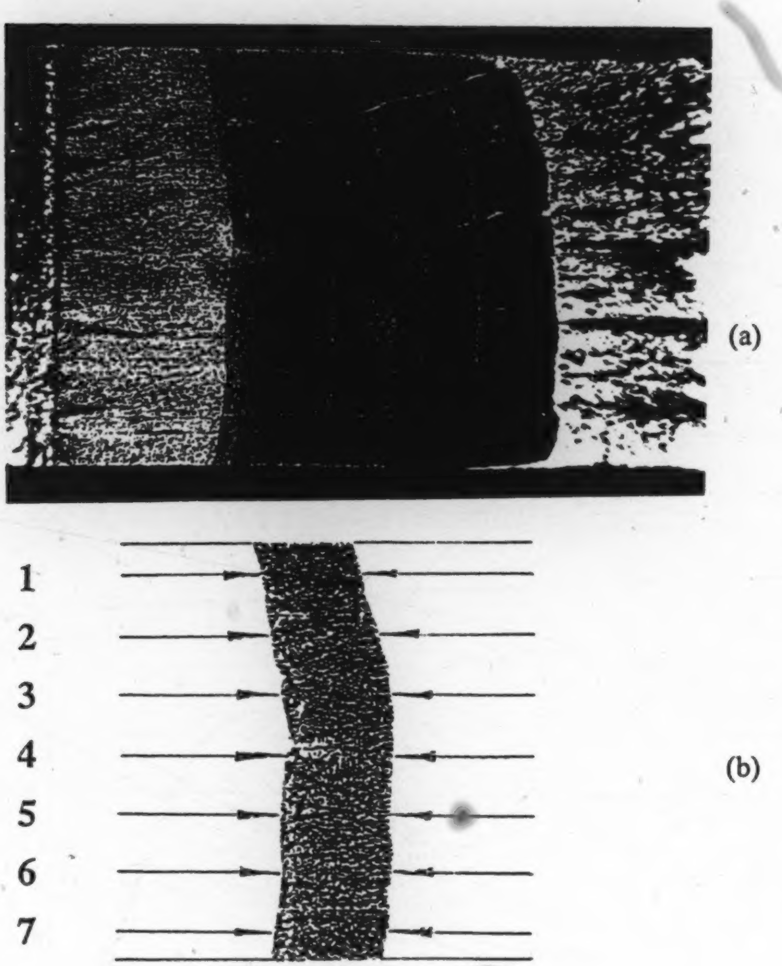

Figure 3-7 Schematic diagram showing the method of measuring crack advance

a) Typical fracture surface of a cracked tapered double cantilever beam specimen

b) Schematic diagram showing the method of mean crack advance measurement

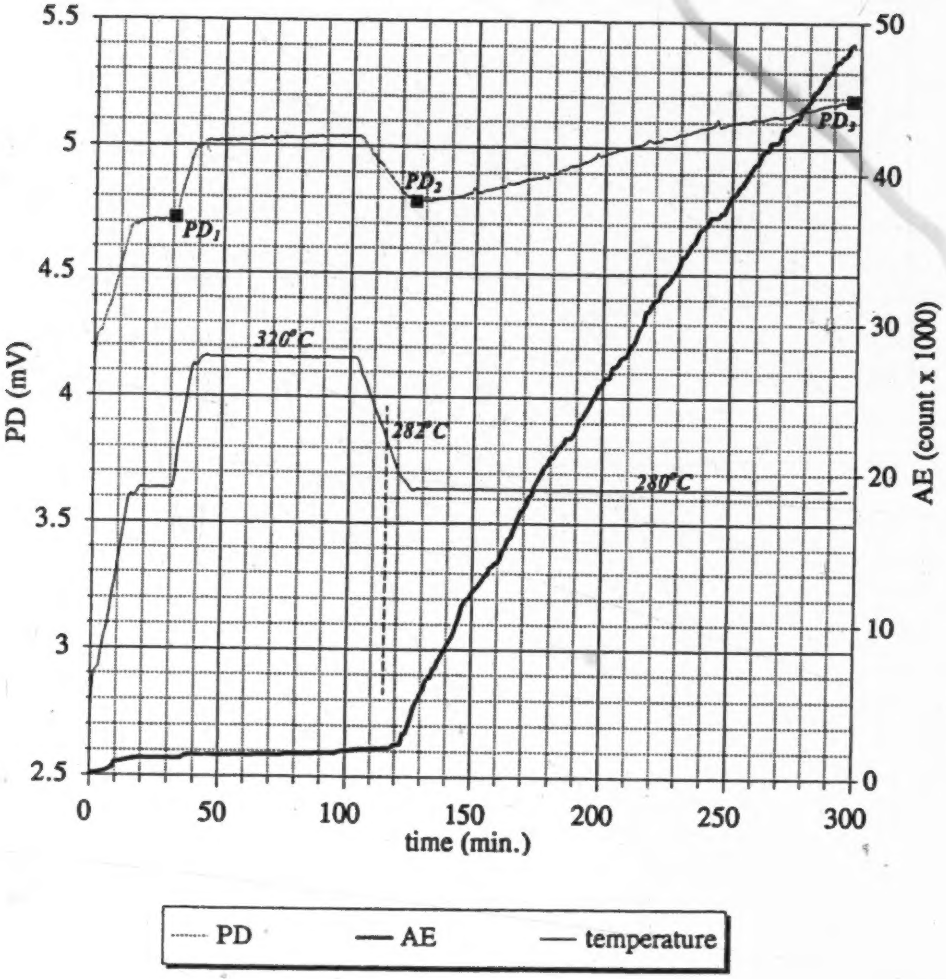

Figure 3-8 Measurement result of AE and PD at 280°C with a peak temperature of 320°C

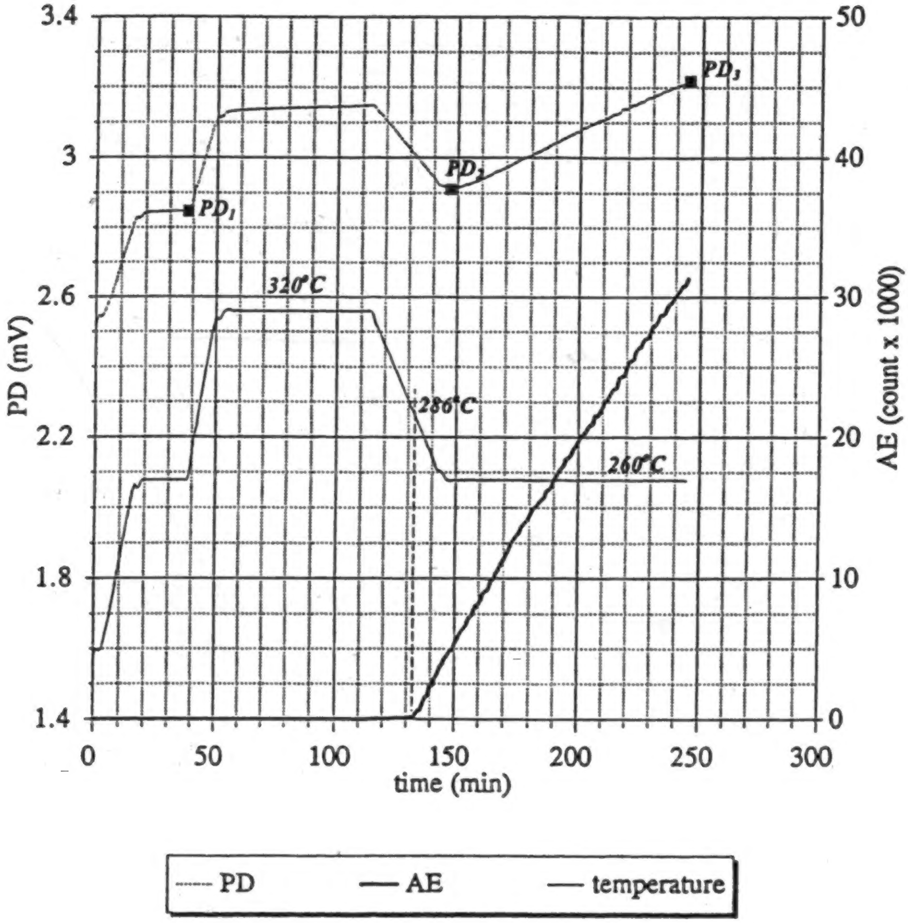

Figure 3-9 Measurement result of AE and PD at 260°C with a peak temperature of 320°C

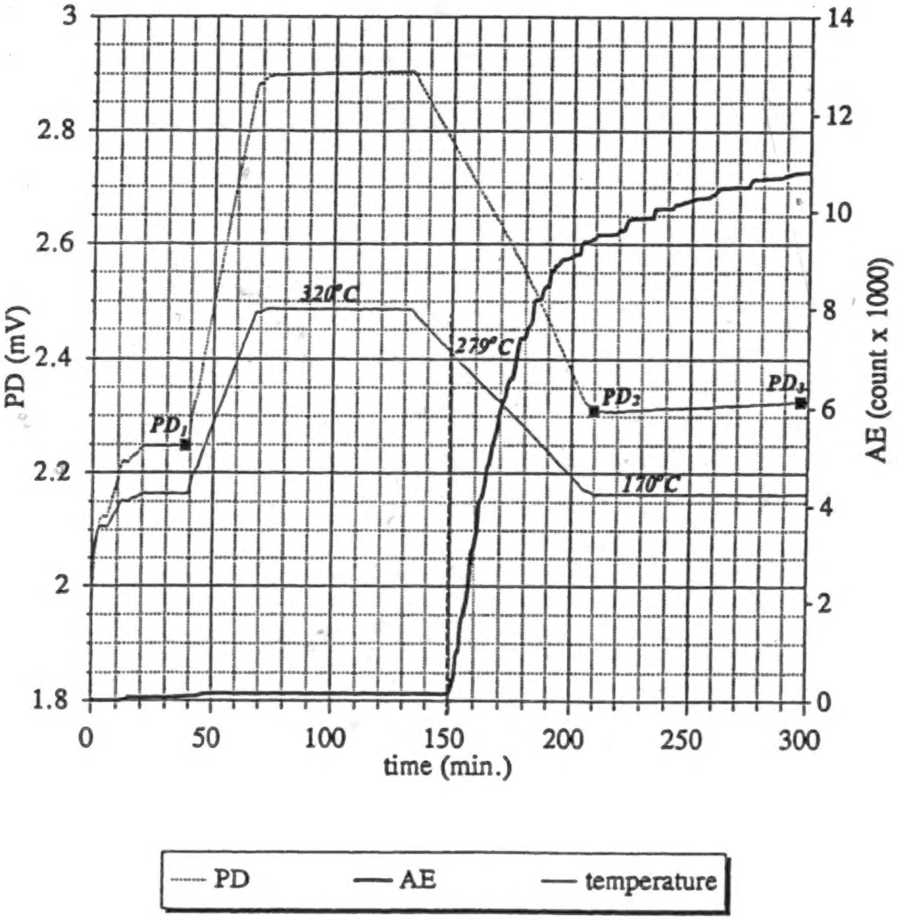

Figure 3-10 Measurement result of AE and PD at 170°C with a peak temperature of 320°C

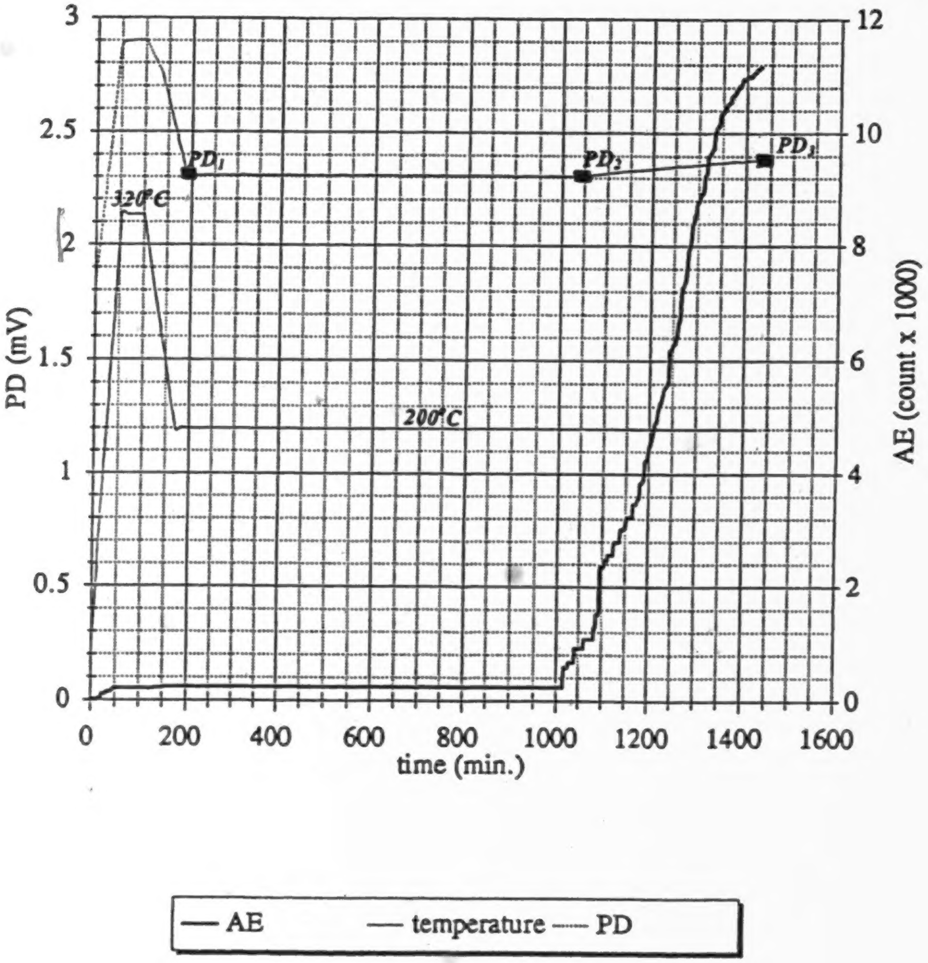

Figure 3-11 Measurement result of AE and PD at 200°C with a peak temperature of 320°C and loading only at the test temperature

Chapter 4 Experimental Results

The testing program on the cracking arrest phenomenon consisted of four parts: pre-analysis, cracking tests, metallography and fractography.

The pre-analyses, so called because they were carried out prior to cracking tests, were set to collect all the necessary information about the specimens such as the specimens' hydrogen content, their matrix hardness, bulk hydride morphology, matrix microstructure, β-phase morphology and so on. This information is believed to be important since these parameters have a profound influence on DHC behavior and, consequently, on cracking arrest behavior as well.

The pre-analyses were followed by cracking tests, which were probably the most important part in the whole testing program. The purpose of the cracking test was to determine the T_{CAT} values and the affecting parameters. In cracking tests, specimens with different matrix strengths or microstructures were tested under various conditions for T_{CAT} value determination. Tests were repeated on the same specimens as well as on nominally identical specimens to see the reproducibility of measurement results. In the investigation of affecting parameters on cracking arrest temperature, efforts were made to vary only the parameter studied while maintaining other parameters constant. The parameters investigated in this work included

- amount of additional cold work
- peak temperature and
- loading condition (stress intensity factor).

In addition to the tests designed for T_{CAT} measurement, cracking tests were also carried out at lower test temperatures to measure the DHC velocities (DHCV) under selected conditions. These tests focused on the temperature dependence of cracking velocity, especially at the temperatures close to T_{CAT} where cracking rates approach zero.

A good portion of the specimens that went through cracking tests have been metallographically or/and fractographically analyzed. Metallographic analysis served for studying hydride formation at T_{CAT} and re-oriented crack tip hydride morphology. Hydride formation was studied because at that time it was not clear if the absence of re-oriented crack tip hydrides or their fracture was the cause of cracking cessation. After confirming the presence of uncracked crack tip hydrides at T_{CAT}, the metallographic examination of crack tip hydrides was continued for quantitatively investigating re-oriented hydride configurations. Crack tip hydrides were studied on both the axial-circumferential and the circumferential-radial planes of the specimens. While hydride images on axial-circumferential planes showed the size and distribution of crack tip hydrides along the crack propagating direction (the axial direction), hydrides observed on circumferential-radial planes exposed their structure along the through-thickness direction of the tube (the radial direction). In addition to the morphology of re-oriented hydrides, the correlation between the original (not re-oriented) and the re-oriented hydrides was also displayed by analyzing hydrides on circumferential-radial planes.

Fractographic analysis was carried out on some of the specimens that had gone through a series of cracking tests. Specimens fractured by DHC were analyzed for fracture features such as pattern distinctness, hydride coverage ratio and the matrix ligament width as well as their dependency on test conditions. Since there is no fracture above T_{CAT}, fractographic analysis could not serve directly in the study of the cracking arrest phenomenon. However, the post-fracture analysis on specimens fractured at lower temperatures revealed information about the temperature dependence of fracture features, which was found helpful in understanding the temperature effects on DHC behavior.

4.1 Results from Pre-analysis

4.1.1 Hydrogen Content

All the specimens used in this study were electrochemically hydrided to ensure ample hydrogen content at test temperatures. The detailed hydriding procedure was introduced in section 3.1. The total hydrogen level in any specimens was determined by the temperature of diffusion annealing, which was carried out after hydriding, see section 3.1 and the dissolution solvus. From the TSSp curve in Figure 2-4 the minimum hydrogen level required for having hydride precipitation at a test temperature could be calculated. A lower average hydrogen content was actually needed for having hydride precipitation at a crack tip region because of the elevated local hydrogen concentration caused by increased stress levels at the crack tip. Therefore, this calculated hydrogen level guaranteed a sufficient hydrogen supply since the hydrogen level was under-estimated. Guaranteed hydrogen supply was important for this project since the possibility of cracking cessation due to depleted hydrogen should be excluded. The nominal hydrogen levels for specimens are listed in Table 4-1. Subsequent sampling of hydrogen contents showed the estimated hydrogen contents were usually ensured.

4.1.2 Amount of Cold Work and Matrix Hardness

In order to see the effect of matrix strength on the T_{CAT} value, some specimens used in this study were prepared from material which had been additionally cold rolled in the axial direction, as previously reported by Shek [72]. Vickers hardness (10 kg load) was measured at room temperature on the axial-circumferential surfaces of these cold worked specimens to estimate their matrix strength (yield strength). The measured hardness values are shown in Figure 4-1. It can be seen that the hardness increases with increasing amount of cold work, being approximately HV 230 in as-manufactured specimens and about HV 270 in specimens of 60% additionally cold worked ones. Based on the correlation between Vickers hardness and tensile strength of Zr-2.5%Nb alloy, see Figure 4-2, [73], the tensile strength of studied specimens are in the range of 730-900 MPa. Considering the fact that the yield strength is roughly 100 MPa lower than its tensile strength, see Figure 4-3 [74], the yield strength level is estimated to be about 630 MPa for as-manufactured specimens and about 800 MPa for 60% additionally cold worked specimens. For the specimens which experienced additional cold working of less than 60%, their yield strength levels are higher than that of the as-manufactured ones but lower than that of the 60% additionally cold worked ones.

The commonly used equations for yield strength estimation are:

$$\sigma_{y(\text{unirradiated})} = 1088 - 1.02T \qquad (4.1)$$

$$\sigma_{y(\text{irradiated})} = 1388 - 1.02T \qquad (4.2)$$

with T, the temperature, in Kelvin and σ_y, the yield strength, in MPa. According to equations 4.1 and 4.2, the yield strength values at room temperature, say 300 K, should be 782 MPa for as-manufactured specimens and 1082 MPa for irradiated specimens. These irradiated values are higher than the estimated values for 60% additionally cold worked based on our hardness measurements.

Using the same relationship with temperature in equations 4.1 and 4.2 but adjusting the first constants according to our hardness test results, we obtain the following equations for yield strength estimation:

$$\sigma_{y(\text{as-manufactured})} = 936 - 1.02T \tag{4.3}$$

$$\sigma_{y(\text{cold-worked})} = 1106 - 1.02T \tag{4.4}$$

As a matter of fact, similar equations for yield strength estimation have been proposed very recently by Shi and Puls [31]:

$$\sigma_{y(\text{unirradiated})} = 958 - 1.02T \tag{4.5}$$

$$\sigma_{y(\text{irradiated})} = 1258 - 1.02T \tag{4.6}$$

These authors had used equations 4.1 and 4.2 in their earlier calculations until 1994 but switched to equations 4.5 and 4.6 in their recent papers because they have also noticed the overestimation of yield strength level given by equations 4.1 and 4.2.

4.1.3 Bulk Hydride Morphology

A significant part of the experimental work done in this study concerned the crack tip hydride morphology. For a better understanding of the re-oriented crack tip hydrides formed during the cracking tests, the bulk hydrides prior to cracking tests were carefully analyzed. These hydrides were formed under the condition of no external loading and were mainly on the axial-circumferential planes, as mentioned in section 2.2.3.2. Thus, their analyses were performed on planes perpendicular to the axial-circumferential orientation, i.e., on the circumferential-radial and axial-radial planes. Figures 4-4a to 4-4h show these bulk hydrides on as-received, 20%, 40% and 60% additionally cold worked specimens observed on circumferential-radial and axial-radial planes. In all the hydride images shown in Figures 4-4, the vertical direction is the radial direction and the horizontal direction is either the axial or the circumferential direction, depending on the images.

The observations of the bulk hydrides suggest the following characteristics of the original hydrides found in the specimens air-cooled to room temperature:

- The bulk hydrides are in a form of platelets of about 100 μm long[1], 20 μm wide[2] and 0.25 μm thick[3] under the experimental conditions used.
- To be more precise, the bulk hydrides are in the form similar to a cornflake circumferential-radial planes, see Figures 4-4b, 4-4d, 4-4f & 4-4h.
- The distribution of bulk hydrides is not homogeneous in the radial direction and the "no-hydride" zones close to the surface are about 100 μm wide in the radial direction.
- The amount of additional cold work does not have a significant effect on bulk hydride morphology.

---

[1] The word "long" is used here to describe the dimension along the axial direction.

[2] The word "wide" is used here to describe the dimension along the circumferential direction.

[3] The word "thick" is used here to describe the dimension along the radial direction.

4.1.4 Matrix Grain Structure

The grain structure of Zr-2.5%Nb pressure tubes has been schematically illustrated in the literature as shown in Figure 4-5 [28]. In as-received specimens, grains are about 15 μm long, 4 μm wide and 0.5 - 1 μm thick. In this study, the microstructure has been analyzed by viewing the β-phase since the β-phase tends to precipitate along grain boundaries. Figures 4-6a to 4-6p are the microstructure for as-received as well as cold worked specimens. Similar to Figures 4-4, the vertical direction in Figures4-6a to 4-6p is the radial direction and the horizontal direction is either the axial or the circumferential direction, depending on the images. Qualitatively, the increasingly "stretched" grains on more severely cold worked specimens are noticeable. A quantitative description of the dimension changes is difficult except for the thickness changes. There seem to be also changes in β-phase thickness, with the β-phase in 60% additionally cold worked specimens being only about half as thick as in as-manufactured specimens, as shown in Figures 4-6b and 4-6h as well as 4-6j and 4-6p.

4.2 Results From Cracking Tests

Cracking tests were designed to measure the cracking arrest temperature under various conditions and to produce a cracking velocity profile over different test temperatures. The cracking test program consisted of two parts. One part was the measurement of crack arrest temperature and its affecting parameters. The other part was the investigation of temperature dependence of cracking velocity.

4.2.1 Determination of Cracking Arrest Temperature (T_{CAT}) and Its Affecting Parameters

The first group of tests was aimed at measuring T_{CAT} values under various conditions. In these tests, the temperatures at which cracking arrested, were approached carefully. A typical test for T_{CAT} determination consisted a series of thermal cycles as shown in Figure 4-7. In each test, a specimen was heated to a peak temperature, usually between 340°C and 370°C, held there for 1 hour and then cooled to a test temperature low enough to get cracking. The heating and cooling rates were 5 K/min and 2 K/min. Heating specimens to a peak temperature and then cooling them down instead of heating them directly to the new test temperatures was necessary because the test temperature had to be approached from above. As soon as cracking was observed at a test temperature by using AE signals, the specimen was re-heated to the peak temperature, held for 1 hour and cooled to a new test temperature which was normally 5K higher than the previous one. This testing process was repeated until a test temperature was reached at which no cracking occurred for at least 24 hours and this temperature was then considered as the T_{CAT} for the tested specimen under the selected condition (applied stress intensity factor, peak temperature etc.). A typical T_{CAT}

measurement normally took anywhere between three days and three weeks and all the T_{CAT} values reported in this work were measured using this testing procedure.

The cracking arrest phenomenon is affected by a number of factors and among them are the amount of cold working, the matrix microstructure and the testing conditions such as the peak temperature and the stress intensity factors. In order to define these factors, cracking experiments were designed to run under different conditions but with only one of these factors being varied at a time.

4.2.1.1 T_{CAT} on As-manufactured Specimens at K=17 MPa√m

Measurements of T_{CAT} values began with the as-manufactured specimens. At K=17 MPa√m, the T_{CAT} value was found to be in a range of 280 to 305°C for a peak temperature of 340°C, Table 4-2. Repeated tests on nominally identical specimens showed that the T_{CAT} value was reasonably repeatable on the same specimen but varied between specimens. That is, for a particular specimen, the temperature range, within which cracking stopped, could be narrowed down to about 5K, for instance being 300-305°C for specimen L1A and 290-295°C for L1B and so on. But for a group of specimens, although they are supposed to be identical, the T_{CAT} range was wider, being about 20 K.

4.2.1.2 T_{CAT} on Additionally Cold Worked Specimens at K=17 MPa√m

T_{CAT} was found to be affected by the amount of cold working. Under the same test conditions, i.e., with the same stress intensity factor, peak temperature, holding time at peak temperature and heating/cooling rates, T_{CAT} values changed if the amount of additional cold working varied, see Table 4-3 for the measured T_{CAT}

values at K=17 MPa√m. The more severe the additional cold working were, the higher the T_{CAT} values would be.

4.2.1.3 T_{CAT} under Different Testing Conditions

In addition to its dependence on the specimen conditions (amount of cold working and heat treatment), T_{CAT} was also found to be dependent on the other test conditions such as peak temperature and stress intensity factor. Under otherwise identical test conditions, the higher the peak temperature was, the higher the T_{CAT} values were, as shown in Tables 4-2 and 4-3. Another important factor for T_{CAT} was the loading condition (stress intensity factor). The trend was that cracking would stop at lower temperatures under lower stress intensity factors, see Table 4-4. There was, however, a decreased reliability of T_{CAT} measurement when stress intensity factors were reduced and the uncertainty was caused by longer incubation periods. According to experimental results, under K=17 MPa√m, a 24 hour-holding time was long enough to ensure that cracking would not occur at the test temperatures, while for situations of K=14 MPa√m, having no cracking within 24 hours did not mean necessarily that cracking would not occur for longer holding time, see Table 4-4a. Thus, when the applied stress intensity factors decreased, the difficulty increased dramatically in deciding if cracking had arrested at a certain test temperature. Tests took longer to run and a larger number of tests had to be carried out to overcome the variation in test results.

4.2.1.4 Reversibility of Cracking Arrest Phenomenon

As mentioned before, stopped cracking activities resumed almost immediately when test temperature was lowered. As shown in Figure 4-8, AE signals were active at 300°C but not at 305°C for as long as 26 hours. However, AE signal became active almost immediately when the test temperature was dropped back to 300°C. This immediate resumption of cracking activities was not observed by Smith and Eadie [6]

4.2.2 Determination of Temperature Dependence of DHC Velocity (DHCV)

The second part of the cracking tests concerned the correlation between cracking velocity and test temperature. The combined AE/PD technique introduced in section 3.2.6 has been used for cracking velocity determination. T_{CAT} means a cessation of cracking activities when test temperatures reach a critical value. This group of tests was designed to quantitatively investigate how cracking activities changed when T_{CAT} was approached.

4.2.2.1 DHCV at Test Temperatures Close to but below T_{CAT}

During T_{CAT} tests, it was noticed that crack activities as measured by AE dropped to zero not abruptly but gradually when T_{CAT} was approached, see Figure 4-7, because the increase rate (slope) of the AE counts decreases when the test temperature increases. After having ceased at T_{CAT}, cracking was found to resume almost immediately if the test temperature was lowered to a temperature below T_{CAT}, see Figure 4-8. These discoveries were quantitatively confirmed by cracking velocity tests at test temperatures slightly below T_{CAT}. The results shown in Tables 4-5 and 4-6 were obtained with K=17 MPa√m. For both as-manufactured and 40% additionally cold worked specimens, cracking velocities decreased gradually when the test temperatures were increased, approaching zero at T_{CAT}.

4.2.2.2 DHCV Distributions with Test Temperature

It has to be pointed out, however, that this trend of slower cracking velocities at higher test temperatures is valid only in a narrow temperature range close to T_{CAT}. As shown in Figures 4-9 to 4-12, there is a temperature range within which DHCV increases with increasing test temperature but there is also a temperature range within which DHCV decreases with increasing test temperature. That is, test temperature dependence of cracking velocity changes in different temperature ranges. For all cases shown in Figures 4-9 to 4-12, which are test results on as-received and 40% additionally cold worked specimens under K=17 MPa√m, there exists a test temperature, $T_{DHCVMAX}$, at which cracking velocity reaches its maximum value for the testing condition. At temperatures below $T_{DHCVMAX}$, cracking velocity increases with increasing test temperature, while at test temperatures above $T_{DHCVMAX}$, cracking velocity decreases with increasing test temperature until it reaches zero. The cracking test results presented in section 4.2.2.1 were all carried out at test temperatures higher than $T_{DHCVMAX}$s' (but lower than T_{CAT}).

In addition to the different responses to test temperature, i.e. DHCV increases with test temperature at temperatures below $T_{DHCVMAX}$ but decreases with test temperature above $T_{DHCVMAX}$, the way the DHCV changes is also different. While DHCV varies with temperature exponentially in the test temperature range up to $T_{DHCVMAX}$, the changing rate of DHCV decreases monotonically with test temperature in the temperature range between $T_{DHCVMAX}$ and $T_{DHCVSTOP}$. The different types of temperature dependence exist in all tested specimens, see Figures 4-9 to 4-12. This difference in temperature dependence suggests that the controlling parameters for DHC may be different in these two different test temperature ranges.

The factors such as amount of cold work, heat treatment and peak temperature, which have been found to have an impact on T_{CAT} values were also found to have influence on cracking velocities. For instance, the profile of cracking velocity distribution has been found to be affected by the peak temperature used for DHCV measurements. The higher the peak temperatures, the higher the $T_{DHCVMAX}$ and the $T_{DHCVSTOP}$ will be, see Figure 4-13 for as-manufactured and Figure 4-14 for 40% additionally cold worked specimens. The $T_{DHCVSTOP}$ is the temperature where the cracking velocity is zero. The values of T_{CAT} and $T_{DHCVSTOP}$ under different peak temperatures have been summarized in Table 4-7.

When re-arranged, data in Figures 4-13 and 4-14 also indicate an effect of cold working on cracking velocities. In Figures 4-15 and 4-16 DHCV results obtained on as-manufactured and 40% additionally cold worked specimens under identical testing condition are compared. A clear dependence of cracking velocity on amounts of cold working can be seen. Cracking velocities on 40% additionally cold worked specimens were up to several times as high as the ones on as-received specimens. Consequently, T $T_{DHCVMAX}$ and $T_{DHCVSTOP}$ were all higher when specimens have experienced additional cold work. This conclusion was supported by a more intensive measurement of DHCV at different temperatures, see Figures 4-17 and 4-18, which was carried out by other members of the same research group [73].

4.3 Results from Metallographic Analysis

Metallographic analysis directly characterizes hydrides and, when combined with cracking test results, reveals the correlation between cracking behavior and re-oriented hydrides causing the cracks. Since the growth rate and morphology of crack tip hydrides dictate the cracking rate, studying crack tip hydrides metallographically benefits DHC study. It is hoped that metallography can also provide hints for the cracking arrest phenomenon. The metallographic analyses reported here were carried out on the samples which have experienced cracking cessation at T_{CAT}. The crack tip hydrides were examined to study their characteristics. After the confirmation of re-oriented hydrides, their morphology was studied, on both axial-circumferential and circumferential-radial planes, to produce a three-dimensional representation of these crack tip hydrides.

4.3.1 Existence of Re-oriented Crack Tip Hydrides at T_{CAT}

The very first point which needed to be clarified was whether re-oriented hydrides existed at crack tips at T_{CAT}. Following the cracking tests, in which the T_{CAT} values were measured, the metallographic analyses of crack tip areas of the specimens used in T_{CAT} measurements were carried out. Cracking cessation at these temperatures indicated that the necessities of DHC were not complete under that particular circumstance. The cracking tests, however, could not provide further information about what was missing. Since the cessation was not caused by deficient hydrogen content - cracking cessation with ample hydrogen - the cause of cracking arrest could only due to either difficulties with the hydride formation (precipitation and growth) or lack of hydride fracture. The metallographic analysis was used to determine which of the speculations was actually happening at T_{CAT} by examining the presence of re-oriented hydrides at crack tip areas.

According to metallographic analysis, T_{CAT} occurred with the presence of uncracked re-oriented hydrides, since re-oriented crack tip hydrides lying on axial-radial planes were observed, see Figures 4-19a and 4-19b. These hydrides were found on the as-received specimens kept at T_{CAT} under K=17 MPa√m for more than 24 hours. Re-oriented crack tip hydrides were also apparent on additionally cold worked specimens. More images of re-oriented hydrides formed at crack tips will be presented in the following sections. These experimentally observed crack tip hydrides indicated that it was not the absence of crack tip hydrides which caused the cessation of cracking but the fact that they could remain uncracked after they were formed.

4.3.2 Morphology of Re-oriented Crack Tip Hydrides Formed at T_{CAT}

After the confirmation of hydride formation, i.e. the observation of uncracked hydrides at crack tips, metallographic analysis was continued mainly to determine why these crack tip hydrides could remain uncracked. Another motivation for continuing with metallography came from the realization that the cracking arrest phenomenon actually provides an unique opportunity for crack tip hydride study, since crack tip hydrides formed and remained uncracked. At this point, the scope of metallographic investigation was extended into a quantitative survey about crack tip hydride configuration. This survey was aimed at obtaining a three-dimensional description of crack tip hydrides which is extremely important for understanding DHC process but has never been done before.

4.3.2.1 Observations of Crack Tip Hydrides on Axial-circumferential Planes

4.3.2.1.1 Crack Tip Hydrides on As-manufactured Specimens

In Figures 4-19a and 4-19b are two typical crack tip hydride images for as-manufactured specimens, obtained after holding the specimen at T_{CAT} for 24 hours. The thick dark lines on the right edge of the pictures are a crack advancing from right to the left along the axial direction. The clustered short thin lines in front of the crack tips are hydrides, which are re-oriented. In other words, these hydride platelets were oriented with their normals in the direction of externally applied stress, i.e., the circumferential direction in this case. It can be seen clearly that the hydrides formed at the crack tip are not in the form of a single piece but rather are a group, or cluster, of tiny platelets. The dimension of individual tiny hydride platelets is about 15 μm along the axial direction and 0.5 μm along the circumferential direction. (The dimension of the hydride platelets along the radial direction can not be viewed on the axial-circumferential planes.) It is also noticeable that these hydride platelets do not lie only on one plane - the cracking plane or the horizontal extension of the cracking plane - but are spread on the planes above and below as well. The dimension of the hydride cluster is about 100 μm along the axial direction (the cracking direction) and spreads out 20 μm in the circumferential direction (the vertical direction).

Careful measurements have been made to evaluate the thickness changes of the hydride platelets along the cracking advance direction. Based on Figures 4-21, the further away from the crack tip, the thinner the hydride platelets are, as indicated in Table 4-8I.

Repeated cracking tests and metallographic analysis on the same specimen resulted in reasonably similar crack tip hydride morphologies. The image in Figure 4-20b, for instance, shows the hydrides observed on a subsequent analysis of the same specimen from which Figure 4-19a was obtained. The crack tip hydrides look quite similar to the one shown in Figures 4-20a.

In addition to showing the reproducibility, comparison of Figures 4-20a and 4-20b also suggests another important characteristic of the crack tip hydrides formed at T_{CAT}: they do not seem to keep growing. Although the time at T_{CAT} has been 120 hours, 5 times as long as in the case of getting hydrides shown in Figure 4-20a, the hydrides shown in Figure 4-20b do not differ significantly in length. This implies that at T_{CAT}, the crack tip hydrides, formed probably shortly after the temperature has been reached, grow with an extremely low rate if they do at all. This apparently "frozen" state of the crack tip hydrides in terms of their dimensional change has been also found in other specimens.

Another hint acquired from metallographic analysis is that the bulk hydrogen level does not seem to have a noticeable impact on crack tip hydride morphology. Despite the fact that the specimen for Figure 4-19b has higher bulk hydrogen level, the hydrides on Figures 4-19a and 4-19b are alike except for the shapes of the cluster.

4.3.2.1.2 Effect of Additional Cold Working

Hydride morphology varies strongly with the amount of additional cold working. Figures 4-21a to 4-21e are crack tip hydrides obtained on 0%, 20%, 30%, 40% and 60% additionally cold worked specimens. Although the crack-tip hydrides in these specimens are all in the form of a cluster of individually precipitated and re-oriented hydride platelets, dimensions of both hydride clusters and individual platelets are different. The higher the percentage of cold working, the shorter the hydride cluster becomes and the finer the hydride platelets are. The measurement results concerning the hydride cluster dimension and the hydride platelet sizes are summarized in Tables 4-8, 4-9 and Figure 4-22. All these radial hydrides are formed at the T_{CAT} values for these samples.

4.3.2.1.3 Crack Tip Areas at Test Temperatures below T_{CAT}

For the purposes of comparison, some metallographic analyses were also performed on specimens cracked at test temperatures below T_{CAT}. Unlike the T_{CAT} tests, the cracking was ongoing when the experiments were terminated. The specimens were air-cooled with the loading removed, metallographically prepared and examined for re-oriented hydrides at the crack tip areas. In general, little hydride was found and typical images were like the ones shown in Figures 4-23.

4.3.2.2 Observations of Crack Tip Hydrides on Circumferential-radial Planes

In order to get a three-dimensional description of the crack tip hydride, only analyzing hydride on axial-circumferential planes is not enough since it does not provide hydride configurations along the crack front. Of course, radial configuration can be obtained by examining hydrides on several axial-circumferential planes arranged in the radial direction, as shown in Figures 4-24a, 4-24b and 4-24c. But the information obtained this way is limited and fragmented, not to mention that repeated metallographic preparations of circumferential-axial planes is very time consuming. A better way of analyzing radial hydride distribution is to do it on circumferential-radial planes. Unfortunately, this approach was associated with problems too and the most difficult part was to get circumferential-radial cross-sections just at the right places where re-oriented hydrides form. Occasionally, cross sections were obtained showing re-oriented hydrides but no crack front, as shown in Figure 4-25. Such an accuracy (obtained only with luck), however, was rarely achieved and, in most cases, cross sections partially cut the crack fronts, ending up showing hydrides and crack front at the same time. Due to the "thumbnail" shape of fractured surfaces, shown in Figure 4-26a, crack fronts were curved away for the cracking direction and the cracked part touched during sectioning was usually in the center of specimen, as schematically illustrated in Figure 4-26b. Another problem with cross-sectioning specimens perpendicular to the axial direction was to keep the specimens from breaking apart, which would happen when the cross sections for examination were too far into the fractured part of the specimens.

Inspections on the circumferential-axial planes indicated that the re-oriented hydrides formed at the crack tip were discontinuous along the radial direction, since they appeared as short line segments or dots as shown in Figures 4-27 and 4-28, depending on the amount of cold working. On the 0% additionally cold worked specimens, see Figure 4-27, the dimension of these hydride platelets along the radial direction was about 3 μm, while on 40% additional cold worked, Figure 4-28, was about 1 μm. The differences in hydride platelets could be compared more clearly in Figures 4-29 and 4-30 under higher magnifications. Being similar to Figure 4-19, these tiny hydrides, in a form of line segments or dots, did not lay just on the crack plane but on the planes above and below as well. Combined together, information about crack tip hydrides obtained on axial-circumferential and circumferential-radial planes portrayed the crack tip hydrides in three dimensions.

Another advantage of analyzing crack tip on circumferential-radial planes was the possibility of viewing the bulk hydrides (vertically oriented in Figures 4-27, 4-28 & 4-29), the re-oriented hydrides (horizontally oriented in Figures 4-27, 4-28 & 4-29) and the cracks (thick dark lines horizontally oriented) simultaneously. This was helpful in understanding their relationships. As indicated in Figures 4-31, re-oriented hydrides were responsible for cracking since most cracks occurred inside these re-oriented ones. Normally, cracks occurred inside the re-oriented hydrides instead of at their boundaries with the matrix. Cracks also preferred going in the middle of the hydrides through the middle of hydride clusters and crack fronts followed the areas where the density of accumulated hydride platelets was the highest. It was of interest to see that in the cases of parallel re-oriented hydride "strips" formed along the radial direction, parallel re-oriented hydride "strips" could break simultaneously to form parallel cracks, as shown in Figures 4-32, or only one of them may break, as shown in Figures 4-33. Closer examination of unbroken hydrides parallel to the broken one showed that the "unharmed" hydrides seemed to be finer and less perfectly re-oriented into the radial direction when compared with the fractured ones, see Figures 4-33a to 4-33d. Also the thickness, the dimension along the circumferential direction, of the hydride cluster seemed smaller for uncracked hydrides. As shown in Figures 4-27 and 4-28, re-oriented hydrides were finer and distributed more evenly along the radial direction when compared to the original hydrides. Although bulk hydrides were not normally involved in fracture process, sometimes their existence can influence the cracking process. It can be seen, for instance, on Figures 4-34a to 4-34d that if some bulk hydrides happened to be in the locations where "climbs" of crack from one group of re-oriented hydrides to another group were needed, these bulk hydrides acted as a " bridge" which linked two groups of hydride together and assisted the fracture process.

Degrees of the crack front variation in the vertical direction, or the roughness, as defined by Luo using an illustration shown in Figure 4-35 [30], can be measured on circumferential-radial planes. Some of crack fronts observed on the circumferential-radial planes are shown in Figures 4-36. Figure 4-37 shows an example of such roughness measurement based on Figure 4-36a. More roughness measurements are summarized in Table 4-10. Two points need to be pointed out here. Firstly, the detail of crack fronts vary from cross-section to cross-section simply because the hydride platelets do not always form on the same plane. As a result, roughness values are not exactly the same at different cross sections. Secondly, simplifications made during roughness measurement, such as for the cases of double-cracking, also brings in errors, with their magnitudes depending on the magnification at which images of hydrides are taken.

4.4 Results from Fractographic Analysis

Fractographic study is a post-fracture analysis, which focuses on features left on fractured surfaces. By direct observation of these features, information about the cracking process can be obtained. Although being seemingly not a suitable analytical means for the cracking arrest phenomenon simply because of lack of fractured surfaces, fractographic analysis does bring useful information for cracking arrest study. Fractographic analysis on fractured surfaces obtained at different test temperatures reveals their characteristics at various test temperatures, which indicates the temperature effect on the cracking process. This, in turn, is helpful in understanding why cracking will eventually cease at a certain critical test temperature.

All the fractographic studies in this work have been carried out microscopically, by using either the optical microscope or the scanning electron microscope (SEM). Optical fractography has been used mainly in cracking extension measurements, as discussed in section 3.2.5. Electron fractography using SEM, on the other hand, has been applied intensively for the studies of finer fracture features such as striations, hydride coverage ratio and ligament widths. In the analysis of the later two fracture surface features, an image analysis technique has been used in conjunction with the SEM.

When examined under the microscope, cracked surfaces by DHC revealed a "fish-scale" pattern, as shown in Figure 4-38. Under high magnifications, the pattern can be recognized as a nested structure, see Figure 4-39. It is generally believed that the bright parts, the ligaments, in Figure 4-39 are matrix based on the fracture patterns. This nested pattern is considered to be indicative of a partial coverage of hydrides on fractured surfaces. In this work, the ratios of the non-ligament parts to the rest, corresponding to the hydride coverage ratios on the fracture surfaces, have been estimated and the width of these ligaments measured for different test temperatures.

As mentioned before, the fractured surface was not fully covered by hydrides. A direct consequence of this partial hydride coverage is an altered fracture strength of the crack tip. The fracture property of the crack tip is, therefore, not only decided by hydrides but also by matrix. Due to the large difference between the fracture properties of the hydride and of the zirconium matrix, the effect of hydride coverage ratio can be significant. A correct estimation of the hydride coverage ratio will be helpful in estimating the amount of matrix involved during fracture. Also, hydride coverage ratios left on surfaces fractured at different temperatures provide hints for the critical condition for crack tip hydrides to fracture.

The hydride coverage ratio, the ratio of the hydrides to matrix on the fractured surface, was estimated with the help of an image analysis technique. The basic principle of the image analysis software, Single Image Phase Analysis or Single IPA, is segmenting an image into a serious of pixels with different gray levels and grouping these pixels into different intensity bands according to threshold values set. The corresponding numbers of pixels which fall into a certain intensity band represent their area percentage of the total image. In this project, only one threshold value has been selected to distinguish between hydride and matrix. As a result, images of fractured surface like the one shown in Figure 4-40a have been transformed into black-and-white patterns, as shown in Figure 4-40b and the percentage of hydride has been estimated. Figure 4-41 is an example of image analysis using Single IPA.

The key point in ratio measurement is to select the right threshold values. That is, to define which pixel represents matrix and which hydrides. It has to be admitted that in producing the in-total 100 image analysis patterns the selection of the threshold was somewhat subjective. Lack of analytical possibilities, variations in brightness and contrast of fractographic pictures left the consultant of original fractographic picture the only way for selecting threshold values. After analyzing over 100 viewfields from more than 10 specimens, the hydride coverage is estimated in a range of 87% to 91%, see Figure 4-42. Figure 4-43 gives a summary of measured striation ridge width values. The hydride coverage ratio increases with test temperature. The striation ridge width increases slightly with test temperature for the "as-manufactured" specimens and remains constant for the additionally cold worked ones.

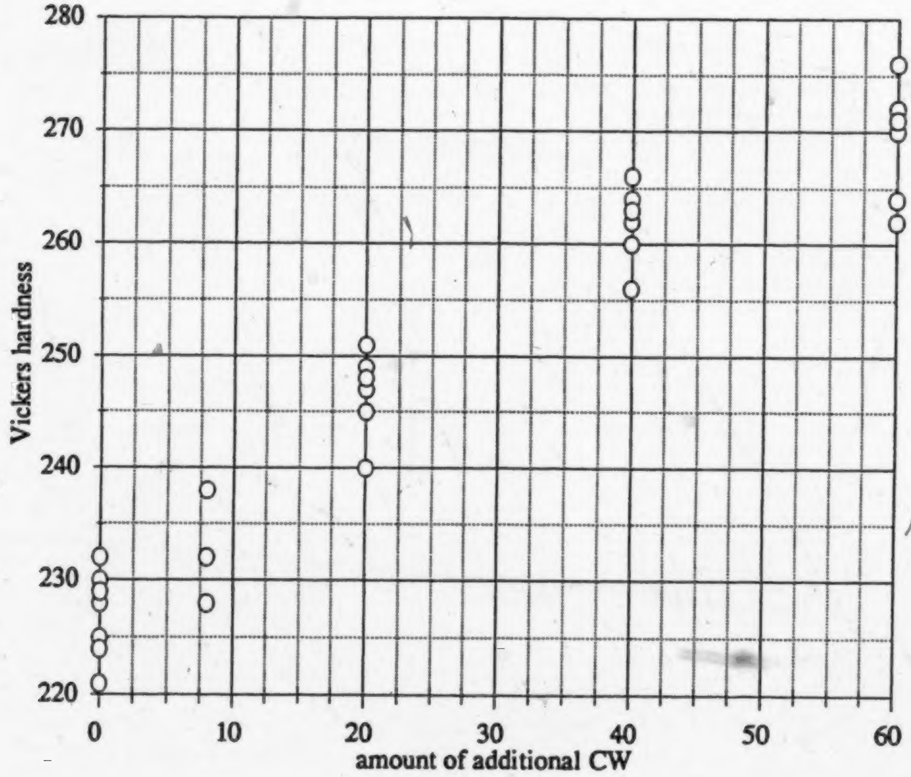

Figure 4-1 Effect of additional cold work on Vickers hardness of Zr-2.5%Nb, measured on the axial-circumferential plans with a 10 Kg-load

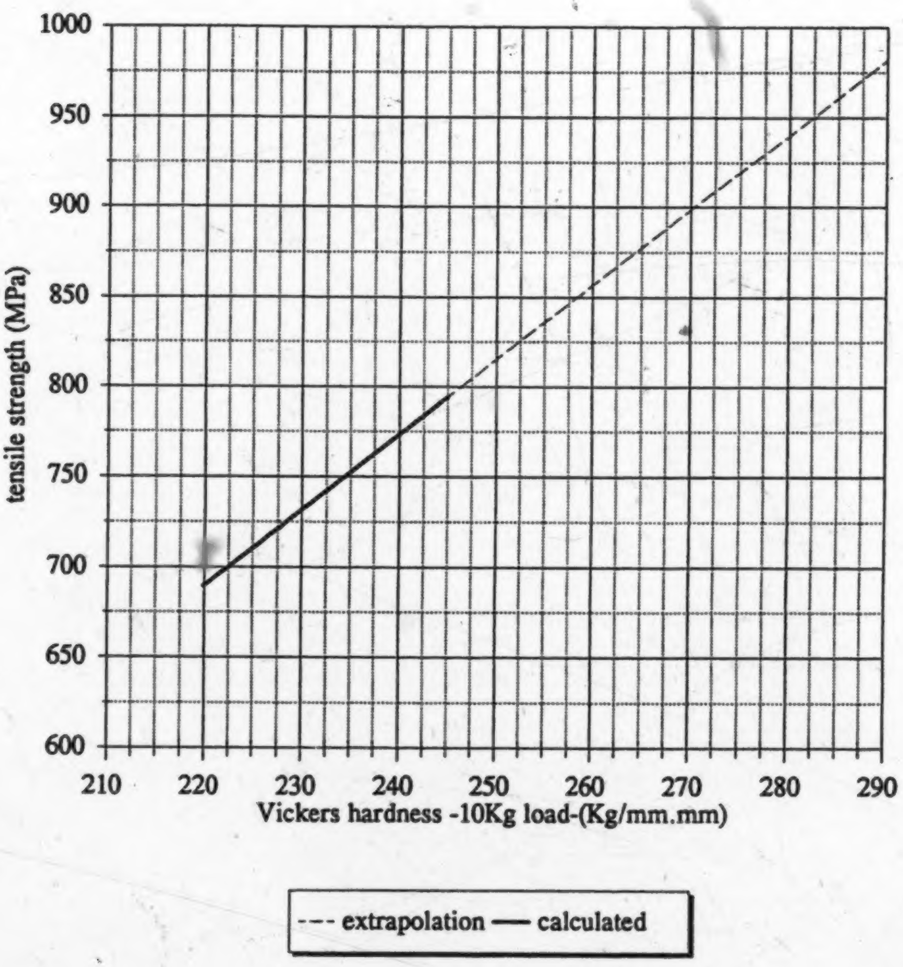

Figure 4-2 Correlation between tensile strength and Vickers hardness of Zr-2.5%Nb [73]

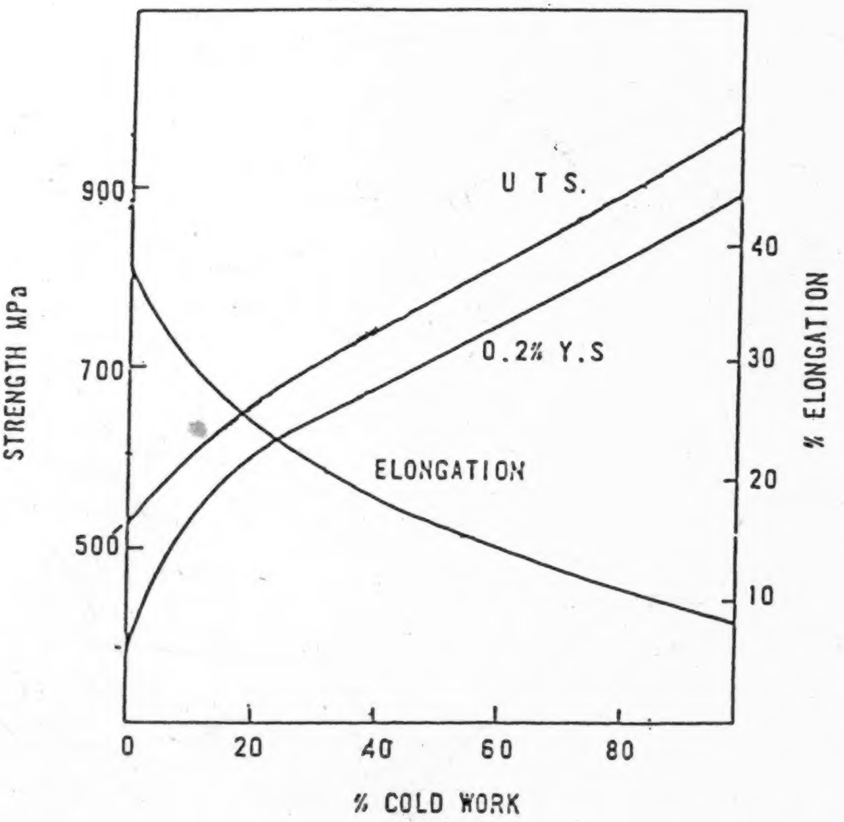

Figure 4-3 The effect of additional cold work on the room temperature tensile strength of Zr-2.5%Nb [74]

(a) axial-radial 0% additional CW 320X

(b) circumferential-radial 0% additional CW 320X

Figure 4-4 Matrix hydride morphology

(c) axial-radial 20% additional CW 320X

(d) circumferential-radial 20% additional CW 320X

Figure 4-4 Matrix hydride morphology (cont.)

(e) axial-radial 40% additional CW 320X

(f) circumferential-radial 40% additional CW 320X

Figure 4-4 Matrix hydride morphology (cont.)

(g) axial-radial 60% additional CW 320X

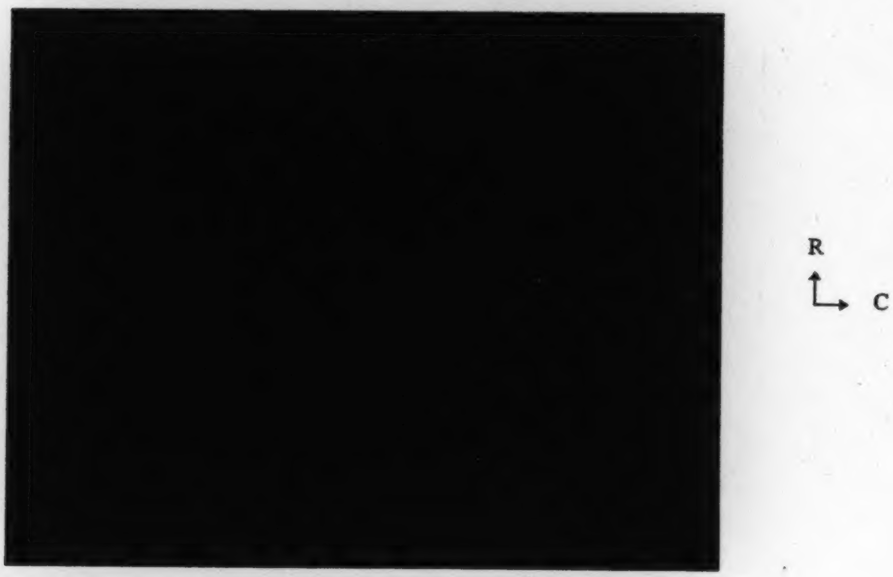

(h) circumferential-radial 60% additional CW 320X

Figure 4-4 Matrix hydride morphology (cont.)

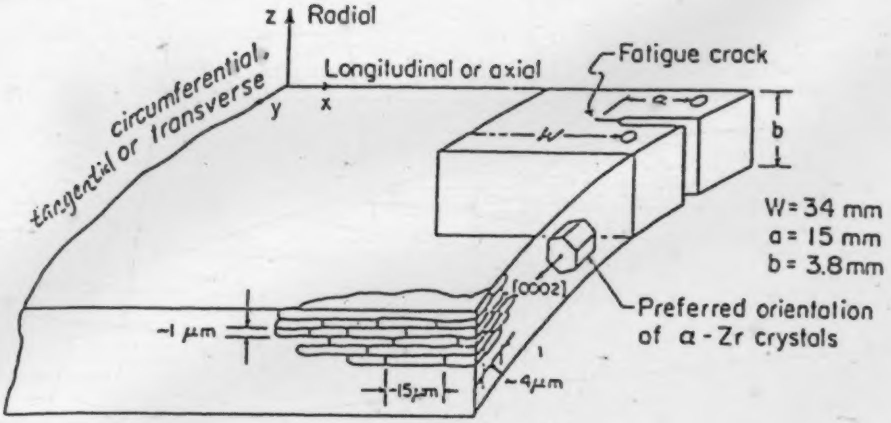
z
Radial
circumferential, tangential or transverse
y
x
Longitudinal or axial
Fatigue crack
a
W
b
W=34 mm
a= 15 mm
b= 3.8mm
[0002]
Preferred orientation of α-Zr crystals
~1 μm
~15μm
~4μm

Figure 4-5 Schematic illustration correlating structural features in a cold worked Zr-2.5%Nb pressure tube with a compact specimen [28]

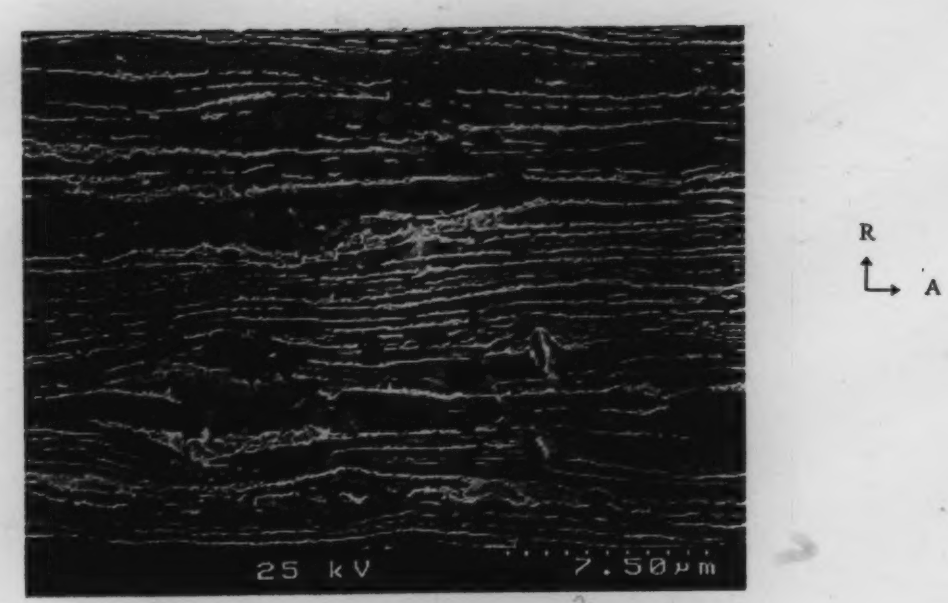
25 kV
7.50µm
R
A

(a) axial-radial 0% additional CW 4000X

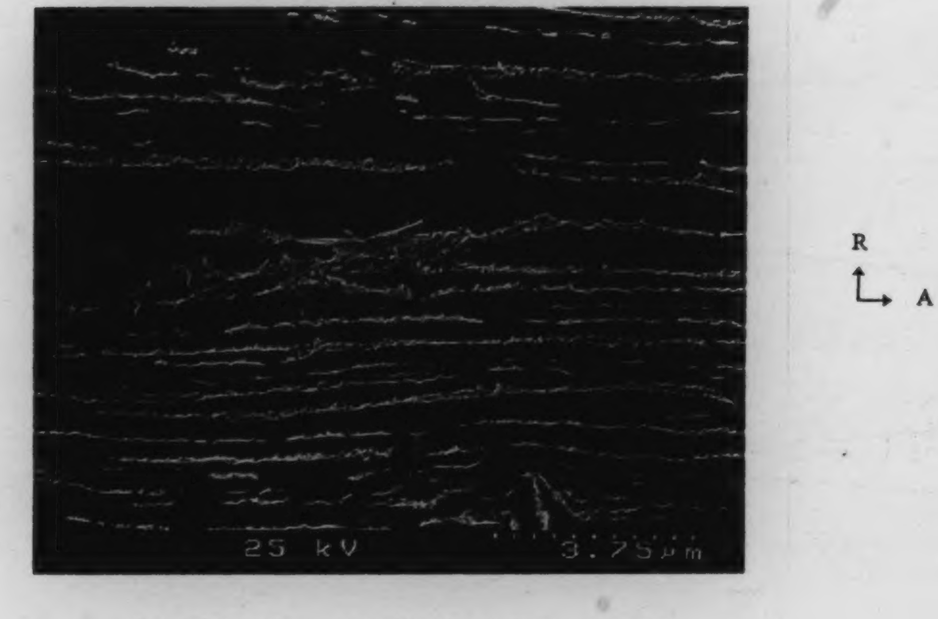
25 kV
3.75µm
R
A

(b) axial-radial 0% additional CW 8000X

Figure 4-6 SEM micrograph of matrix material

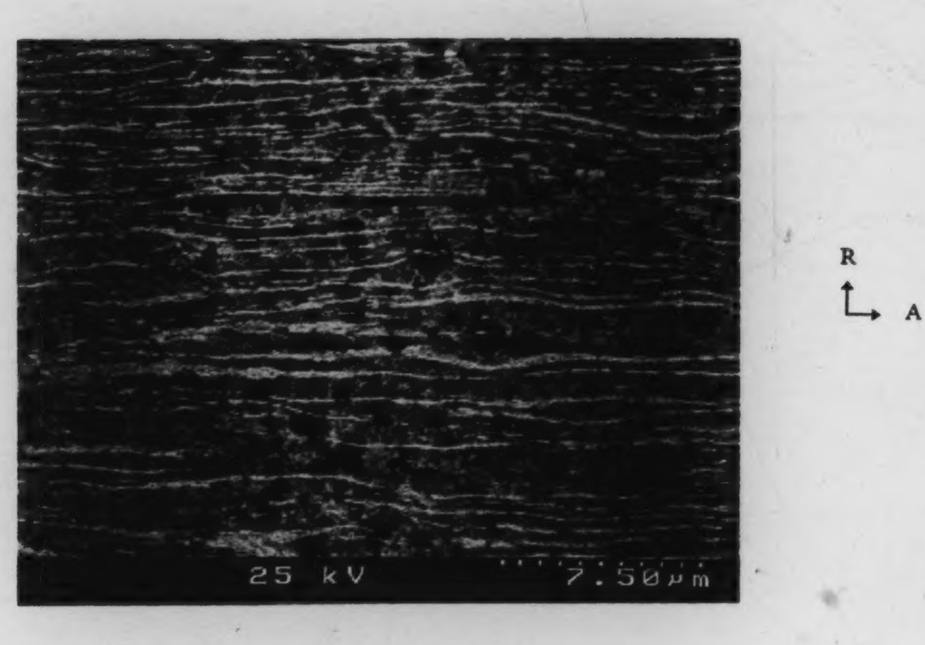
25 kV
7.50μm
R
A

(c) axial-radial 20% additional CW 4000X

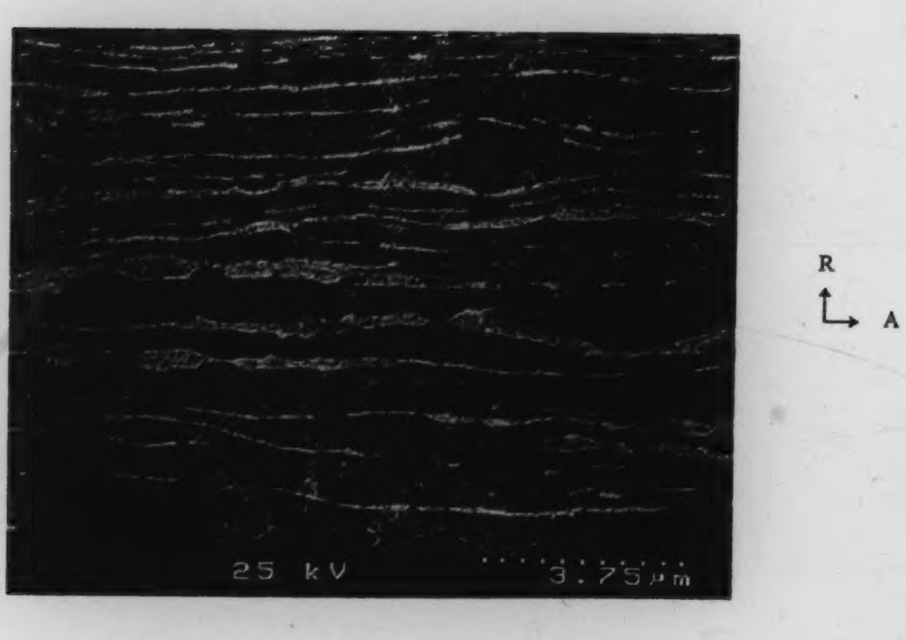
25 kV
3.75μm
R
A

(d) axial-radial 20% additional CW 8000X

Figure 4-6 SEM micrograph of matrix material (cont.)

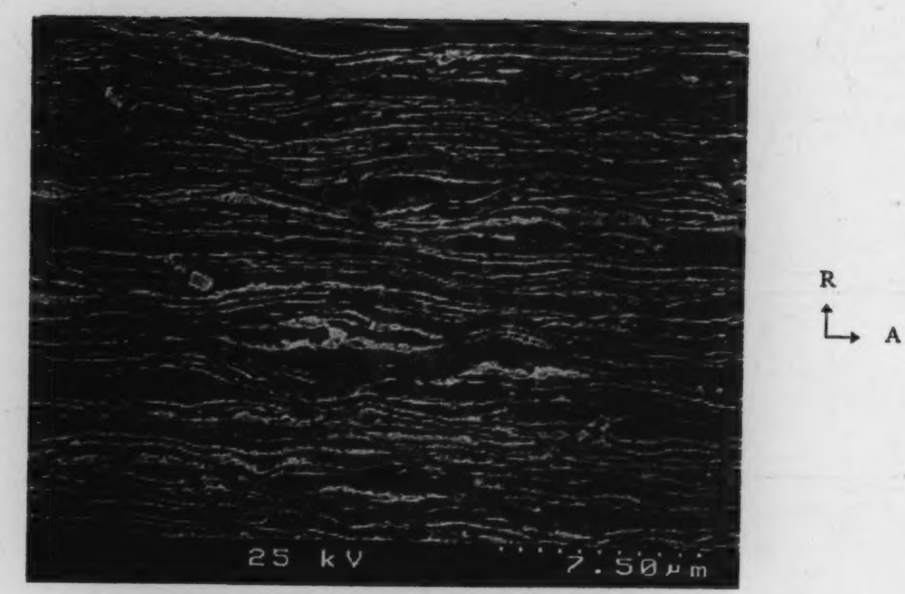
25 kV
7.50μm
R
A

(e) axial-radial 40% additional CW 4000X

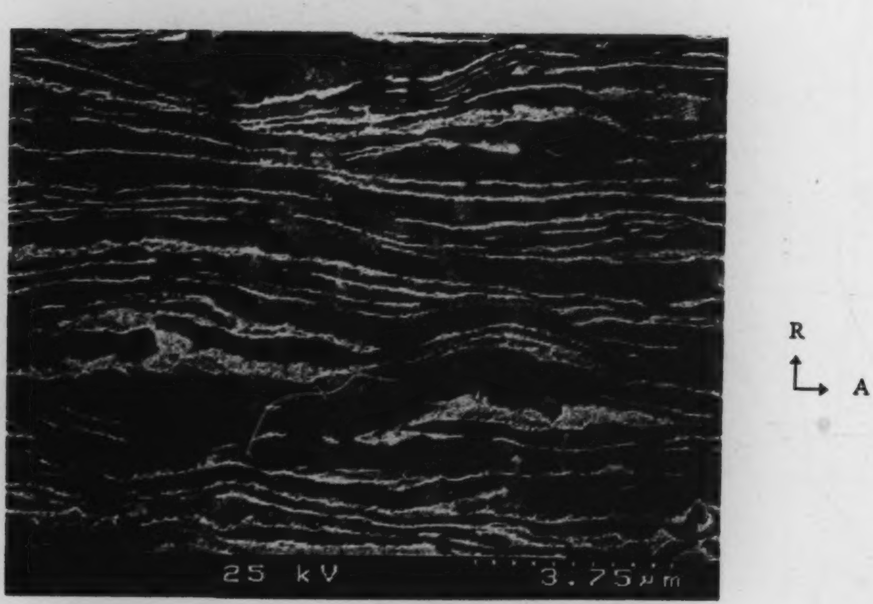
25 kV
3.75μm
R
A

(f) axial-radial 40% additional CW 8000X

Figure 4-6 SEM micrograph of matrix material (cont.)

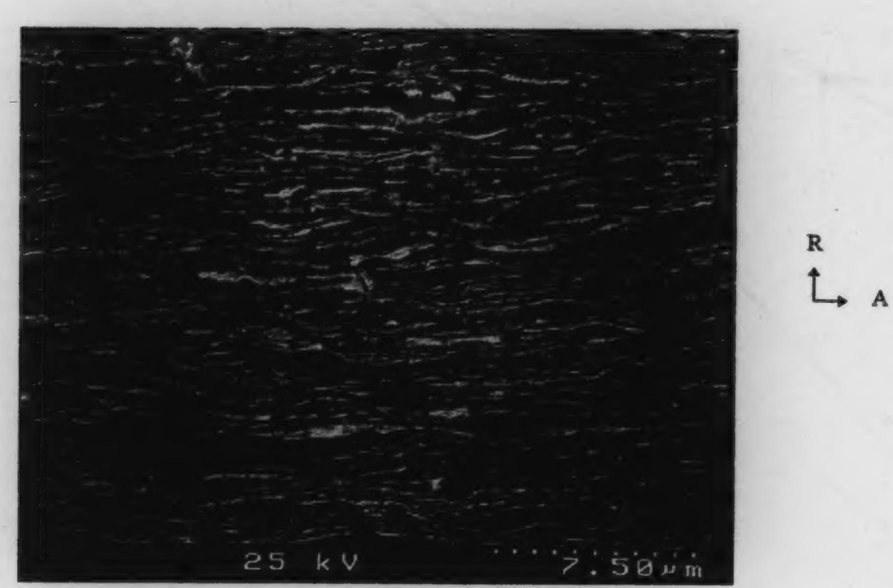
25 kV
7.50 μm
R
A

(g) axial-radial 60% additional CW 4000X

25 kV
3.75 μm
R
A

(h) axial-radial 60% additional CW 8000X

Figure 4-6 SEM micrograph of matrix material (cont.)

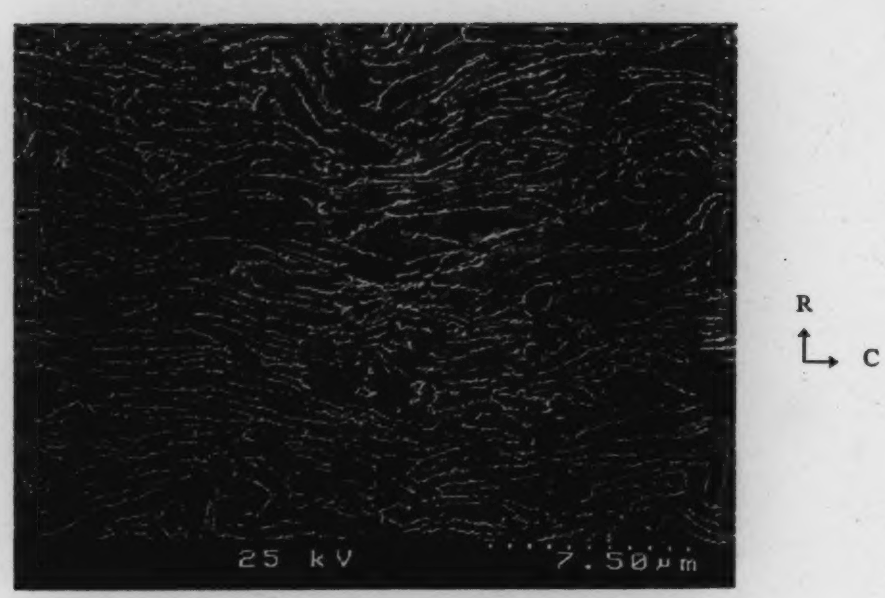
25 kV
7.50μm
R
C

(i) circumferential-radial 0% additional CW 4000X

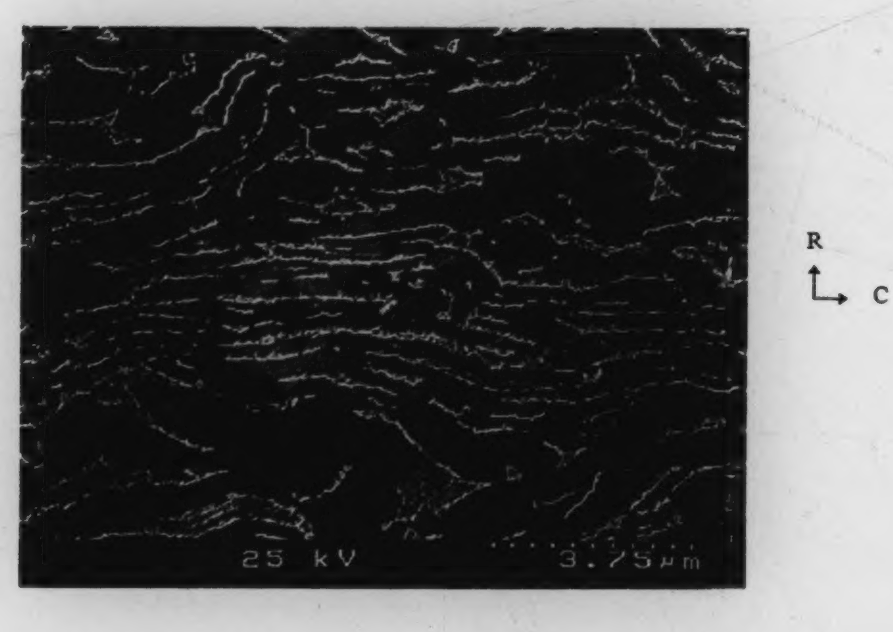
25 kV
3.75μm
R
C

(j) circumferential-radial 0% additional CW 8000X

Figure 4-6 SEM micrograph of matrix material (cont.)

25 kV
7.50μm
R
C

(k) circumferential-radial 20% additional CW 4000X

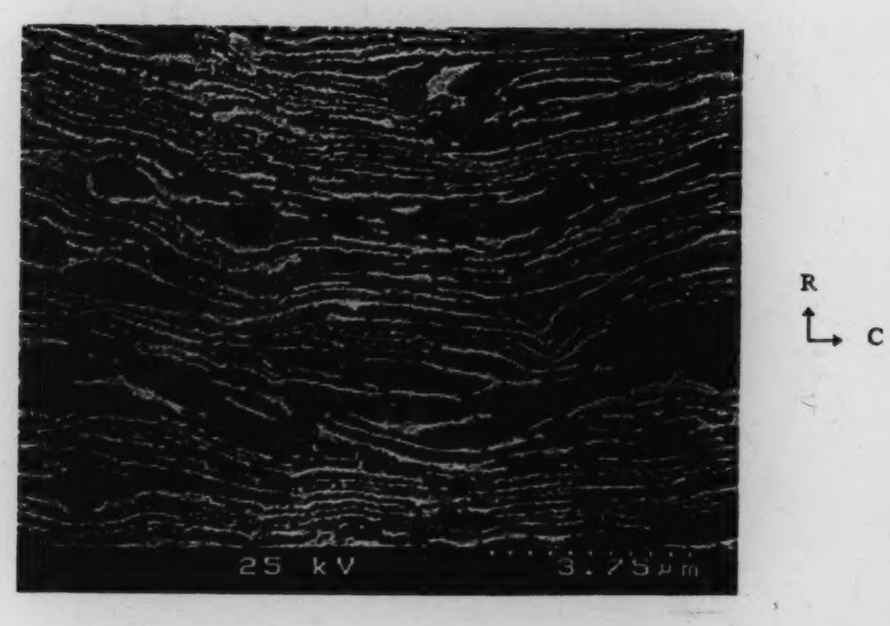
25 kV
3.75μm
R
C

(l) circumferential-radial 20% additional CW 8000X

Figure 4-6 SEM micrograph of matrix material (cont.)

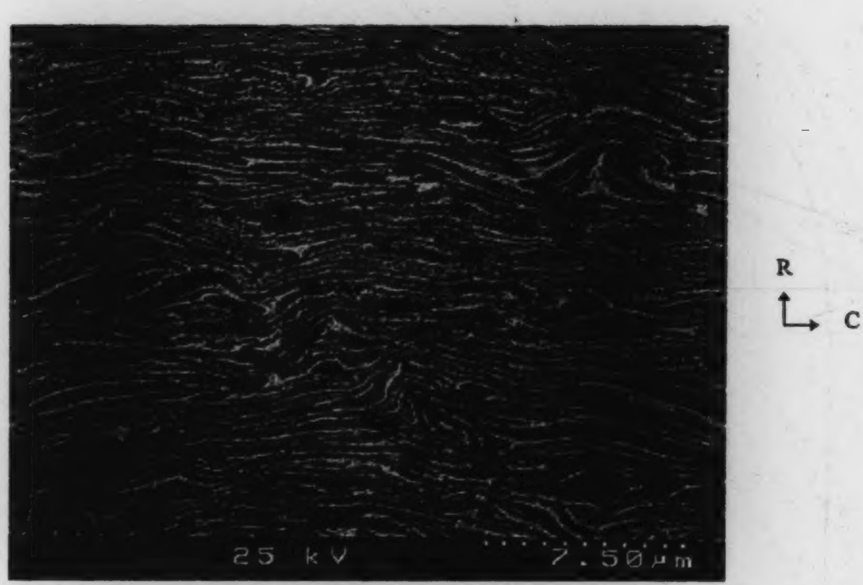
25 kV
7.50µm
R
C

(m) circumferential-radial 40% additional CW 4000X

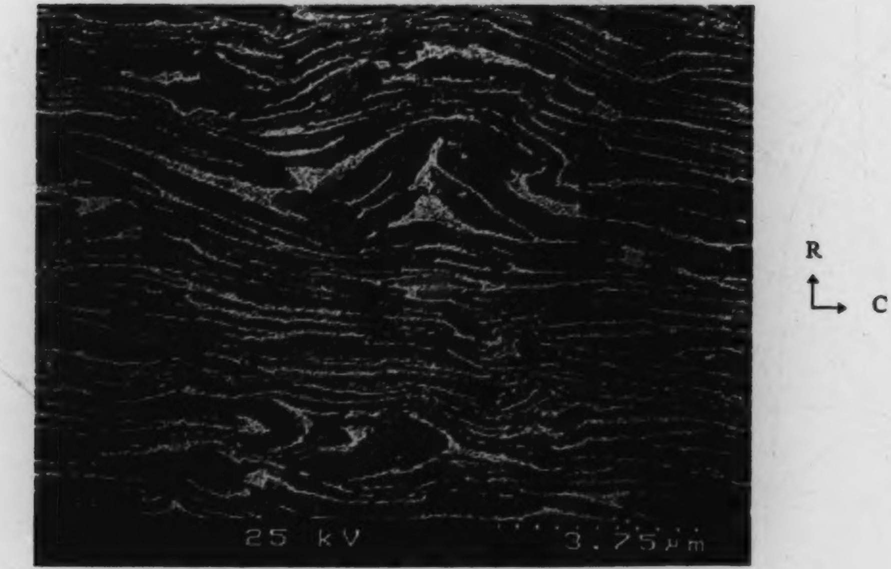
25 kV
3.75µm
R
C

(n) circumferential-radial 40% additional CW 8000X

Figure 4-6 SEM micrograph of matrix material (cont.)

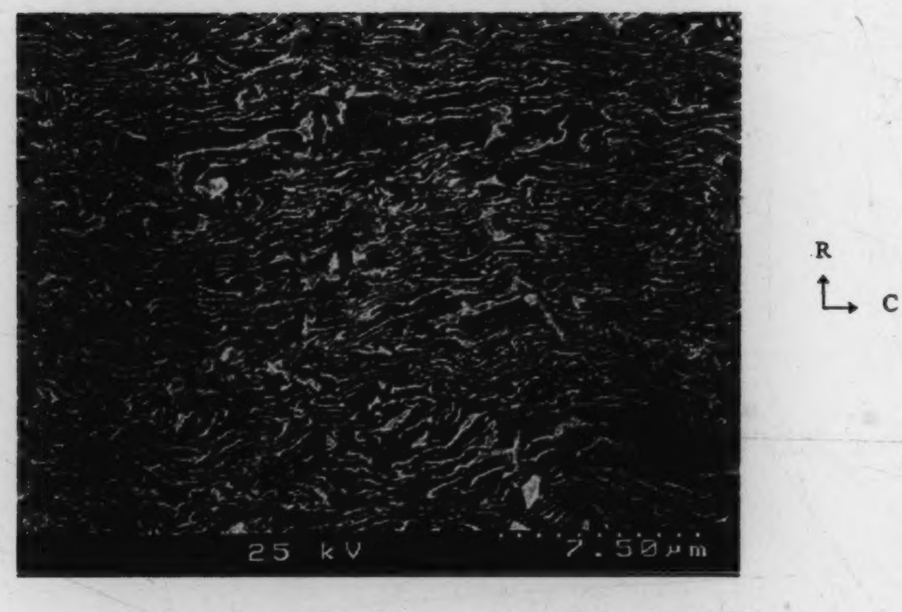
25 kV
7.50μm
R
C

(o) circumferential-radial 60% additional CW 4000X

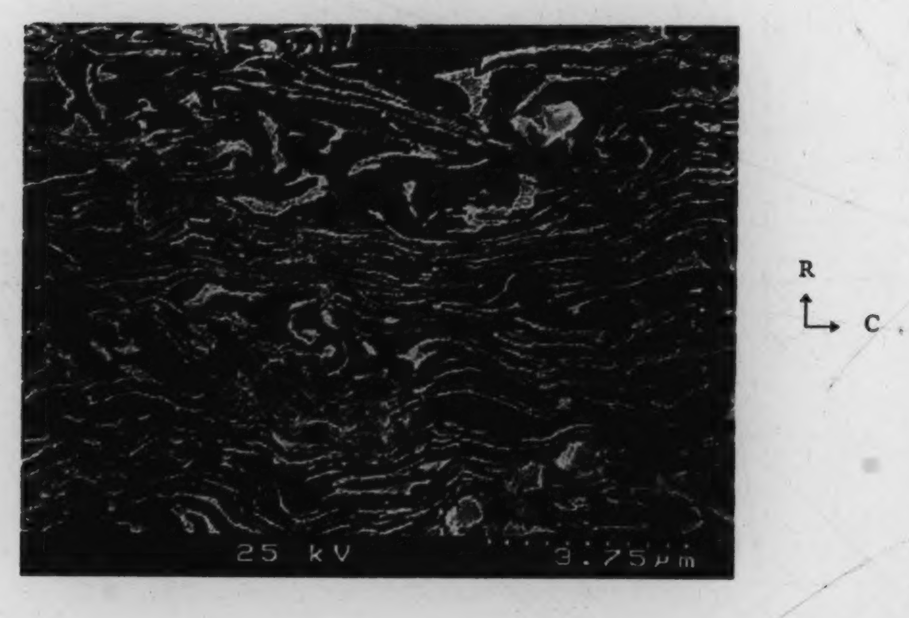
25 kV
3.75μm
R
C

(p) circumferential-radial 60% additional CW 8000X

Figure 4-6 SEM micrograph of matrix material (cont.)

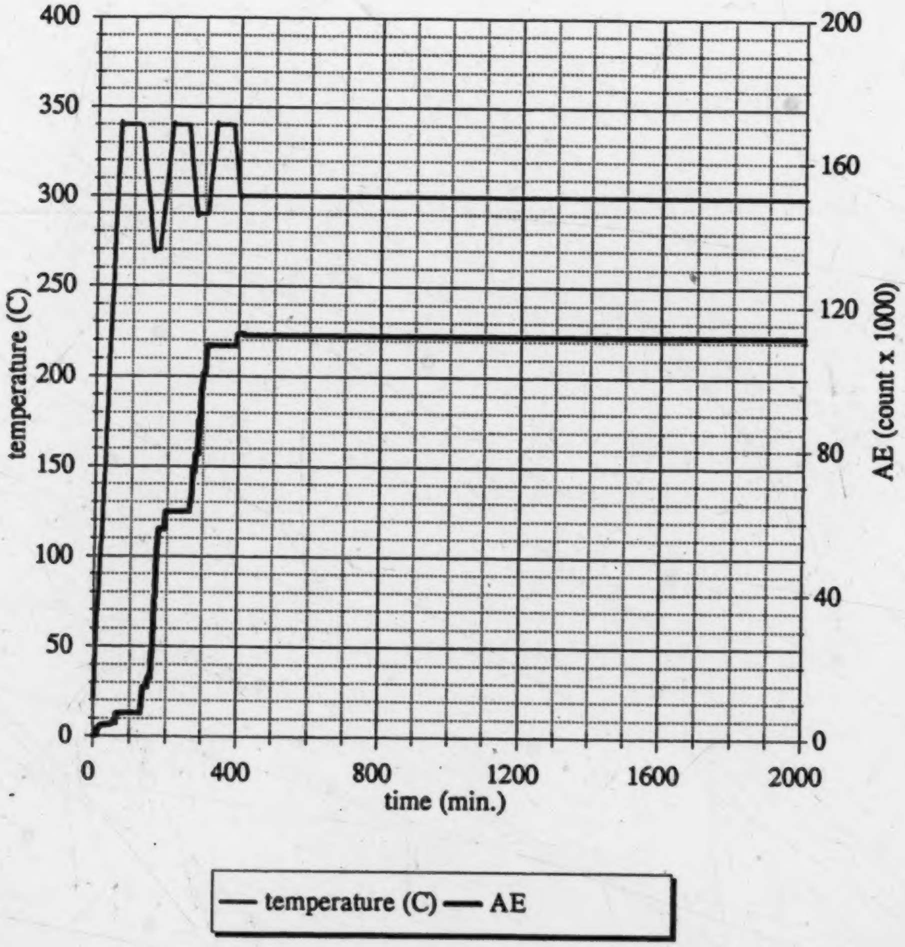

Figure 4-7 Typical AE measurement result for determining the Cracking Arrest Temperature (T_{CAT})

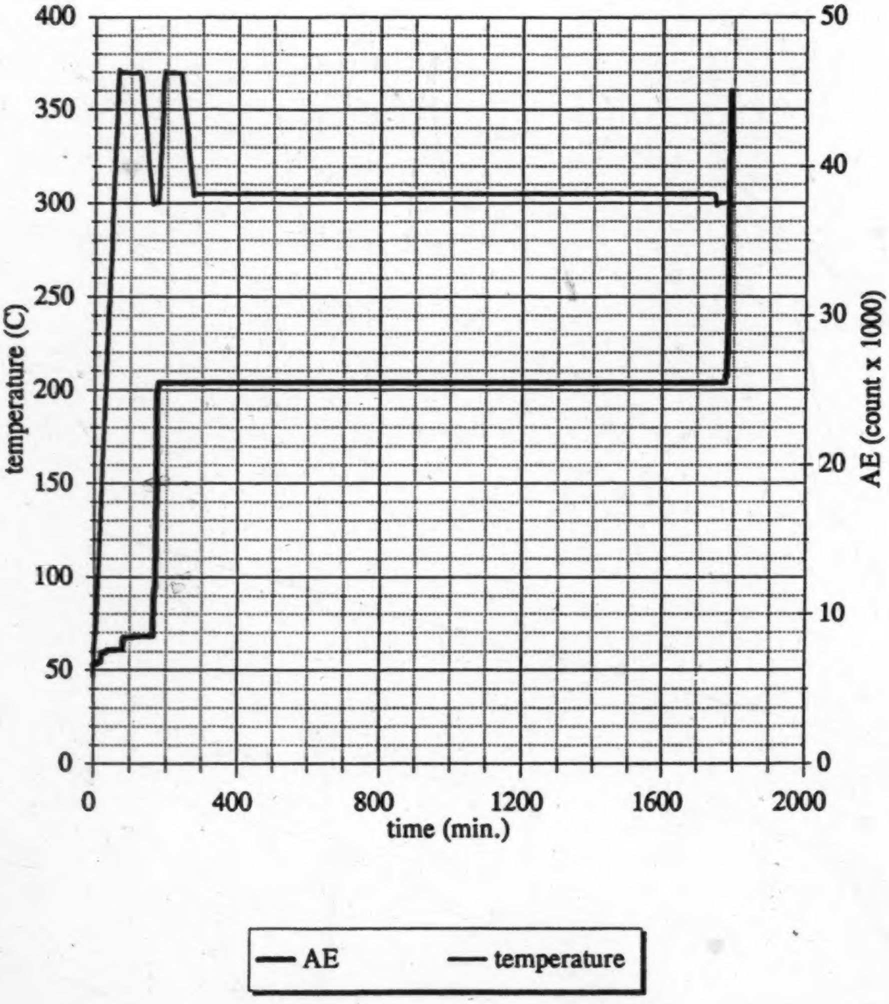

Figure 4-8 AE measurements at T_{CAT} (305°C) and at the temperature just below T_{CAT} (300°C). (Note the significant jump of acoustic emission when the test temperature is dropped from at 305 to 300°C.) H% =160 μg/g, K=17 MPa√m

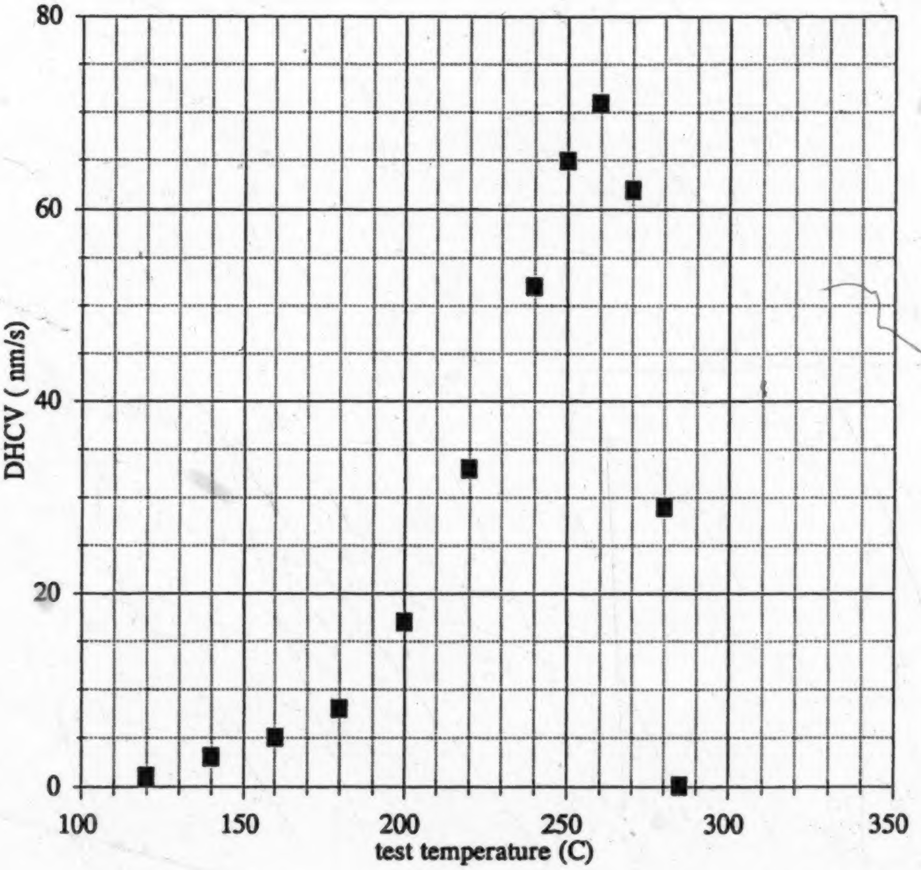

Figure 4-9a DHCV versus test temperature (0% additional CW, H%=160 μg/g, peak temperature = 320°C, K=17 MPa√m)

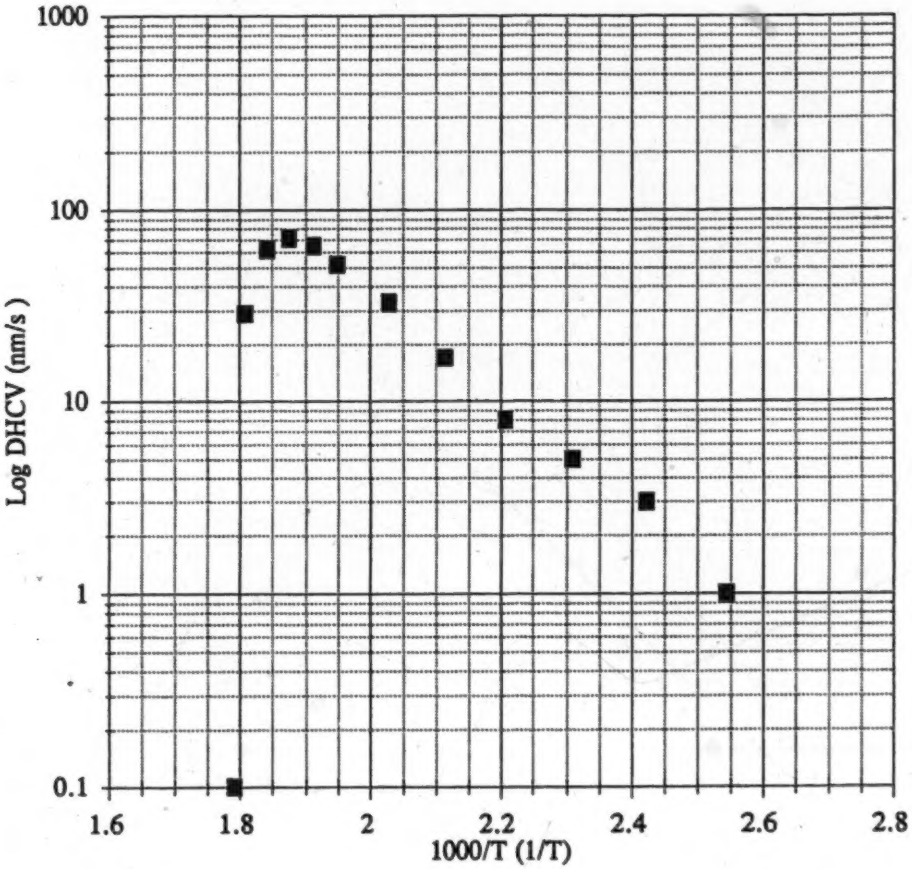

Figure 4-9b DHCV (log) versus test temperature (0% additional CW, H%=160 μg/g, peak temperature = 320°C, K=17 MPa√m)

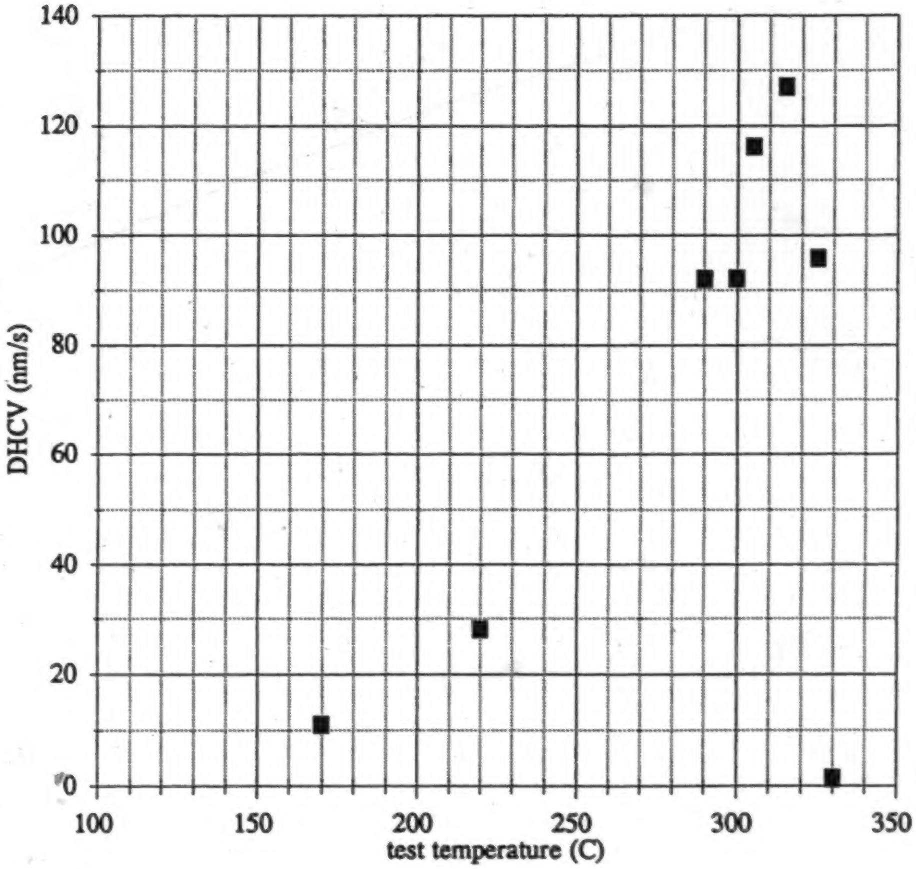

Figure 4-10a DHCV versus test temperature (0% additional CW, H%=160 μg/g, peak temperature = 370°C, K=17 MPa√m)

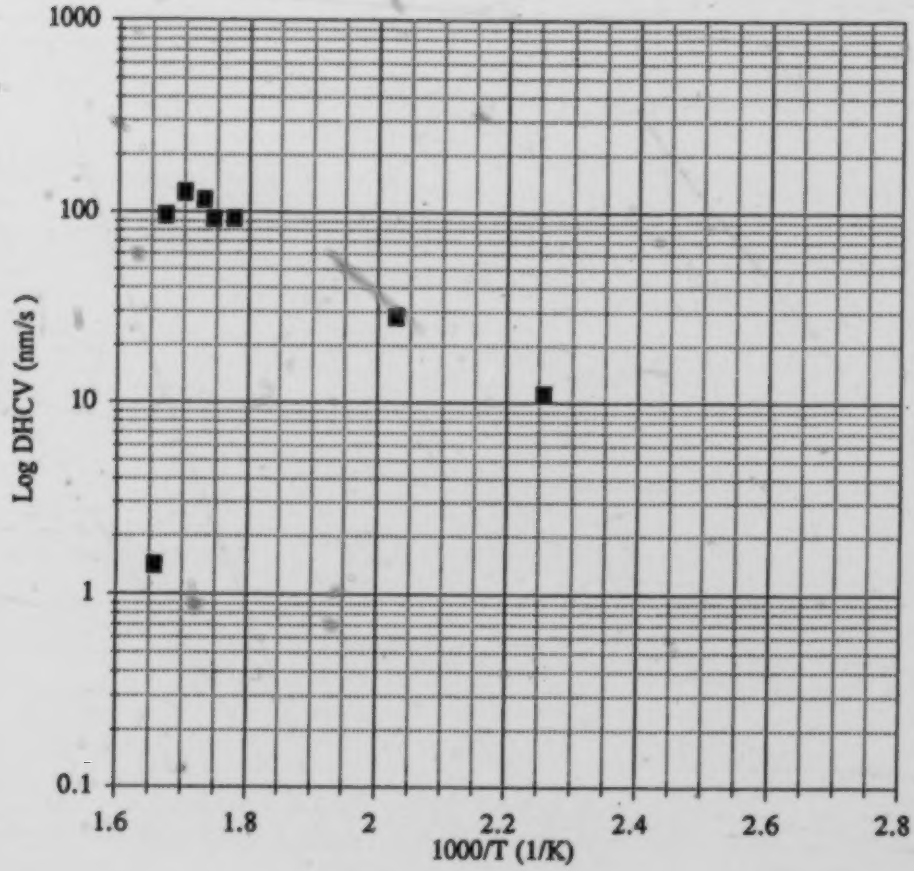

Figure 4-10b DHCV (log) versus test temperature (0% additional CW, H%=160 μg/g, peak temperature = 370°C, K=17 MPa√m)

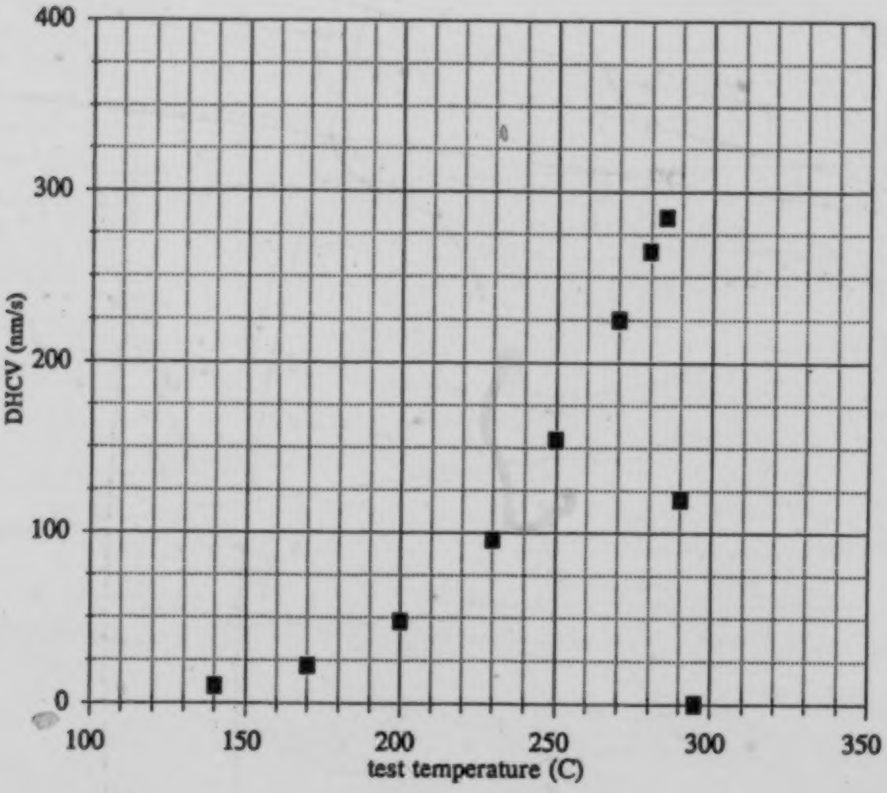

Figure 4-11a DHCV versus test temperature (40% additional CW, H%=160 μg/g, peak temperature = 320°C, K=17 MPa√m)

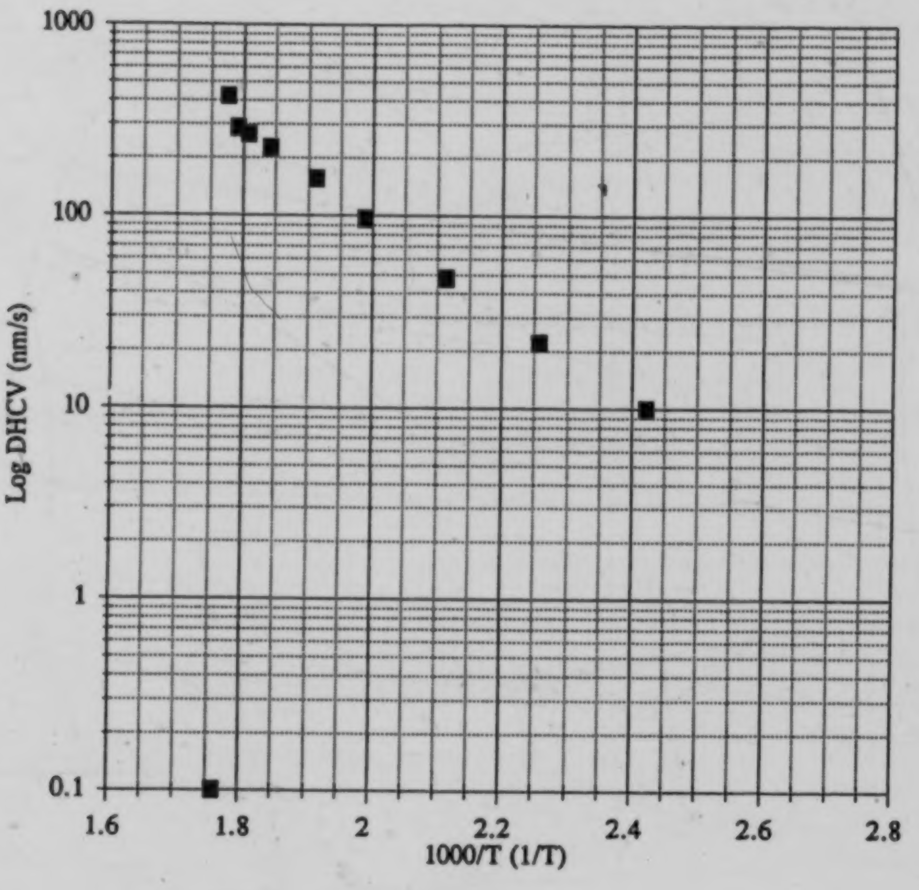

Figure 4-11b DHCV (log) versus test temperature (40% additional CW, H%=160 µg/g, peak temperature = 320°C, K=17 MPa√m)

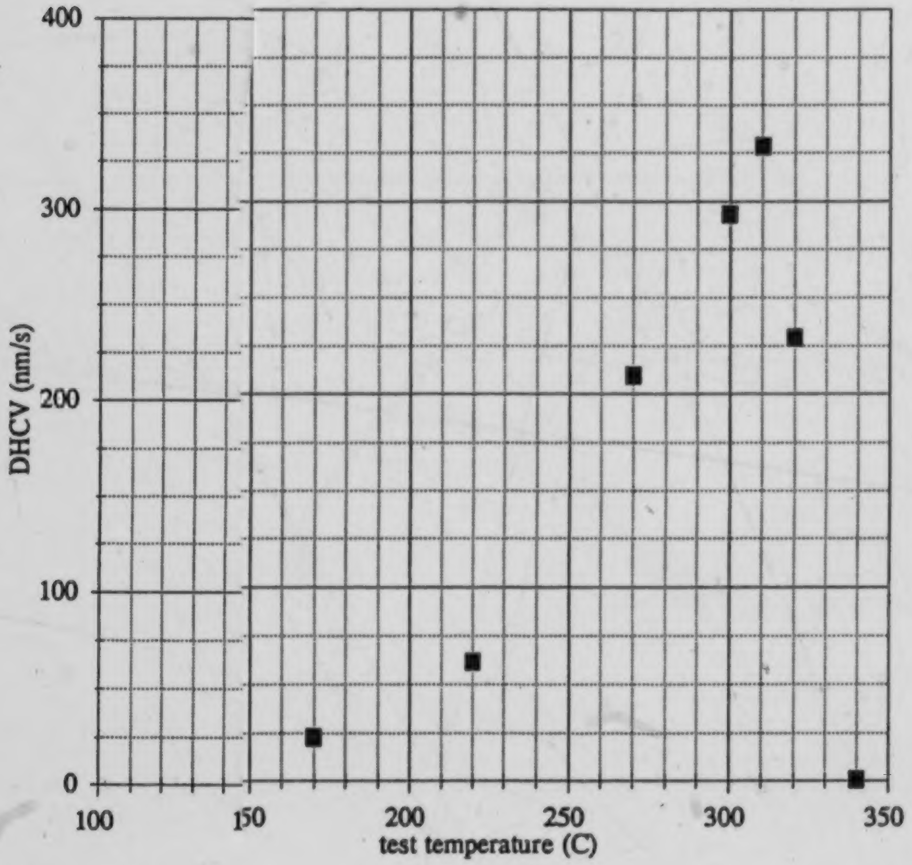

Figure 4-12a DHCV versus test temperature (40% additional CW, H%=160 µg/g, peak temperature = 370°C, K=17 MPa√m)

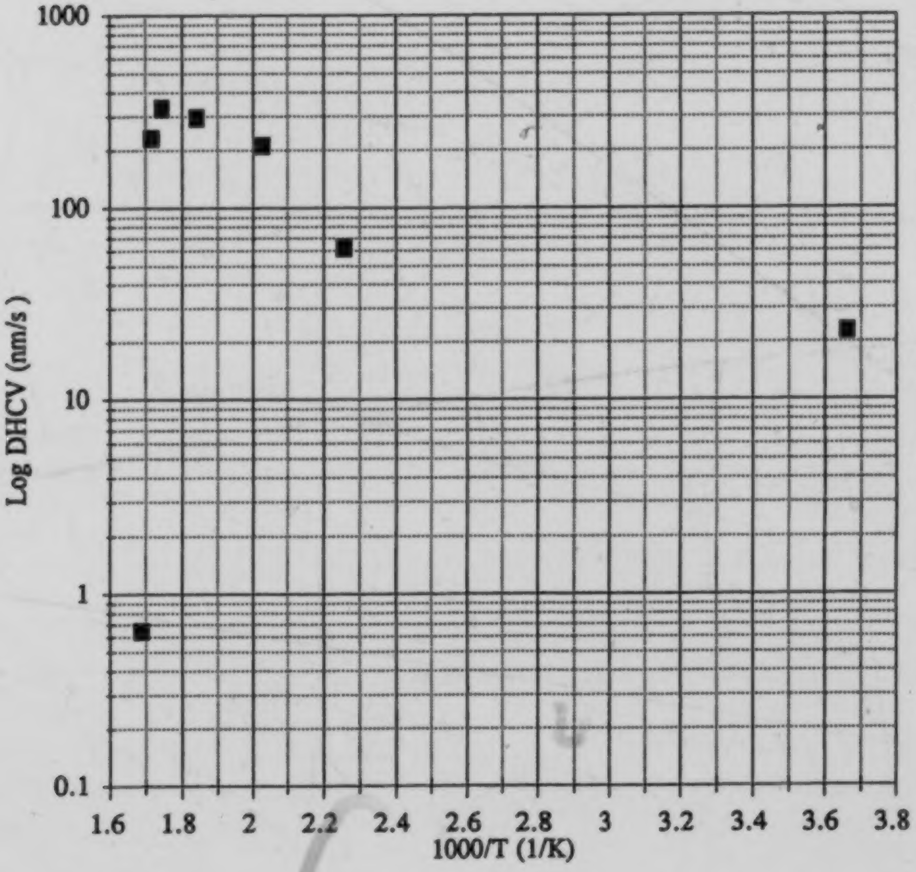

Figure 4-12b DHCV (log) versus test temperature (40% additional CW, H%=160 μg/g, peak temperature = 370°C, K=17 MPa√m)

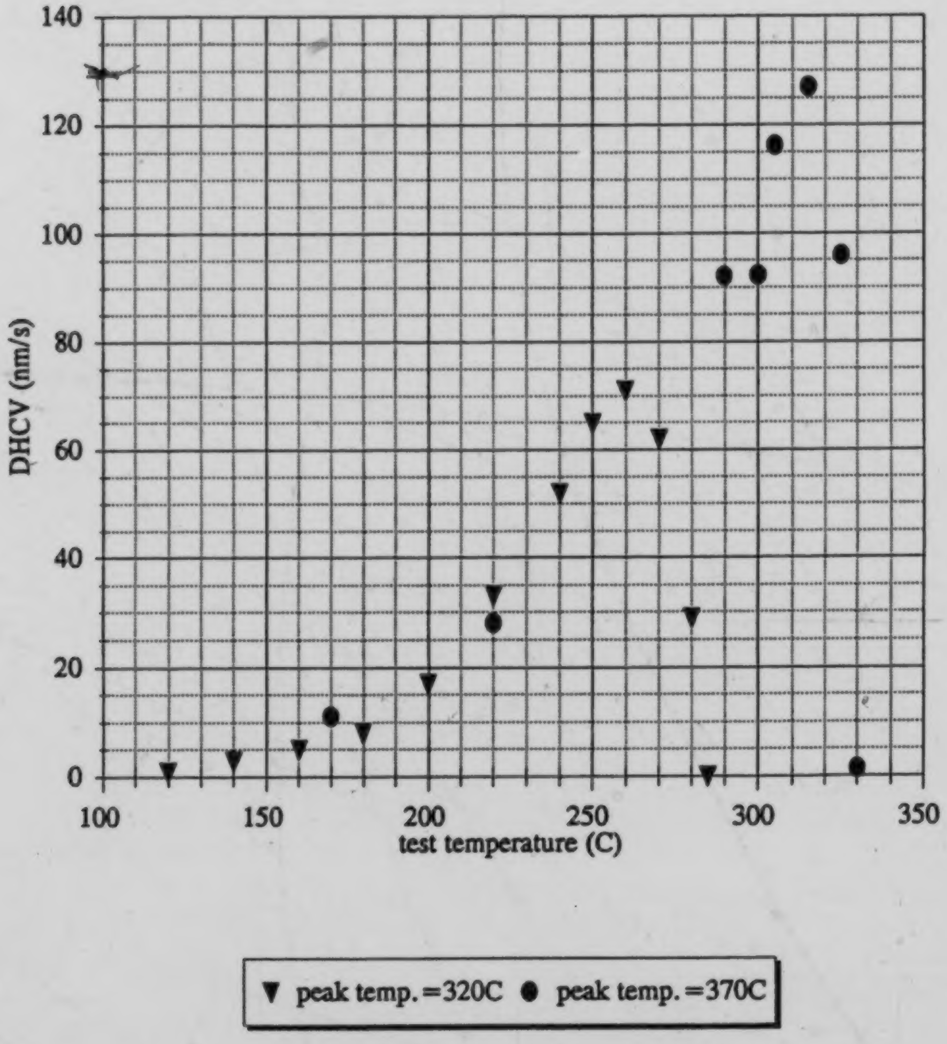

Figure 4-13 Summary of DHCV on as-manufactured (0% CW) specimens for different peak temperatures (H%=160 μg/g, K=17 MPa√m)

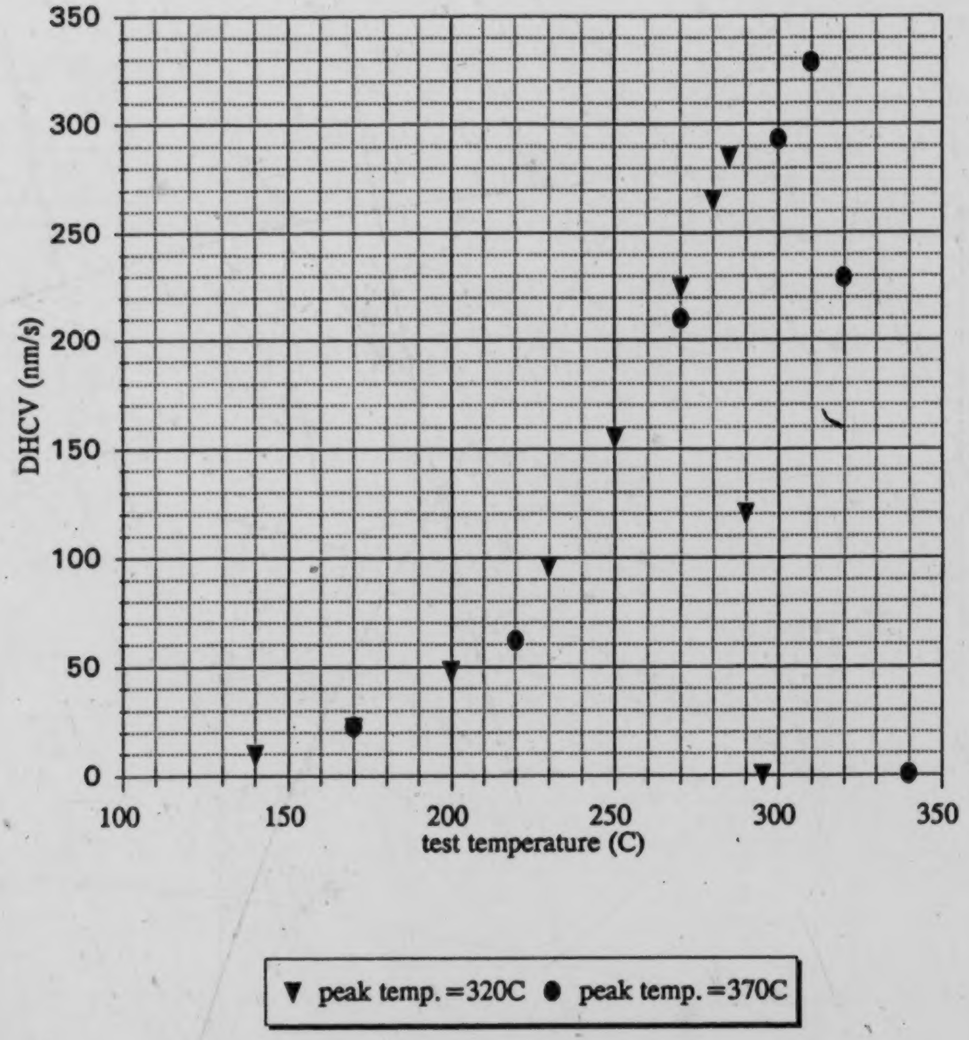

Figure 4-14 Summary of DHCV on additionally cold worked (40%CW) specimens for different peak temperatures (H%=160 μg/g, K=17 MPa√m)

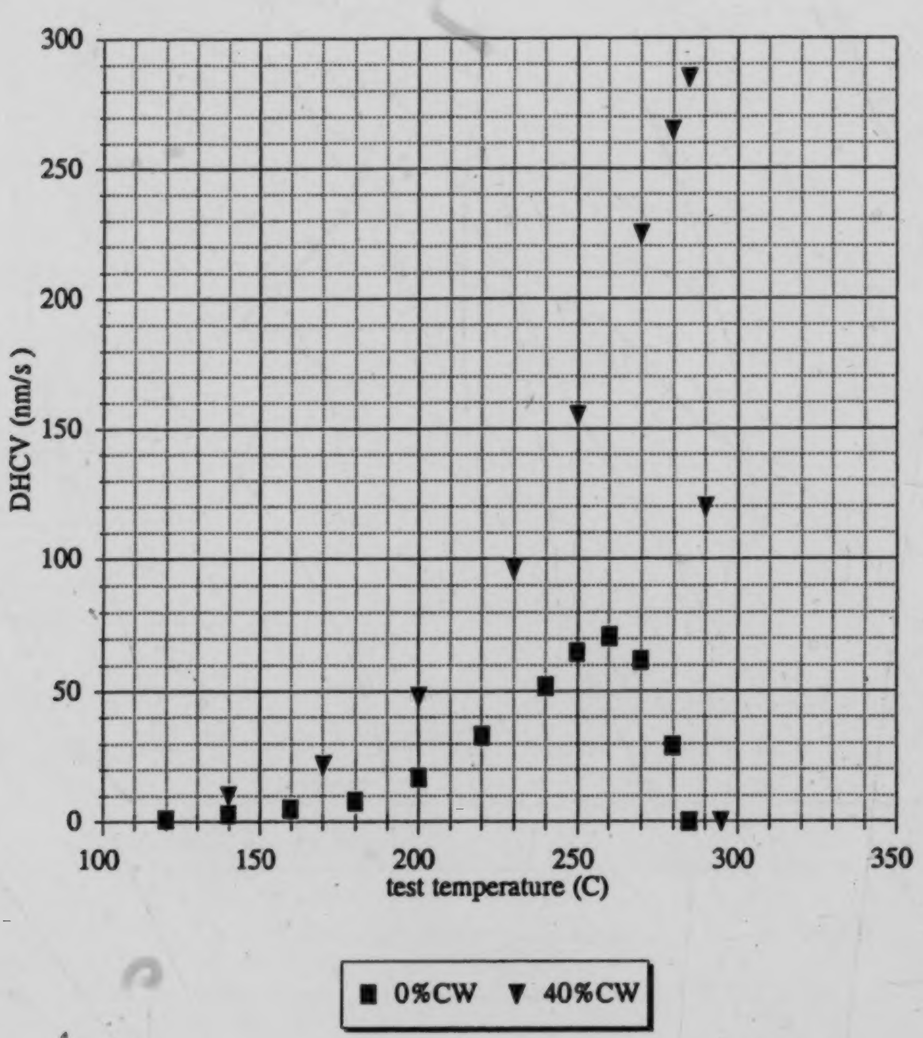

Figure 4-15 Measured DHCV on as-manufactured (0% CW) and additionally cold worked (40%CW) specimens under the same testing conditions (H%=160 μg/g , peak temperature = 320°C, K=17 MPa√m)

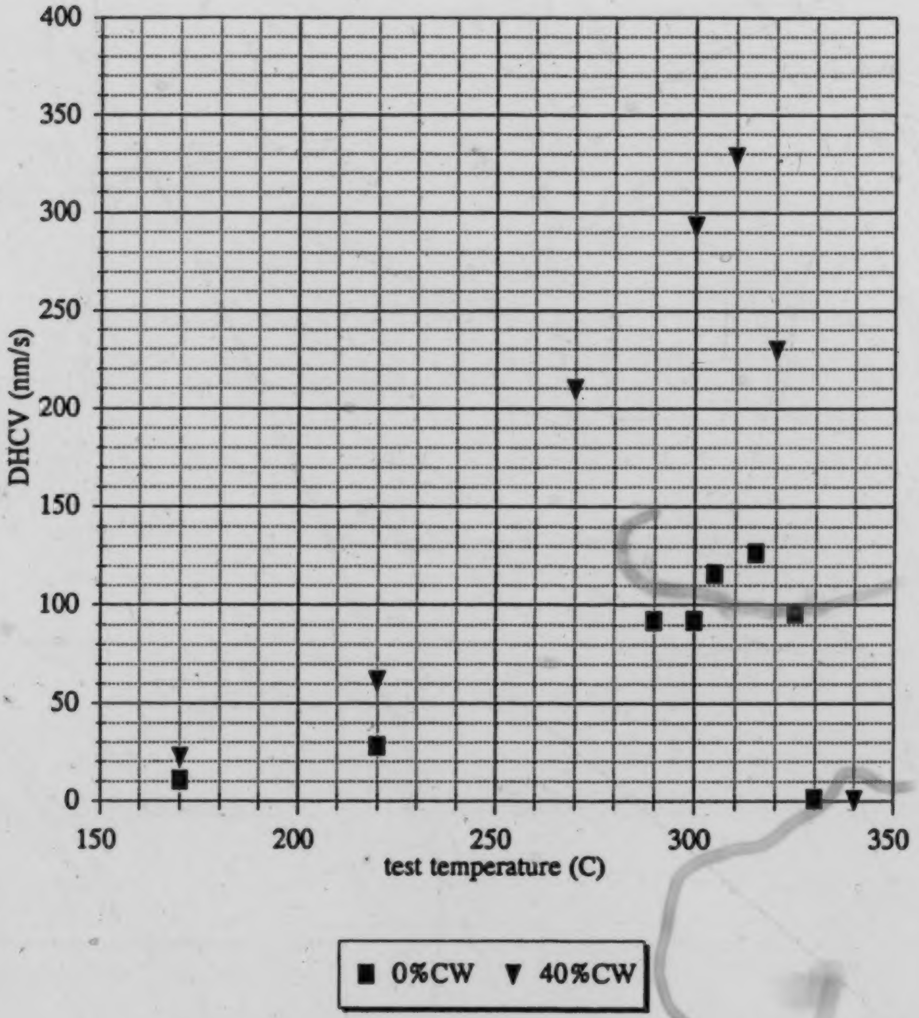

Figure 4-16 Measured DHCV on as-manufactured (0% CW) and additionally cold worked (40%CW) specimens under the same testing conditions (H%=160 μg/g , peak temperature = 370°C, K=17 MPa√m)

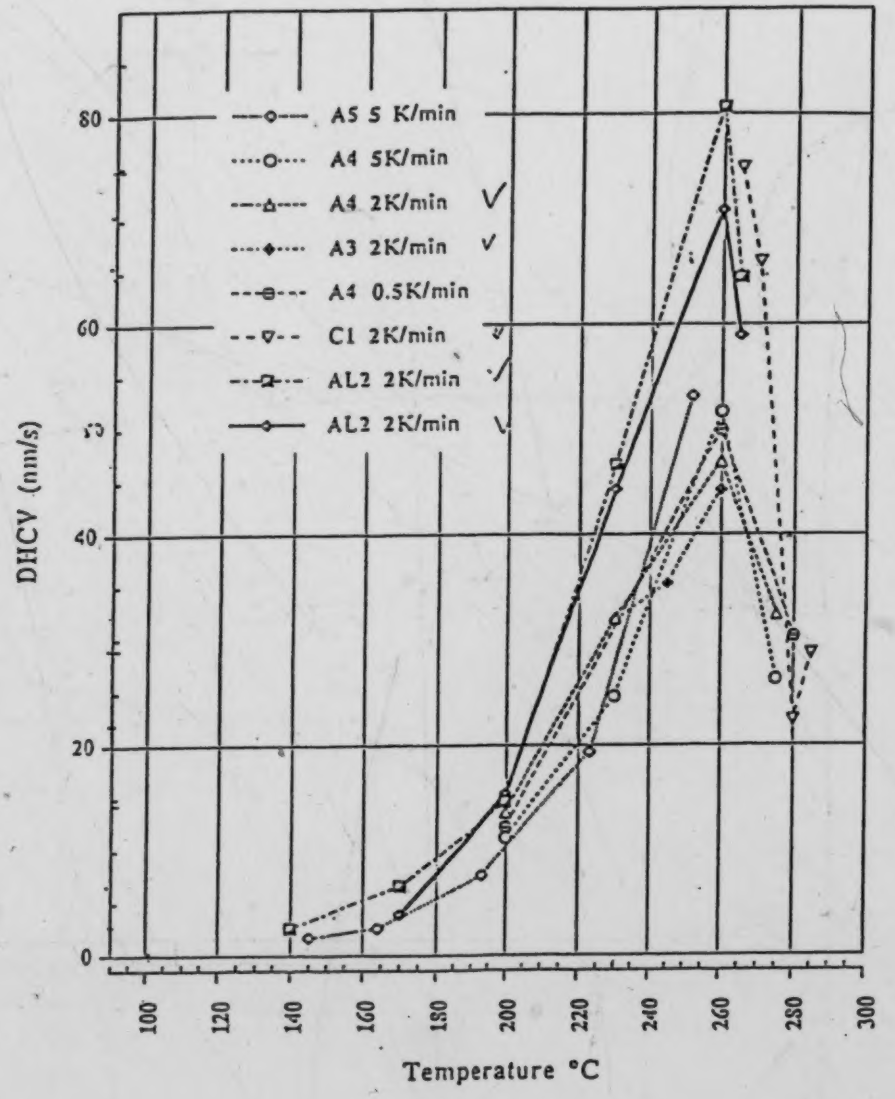

Figure 4-17 Summary of measured DHCV on as-manufactured specimens (peak temperature = 360°C, K=17 MPa√m) [73]

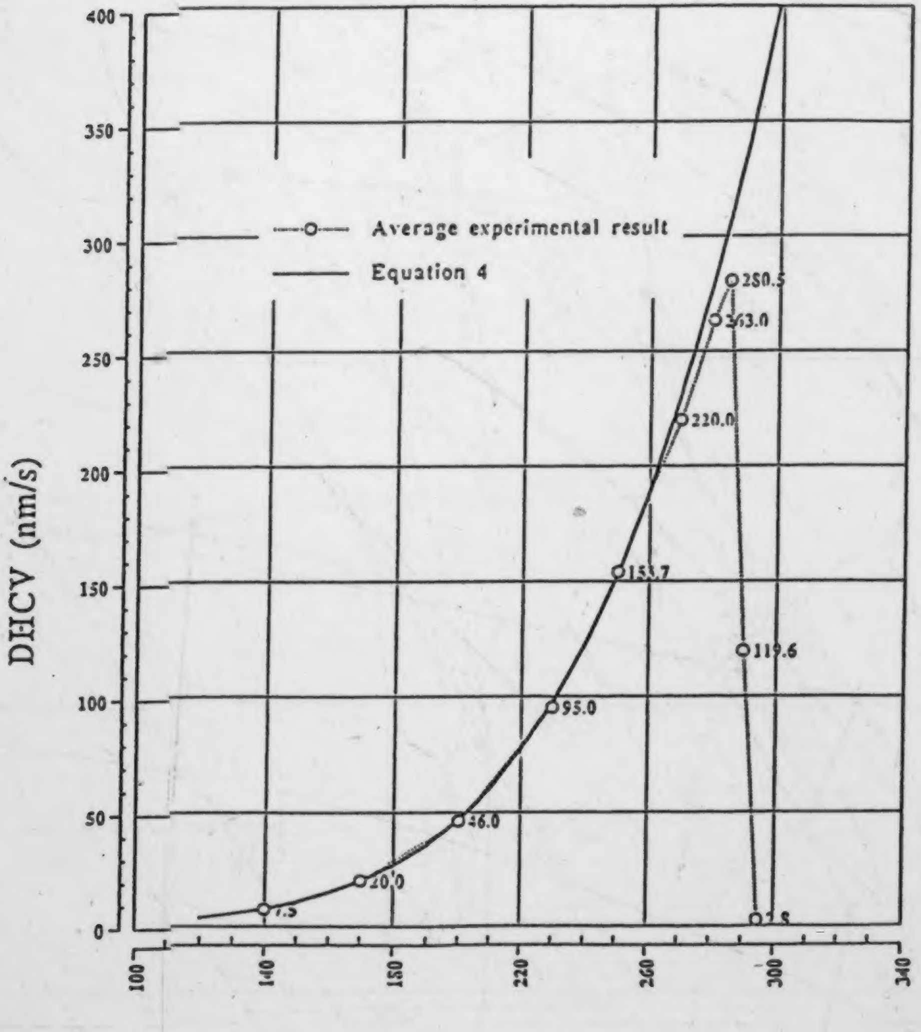

Figure 4-18 Summary of measured DHCV on 40% additionally cold worked specimens (peak temperature = 360°C, K=17 MPa√m) [73]

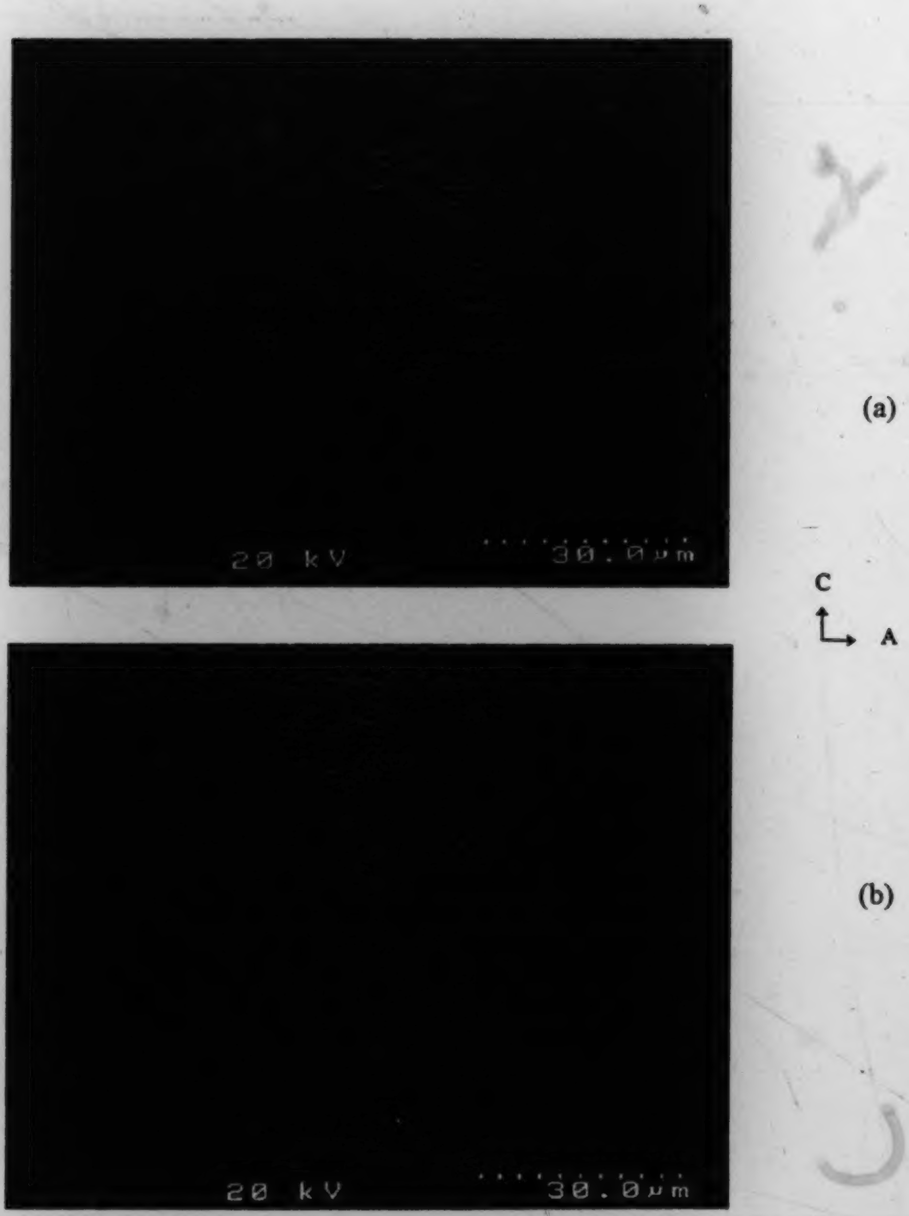
20 kV
30.0µm
(a)
C
A
20 kV
30.0µm
(b)

Figure 4-19 SEM micrograph (BSE image) of crack tip hydride image on axial-circumferential plane (0% additional CW) 1000X

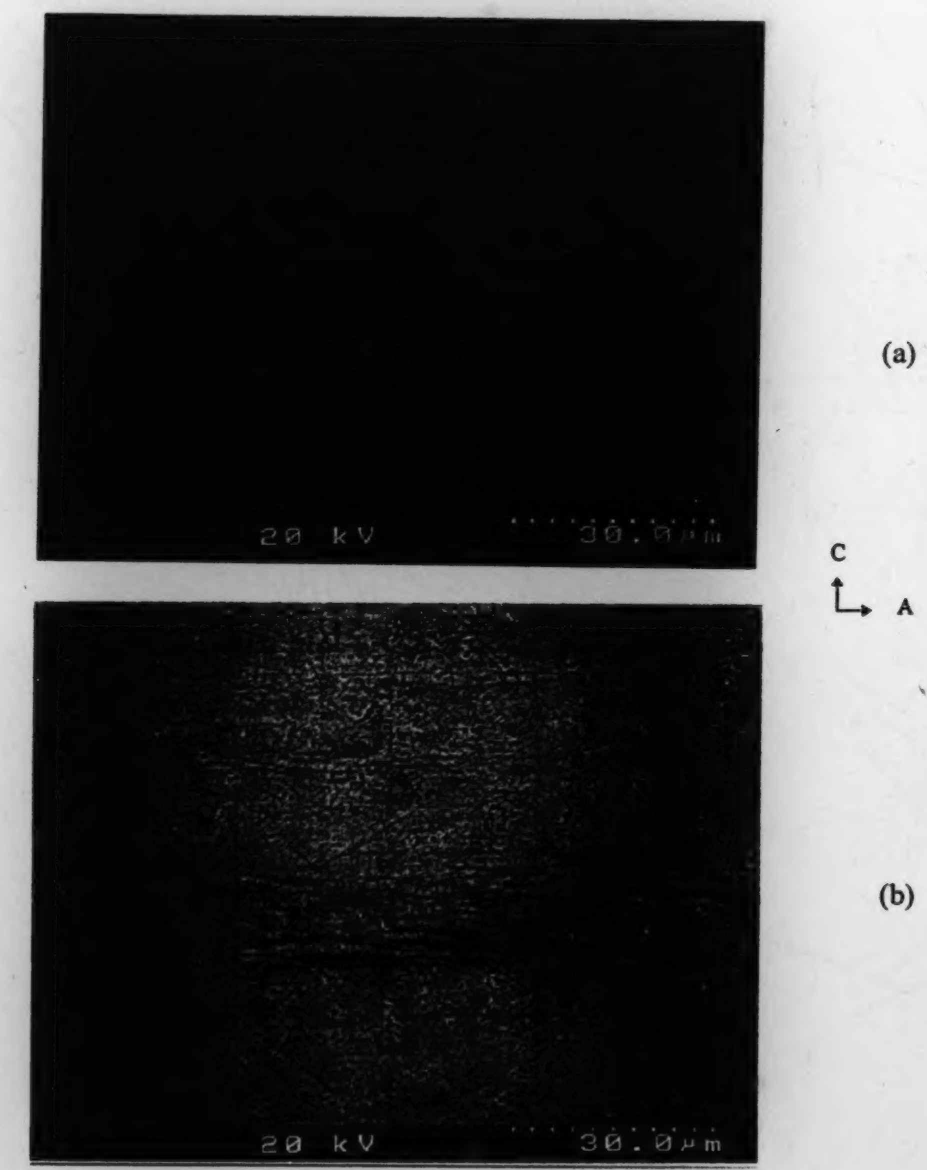
20 kV
30.0 μm
(a)
C
A
20 kV
30.0 μm
(b)

Figure 4-20 Axial-circumferential crack tip hydride image obtained in repeated tests on the same specimen used for obtaining Figure 4-19 (0% additional CW) 1000X

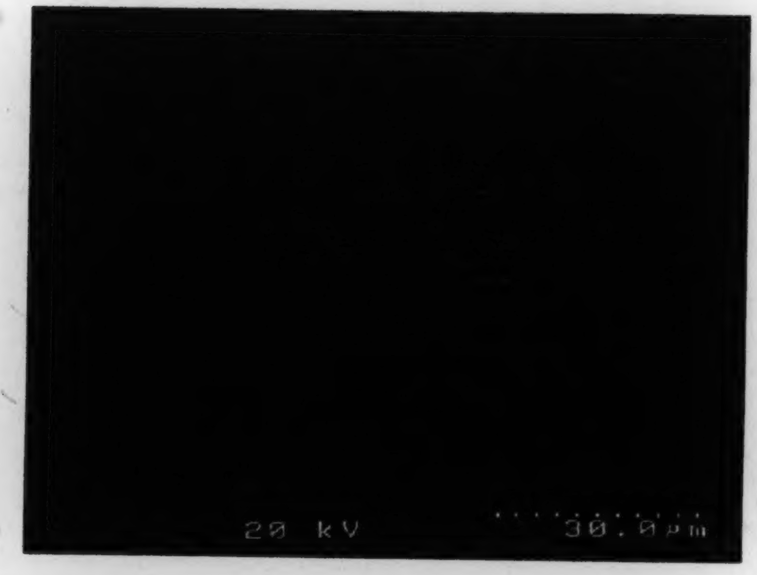

(a) 0%CW

Figure 4-21 Axial-circumferential crack tip hydride image obtained on specimens with different amounts of additional cold work 1000X

20 kV
30.0µm

(b) 20%CW

C
A

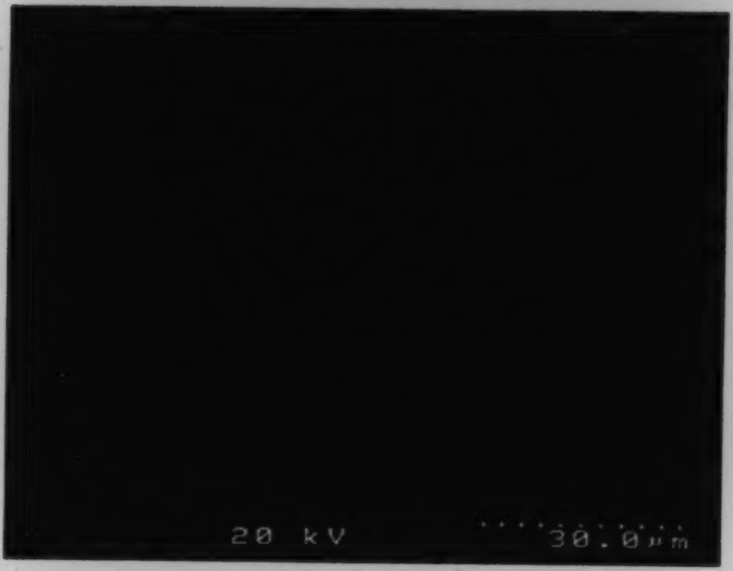

(c) 30%CW

Figure 4-21 Axial-circumferential crack tip hydride image obtained on specimens with different amounts of additional cold work (cont.) 1000X

20 kV
30.0µm

(d) 40%CW

C
A

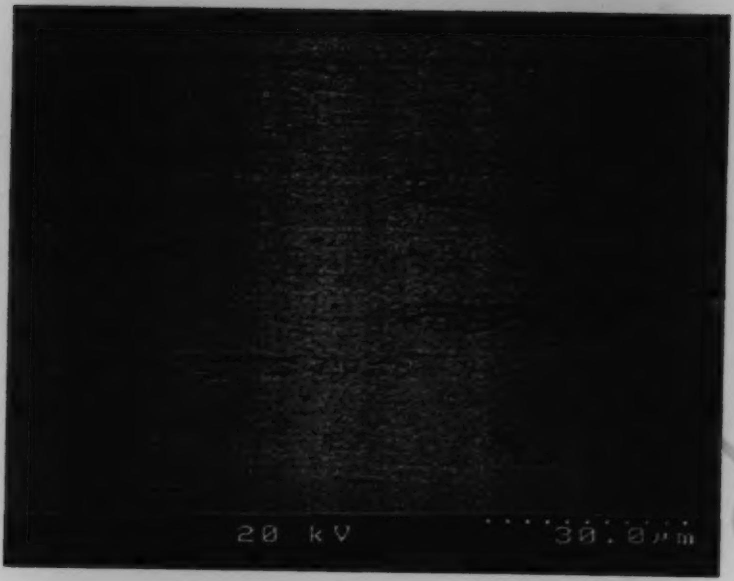

(e) 60%CW

Figure 4-21 Axial-circumferential crack tip hydride image obtained on specimens with different amounts of additional cold work (cont.) 1000X

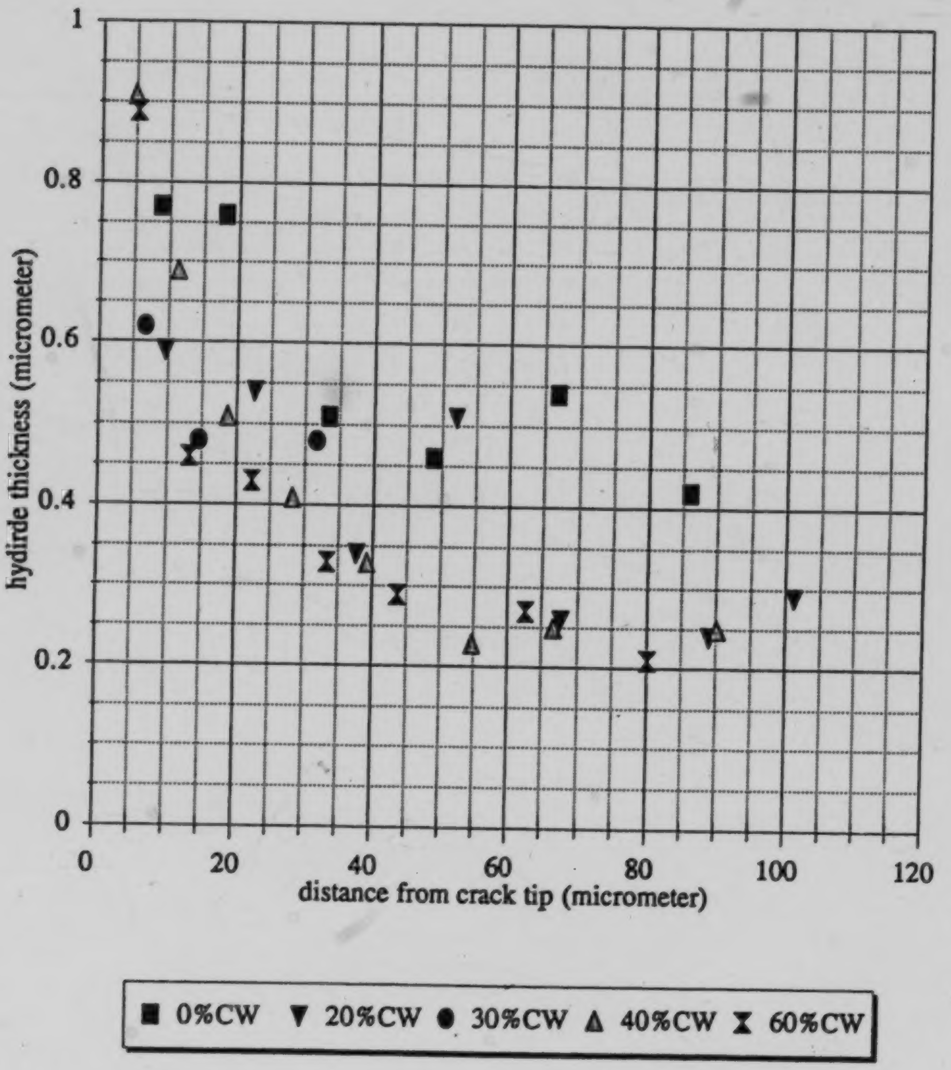

Figure 4-22 Hydride thickness versus location (see also Table 4-8)

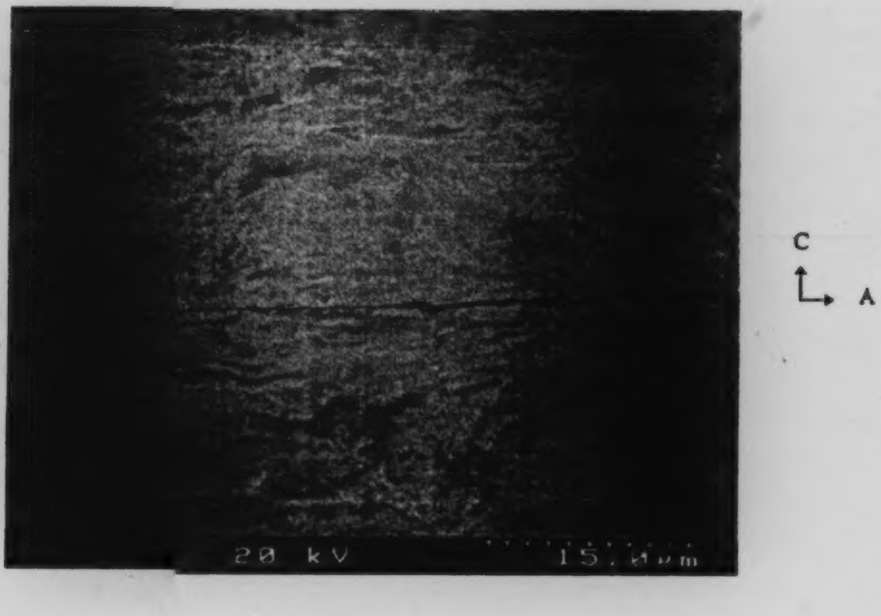

Figure 4-23 SEM micrograph (BSE image) of crack tip area at test temperatures below T_{CAT} on axial-circumferential plane

500X

20 kV
30.0 µm
C
A

Figure 4-24a Axial-circumferential crack tip hydride obtained after the first polish (0% additional CW) 1000X

20 kV
30.0µm
C
A

Figure 4-24b Axial-circumferential crack tip hydride obtained after the second polish (The specimen has been re-polished after getting Figure 4-29a. The specimen's thickness before re-polishing was 2.4 mm and after re-polishing was 2.36 mm.) (0% additional CW)

20 kV
30.0μm
C
A

Figure 4-24c Axial-circumferential crack tip hydride obtained after the third polish (The specimen's thickness after the third polish was 1.30 mm.) (0% additional CW) 1000X

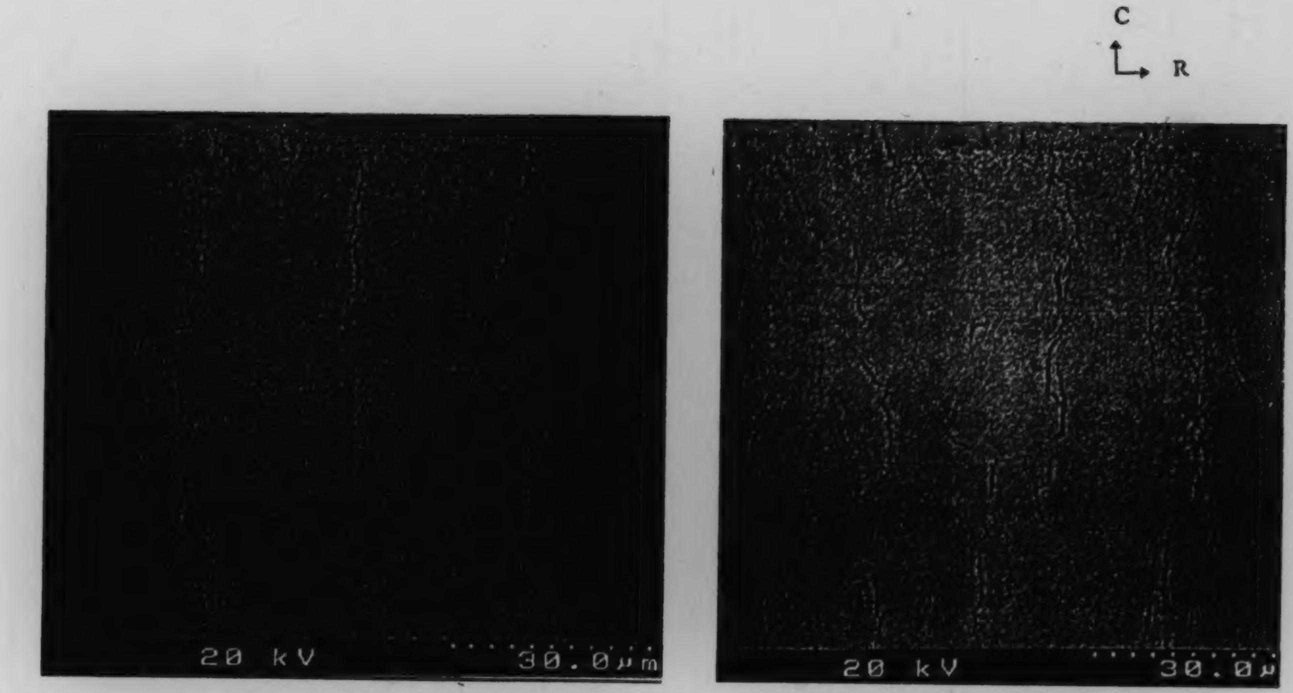
C
R
20 kV
30.0µm
20 kV
30.0µ

Figure 4-25 SEM micrograph (BSE image) of crack tip hydrides on circumferential-radial plane (0% additional CW) 1000X

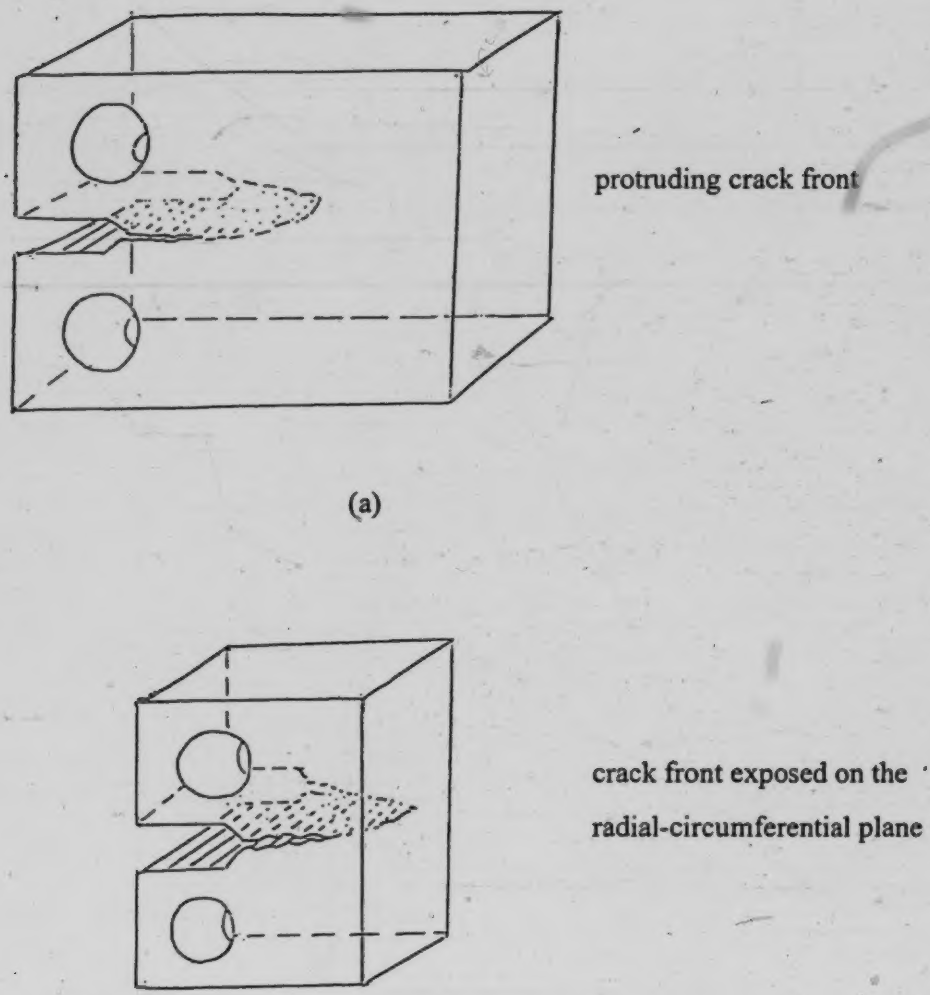
protruding crack front
crack front exposed on the
radial-circumferential plane

(a)

(b)

Figure 4-26 Schematic illustration of crack front

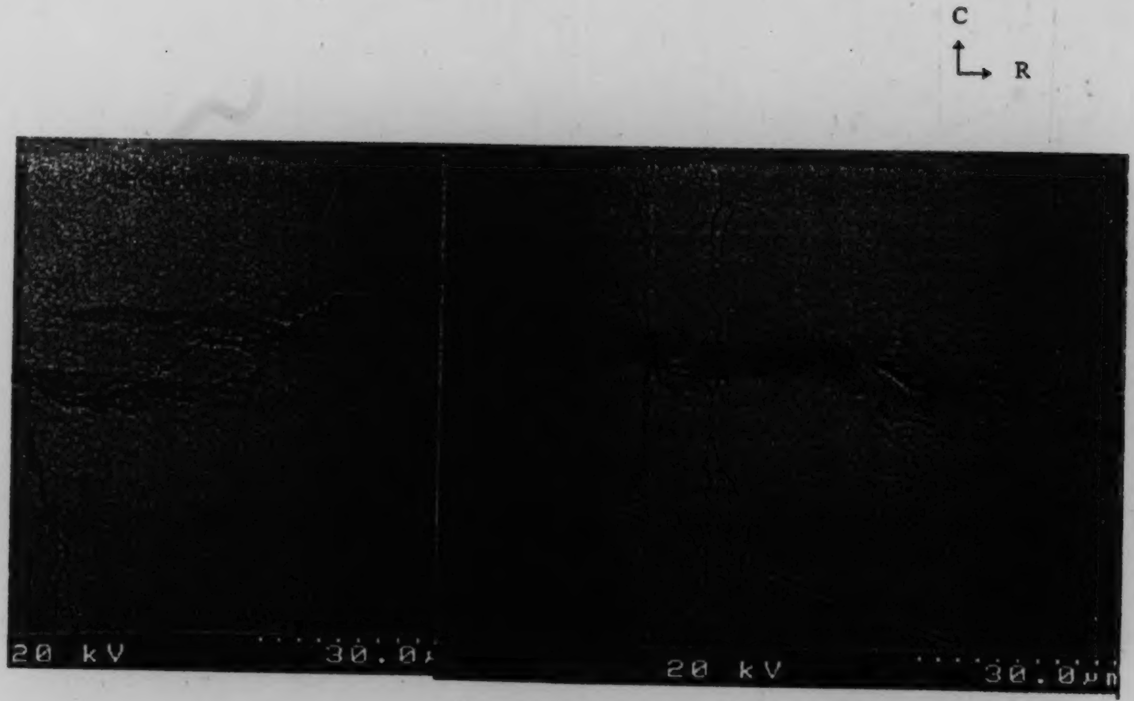
C
R
20 kV
30.0
20 kV
30.0μm

Figure 4-27 SEM micrograph (BSE image) of crack tip hydrides on circumferential-radial plane (0% additional CW) 1000X

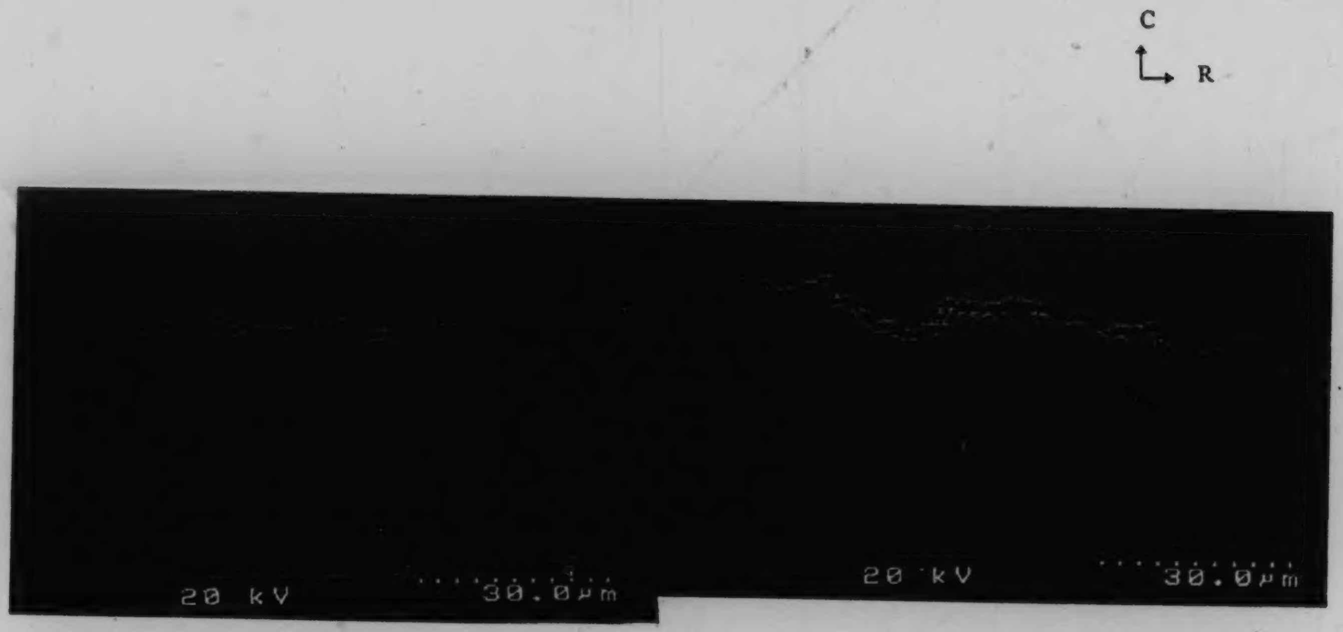
C
R
20 kV
30.0μm
20 kV
30.0μm

Figure 4-28 SEM micrograph (BSE image) of crack tip hydrides on circumferential-radial plane (40% additional CW) 1000X

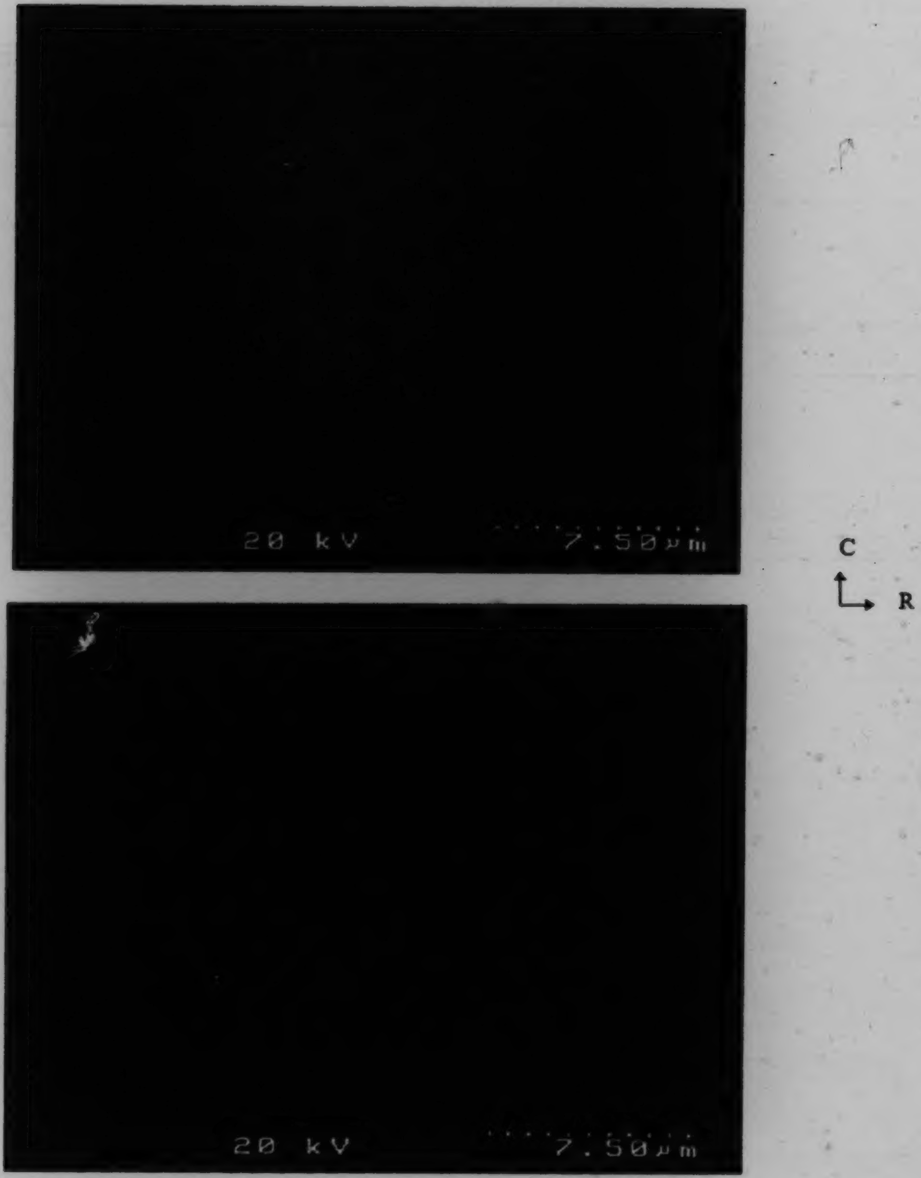
20 kV
7.50µm
C
R
20 kV
7.50µm

Figure 4-29 SEM micrograph (BSE image) of crack tip hydrides on circumferential-radial plane (0% additional CW) 4000X

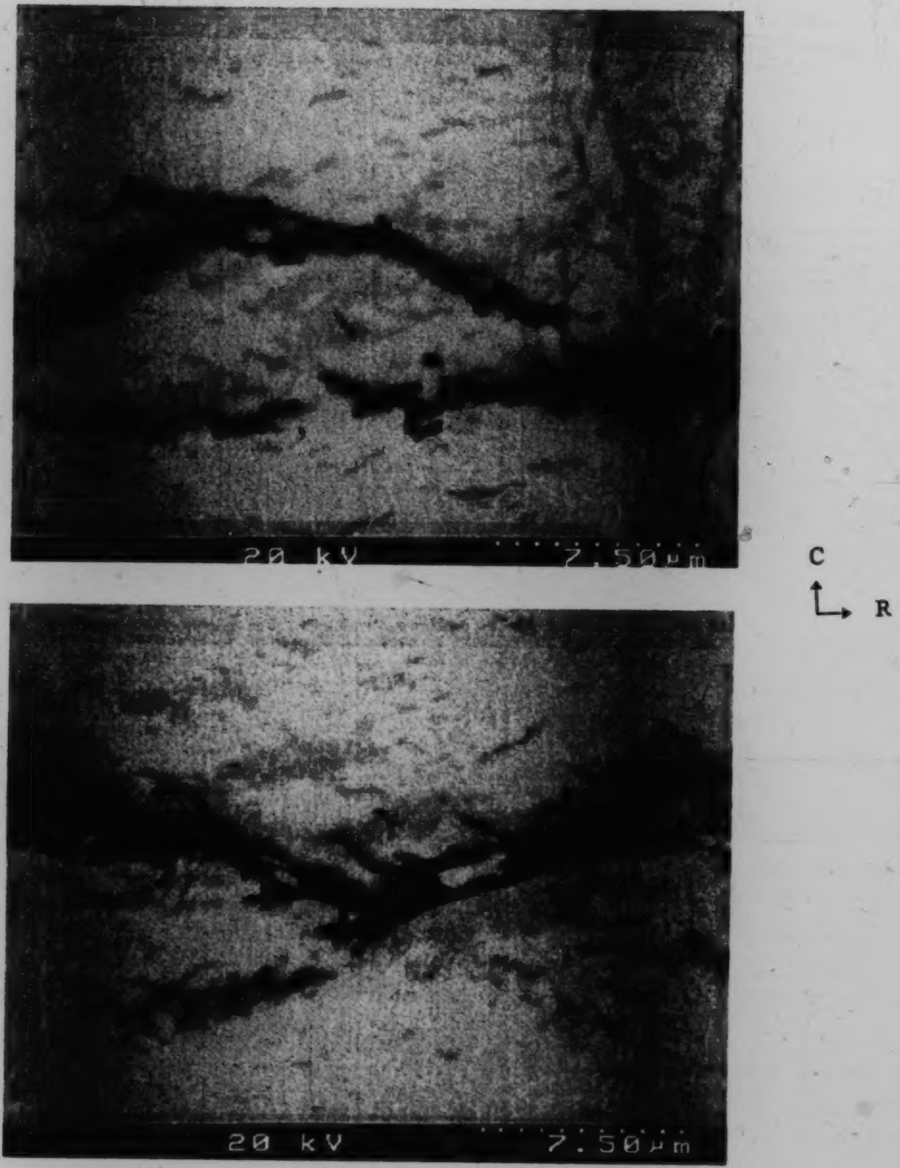
20 kV
7.50µm
C
R
20 kV
7.50µm

Figure 4-30 SEM micrograph (BSE image) of crack tip hydrides on circumferential-radial plane (0% additional CW) 4000X

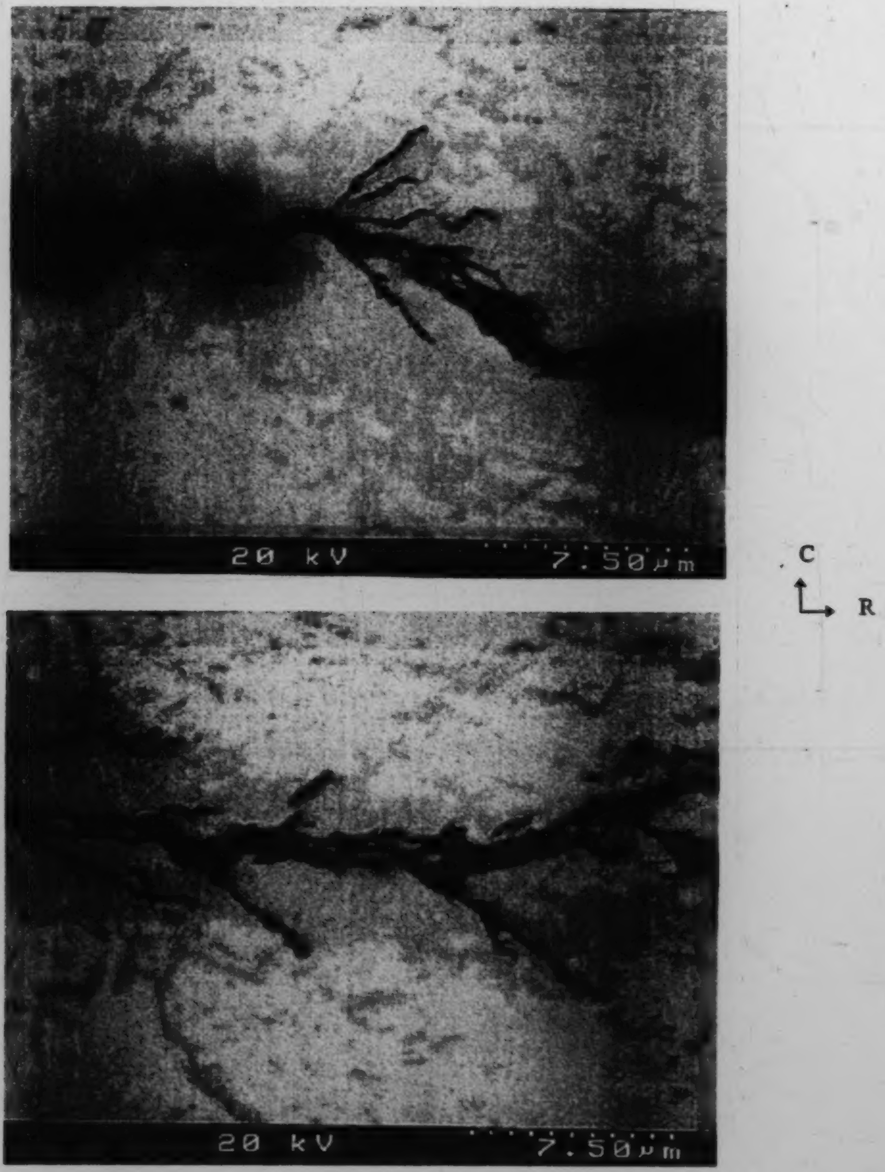
20 kV
7.50 μm
C
R
20 kV
7.50 μm

Figure 4-31 SEM micrograph (BSE image) of crack tip hydrides on circumferential-radial plane (0% additional CW) 4000X

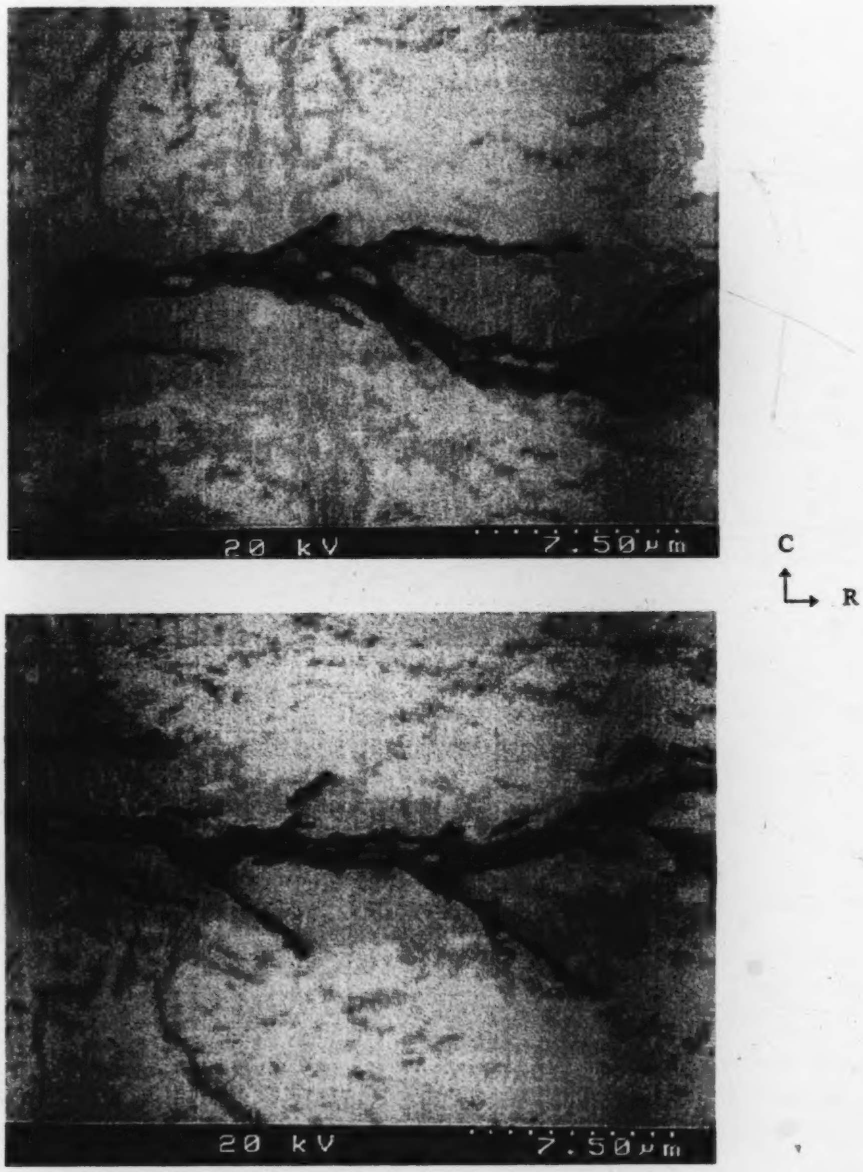
20 kV
7.50µm
C
R
20 kV
7.50µm

Figure 4-31 SEM micrograph (BSE image) of crack tip hydrides on circumferential-radial plane (0% additional CW) (cont.) 4000X

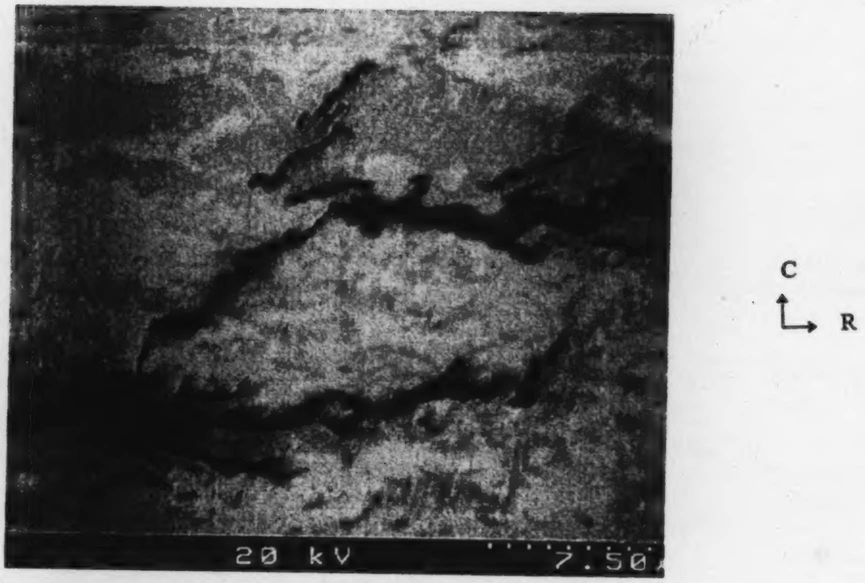

Figure 4-32 SEM micrograph (BSE image) of crack tip hydrides on circumferential-radial plane (0% additional CW) 4000X

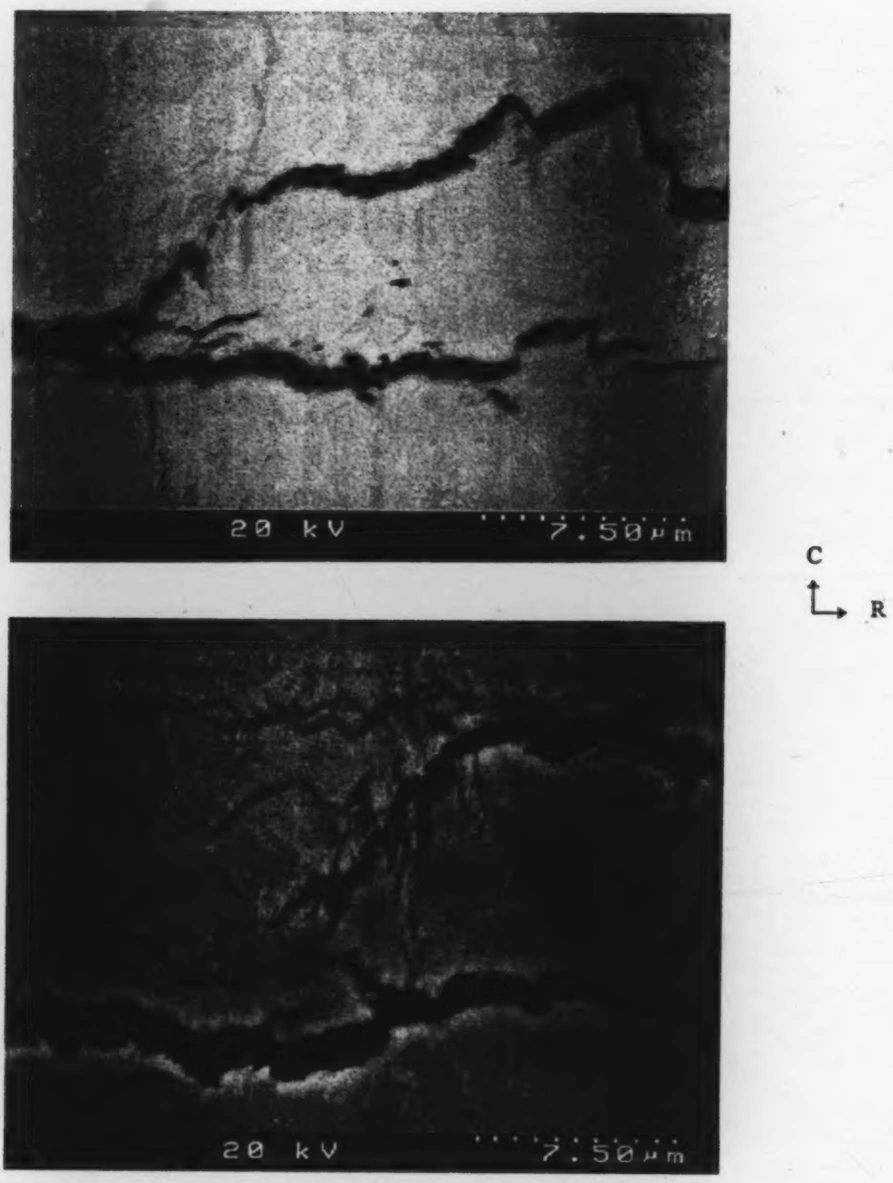
20 kV
7.50µm
C
R
20 kV
7.50µm

Figure 4-32 SEM micrograph (BSE image) of crack tip hydrides on circumferential-radial plane (0% additional CW) (cont.) 4000X

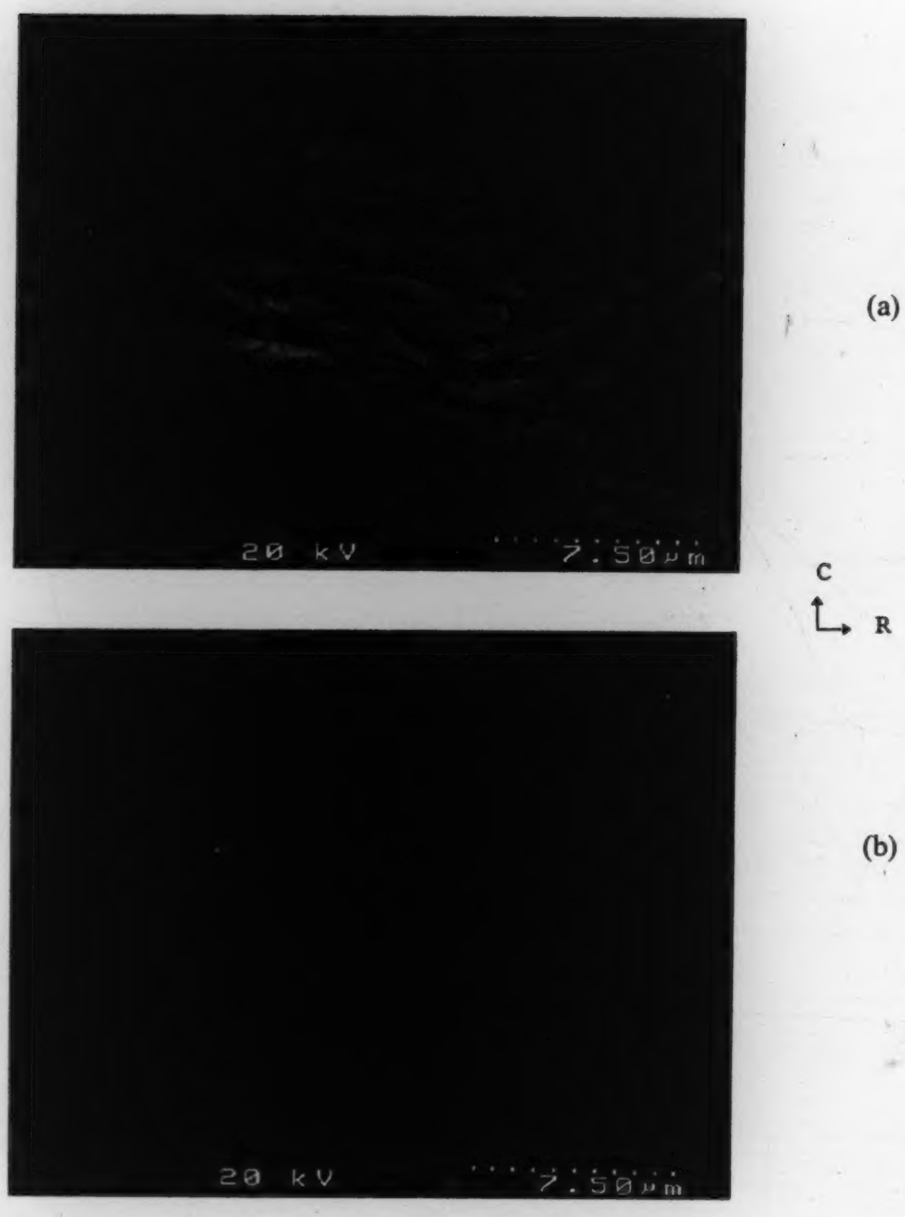
20 kV
7.50μm
(a)
C
R
20 kV
7.50μm
(b)

Figure 4-33 SEM micrograph (BSE image) of crack tip hydrides on circumferential-radial plane (0% additional CW) 4000X

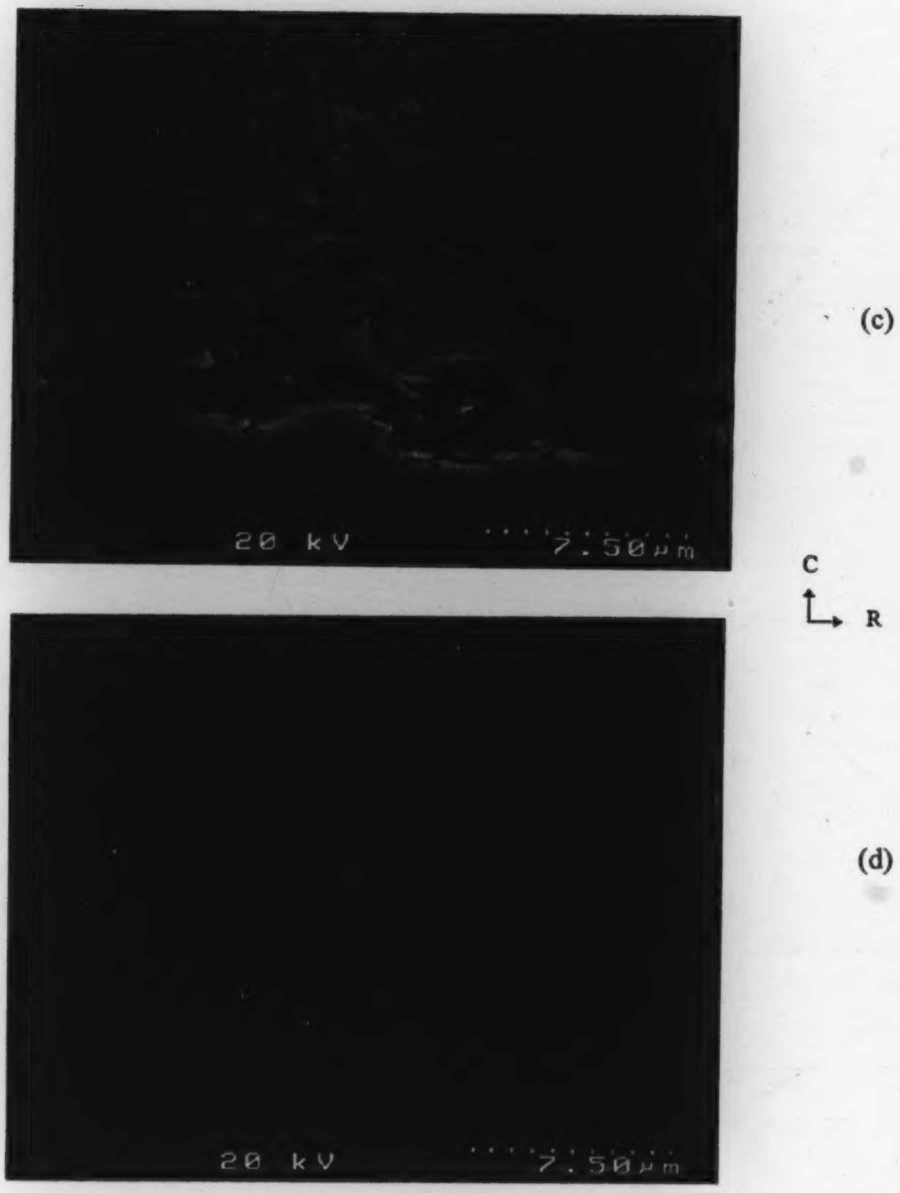
20 kV
7.50 μm
(c)
C
R
20 kV
7.50 μm
(d)

Figure 4-33 SEM micrograph (BSE image) of crack tip hydrides on circumferential-radial plane (0% additional CW) (cont.) 4000X

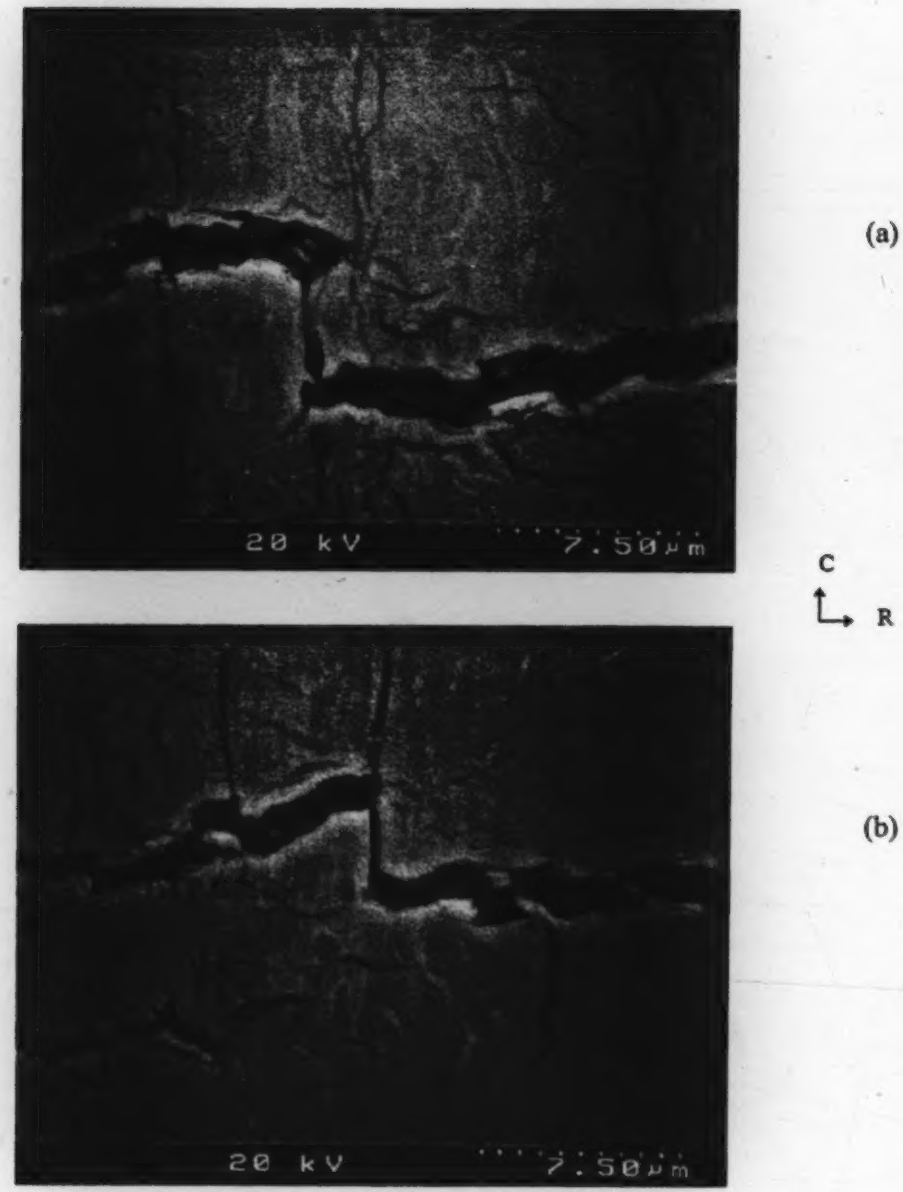
20 kV
7.50µm
(a)
C
R
20 kV
7.50µm
(b)

Figure 4-34 SEM micrograph (BSE image) of crack tip hydrides on circumferential-radial plane (0% additional CW) 4000X

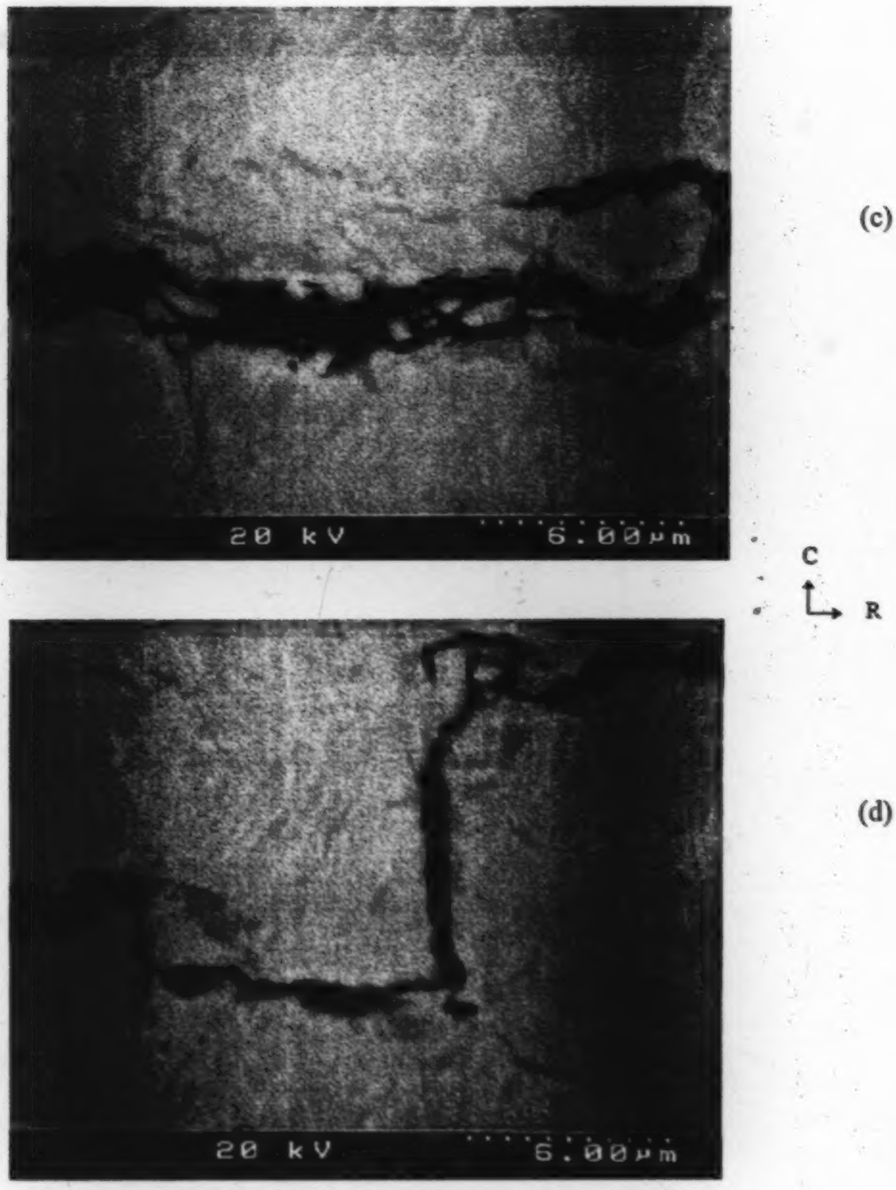
(c)
20 kV
6.00µm
C
R
(d)
20 kV
6.00µm

Figure 4-34 SEM micrograph (BSE image) of crack tip hydrides on circumferential-radial plane (0% additional CW) (cont.) 4000X

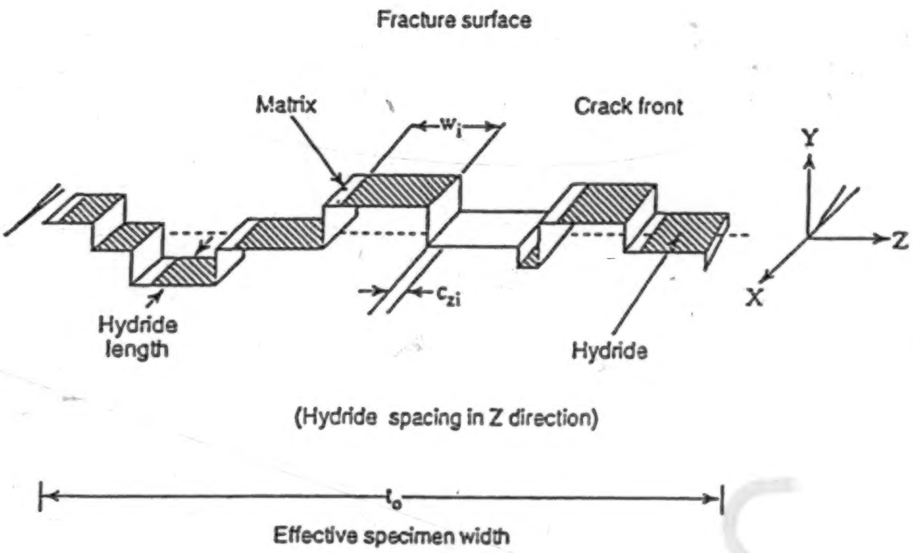
Fracture surface
Matrix
w_i
Crack front
Y
Z
X
c_{zi}
Hydride length
Hydride
t_o
Effective specimen width

(Hydride spacing in Z direction)

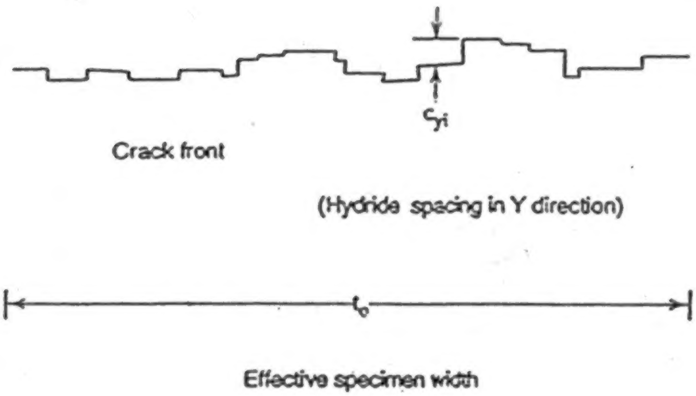
c_{yi}
Crack front
t_o
Effective specimen width

(Hydride spacing in Y direction)

Figure 4-35 Cross-section of a fractured surface [30]

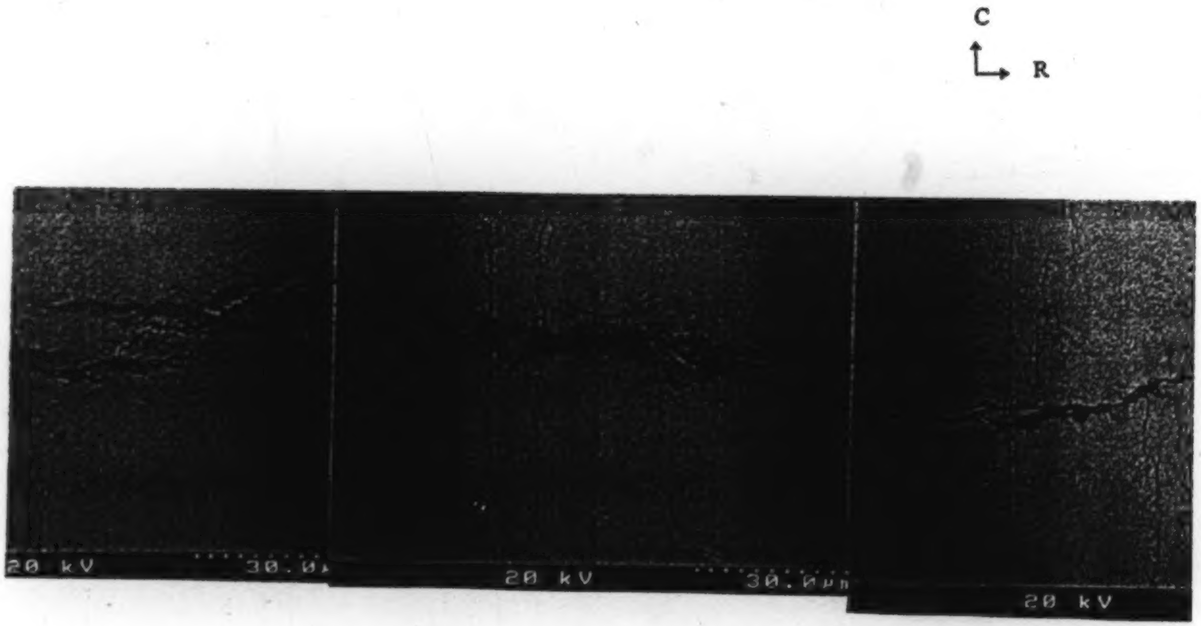
C
R
20 kV
30.0
20 kV
30.0μm
20 kV

Figure 4-36a SEM micrograph (BSE image) of crack tip hydrides on circumferential-radial plane (0% additional CW) 1000X

Figure 4-36b SEM micrograph (BSE image) of crack tip hydrides on circumferential-radial plane (0% additional CW) 1000X

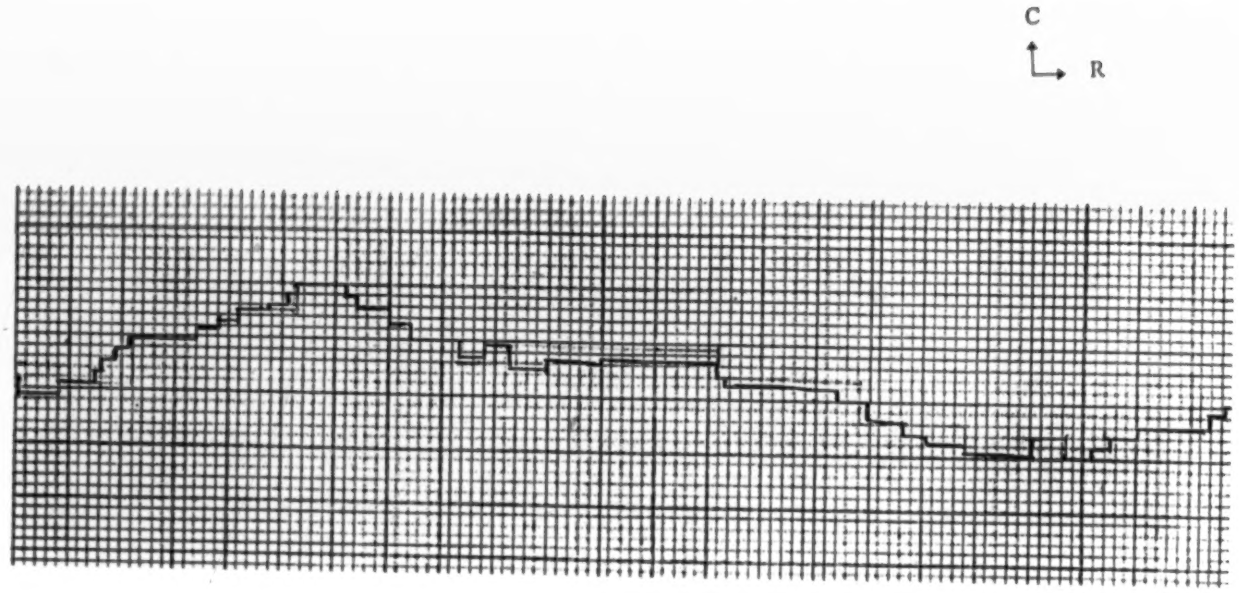

Figure 4-37 Measurement result of roughness according to the definition given by Luo in [30]

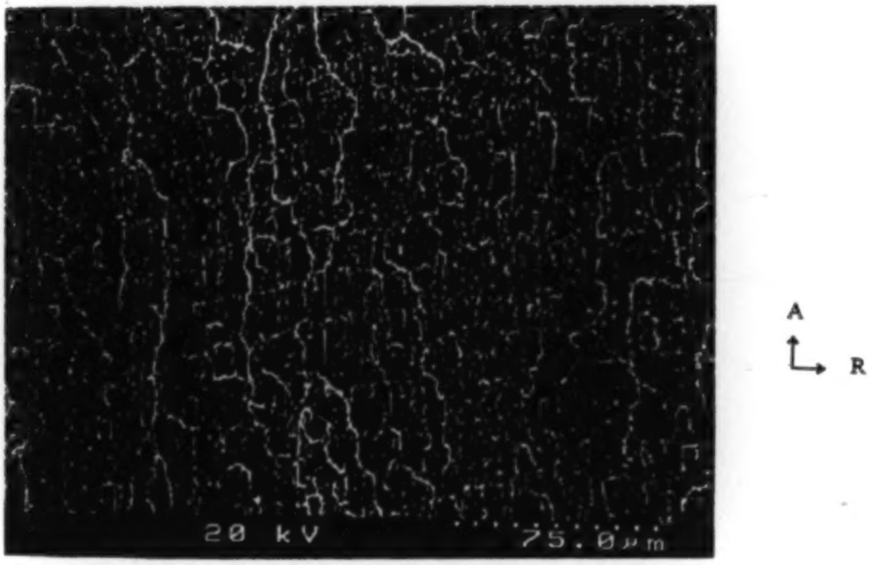
20 kV
75.0 µm
A
R

Figure 4-38 A typical "fish-scale" pattern observed on fractured surface 400X

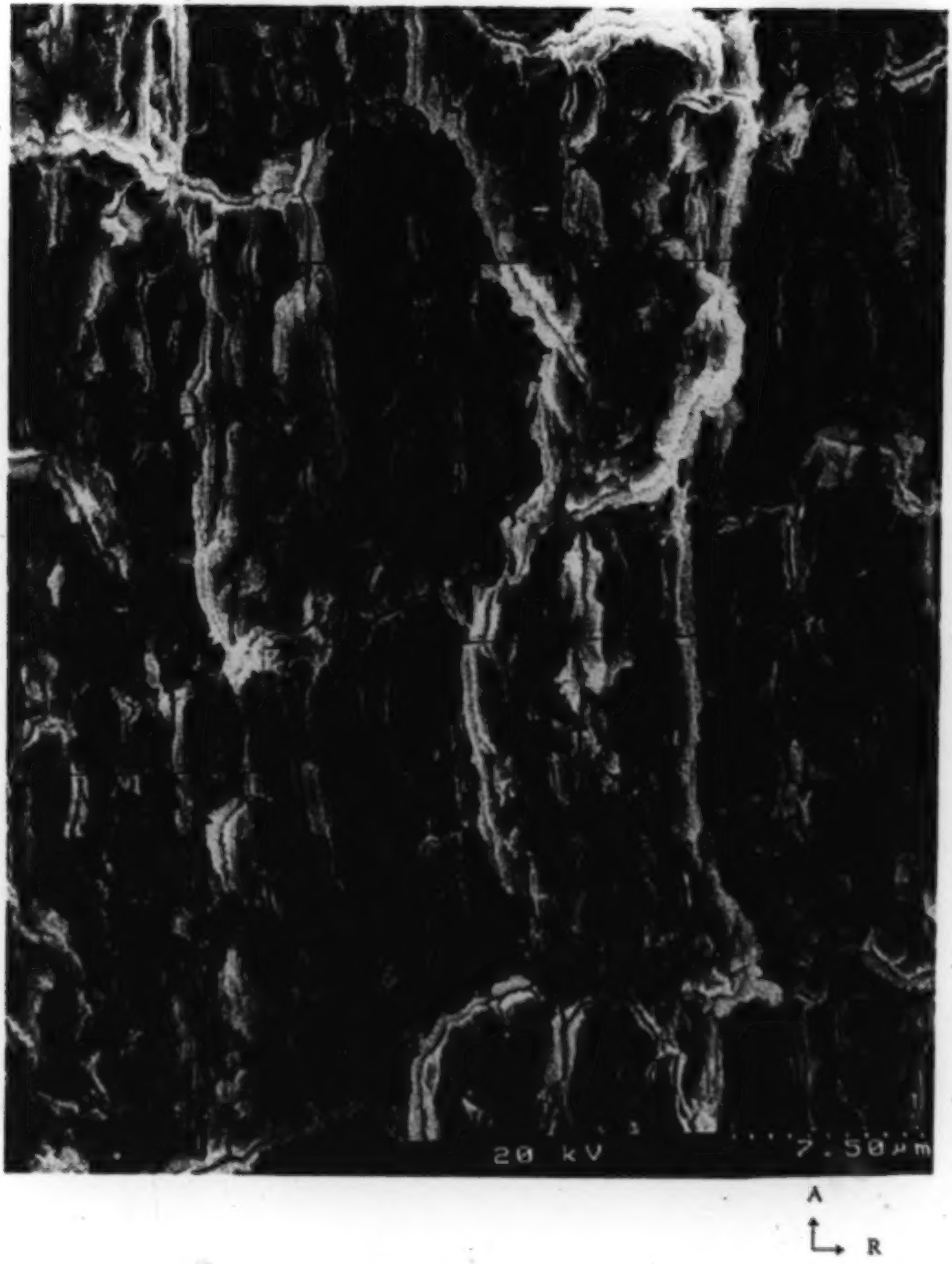
20 kV
7.50 μm
A
R

Figure 4-39 A typical "fish-scale" pattern observed on fractured surfaces under high magnification 4000X

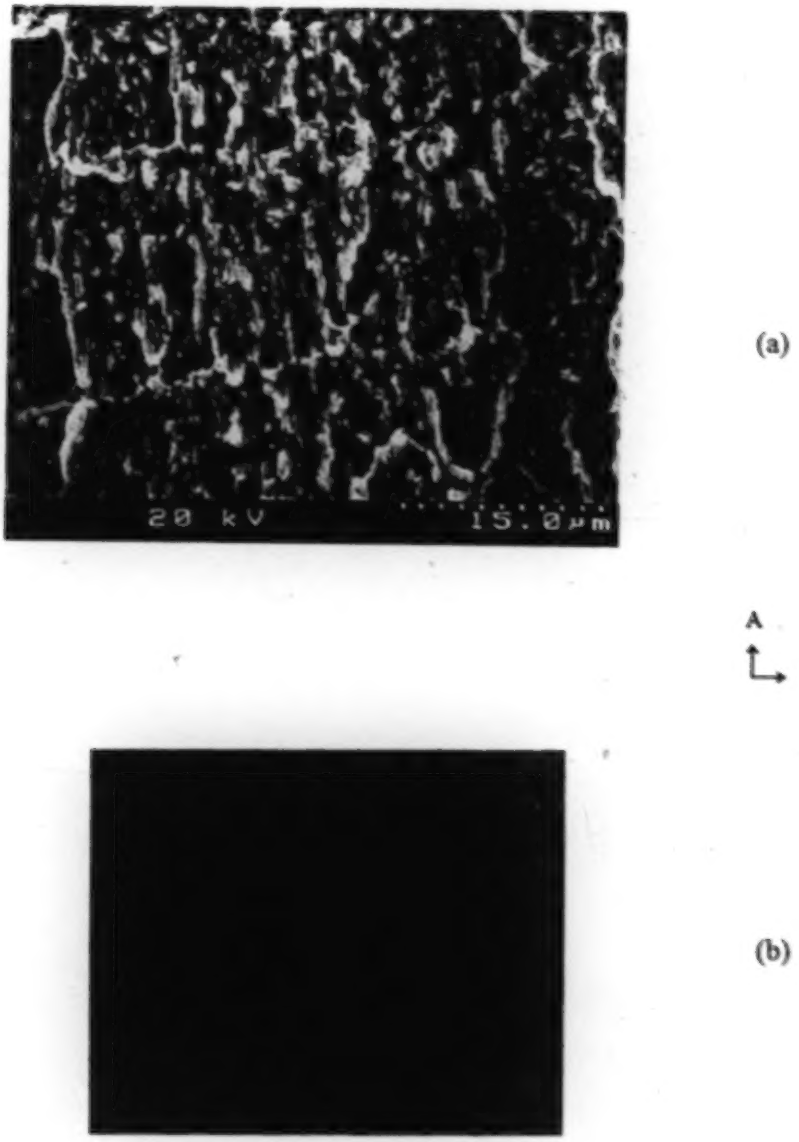

Figure 4-40 SEM and digitized images of striations on fractured surfaces
a) Striations on fractured surfaces 2000X
b) Digitized image of striations on fractured surfaces

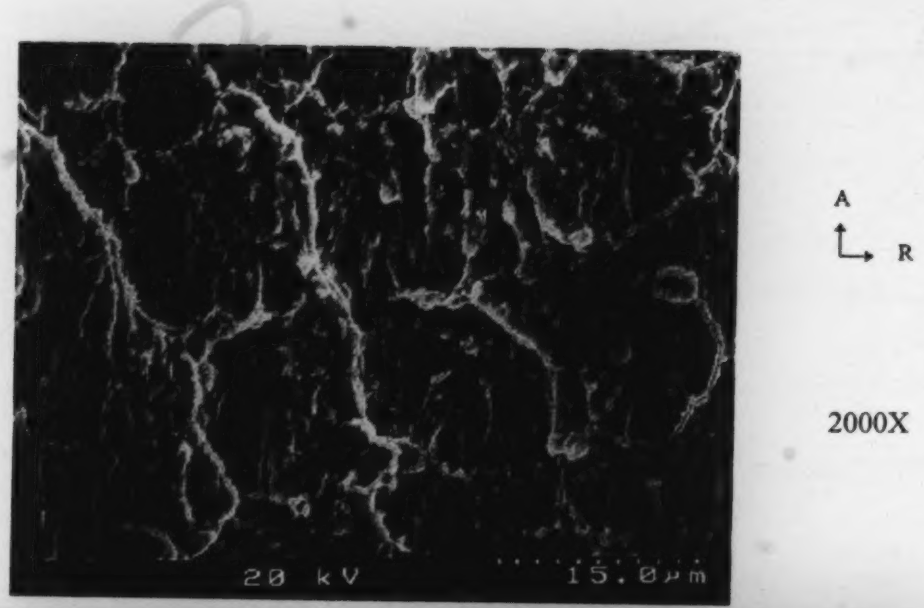

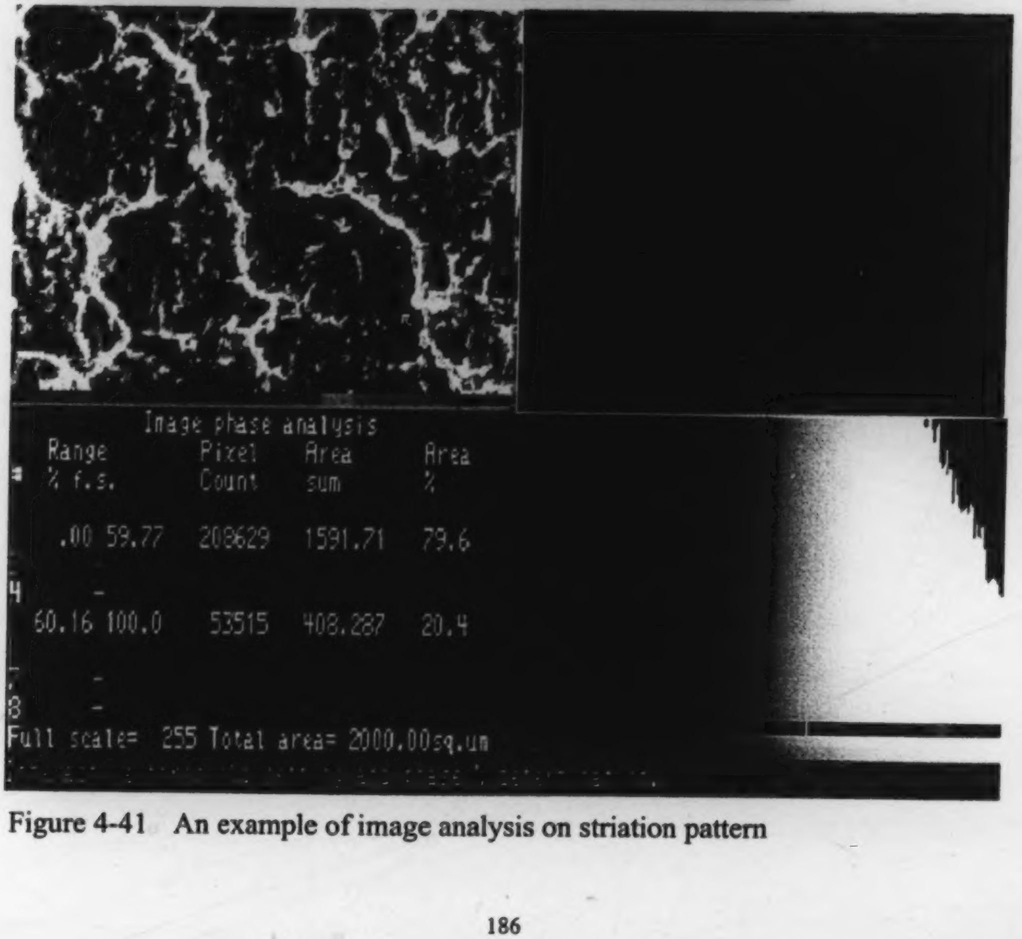

```
       Image phase analysis
 Range         Pixel   Area      Area
 % f.s.        Count   sum       %

  .00 59.77    208629  1591.71   79.6

4      -

60.16 100.0     53515  408.287   20.4

7      -
8      -
Full scale=  255 Total area= 2000.00sq.um
```

Figure 4-41 An example of image analysis on striation pattern

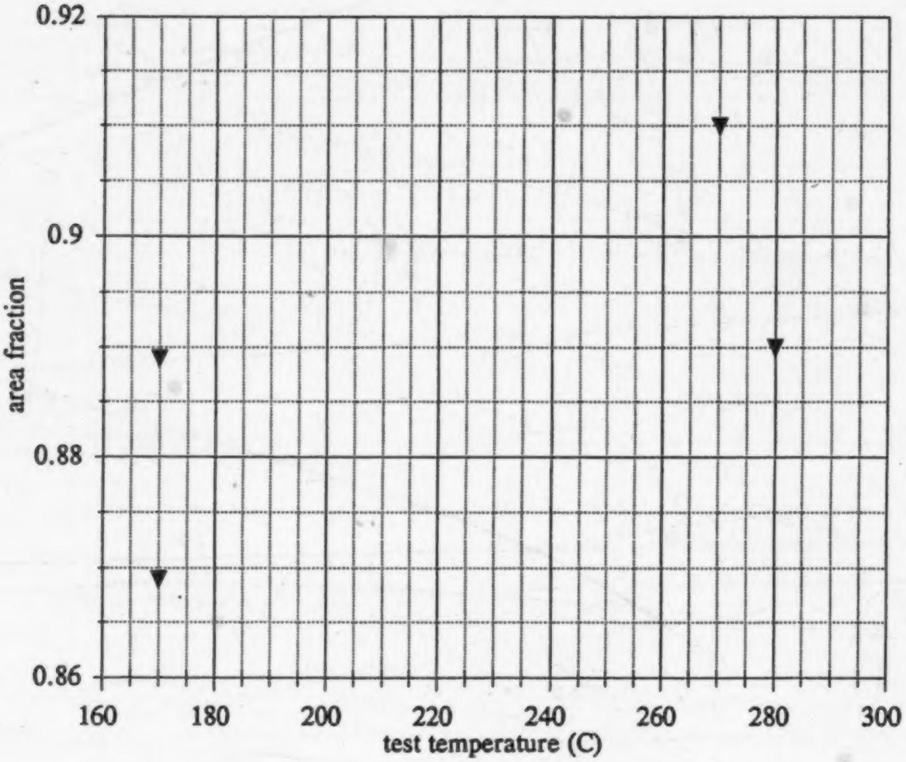

Figure 4-42 The area fractions of crack tip hydrides versus test temperature

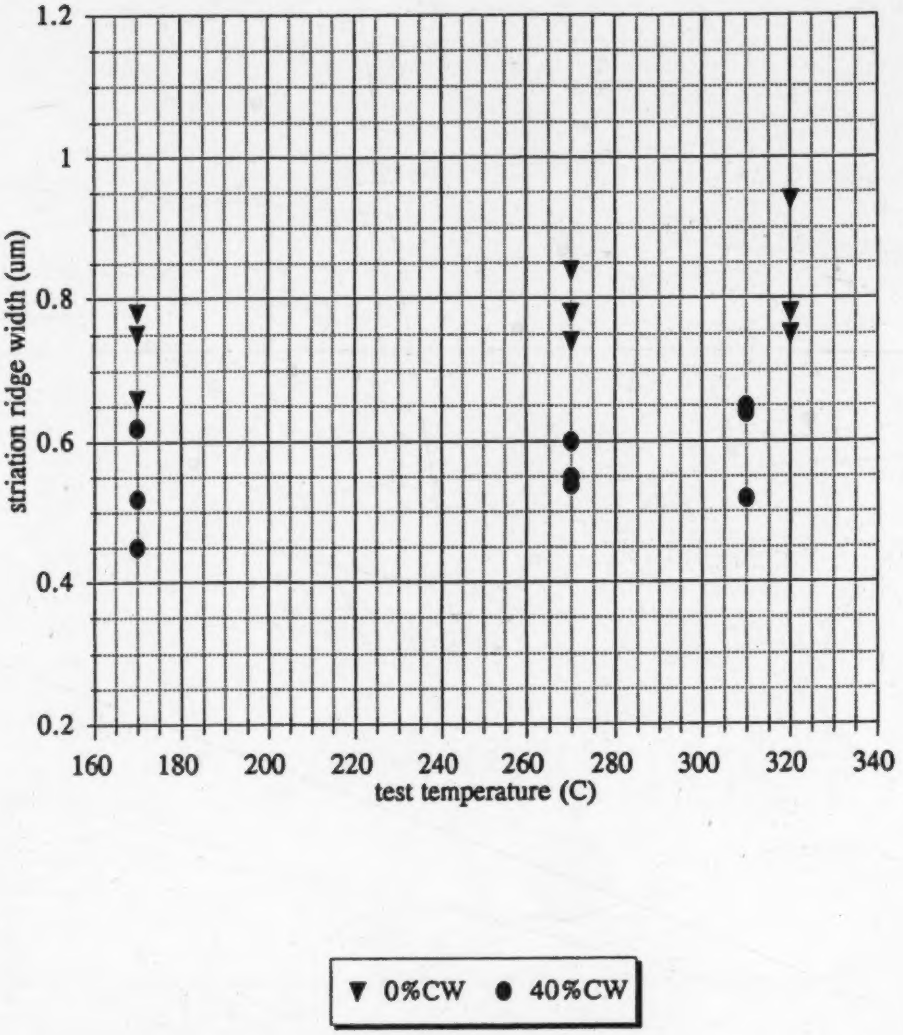

Figure 4-43 Striation ridge width versus test temperature

Table 4-1 Initial conditions of tested specimens including their amount of additional cold work and hydrogen concentration

No.	CW (%)	H^{*} (μg/g)	H^{**} (μg/g)	No.	CW (%)	H^{*} (μg/g)	H^{**} (μg/g)	No.	CW (%)	H^{*} (μg/g)	H^{**} (μg/g)
L1A	0	80	77	L3A	0	120	119	L4A	0	160	
L1B	0	80	80	L3B	0	120		L4B	20	160	
L1C	0	80	90	L3C	20	120		L4C	20	160	
L1D	0	80	90	L3D	20	120		L4D	40	160	
L1E	0	80	163	L3E	22	120		L4E	40	160	
L1F	0			L3F	22	120		L4F	60	160	
				L3G	22	120		L4G	60	160	
L2A	8	80		L3H	25	120		L4H		160	
L2B	8	80		L3I	32	120					
L2C	8	80		L3J	32	120		L5A	0	160	
L2D	8	80		L3K	32	120		L5B	0	160	
L2E	20	80		L3L	32	120		L5C	0	160	
L2F	20	80		L3M	32	120		L5D	0	160	
L2G	20	80		L3N	32	120	196	L5E	0	160	
L2H	40	80		L3O	40	120		L5F	0	160	
L2I	40	80		L3P	40	120	190	L5G	0	160	196
L2J	40	80		L3Q	60	120	239				
				L3R	60	120					
				L3S	60	120					

H^{*}: estimated hydrogen level, H^{**}: analyzed hydrogen level

Table 4-2 Measured T_{CAT} values for as-manufactured specimens

(peak temperature = 340°C, K =17 MPa√m)

	% additional CW	H% (μg/g)	T_{CAT} (°C)
L1Aa	0	80	300
L1Ab	0	80	300
L1Ac	0	80	305
L1Ba	0	80	290
L1Ba	0	80	290
L1Ba	0	80	295
L1Bd	0	80	290
L1Fa	0	80	280
L1Fb	0	80	285

Table 4-3 Measured T_{CAT} values for as-manufactured and additionally cold worked specimens (peak temperature = 360°C, K =17MPa√m)

	% additional CW	H% (μg/g)	T_{CAT} (°C)
L3Ba	0	120	320
L2Aa	8	120	325
L2Ab	8	120	325
L2Ac	8	120	320
L2Bb	8	120	310
L2Ca	8	120	320
L2Cb	8	120	320
L2Cc	8	120	325
L2Da	8	120	325
L2Db	8	120	315
L3Ga	20	120	330
L2Ga	20	120	330
L2Gb	20	120	335
L2Ha	40	120	330
L2Hb	40	120	330
L2Ia	40	120	330
L2Ja	40	120	335
L3Qa	60	120	330
L3Qb	60	120	335

Table 4-4a Measured T_{CAT} values on as-manufactured specimens under various stress intensity factors (peak temperature = 370°C)

	H% (μg/g)	test temperature (°C)	result
K=10			
L3Aa	120	220	cracked after 53 hrs.
L3Ab	120	220	cracked immediately
L3Ac	120	220	cracked after 2 hrs.
K=12			
L4Aa	160	250	no cracking for 24 hrs.
		220	no cracking for 27 hrs.
L4Ab	160	200	cracked after 44 hrs.
L4Ac	160	200	cracked after 124 hrs.
L4Ad	160	200	no cracking for 101 hrs
L4Ae	160	200	cracked after 20 hrs.
		250	no cracking for 40 hrs.
L4Ae	160	200	no cracking for 30 hrs.
L4Af	160	190	no cracking for 25 hrs.
K=14			
L4Ah	160	250	no cracking for 29 hrs.
L4Ai	160	240	no cracking for 26 hrs.
l4Aj	160	220	no cracking for 43 hrs.
L4Ak	160	210	cracked after 4 hrs.
L5Ba	160	190	cracked after 21 hrs.
L5Bb	160	170	cracked after 13 hrs.
L5Bc	160	220	cracked after 4 hrs
L5Bd	160	260	cracked after 2 hrs.

Table 4-4b Measured T_{CAT} values on 20% additionally cold worked specimens under various stress intensity factors (H%=160 μg/g, peak temperature = 370°C)

	test temperature (°C)	result
K=10		
L4Ba	190	no cracking for 5 hrs.
	150	no cracking after 2 cycles* & 67 hrs
L4Bb	150	cracked after 23 hrs.
	200	no cracking for 23 hrs.
	180	no cracking for 20 hrs.
	165	no cracking for 165 hrs.
K=12		
L4Bc	250	no cracking after 2 cycles and 20 hrs
L4Bd	220	cracked after 2nd cycle and 20 hrs.
	225	cracked after 47 hrs.
L4Be	230	no cracking after 2 cycles and 54 hrs
L4Ca	260	no cracking for 17 hrs.
L4Cb	250	no cracking for 34 hrs.
	240	no cracking for 54 hrs.
L4Cc	235	cracked after 5 hrs.
	235	cracked after 2 hrs.

* A cycle consists of a re-heating to 370°C, holding at 370°C for 1 hour and cooling down to the original test temperature again.

Table 4-4c Measured T_{CAT} values on 40% additionally cold worked specimens under various stress intensity factors (H%=160 μg/g, peak temperature = 370°C)

	test temperature (°C)	result
K=12		
L4Da	260	no cracking for 24 hrs.
L4Db	260	cracked after 48 hrs.
K=14		
L4Dc	230	cracked after 2.5 hrs.
L4Dd	250	cracked after 2 hrs.
L4De	270	no cracking for 25 hrs.

Table 4-4d Measured T_{CAT} values on 60% additionally cold worked specimens under various stress intensity factors (H%=160 μg/g, peak temperature = 370°C)

	test temperature (°C)	result
K=12		
L4Fa	250	no cracking for 15 hrs.
	220	cracked after 6 hrs.
L4Fb	250	no cracking after 2 cycles and 43 hrs.
	230	no cracking for 26 hrs.
L4Fc	230	no cracking for 17 hrs.
	210	no cracking for 27 hrs.
	200	no cracking for 24 hrs.
K=14		
L4Fd	270	no cracking for 68 hrs.
L4Fe	270	no cracking for 48 hrs.

* A cycle consists of a re-heating to 370°C, holding at 370°C for 1 hour and cooling down to the original test temperature again.

Table 4-5 DHCV in nm/s for as-manufactured specimens under K=17 MPa√m (H%=160 μg/g)

test temperature (°C)	peak temperature (°C)	
	320	**370**
235		
245		
250		
255		
260	71	
270	63	
280	29	
285	0	
315		127
325		96
330		1

Table 4-6 DHCV in nm/s for 40% additionally cold worked specimens under $K=17\ \mathrm{MPa}\sqrt{\mathrm{m}}$ (H%=160 μg/g)

test temperature (°C)	peak temperature (°C)	
	320	370
285	285	
290	120	
295	0	
310		329
320		230
340		1

Table 4-7 Comparison between T_{CAT} and $T_{DHCVSTOP}$

0% add. CW	**$K=17\ MPa\sqrt{m}$**	**peak temperature =**	**370°C**
T_{CAT} (°C)	330	$T_{DHCVSTOP}$ (°C)	330
40% add. CW	**$K=17\ MPa\sqrt{m}$**	**peak temperature =**	**370°C**
T_{CAT} (°C)	340	$T_{DHCVSTOP}$ (°C)	340

Table 4-8 Measurement results of hydride thickness

I as-received sample (from Figure 4-21a)

Distance from crack tip (μm)	# of platelets	total platelet thickness (μm)	average platelet thickness (μm)
8.81	10	7.74	0.77
18.17	7	5.33	0.76
33.45	8	4.09	0.51
48.75	7	3.25	0.46
66.85	4	2.17	0.54
85.92	3	1.27	0.42

II 20% additionally cold worked specimen (from Figure 4-21b)

Distance from crack tip (μm)	# of platelets	total platelet thickness (μm)	average platelet thickness (μm)
9.62	4	2.35	0.59
22.64	4	2.18	0.54
37.63	5	1.71	0.34
52.11	4	2.04	0.51
67.65	5	1.29	0.26
88.99	3	0.71	0.24
101.13	1	0.29	0.29

III 30% additionally cold worked specimen (from Figure 4-21c)

Distance from crack tip (μm)	# of platelets	total platelet thickness (μm)	average platelet thickness (μm)
6.72	9	5.60	0.62
14.57	6	2.90	0.48
22.77	9	2.84	0.32
31.69	3	1.45	0.48

IV 40% additionally cold worked specimen (from Figure 4-21d)

Distance from crack tip (μm)	# of platelets	total platelet thickness (μm)	average platelet thickness (μm)
4.86	5	4.55	0.91
11.35	5	3.47	0.69
18.73	5	2.56	0.51
28.28	6	2.54	0.41
39.19	5	1.65	0.33
54.85	5	1.13	0.23
66.63	5	1.23	0.25
90.17	3	0.76	0.25

V 60% additionally cold worked specimen (from Figure 4-21e)

Distance from crack tip (μm)	# of platelets	total platelet thickness (μm)	average platelet thickness (μm)
5.19	6	5.32	0.89
13.26	7	3.20	0.46
22.35	4	1.73	0.43
33.41	5	1.63	0.33
43.70	5	1.45	0.29
62.68	3	0.81	0.27
80.07	3	0.63	0.21

Table 4-9 Dimensions of hydride cluster and individual hydrides obtained on the specimens with and without additional cold work

amount of additional CW (%)	length of hydride cluster (µm)	length to thickness ratio of hydride luster	length of individual hydride (µm)
0	100	8.7	10-15
20	80	7.3	8-13
30	50	4	5-8
40	40	3	2-5
60	30	3	1-3

Table 4-10 Roughness measurement results

	amount of additional cold work (%)	measured roughness
L2B	8	0.303
L2D	8	0.361
L2F	20	0.486
L2G	20	0.332
L3D	20	0.257
L3G	20	0.226

Chapter 5 Discussion

5.1 About The Cracking Arrest Phenomenon

5.1.1 Summary of Experimental Evidence about the Cracking Arrest Phenomenon

In addition to what was already known about the cracking arrest phenomenon when this work was started, the following are the new characteristics about cracking arrest phenomenon discovered in this work.

- The cracking activity diminishes when T_{CAT} is approached.
- At T_{CAT}, cracking stops with uncracked radial crack tip hydrides present.
- Cracking arrest behavior is closely related to the morphology of the radial hydrides. That is, large, tapered radial hydrides are found associated with T_{CAT}.
- Cracking arrest behavior is a function of the peak temperature used before a test temperature is reached. The higher the peak temperature is, the higher is the T_{CAT}.
- Loading condition of the specimens affects the T_{CAT} values. T_{CAT} increases with increasing K_I.
- Cracking arrest temperature is also influenced by the amount of additional cold work, with additional cold work increasing the T_{CAT}.
- T_{CAT} values can be reasonably repeated on the same specimen but vary on different specimens even from the same pressure tube.

The meaning of the following phrases used in presenting the experimental results need to be re-addressed.

Peak Temperature As discussed in section 2.2.6.1.1, peak temperature is defined as the highest temperature a specimen has experienced directly prior to approaching a test temperature. As briefly addressed in the previous sections, in this work different peak temperatures represent different hydrogen levels in solution, because, with sufficient matrix hydrides available, the highest temperature a specimen has reached before reaching a test temperature determines how much hydride has dissolved and gone into solution. In this project, all the specimens have been provided with "more-than-enough" matrix hydrides and have been heated to a peak temperature and held before being cooled down to test temperatures. The hydrogen level in solution, which is the hydrogen available for forming re-oriented crack tip hydrides, depends, therefore, solely on the peak temperature. For instance, for a specimen with a matrix hydrogen concentration of 120 μg/g (e.g. L3A, see Table 4-1) a peak temperature of 320°C will bring 70.5 μg/g hydrogen into solution while a peak temperature of 340°C will increase the level of diffusible hydrogen to 87.9 μg/g. That is to say, for all the specimens with a matrix hydrogen concentration of 120 μg/g, there is a unique dependency of diffusible hydrogen on the peak temperature as long as the peak temperature is below 370°C because the 370°C is the temperature needed to dissolve all the 120 μg/g matrix hydrogen. Experimentally, both cracking rates and cracking arrest temperatures have been found to decrease when tested with lower peak temperature. The amount of hydrogen in solution dictates both cracking initiation and propagation processes. The abrupt drops in cracking velocity when test temperature exceeds $T_{DHCVMAX}$ and the cessation of cracking activities at T_{CAT} all seem to be the result of a diminished source of diffusible hydrogen. In other words, a minimum amount of diffusible hydrogen is needed for both fracture initiation and/or propagation at a given temperature. The importance of the amount of diffusible hydrogen, which is determined by the difference between the peak temperature and the test temperature, in the DHC process will be further discussed in section 5.1.4.

Loading Condition In order to get cracking, the specimens have to be loaded under tension. For the pressure tubes in *CANDU* reactors, it is the externally applied load(s) and the internally existing stresses, such as the residual stresses caused by over-extended rolling mentioned in section 2.1, that determine the level of overall stress. In the laboratory, specimens are loaded under tension by using a device introduced in section 3.2. The applied load and the geometry of the specimens dictate the stress level and distribution at the crack tip regions. The loading condition is represented as the applied stress intensity factor (K_I). As the applied K_I decreases, cracking initiation becomes more and more difficult.

Cold Working The effect of additional cold working on T_{CAT} values has been confirmed by cracking tests, see section 4.2.1.2. Why does cold working affect T_{CAT} value? It has been proved that cold working brings two changes to the specimens. The first one is an increased matrix strength and the second one is morphological and texture change. As indicated in section 2.2.5.4, in this project cold working the specimens is designed to simulate the hardening effect of irradiation and the increased matrix strength after cold working can be seen from Figures 4-1 and 4-2 in section 4.1.2. Thus, matrix strength should be considered as one of the affecting parameters on T_{CAT} values. This consideration fits into DHC theory that crack tip stress levels affect the DHC process due to their influence on crack tip hydride formation and fracture. Increases in matrix strength enhance crack tip stress level and, therefore, affect DHC behavior including cracking arrest temperatures. As indicated in section 4.1.2, neutron irradiation during service in reactors increases the matrix strength of pressure tubes. The length of service time of the pressure tubes, therefore, should have an influence on the cracking arrest temperature. Another possible outcome of additional cold working in the axial direction is morphological texture changes, with the grain and β-structure being more elongated and the degree of random orientation of basal poles being decreased. According to recent x-ray diffraction analysis results, additional cold work affects the fraction (or percent) of the basal poles in each direction of the 3 axes of the pressure tubes, as shown in Table 5-1 [75]. Texture change should have effects on crack tip hydride precipitation and cracking initiation. A complete picture about textural and morphological changes in Zr-2.5%Nb pressure tube material after additional cold working and their consequences on cracking arrest phenomenon needs further investigation. The possible influence on the diffusion process from the dislocations introduced by cold working is not considered in this work because the dislocation diffusion mechanism is believed not important for the hydrogen levels dealt with in this work.

5.1.2 Indications of the Experimental Evidence

The aforementioned experimental results indicate the following characteristics of the DHC process.

The cracking tests introduced in section 4.2 show that, with other testing parameters kept constant, the cracking activity is a function of test temperature and T_{CAT} is the upper limit for DHC to occur. The metallographic results shown in section 4.3 indicate clearly that re-oriented hydrides form at the crack tip at T_{CAT}

but remain uncracked. That is, cracking cessation at T_{CAT} is caused not by an absence of re-oriented hydrides but by an inability of these hydrides to fracture. The fractographic analysis results given in section 4.4 reveal the fact that the fracture property of hydrided Zr-2.5%Nb depends on both the hydride and the matrix since the fractured surfaces are not fully covered by the radial hydrides. At this time, it is believed that it is the temperature dependent material property changes of the hydrided Zr-2.5%Nb, due to the precipitation and growth of the re-oriented hydrides at the crack tips, that causes the cracking cessation.

Temperature, including the test temperature and the peak temperature, is certainly one of the principal affecting parameters in the DHC process. The importance of test temperature is reflected by the fact that cracking becomes more difficult when T_{CAT} is gradually approached (i.e. when the test temperature is further increased). The cracking activity can even cease when the test temperature is at T_{CAT}. The exact value of the test temperature at which cracking arrests depends on the peak temperature used. The peak temperature actually represents a certain amount of diffusible hydrogen. In all the tests carried out in this thesis, raising test temperature means both increasing the absolute value of the temperature at which a test is run and decreasing the difference between the peak and test temperatures. The results in section 4 suggest that both the absolute value of test temperature and the difference between the test and peak temperature are important. Other testing parameters such as the applied stress intensity factor K_I and the condition of the sample used (i.e. whether it is as-manufactured or additionally cold-worked) need also to be considered.

From all the evidence obtained, it is suggested that the formation of the radial hydrides is just one of the necessities for DHC to occur because having radial hydrides formed, or starting to form, does not guarantee fracture initiation, because the radial hydrides can be formed at T_{CAT} but can stay uncracked. T_{CAT} represents a critical condition where the combination of testing parameters, including test temperature, diffusible hydrogen level and stress intensity factor, makes it possible for the radial hydrides to form but not to fracture because the further growth of these hydrides seems to be arrested.

5.1.3 The Effect of Test Temperature, Diffusible Hydrogen and Stress Intensity Factor on DHC Initiation

Understanding the dependence of T_{CAT} on test temperature, peak temperature and K_I starts from understanding the effects of these parameters on the DHC initiation process. The effect of test temperature on the DHC process stems from its effect on both the fracture process and the hydrogen diffusion process which causes the formation of radial hydrides needed for DHC. According to Griffith [76], fracture processes, like any other natural process, follow the basic principles of thermodynamics, occurring to lower the total energy of the system. When a piece of material is loaded under tension, strain energy is stored. When the material is fractured this energy is released and the total energy level of the system is reduced. For any fracture to occur, the stored elastic energy, which is the driving force of the fracture process, has to be high enough to overcome the resistance of the process. In the case of DHC, the fracture resistance is related to the local toughness of the crack tip region because it is the local toughness of this region that dictates how much energy is required to move the crack forward. For hydrided Zr-2.5%Nb, the overall toughness of the material is determined by the toughness values of both the matrix (Zr-2.5%Nb) and the hydride (δ-hydride) as well as the hydride coverage ratio, the ratio of the hydride to matrix on the fractured surface.

The experimental results introduced in section 4.4 (Figure 4-42) indicate that the hydride/matrix ratio increases with increasing test temperature. This increased hydride/matrix ratio is necessary for fracturing specimens at a higher test temperature. It is known that the toughness of both δ-hydride and Zr-matrix increase with increasing temperature [26] because both the matrix and the hydride become tougher as temperature rises. The only way to lower the local toughness then is to increase the percentage of the more brittle phase, which in this case is the δ-hydride. To put it differently, when tested at a higher test temperature, the specimen needs to have a higher hydride/matrix ratio to satisfy the necessity of the driving force being higher than the cracking resistance. This higher ratio is obtained by the radial hydrides growing larger before fracture can initiate. That a higher percentage of hydride is needed for fracture at a higher test temperature can also be seen from the temperature-dependent striation spacing changes. The concept of striation spacing has been introduced in section 2.2.6.4. According to Anderson [77], striation spacing shows an Arrhenius type increase with test temperature, as shown in Figure 5-1 [77]. Since a larger striation spacing means a larger portion of hydrided region, therefore a higher hydride/matrix ratio, the increases in striation spacing are equivalent to increases in the hydride/matrix ratio.

Test temperature also affects the hydrogen diffusion process which brings hydrogen into the crack tip region to form hydrides there. The growth of the radial hydrides at the crack tip is made possible by the stress-induced diffusion of hydrogen and this stress induced diffusion process becomes less feasible when the test temperature increases. The negative influence of increasing test temperature comes from the fact that the amount of diffusible hydrogen relative to the precipitation solvus decreases when the test temperature gets closer to peak temperature. As mentioned in section 2.2.2, the ultimate cause for the stress induced hydrogen diffusion to the crack tip region is the chemical potential difference between the crack tip region and the surrounding area (which is at a lower stress). The chemical potential of diffusible hydrogen, $\mu_{H,p}$, in a stressed solid is given by

$$\mu_{H,p} = \mu'_{H,o} + RT\ln C_H - pV_H \tag{5.1}$$

Or, the relationship between the chemical potential ($\mu_{H,p}$), the diffusible hydrogen content (C_H) and the local stress level (p) can be given as

$$\Delta\mu_{H,p} = RT(\Delta\ln C_H) - \Delta pV_H \tag{5.2}$$

That is, chemical potential difference between the crack tip and the adjacent region is determined by the differences in the diffusible hydrogen content and the stress levels. As mentioned earlier, the difference between the test temperature and the peak temperature inevitably decreases when the test temperature increases under the test conditions used in this work. As a result, the diffusible hydrogen level decreases when the test temperature approaches T_{CAT}. This lowered diffusible hydrogen level limits the supply of hydrogen for the growth of radial hydrides at the crack tip. On one hand, larger radial hydrides are needed to induce fracture at a higher test temperature. On the other hand, the hydrogen supply decreases when test temperature rises. These two factors combined make the formation of sufficiently large radial hydrides more difficult. The observed dependence of DHCV on test temperature at the temperatures above the $T_{DHCVMAX}$ and the effect of peak temperature on DHCV, as shown in section 4.2.2, proves the validity of the above reasoning. After the $T_{DHCVMAX}$ is exceeded, any increase in test temperature means that the crack tip hydrides need to grow larger, with less available diffusible hydrogen, before they fracture. Therefore, DHC becomes more difficult. When the peak temperature increases, the amount of diffusible hydrogen increases for a given test temperature, making the crack process more feasible.

The stress intensity factor K_I affects the process in at least the following two ways: 1) It affects the process of stress induced diffusion of diffusible hydrogen, therefore, affects the hydrogen supply for the formation of the radial hydrides. 2) It also influences the fracture of the radial hydrides formed at the crack tip. At any given test temperature, fracture can only occur when the applied K_I remains high enough to promote hydrogen diffusion and to fracture the radial hydrides. Shek and Metzger have shown that the lower the applied K_I is, the more significant the re-modifying effect of the radial hydrides on the peak stress, Figure 5-2 [78]. That is, the peak stress at the crack tip is more readily reduced by the precipitation of these hydrides at a lower K_I. At test temperatures close to T_{CAT}, the supply of diffusible hydrogen is limited and a larger concentrating effect is required to bring in enough hydrogen to form radial hydrides at the crack tip. But a lowered K_I means a reduction in peak stress both regarding the magnitude and the size of the highly stressed region. The stress field at the crack tip is also more sensitive to the growth of the radial hydrides. Under a low K_I, the peak stress will decrease significantly with the growth of the radial hydrides. As a consequence, the resultant stress gradient will not be high enough to move sufficient hydrogen to grow the radial hydrides large enough to initiate fracture. A reduction in stress also means that the available energy for fracture is less because this energy is a function of the second power of the stress (σ^2). At this point, cracking stops with the crack tip hydrides formed but remaining uncracked.

5.1.4 The Causes of Cracking Arrest Phenomenon at High Temperatures

Based on the experimental results obtained in this work and the understanding about the DHC process at this time, a sketch of cracking arrest at high test temperatures can be drawn. Since metallography indicates that cracking activity ceases with crack tip hydrides present, the question needed to be answered about the cracking arrest phenomenon is actually why the radial crack tip hydrides can form but do not crack at T_{CAT}.

Since the radial hydrides will fracture when they reach a critical dimension, only under two circumstances can these radial hydrides remain uncracked. The first possible scenario is that the critical dimension for hydride to fracture becomes unlimitedly large, so large that the crack tip hydrides will never reach that threshold value no matter how large they grow. The second one is that the critical dimension remains unchanged but the crack tip hydrides can never reach the critical dimension because they grow at an extremely low rate or do not grow at all. Among these two possibilities, the latter seems to be what is happening when a T_{CAT} is reached. The most direct support of this belief comes from the metallographic observations of the crack tip hydrides. Metallographic analysis reported in section 4.3.2.1.1 indicates that the dimension of the crack tip hydrides does not increase significantly even when the holding time at T_{CAT} has been quintupled. This observation has been confirmed by the repeated "cracking" tests at T_{CAT} and metallographic analysis thereafter.

There are at least two contributory factors for the cracking arrest at T_{CAT}. The first one is a decreased supply of diffusible hydrogen at T_{CAT} because of the smaller difference between the test temperature and peak temperature. The reduced hydrogen supply limits the growth of the radial hydrides. A cracking process can not occur when the amount of diffusible hydrogen is not sufficient for the radial hydrides to grow large enough to initiate fracture. The other contributory factor is the interaction between the precipitated hydride platelets and the local stress distribution. The local stress level and its distribution is essential to the DHC process because it affects two of the three processes involved in DHC: hydrogen diffusion into the crack tip region and the fracture of the radial hydrides in that region. The stress level at the crack tip is affected by the growth of the radial hydrides formed in that region. Work done in this area show that hydride precipitation and growth modifies the stress field at the crack tip [34,37]. Metzger, for instance, has suggested that the total stress level decreases when crack tip hydrides grow larger as shown in Figure 5-3 [37]. When the local stress level decreases, so does the stress induced diffusion process of hydrogen. At T_{CAT}, a combination of high test temperature, which reduces matrix strength of the specimens, and the limited amount of diffusible hydrogen, which restricts the growth of the hydride platelets, creates a condition that the radial hydride precipitation can start but can not continue. Because, with the growth of these radial hydrides, diffusible hydrogen is being consumed and the stress field around the crack tip is being flattened. Further growth of the radial hydride platelets becomes more difficult. Eventually, a situation is created in which the growth of the radial hydrides stops and these hydride platelets remain uncracked. At this point, the DHC process ceases with uncracked radial hydrides present.

There is no doubt that T_{CAT} represents a threshold test temperature as far as crack tip hydride formation, growth and its fracture are concerned. At the first instance when a T_{CAT} is reached by cooling, the excess diffusible hydrogen and the high crack tip stress make the precipitation of these hydrides possible. The consequence of this hydride precipitation process has, however, a negative impact on the further growth of these radial hydride platelets, because the precipitated hydride platelets consume the diffusible hydrogen available and the expansion of the hydrides tends to reduce the crack tip stress. As a result, these precipitated hydride platelets stop growing due to discontinued hydrogen supply before they can reach the critical dimension to fracture. At this point, the process of hydride growth/hydride fracture can not continue. This state of process "*PAUSE*" lasts as long as all the testing parameters remain unchanged. When, for instance, the test temperature is decreased from this threshold temperature, even by just a few degrees, re-oriented hydrides will soon crack due to the resumed hydride growth. In other words, at a test temperature equaling T_{CAT}, the necessities for further crack tip hydrides to form must be just barely unfulfilled.

Recall from previous sections that the governing factor in DHC is the localized stress concentration at the crack tips and a resultant stress induced hydrogen diffusion into the area. If the diffusible hydrogen level is C_o and the increased hydrogen level in solution at the crack tip is C_{MAX}, their relationship can be expressed as

$$C_{MAX} = \beta C_o \qquad (5.3)$$

with β being the hydrogen concentration factor.

The hydrogen concentration factor, β, is not a constant because it decreases when temperature increases, as shown in Figure 5-4, and the reduction of β is caused by the reduction of the yield strength at higher temperatures. The actual value of β will be also affected by the existence of the crack tip hydrides because of the interaction between the hydrides and the local stress field. This effect is ignored in producing Figure 5-4. As a consequence of the dependence of β on test temperature, the hydrogen gradient caused by this stress induced hydrogen diffusion varies when test temperature changes. At the first instance when a T_{CAT} is reached, the hydrogen concentration must be just high enough to bring hydrogen into the crack tip region to have re-oriented hydrides formed. But this hydrogen gradient must be so small that it is immediately counter-balanced as soon as some tiny hydride platelets have precipitated. This counter-balancing effect of hydride precipitation on stress gradient comes from the dilation accompanying hydride formation, see section 2.2.4.2. When the hydrogen gradient vanishes, so does the hydrogen flow to the crack tip area, resulting in a "frozen" hydride size because the crack tip hydride growth halts temporarily. The result is a "*PAUSE*" state of cracking process at which crack tip hydrides remain uncracked because they have stopped growing when they are still smaller than the critical dimension needed for fracture.

The reversibility of the cracking arrest phenomenon at T_{CAT}, which has been discussed in section 4.2.1.4, is an indication on how vulnerable the balance is between the uncracked crack tip hydrides and the local hydrostatic stress field/hydrogen gradient reached at a T_{CAT}. The immediate resumption of cracking activities with a decrease in test temperature suggests that the balance is destroyed instantaneously when the testing condition is changed. When test temperatures are dropped from T_{CAT} to a lower test temperature, three alterations exist. The first one is a decreased $C_H{}^d$ value whose occurrence increases the relative level of diffusible hydrogen in the crack tip region. The second change is an increased matrix strength which will cause the hydrogen concentration factor, β, to increase. The third change is a decrease of the material toughness. Crack tip hydrides start growing again due to the resumed hydrogen supply. These hydrides will soon break when they reach the critical dimension and the fracture becomes easier because of the lowered toughness. The immediate resumption of cracking activity also indicates that the cracking arrest at T_{CAT} is "*elastic*" rather than "*plastic*" in nature. No permanent, or irreversible, changes have been made either to the specimen matrix or to the re-oriented hydrides when the cracking process halts at $T_{CAT.}$ Otherwise specimens will not be able to respond almost immediately to the changes in testing conditions to re-start cracking. That is to say, cracking has just "paused" but not "stopped" at T_{CAT}.

The high sensitivity of the cracking "*PAUSE*" to crack tip stress and its distribution is also the reason why additional cold work and applied stress intensity factors have an influence on cracking arrest temperatures. When the amount of cold work increases, so does the matrix strength level, see section 4.2.1.2. Harder materials require a higher temperature to soften. That is, for additionally cold worked specimens, the balance can be reached only at a higher test temperature. The more cold worked a specimen is, the higher is the test temperature required to reach the balance as reported in section 4.2.1.2. This same argument holds for the effect of applied stress intensity factor. Stress intensity factor affects both the stress distribution and the stress drop-off due to hydride formation. It will, therefore, affect the point at which the balance can be reached.

DHCV profiles over different test temperature ranges, such as the ones shown in Figures 4-9 to 4-12, are another relevant indicator about DHC behavior being a composite result of all the affecting parameters. Shown by cracking tests, there always exists a $T_{DHCVMAX}$, which gives the test temperature for the highest DHCV for the material tested, the peak temperature used and the stress intensity factor applied. Since DHCV reaches its maximum value at $T_{DHCVMAX}$, the testing condition at this temperature must represent an optimal combination of all the testing parameters in terms of creating a most favorable condition for the DHC process to proceed. At any test temperature below $T_{DHCVMAX}$, the relative amount of diffusible hydrogen increases, the matrix strength level increases, the stress level at the crack tip increases, but the hydrogen diffusion coefficient decreases. At any test temperatures higher than the $T_{DHCVMAX}$, the situations reverses: the diffusion rate becomes higher but the total amount of diffusible hydrogen available for hydride formation is limited and so is the local stress level at the crack tip. The slowest step in a process being the controlling step, the hydrogen diffusion is the controlling step of The DHC process in the pre-$T_{DHCVMAX}$ temperature range and the increased DHCV is the result of an accelerated hydrogen diffusion process. In the post- $T_{DHCVMAX}$ temperature range, on the other hand, the controlling step must have changed, because the DHCV now decreases with the increasing test temperatures. Since increasing test temperature means a smaller difference between the peak temperature and test temperature, the decreased DHCV must be associated with the decreased level of diffusible hydrogen. The effect of peak temperature on DHCV and on T_{CAT} can be also easily integrated into the above analysis. Since a higher peak temperature means a higher relative amount of diffusible hydrogen, increasing peak temperature will cause increased DHCV regardless of the test temperature range, see section 4.2.2. An increased amount of diffusible hydrogen also makes reaching the balance more difficult, therefore gives higher T_{CAT} values, see section 4.2.1.

The observed variations of the hydride coverage ratio with test temperature, as reported in section 4.4 are the consequence of local toughness changes required to initiate fracture. The local toughness of the crack tip region in a hydrided Zr-2.5%Nb specimen is determined by the toughness of the specimen matrix, the hydrides formed and the percentages of these two phases. Expressed in energy, the above idea can be represented as [32]:

$$E_{total} = f_{hydride} E_{hydride} + f_{matrix} E_{matrix} \qquad (5.4)$$

where E_{total} is the total fracture energy per unit area of hydrided material,

$E_{hydride}$ is the hydride fracture energy,

E_{matrix} is the matrix fracture energy,

$f_{hydride}$ is the area fraction of hydrides at crack initiation,

f_{matrix} is the area fracture of matrix at crack initiation, and

$f_{hydride}+f_{matrix}=1$.

Equation 5.4 can be used to understand why the hydride coverage ratio varies with test temperature. The hydride coverage ratio, calculated by $f_{hydride}/f_{matrix}$, is directly related to the concept of "striation spacing" discussed in section 2.2.6.4. Striations, whose presence is a direct evidence that the crack front moves in a discontinuous manner in the DHC process, are fracture features left on the fractured surfaces in forms of bands perpendicular to the fracture advance direction. The striation spacing is the width of a striation "band". Each striation starts with a primarily brittle fracture portion and is followed by a much narrower ductile fracture strip. The brittle portion of a striation is believed to be caused by the fracture of radial hydrides and the ductile portion the fracture of the Zr-matrix not covered by the radial hydrides. Every "jump" of the crack front starts with the fracture of the radial hydrides formed at the crack tip and then is arrested when the crack proceeds into the Zr-matrix. Since both $E_{hydride}$ and E_{matrix} are fixed values at any given test temperature, the specific E_{total} value at that temperature is determined solely by the ratio of $f_{hydride}/f_{matrix}$. This ratio changes when the radial hydrides grow larger. As has been experimentally observed, the width change of the matrix ligament in the striations is minimal, see Figure 4-43, when the total striation spacing increases with test temperature. The increases in the total striation spacing is caused mainly by the increases in the brittle portion of the "jumps". Due to the fact that $E_{hydride} << E_{matrix}$ (i.e. the hydride is a lot more brittle than the matrix), an increased $f_{hydride}/f_{matrix}$ value means a reduced local toughness of the crack tip area which is necessary to initiate fracture at a higher test temperature.

To summarize, the following is believed to be the reason for cracking cessation at T_{CAT} with the uncracked radial hydrides present. When the test temperature is higher, larger radial hydrides have to be formed before fracture can occur. But the growth of the radial hydrides at a higher test temperature becomes more difficult due to the reduced relative diffusible hydrogen resulting from the drop in stress. Therefore, cracking becomes less feasible. This is why DHCV decreases with increasing test temperature when T_{CAT} is approached with a fixed peak temperature. Eventually a threshold test temperature is reached. At the first instant when this threshold test temperature is reached, the local hydrogen level still allows radial hydrides to precipitate at the crack tip. The slim excess diffusible hydrogen created at that temperature and the modification on the stress field caused by the existing hydrides, however, can not maintain the growth of these precipitated crack tip hydrides. With the hydride growth being halted, fracture can not occur and these formed crack tip hydrides remain uncracked. This threshold test temperature is the T_{CAT} for the peak temperature used, at the applied K_I for the given material with respect to its matrix yield strength and the hydrogen content. Any changes in one of these parameters, be it matrix strength, applied K_I or the diffusible hydrogen level caused by using a different peak temperature, will set the T_{CAT} to a new value which reflects the fact that a new "balance" has to be reached.

Despite a strong tendency to believe that the cracking cessation at T_{CAT} is caused by hydride stopping growing, as presented earlier, the author has to admit, at this point of cracking arrest phenomenon study, that other possibilities can not be yet totally excluded. For instance, it could be that crack tip hydride platelets do not stop growing after their precipitation but they grow at an extremely low rate instead. A simple calculation based on the cracking velocity at a test temperature of 300°C suggests that the time needed for hydrides to grow to 25 micrometers long, which is the inter-striation distance for that temperature, is only three thousandth of a second. At this stage of T_{CAT} study, it is not clear yet, if the crack tip hydrides observed on the specimens being kept at T_{CAT} for more than 24 hours have been formed only at the initial portion of the holding time or the hydride growth process actually has lasted for the entire period of time held at T_{CAT} but with an extremely low growth rate. Efforts made to compare the uncracked crack tip hydrides obtained after holding specimens at T_{CAT} for 10 hours and 24 hours, respectively, have failed to produce convincing results about whether the growth of these re-oriented crack tip hydrides continues after their precipitation. More sophisticated measurements are required to bring a better description of crack tip hydride precipitation and growth process at T_{CAT}.

5.1.5 Estimation of Temperature Ranges for T_{CAT} Existence

Observations of uncracked crack tip hydrides indicate that T_{CAT} is lower than the temperature at which hydride precipitation just becomes feasible. If we term the highest possible temperature for hydride precipitation to occur as T_P, T_{CAT} should be lower than T_P. At temperatures above T_P, no hydride precipitation is possible. On the other hand, the temperature difference between a T_{CAT} and a T_P has to be minimal, because otherwise re-oriented crack tip hydrides can not remain uncracked as already discussed. That is, T_{CAT} represents a temperature below T_P at which a balance is reached between the crack tip hydrostatic stress and the re-oriented hydride platelets.

The values of T_P can be calculated since it is nothing but the temperature at which local hydrogen level exceeds the precipitation solvus. Mathematically, T_P is the temperature at which

$$C_{local} = C_H^{\ P} \qquad (5.5)$$

and C_{local} is the local hydrogen level at crack tip, which can be calculated by using

$$C_{local} = \beta\, C_H^{\ d} \qquad (5.6)$$

β is the hydrogen concentration factor mentioned in section 5.1.4, which reflects the difference between the average matrix hydrogen level and the elevated hydrogen level at crack tip due to local stress concentration. The average hydrogen level at test temperatures is decided by the peak temperature prior to cooling, which sets the hydrogen level in solution.

According to Shi *et al.* [79]:

$$\beta = \exp[\Phi(r_p) - \Phi(L)]/[1+1/3\ \Phi(L)] \qquad (5.7)$$

The stress potential, $\Phi(r)$, in the above equation is defined as

$$\Phi(r)=(V_H/RT)P(r) \qquad (5.8)$$

where V_H is the molar volume of hydrogen in solution and P(r) the hydrostatic stress which is given by

$$P(r)=[2(1+\nu)\, K_I]/[3\sqrt{2\pi r}] \qquad (5.9)$$

R and T in equation 5.8 have their usual meanings. ν in equation 5.9 is the Poisson's ratio and K_I the stress intensity factor. L in equation 5.7 is the size of the effective diffusion field, as Shi *et al.* have called it. When L is of the order of a few thousand micron, β in equations 5.6 and 5.7 is close to $\exp\Phi(r_p)$.

$$P(r_p) \approx P(r_{pz}) = [2(1+\nu)\, \sigma_y]/[3(1-2\nu)] \qquad (5.10)$$

Figure 5-4 shows the value of β as a function of temperature for unirradiated and irradiated materials when $L \rightarrow \infty$. Of course, the curves depend on the equations used for matrix strength calculation. The curves in Figure 5-5, for instance, show the effect of using different equations for matrix strength.

Based on equations 5.5, 5.6 and 5.7, we can get Figure 5-6, which shows that the highest temperature where hydride can be formed is about 312°C if the peak temperature is 340°C. Peak temperature is important here because it decides the average hydrogen level in solution. According to equation 2.1

$$C_H^d = 6.86 \times 10^4 \exp\{-4061/T\} \qquad (2.1)$$

the hydrogen level in solution is 91 μg/g for 340°C, which is the value used in getting Figure 5-6. If $\sigma_{y(\text{as-manufactured})}$ = 936-1.02T (equation 4.3) instead of $\sigma_{y(\text{as-manufactured})}$ = 1088-1.02T (equation 4.1) is used, the T_p is about 305°C as shown in Figure 5-7. This is the upper limit of measured T_{CAT} value for peak temperature of 340°C, see Table 5-2. For a peak temperature of 360°C, the hydrogen level in solution is 112 μg/g according to equation 2.1 and calculations show that the T_P values increase to 321°C for unirradiated and 332°C for irradiated materials, see Figure 5-8. The measured T_{CAT} values for corresponding peak temperatures are 320°C and 335°C, Table 5-2. If the peak temperature is further increased to 370°C, the T_p will reach 330°C for unirradiated and 340°C for irradiated, Figure 5-9, while measured T_{CAT} are 330°C for as-received and 340°C for 40% additionally cold worked specimens. The hydrogen level in solution is 124 μg/g for a peak temperature of 370°C. To make the comparison easier, the calculated T_P values and measured T_{CAT} values for different peak temperatures are listed in Table 5-2.

From Table 5-2, it can be seen that the calculated T_p values are the upper limits of the measured T_{CAT} ranges. The DHC process can not occur at temperatures above T_P because at test temperatures higher than T_P re-oriented hydrides can not be formed. However, at temperatures of T_P, or slightly lower, cracking might not occur either, since re-oriented hydrides can remain uncracked. That is, the real upper limit for DHC to occur is represented by T_{CAT} not by T_P, with the latter used to be considered as the most upper limit for DHC. Since T_P is just a necessity but not a guarantee for The DHC process to occur, using it as the upper limit is conservative.

The existence of a T_{CAT} is an outcome of delicate relationships between local stress gradient and the fracture toughness of the hydrided region at the crack tip. Experimentally, the temperature difference between T_P and T_{CAT} for a given specimen is estimated to be less than 5°C. It was found, in cracking tests and metallographic analysis afterwards, that the likelihood of being able to observe re-oriented hydrides was only 30% when a 10°C temperature interval was used between consequent increases in test temperatures in approaching a T_{CAT}. But the chance of metallographically observing re-oriented hydrides was increased to about 70% if the temperature interval was reduced to 5°C. Assuming that the failure to obtain crack tip hydrides was not caused by improper specimen preparation but due to absence of crack tip hydrides, the probability of having crack tip hydrides should be 100% if the T_{CAT} range was 5°C or larger. In other words, the situation of having no crack tip hydrides observed was caused by increasing test temperature from below T_{CAT} to above T_P, skipping the T_{CAT} in between. The fact that a 5°C interval can not guarantee a hundred percentage success in revealing re-oriented hydride platelets indicates that the T_{CAT} range might be smaller that 5°C, being probably 3 to 4°C. Within this temperature range, crack tip hydrides form and remain uncracked.

There are two problems which make precise calculations of T_P values impossible. The first problem is associated with the fact that calculated T_P values are very sensitive to parameters used in the calculations. Yield strength of the specimen matrix, for instance, is one of these parameters and calculations based on different matrix strength equations give different results, as shown in Figure 5-10. The dissolution solvus is another parameter affecting the calculation results, as shown in Figure 5-10. The other C_H^d equation used in producing Figure 5-10 is suggested by Shi [79]:

$$C_H^d = 3.9153 \times 10^4 \exp\{-31000/RT\} \qquad (5.11)$$

and by using it, the T_p values go down by about 4°C.

The strongest effect on the calculated T_P values comes from using different values of precipitation solubility C_H^P. In plotting Figures 5-6 to 5-10, the equation used for the precipitation solubility calculation is equation 2.2

$$C_H^P = 4.11 \times 10^4 \exp\{-3368/T\} \qquad (2.2)$$

There are also other equations used for precipitation solubility calculation and the one suggested by Shi is

$$C_H^P = 3.9153 \times 10^4 \exp\{-28942/RT\} \qquad (5.12)$$

Using equation 5.12 will bring the T_P values up, giving 332°C instead of 318°C for unirradiated and 343°C instead of 328°C for irradiated materials, see Figure 5-11. The difference in calculated T_p values is about 14°C, larger than the 4°C difference caused by using different C_H^d equations.

The second problem in calculating T_P values has to do with the nature of hydride precipitation. Unlike dissolution temperature, precipitation temperature can vary slightly due to fluctuating total molar energy for hydride precipitation [79] and the cooling rate. As a result, instead of being a line in a concentration versus temperature plot, the precipitation temperature is actually a temperature band between $C_H^{p,1}$ indicating the upper bound and $C_H^{p,2}$ indicating the lower bound, as shown in Figure 5-132. The equation 5.12 represents the $C_H^{p,1}$ and the $C_H^{p,2}$ is given by

$$C_H^{p,2} = 3.9153 \times 10^4 \exp\{-27704/RT\} \qquad (5.13)\ [79]$$

Physically, using a temperature range to describe precipitation is more realistic. Mathematically, however, this practice means that T_P will not be a specific temperature any more. Instead, it can be any temperature in a temperature range, as shown in Figure 5-13. For a peak temperature of 360°C, the T_P can be any value between 317 and 332°C for specimens with no additional cold work and between 327 and 343°C for specimens with additional cold work. In terms of predicting T_P values, the yield strength values from our hardness measurements based on equations 4.3 and 4.4 seem to be more acceptable than the values suggested by traditional equations, equations 4.1 and 4.2. There is, however, no evidence about which equation should be preferred in calculating dissolution/precipitation solubilities. Selecting different yield strength values will result in different T_P values. Thus, the accuracy of T_P calculation is compromised.

Remember that the conclusion of T_{CAT} being within 4°C of T_P is only valid for any given specimen. The existence range of T_{CAT} for a set of nominally identical specimens is larger, being about 20°C for as-received specimens with a peak temperature of 340°C see Table 4-2. The fluctuation of T_{CAT} values between nominally identical specimens is believed to be associated with the inherent properties of the fracture process and the fact that no two specimens can be absolutely identical. In order to estimate the T_{CAT} values, all the factors have also to be considered. For instance, the matrix strength of the specimens will likely not be a constant value for all the specimens. Figure 4-1 shows that ten units of difference in Vickers hardness is not unusual for specimens that have experienced the same amount of additional cold work. According to Figure 4-2, ten units of Vickers hardness difference is equivalent to about 40 MPa in tensile strength variation and this matrix strength level change has a direct impact on the precipitation temperature. All these factors - hydrogen level, matrix strength, microstructure and even microstructural defects - affect the actual precipitation temperature for any given specimens. With all of these factors being not identical, variations in T_{CAT} temperature between specimens should be a well anticipated consequence.

5.1.6 Critical Stress Intensity Factor (K_{IH}) and Critical Test Temperature for DHC (T_{CAT})

The concept of critical stress intensity factor, K_{IH}, has been introduced in section 2.2.6.2. The basis for discussing K_{IH} and T_{CAT} together in this section is that both of them represent a critical condition in terms of cracking initiation. The most commonly used definition of K_{IH} reads " K_{IH} is a threshold value of stress intensity factor, K_I, below which DHC is not possible" [80]. K_{IH} study has drawn increasing attention because of its practical and theoretical significance. The theoretical significance of K_{IH} comes from its importance in understanding crack initiation criteria. The practical importance of K_{IH} stems from the fact that if a pressure tube contains a pre-existing crack for which the crack tip stress intensity at the applied load is less than K_{IH}, it is then unlikely that such a crack will grow by a DHC mechanism.

Since both T_{CAT} and K_{IH} are near-threshold phenomena, they are somehow related. Fracture tests under low stress intensity factors, for instance under a $K_I = 14$ MPa√m, indicate that cracking will stop at a lower temperature under a reduced K_I. This mirrors the fact that DHC behavior, especially cracking initiation, is a consequence of combined testing parameters including temperature and loading conditions. In considering this fact, the critical condition for cracking to occur can be defined by using either one of these two parameters if another one is known. That is, at any given test temperature, there is always a critical K_I value below which DHC is not possible and this critical K_I value is K_{IH}. If a K_I value is given, on the other hand, there should be also a critical value of test temperature above which DHC will not occur. Imagine that there is a physical quantity, Θ_{DHC}, which decides if cracking can occur, this quantity has to be a function of, among others, both test temperature and stress intensity factor. That is, this quantity Θ_{DHC} should be expressed as:

$$\Theta_{DHC} = f(T, K_I, \ldots\ldots) \qquad (5.14)$$

T_{CAT} is actually a way of defining this quantity by giving the temperature at which cracking will not start under a given stress intensity factor, while K_{IH} is nothing but a stress intensity factor value below which cracking will not occur at a given test temperature. It is no wonder, therefore, K_{IH} value is temperature dependent, as shown in Figure 5-14 [31], while T_{CAT} values are found to be stress intensity factor dependent, as has been reported earlier. Being similar to the fact that cracking can be stopped by increasing test temperatures, cracking processes can also be terminated by reducing the stress intensity factor applied to the specimens, see Figure 5-15. Notice that the reduction of the stress intensity factor has been carried out gradually not abruptly to avoid causing cracking to arrest due to the "compressive zone effect". It can been seen in Figure 5-15 that the increase rate (slope) of the AE counts changed gradually, not abruptly, to zero which means that the specimen was kept cracking during the stress intensity factor reduction process. The specimen finally stopped cracking because the K_{IH} for that test temperature was reached.

To examine how well the above analysis will stand, measured T_{CAT} values under different stress intensity factors have been transformed into the corresponding temperature dependent critical stress intensity factors "K_{IH}" values. Adding these indirectly obtained "K_{IH}" data to Figure 5-14 produces Figure 5-16. The new "K_{IH}" points converted from T_{CAT} measurements fit very well into the original trend shown by the directly measured K_{IH} data points. Regressions show that the curve of combined K_{IH} and "K_{IH}" data even gives a higher R^2 value. Mathematically, this increased R value means that the addition of these converted K_{IH} values has not increased the scatter shown by the measured K_{IH} data. Physically, Figure 5-16 implies that there is a relationship between T_{CAT} and K_{IH} because one of them can be somehow expressed by using the other.

5.1.7 Incubation Phenomenon and Cracking Arrest Phenomenon

As was briefly mentioned earlier, incubation is another phenomenon, which is associated with the cracking initiation process. The incubation period is usually defined as the time span required to get the first crack "jump" after cooling loaded specimens from a peak temperature to a test temperature. This phenomenon is linked to T_{CAT} because it can be considered as a kind of temporary cracking cessation as well. Under some circumstances, cracking does not occur within a certain time period but it will eventually do so when the specimens are held under that condition long enough. This is the difference between incubation and cracking arrest, because when a T_{CAT} is reached, cracking will not occur until the test temperature is lowered again. During incubation, however, cracking is not impossible but just more difficult. A longer holding period is needed for cracking to start.

In T_{CAT} study, a correct judgment about incubation is essential to T_{CAT} measurements because the latter is a cracking "*PAUSE*" while the former is just a "*DELAY*" in cracking initiation. Differentiations have to be made between situations when cracking has really arrested, therefore will not occur no matter how much longer the specimens are going to be kept at the test temperature and situations when cracking activities have not started yet but will do so when the holding period becomes long enough. This kind of differentiation is especially crucial when T_{CAT} measurements are carried out with stress intensity factors below 14 MPa√m, see Tables 4-4a, 4-4b, 4-4c and 4-4d.

In a sense, T_{CAT}, incubation and the K_{IH} discussed earlier are related to each other since they have several things in common. Firstly, they all represent a condition which is associated with some type of cracking initiation difficulties. T_{CAT} and K_{IH} are temperature and loading limits, respectively, because cracking is not possible either at a test temperature above T_{CAT} or under an applied K_I below H_{IH}. Incubation is a time limit which has to be exceeded otherwise cracking will not start. Incubation occurs when cracking initiation becomes so unfavorable that a prolonged preparation (incubation) is needed. Secondly, these three phenomena are all "individual" quantities. Extensive research works on all these three phenomena are needed to thoroughly understand their mechanism. Any improved knowledge on one of these three phenomena will undoubtedly benefit the study of the other two. Although the models about the DHC process which have been developed so far are successful for averageable cracking behaviors such as DHCV, they appear to be less satisfactory in explaining the "individual" behaviors including K_{IH}, T_{CAT} and incubation. To a certain degree, the lack of reliable physical descriptions on "individual" processes retards the development of microscopic models for DHC. Experimental study of "individual" properties is more difficult when compared with measuring averageable behavior because measurements of "individual" quantities require more sophisticated instrumentation, higher level of skills in specimen preparation and larger amount of testing work because of the larger data scatter due to the probabilistic nature of "individual" DHC behavior.

5.1.8 A Possible Existence of an Absolute Cracking Arrest Temperature ($T_{CAT}^{ABSOLUTE}$)

It has been mentioned in section 1, "Research Topic Selection", that one of the objectives of this project is to explore the possible existence of an absolute cracking arrest temperature, $T_{CAT}^{ABSOLUTE}$, above which DHC will occur under no circumstance. Does such an absolute cracking arrest temperature exist?

Experimentally, the peak temperature used in T_{CAT} measurements has been raised to 400°C. With the peak temperature increased to 400°C, cracking arrest temperature has been found also increased to around 360°C, see Figure 5-17. That is, T_{CAT} value keeps increasing when peak temperature increases. In other words, no unconditional independence of T_{CAT} has been found with peak temperature being as high as 400°C. Thus, T_{CAT} measured in the scope of this work is just a state in the cracking process under specific testing condition not a material property of the Zr-2.5%Nb. T_{CAT} measurements with higher peak temperatures have not been carried out since 400°C is the highest temperature pressure tubes encounter both during their production after the extrusion process and in their service, see Figure 3-1. Using peak temperatures above 400°C will bring changes to the microstructure of the specimens [22], making interpretation of the test results difficult. The answer to the question whether or not a $T_{CAT}^{ABSOLUTE}$ exists remains unclear and further work will be needed.

5.2 About Crack Tip Hydride Morphology and Fracture Initiation Criteria

As mentioned in section 1 Research Topic Selection, the study on morphology of crack tip hydrides is an extension of the originally planned work. This extension was made after it had been realized that T_{CAT} provides a unique opportunity for direct observation of the re-oriented crack tip hydrides. The result of this "extra" work, however, later turns out to fit perfectly into the frame of cracking arrest studies simply because T_{CAT} study is about cracking initiation and crack tip hydride morphology is a key issue in controlling the cracking initiation process. The studies of T_{CAT}, crack tip hydrides and fracture initiation criterion are closely related to each other and a thorough understanding of hydride precipitation, growth and fracture will explain a lot of phenomena in DHC, including cracking arrest at high temperatures. Successful development of such fracture initiation criteria will heavily rely on a solid knowledge of crack tip hydride morphology. The semi-quantitative, three dimensional description of crack tip hydrides obtained from this work provides a basis for developing a microscopic model about the fracture initiation process. The hydride morphology study carried out in this work coincides with the increasingly active studies of DHC fracture criteria carried out by other institutions. Since developing a crack tip hydride fracture criterion is not this work's objective, the following discussion is only intended to summarize the metallographic results obtained in this work on crack tip hydrides and to address the possible impact of these developments on the fracture initiation process.

5.2.1 Effect of Hydride Shape on the Stress Distribution near a Crack Tip

The importance of crack tip stress field in the DHC process can not be overstressed and the shape of the precipitated crack tip radial hydride plays a critical role in determining the redistributed local stress field. As introduced in section 2.2.4.2, there are two models dealing with the effect of an existing hydride on the stress distribution near a crack tip: the Ellyin-Wu model [36] and the Metzger-Sauve model [37]. The importance of the hydride shape has been clearly demonstrated by both models.

By using an elstoplastic finite element analysis, Ellyin and Wu have demonstrated that the dimension of the crack tip hydrides, their thickness and length, has influence on the local stress field [36]. Some of their predications have been experimentally validated. For instance, they suggest that irrespective of the location of the initial hydride precipitation, at the crack tip or slightly away from it, the hydride geometry will be similar after a certain amount of growth. This prediction has been confirmed by the metallographic studies of the radial crack tip hydrides carried out in this work, see Figure 4-20. There are, however, indications that some of the assumptions utilized by Ellyin-Wu model need to be modified. Both Figure 2-9 and 2-10 show the presence of a compressive stress region which is impossible because the stress induced hydrogen diffusion can not continue unless the region is loaded under tension, as indicated by equation 2.5. The suggested existence of compressive stress region shown in Figure 2-9 and 2-10 has to do with the assumptions adopted for the modeling process. One of these assumptions is that the crack tip hydride platelets have a rectangular shape with a constant thickness. This assumption has been proven to be inaccurate by the metallographic evidence obtained after the Ellyin-

Wu model had been published. Had a different shape for hydride platelet been used, the drastic variation in the redistributed stress would have been reduced because the importance of the geometry of hydride platelet has been clearly indicated by Figure 13 in [36]. For a piece of hydride platelet of 10 μm long and 0.1 μm thick, having a gradual end shape change eliminates the compressive stress predicted for a sudden end shape change. A careful examination of Figure 2-9 reveals that the stress in a certain region becomes more compressive when the uniformly sized hydride platelet becomes thicker. Since the length of the hydride has been kept constant in Figure 2-9, the results can be interpreted as follows: the redistributed stress will enter a compressive territory when the ratio of thickness/length keeps increasing. Since diffusion would stop before compressive stresses occur, there can be no region of compressive stress, so this implies that uniform thickening of the hydrides is not possible. This implication agrees with the commonly accepted fact about crack tip hydride growth: it grows predominately along the longitudinal direction (becomes longer). As indicated in Figure 2-10, the compressive stress starts to disappear when the ratio thickness/length exceeds a certain value.

The effect of hydride shape on the crack tip stress has been fully explored in Metzger-Sauve model [37]. According to their results, the crack tip hydride platelet should possess a wedged shape. It is also possible that more than one hydride may be formed at a crack tip. In this case, hydride platelets form in a distribution that is concentrated on the plane of symmetry ahead of the notch and the tapering shape reflects the overall shape of the hydrided region. This type of "hydride cluster" is observed repeatedly in this work, as illustrated in Fig. 4-21 and Table 4-8. A tapering shape away from the crack tip is visible for all the radial hydride clusters viewed on the axial-circumferential planes of the specimens. As indicated in Table 4-8, both the number of platelets and the total plate thickness decrease when the measuring location is moved away from the crack tip. Because of the adoption of a wedged shape for hydride platelet(s) in their modeling, Metzger-Sauve model predicts a monotonic stress redistribution which seems to be more realistic.

The fracture initiation of DHC can be viewed as an outcome of the competition between hydride growth and hydride fracture. Fracture occurs when hydrides can precipitate, keep growing and reach the critical fracture condition. In the case of T_{CAT}, the fracture arrest with the presence of uncracked radial hydrides suggests that these hydrides can form but can not grow large enough to initiate fracture. The temperature at which the radial hydrides form but stop growing before they become sufficiently large to fracture is T_{CAT}. At T_{CAT}, the crack tip stress field must be such that hydride precipitation is possible when there are no radial hydrides. As soon as these hydrides have formed, however, the local stress field must have been modified in a way that further growth of these hydride platelets becomes impossible. Because the factors such as test temperature, the amount of cold work and the applied K_I influence the stress distribution near a crack tip, it is the combination of these factors that determines the circumstance under which the radial hydrides form but can not grow. This circumstance, presented in temperature, is the crack arrest phenomenon being studied in this work. The modifying effect of the existing radial hydrides on the crack tip stress field suggested by Ellyin-Wu model and Metzger-Sauve model is one of the key points in understanding the T_{CAT} phenomenon. Based on the aforementioned analyses, it is clear that the geometry of the crack tip hydride is an essential parameter in defining the redistributed stress field. The intensive metallographic examination of the crack tip hydrides carried out in this work has no doubt contributed to a more precise description of the geometry of the crack tip radial hydrides, which provides a better basis for the future modeling of the interaction between the precipitated hydrides and the local stress field.

5.2.2 Describing the Crack Tip Radial Hydrides using a "Multi-hydride" instead of a "Mono-hydride" Configuration

The classic picture of crack tip hydride is disappointedly vague and extremely primitive. Up to quite recently, a "mono-hydride" configuration has been used in DHC process modeling. This configuration assumes that crack tip hydride is in the form of single planar piece lying on the plane of crack. Modeling DHC process using this hydride configuration can give acceptable results when describing averageable behaviors such as DHCV but is impotent in dealing with all the DHC behavior which are non-averageable. Theoretical modeling of the DHC process, either analytically or numerically, which is capable of dealing with "individual" behavior requires a better and more realistic description of crack tip hydride configuration so that the process of hydride precipitation, growth and fracture can be better understood and, eventually, quantitatively defined.

The adoption of the over-simplified "mono-hydride" configuration was mainly because of an absence of a detailed characterization of crack tip hydrides when DHC process modeling started more than 20 years ago. In terms of macroscopic DHC process modeling, ignoring the detailed crack tip hydride configuration does not damage the validity of the derived conclusion. Modifications made to the model have further improved the results derived from the model. Today, 20 years after the model has been developed, it seems that a revolutionary modification of this "mono-hydride" configuration has to be made, otherwise DHC modeling can only remain macroscopic. People have realized that instead of a "mono-hydride" configuration, a "multi-hydride" one should be used in modeling. Such a configuration, although urgently needed, is not available yet, mainly because of the difficulties in preserving crack tip hydrides and the tedious metallographic procedures in revealing these hydrides. Results presented in this work are believed to be the first and the only semi-quantitative, three dimensional description of uncracked fracture tip hydrides published.

Following are some of the characteristics of crack tip hydrides based on metallographic studies carried out in this work:

- Crack tip hydrides are confirmed to be not in the form of single piece but a cluster of platelets, especially at T_{CAT} conditions.
- Individual hydride platelets have platelike shapes.
- The usually observed hydride platelet arrangements are aligned and stacked.
- The hydride cluster, if not every single hydride platelet, has a "wedge" shape.
- The dimensions of both individual hydride platelets and hydride clusters decrease with the amount of cold work done to the specimens.
- The morphology of these hydride platelets can also change with the heat treatments the specimens have experienced.
- These hydride platelets seem to grow along the axial direction as well as along the circumferential direction and become, therefore, longer and thicker synchronously but not necessarily at the same rate.
- At T_{CAT}, re-oriented hydrides form not only on the crack plane but also on planes below and above the crack plane. At temperatures below T_{CAT}, hydrides seem to be less spatially diversified.
- Although the re-oriented, i.e. the axial-radially oriented, hydrides are

responsible for DHC process, the bulk hydrides, i.e. the axial-circumferentially oriented, are not totally irrelevant to the DHC process, since the "bridging" effect of these bulk hydrides may assist fracture initiation.

Based on these observations about crack tip hydrides, it is obvious that the crack tip hydride is more than being a single piece and the "mono-hydride" model has to be replaced. It is just impossible that the critical condition for fracture initiation can be defined by using such a over-simplified "mono-hydride" model. The practice of defining the fracture criterion by using a single quantity - the "critical length" of crack tip hydride - as it is often done until now has to be abandoned. The term "critical length" has to be replaced by "critical condition". At least, the number, size, shape, positions, distribution and orientation of the re-oriented crack tip hydride platelets have to be considered. The morphological effects of specimen strength level, microstructure, thermal history and β-phase morphology on crack tip hydrides, together with some other possible parameters, have to be also clarified. Even the bulk hydrides may play a role in inducing fracture initiation due to the "bridging effect" mentioned earlier, therefore, the density of the bulk hydride which is directly related to matrix hydrogen level may also need to considered. Fractographic analysis shown in section 4.4 indicates that especially the area fraction of re-oriented crack tip hydrides increases with increasing test temperature, see Figures 4-42. It may be possible, that fracture initiation is determined by the hydride coverage ratio, as proposed by Luo [30], not by the dimension of individual hydride platelets or hydride clusters. When the ratio of hydride/matrix becomes high enough, the local toughness of the crack tip region becomes low enough that fracture of this region can occur. The striation spacing changes with test temperature, shown in Figure 5-1, basically support the above argument since the striation spacing changes are equivalent to the changes of hydride/matrix ratio.

While there is no doubt that its application will provide better results in modeling the DHC process, application of a "multi-hydride" certainly brings a higher level of difficulty. Not only more parameters have to be determined, but also the inter-relationships between these parameters need to be well understood, which requires a large amount of theoretical and experimental work.

First of all, metallographic examinations have to be carried out in conjunction with cracking tests to characterize the crack tip morphology under various testing conditions. Combined study of cracking behavior and hydride morphology can also reveal the correlation between the cracking initiation and crack tip hydride configuration. Surveys of crack tip hydrides along the axial direction (the cracking direction), the radial direction (the direction parallel to crack front but perpendicular to the cracking direction) and the circumferential direction (the direction perpendicular to both the cracking direction and the direction parallel to crack front) have to be made. Variations of hydride configuration with respect to test temperature, matrix condition and applied stress-intensity factors have to be determined. It has to be determined what is (are) the dictating parameter(s) for fracture initiation. Is it the length of the individual hydride platelets or the length of the hydride cluster? Or is it the thickness of the re-oriented hydride platelets that governs the fracture initiation condition? Since the thickness increases with length, as suggested theoretically by Metzger [37] and observed experimentally, the thickness and the length of the re-oriented hydrides are related to each other and both of them are important for controlling fracture initiation. There could be other parameters which are decisive for the fracture initiation, for instance the hydride/matrix ratio. To ultimately determine the decisive parameters in the fracture initiation process, measurements of all the affecting parameters need to be carried out. Enough specimens have to be analyzed to get a statistical conclusion.

Secondly, caution has to be applied when any averaged quantity is used in defining the critical threshold values. For instance, it can not simply be assumed that the average crack tip hydride dimension measured metallographically represents the critical dimension for fracture initiation, because this averaged value is a calculated result from all the observed hydrides including those which have only grown to a fraction of their critical dimension. Using such an averaged value will underestimate the critical condition for fracture initiation. A more acceptable practice would be to consider the critical hydride length to be equal to the value of an upper confidence level of all observed crack tip hydride lengths. To avoid any underestimation, the critical dimension should be calculated by multiplying the value of mean hydride dimension by a correction factor which is greater than one.

Thirdly, the interaction between re-oriented hydrides and crack tip stress level has to be further investigated. This interaction has been widely acknowledged but not always integrated in modeling DHC behavior [78]. Improved knowledge on this interaction will help us to understand the hydride growth process, which in turn, will benefit the study of the fracture initiation process.

Fourthly, the interaction between the re-oriented hydrides (the radial hydrides) and the "original" bulk hydrides (the longitudinal hydrides) needs to be clarified as well. The interaction between re-oriented and the bulk hydrides means that the matrix hydrides are not totally irrelevant to the cracking initiation/propagation process because these bulk hydrides can sometimes “bridge” two re-oriented hydrides to make their fracture possible. It is not clear, though, how decisive this “bridging” effect is in fracture initiation/propagation process.

5.3 About DHC Process and The Parameters Affecting It

Being able to explain all the DHC behavior of Zr-2.5%Nb is the ultimate goal of any DHC study. To be able to describe the process quantitatively, a qualitative characterization of the process is necessary. It is like a study of any process, a mathematical description of the process comes only after a physical characterization of the process becomes available. The classic DHC model assumes that a single-pieced, through-thickness hydride forms at the crack tip and it grows in the cracking direction. This piece of hydride breaks when it reaches a "critical length". With this hydride broken, the crack front jumps forward and the formation of crack tip hydride re-starts. Previous discussion and all the papers on DHC published recently have indicated that this "mono-hydride" configuration is greatly oversimplified and has to be replaced by a "multi-hydride" configuration which is closer to reality. Following is some visualization on how a DHC process actually progresses based on the experimental evidence collected in this work.

In considering the fact that fractured surfaces often show a nested structure consisting of squares, Figure 5-18, a "disk-like" ("cornflake-like") configuration of crack tip hydride as shown in Figure 5-19 seems to be a logical consequence. As mentioned in section 4.4, the fractured surface is not totally covered by hydride and the nest is made of matrix material and the openings of the nest are the places where hydrides have existed. A schematic drawing shown in Figure 5-20 about how these crack tip hydride disks are developed appears then to be acceptable. Figure 5-21 schematically illustrates the hydride configurations on the axial-circumferential (A-C) and circumferential-radial (C-R) planes if the crack tip hydrides had "disk-like" ("cornflake-like") shapes. It is more likely, however, that crack tip hydrides are actually developed in a way illustrated in Figure 5-22.

Considering the fact that re-oriented crack tip hydrides precipitate more or less uniformly along the crack front, situations presented in Figure 5-23 may be more realistic. Figure 5-24 suggests the possible hydride morphologies on both axial-circumferential (A-C) and circumferential-radial (C-R) planes based on this "strip-like" configuration. Referencing to the metallographic observations introduced in section 4.3, the author believes that the development model portrayed in Figure 5-25 is the best one in terms of representing what is actually happening when a specimen is cracking via DHC. The author's belief stems from the following reasoning. First of all, the hydride configurations proposed by Figure 5-26 closely resemble the experimentally observed re-oriented hydrides introduced in section 4.3. Secondly, the three dimensional metallographic measurements show that there can be more than one hydride platelet lined up along the axial direction and the hydride width (the dimension along the radial direction) is always shorter than the hydride length (the dimension along the axial direction). Thirdly, being in the shape of a stripe does not mean that the pattern shown in Figure 5-18 can not be produced, as shown in Figure 5-27. Comparison of Figures 5-19 and 5-27 shows the later is closer to the real image of fracture surface shown in Figure 5-18. The fractographic details inside the quasi-square units observed on fractured surfaces indicate that crack tip hydrides are not in a form of square disks but in a rectangular or a lenticular shape.

In terms of affecting parameters in DHC process, some reasoning can also be made based on the discoveries of this work. As shown in equation 5.14, test temperature relative to peak temperature and applied stress intensity factor appear to be two of the important parameters in the DHC process. Considering the proper influence of matrix strength on DHC behavior, Figure 5-16 given in section 5.1.6 can actually be expanded into a three dimensional graph. In addition to test temperature and loading condition, the matrix strength should be added as the third axis and Figure 5-28 is the resultant graph. Figure 5-28 indicates that a critical condition for crack initiation can be defined by a point in a three-dimensional coordinate system made of test temperature, applied stress intensity factor and matrix strength. The equation 5.14 can now modified into

$$\Theta_{DHC} = f\,(T, K_I, \sigma_y \,.....) \qquad (5.15)$$

Since the diffusible hydrogen level has been proved to affect the DHC behavior too, the equation 5.15 can be further expanded to

$$\Theta_{DHC} = f\,(T, K_I, \sigma_{y,}\ C_{H(DIFF)}, \,....) \qquad (5.16)$$

Equation 5.16 will be further expanded based on the continuously improving knowledge about the DHC process. Until the completion of a physically correct visualization of DHC process, a complete scientific model of DHC will not be possible.

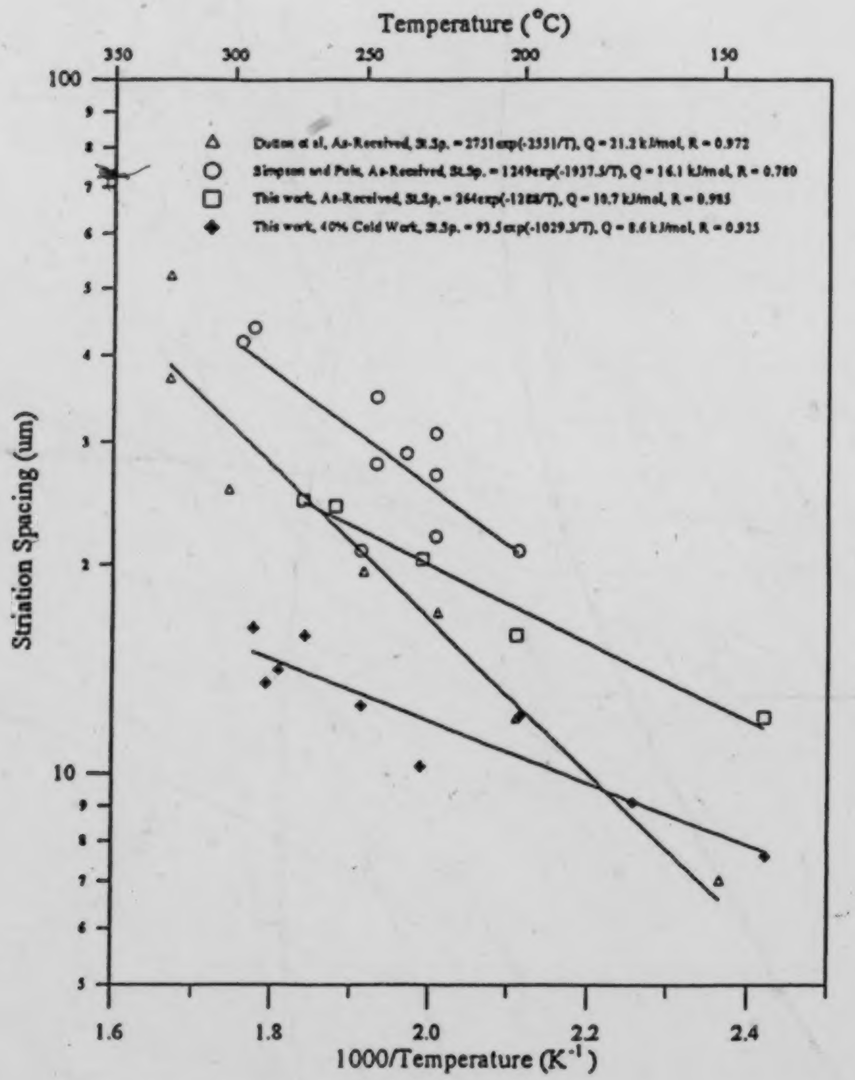

Figure 5-1 Effect of temperature on striation spacing [77]

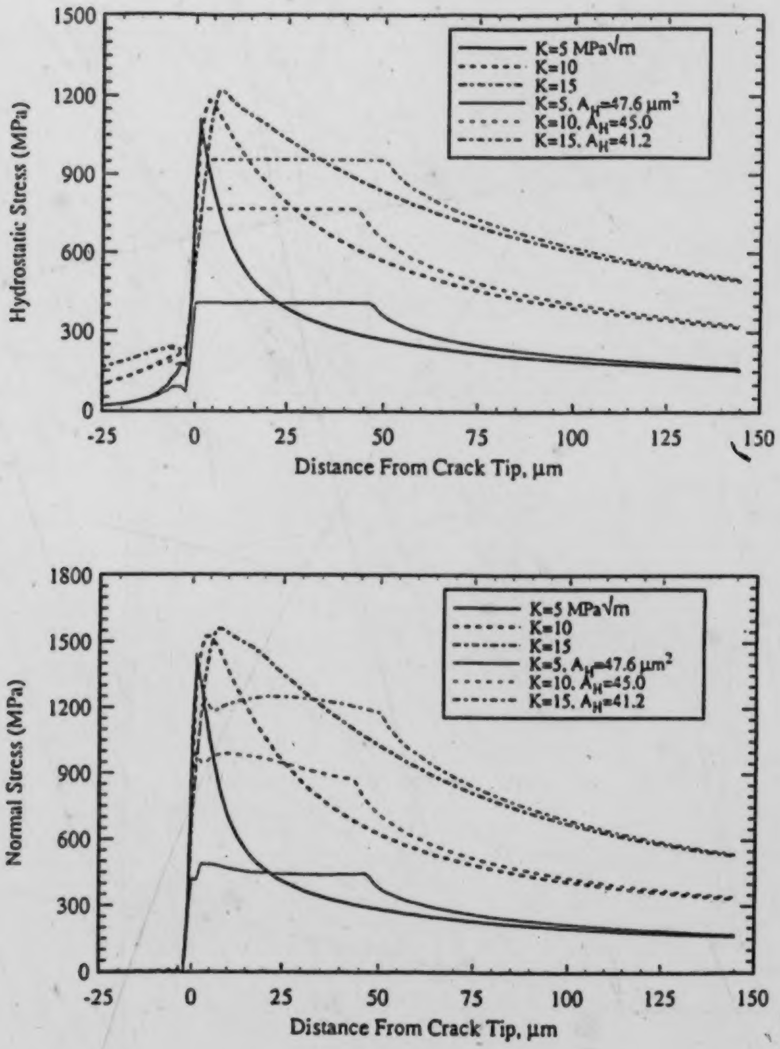

Figure 5-2 Change in crack tip stress due to growth of hydride elastic-perfectly plastic, $\sigma_y = 550$ MPa, E= 80 GPa [78]

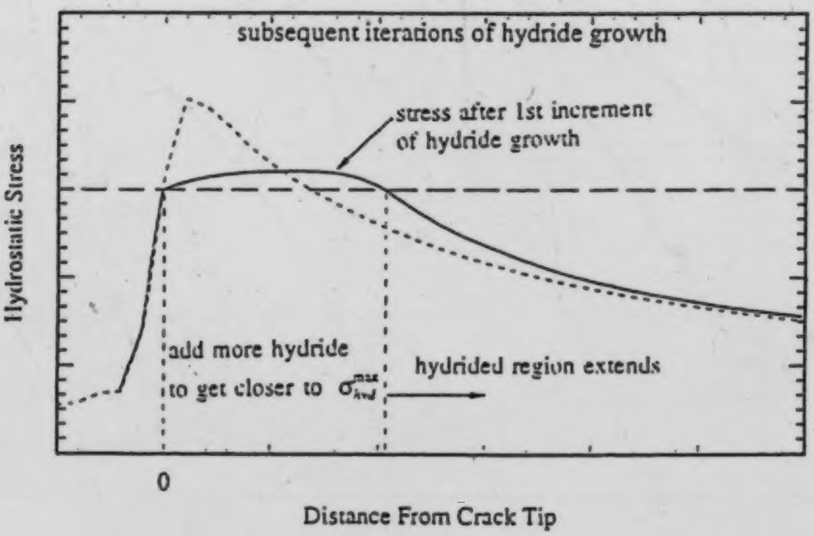

Figure 5-3 Increments of hydride growth reducing hydrostatic stress [37]

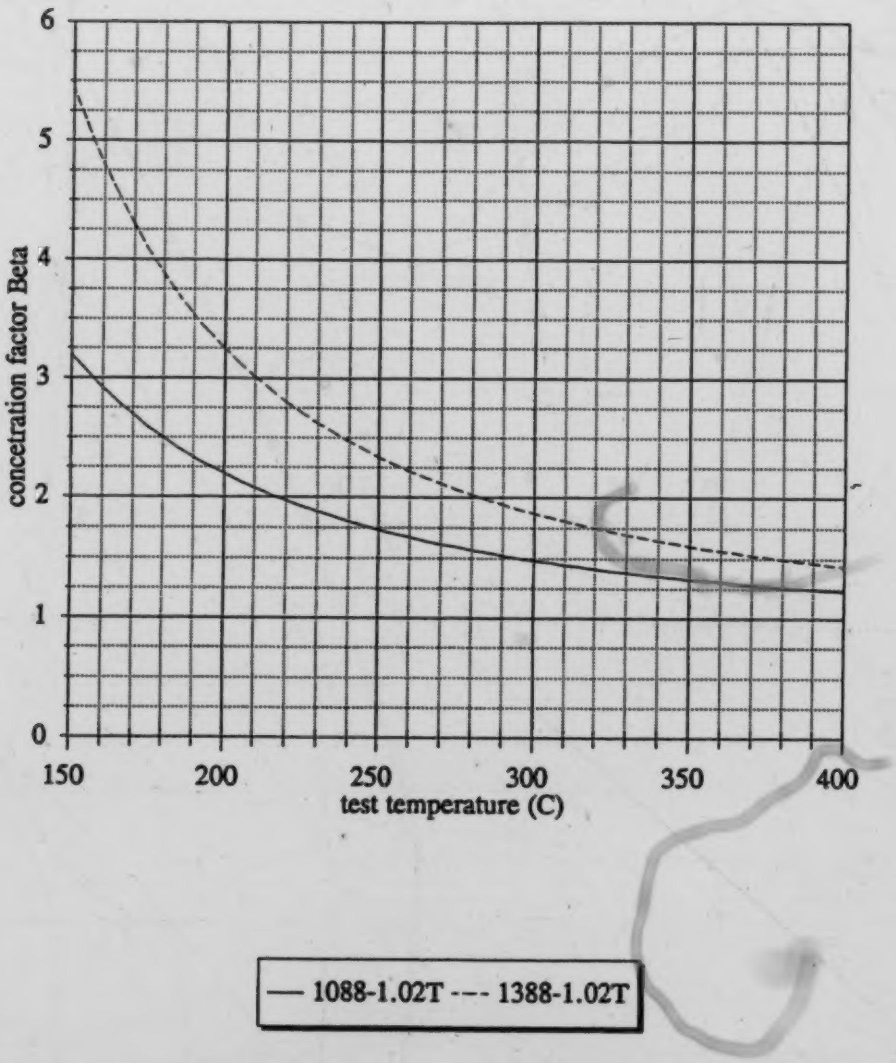

Figure 5-4 Temperature dependence of hydrogen concentration factor β

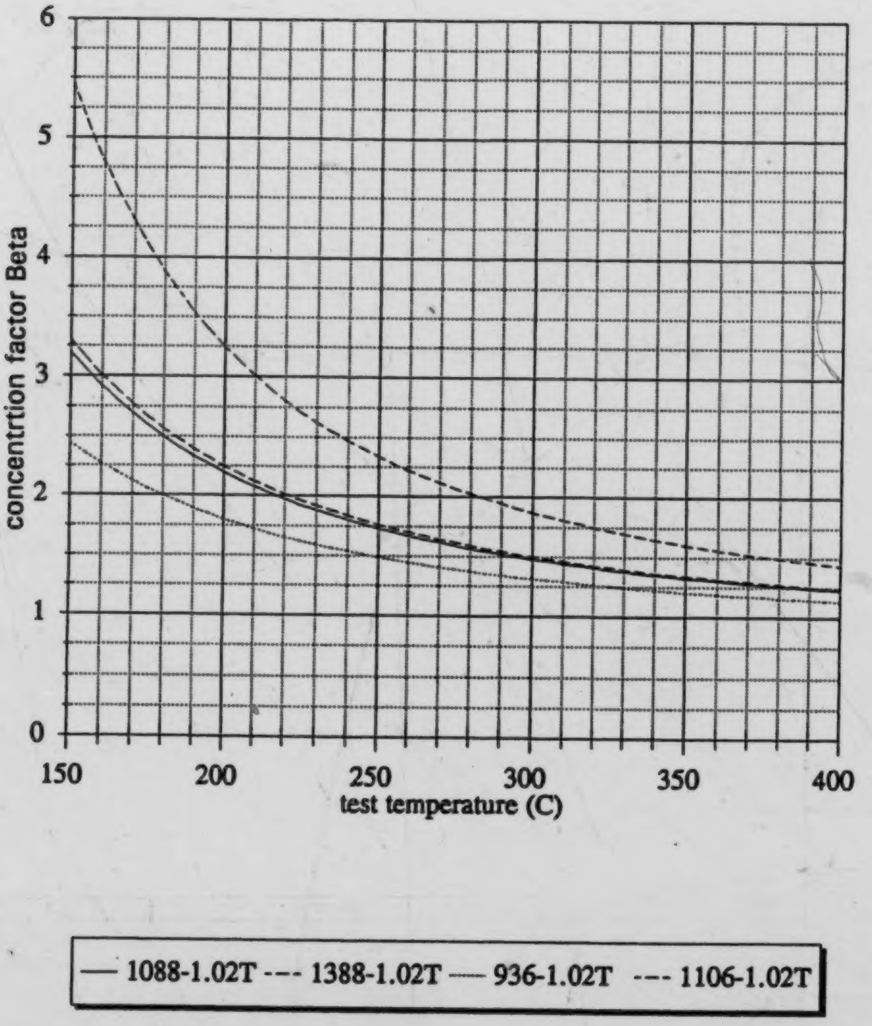

Figure 5-5 Effect of matrix strength values in calculating hydrogen concentration factor β

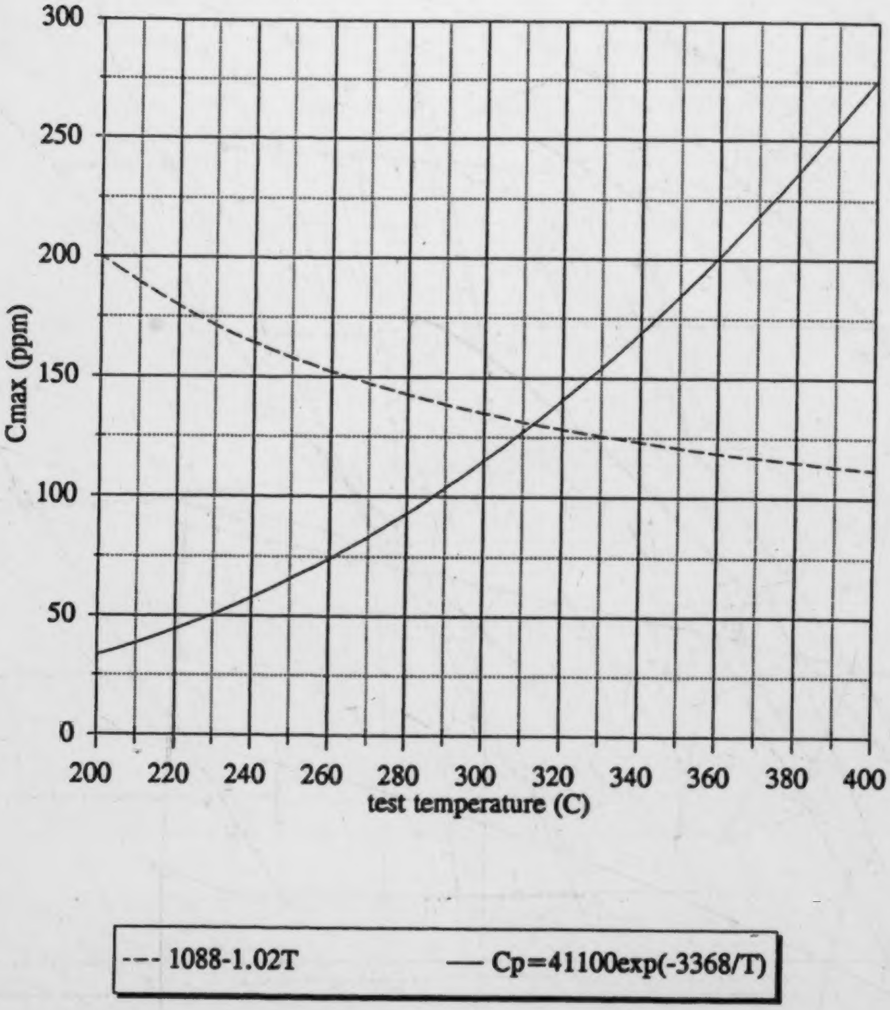

Figure 5-6 Graphical calculation of the highest possible temperature for hydride precipitation (T_p) with a peak temperature of 340°C

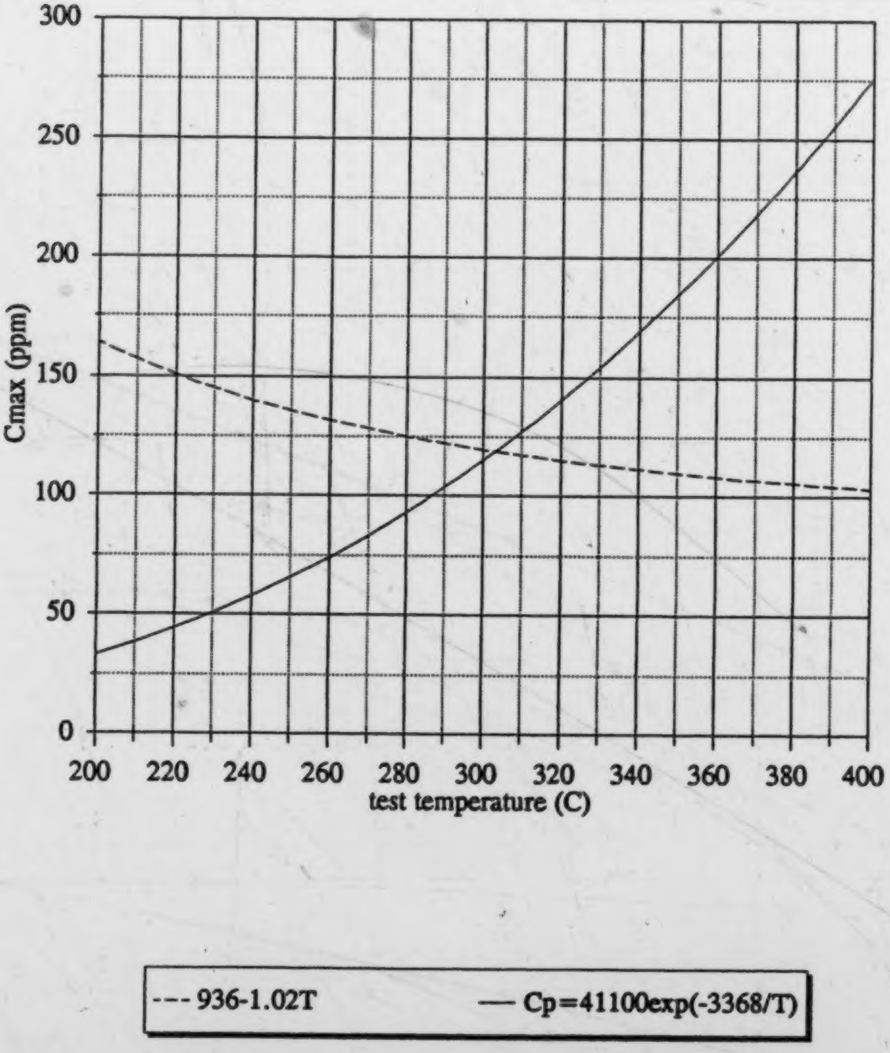

Figure 5-7 Effect of matrix strength values on calculating the highest possible temperature for hydride precipitation (T_p) with a peak temperature of 340°C

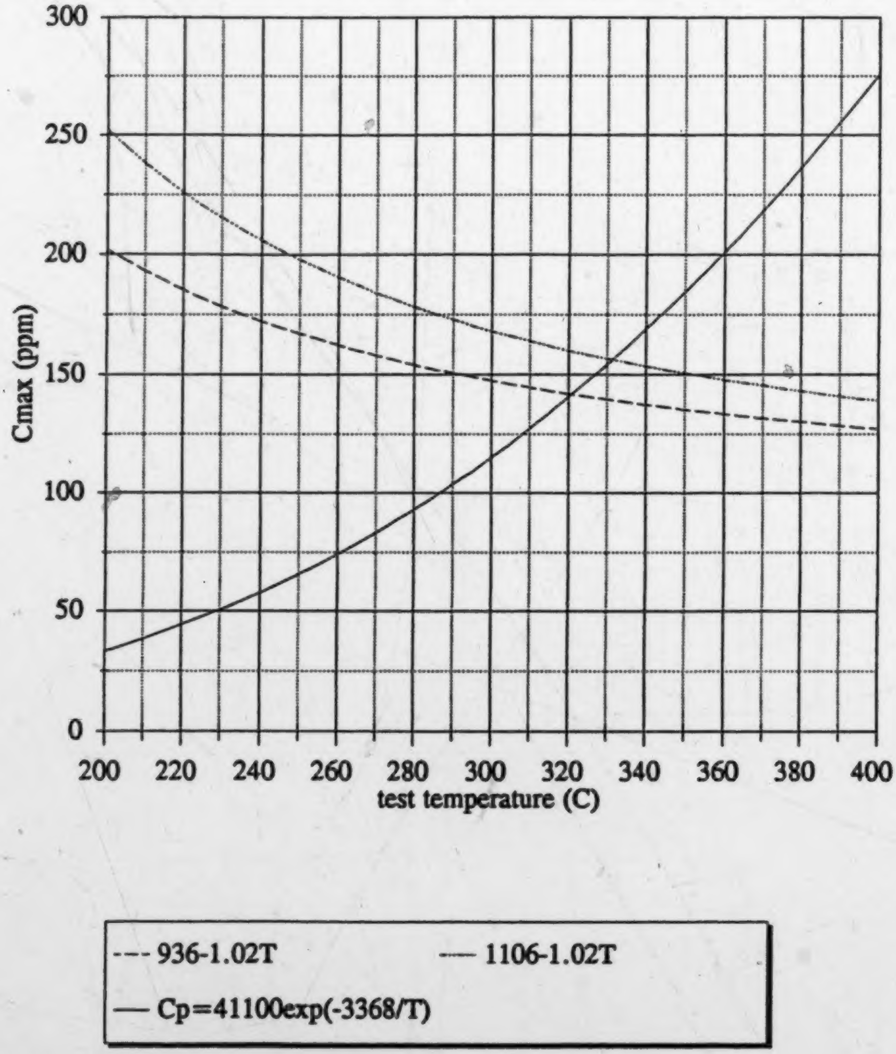

Figure 5-8 Graphical calculation of the highest possible temperature for hydride precipitation (T_p) with a peak temperature of 360°C

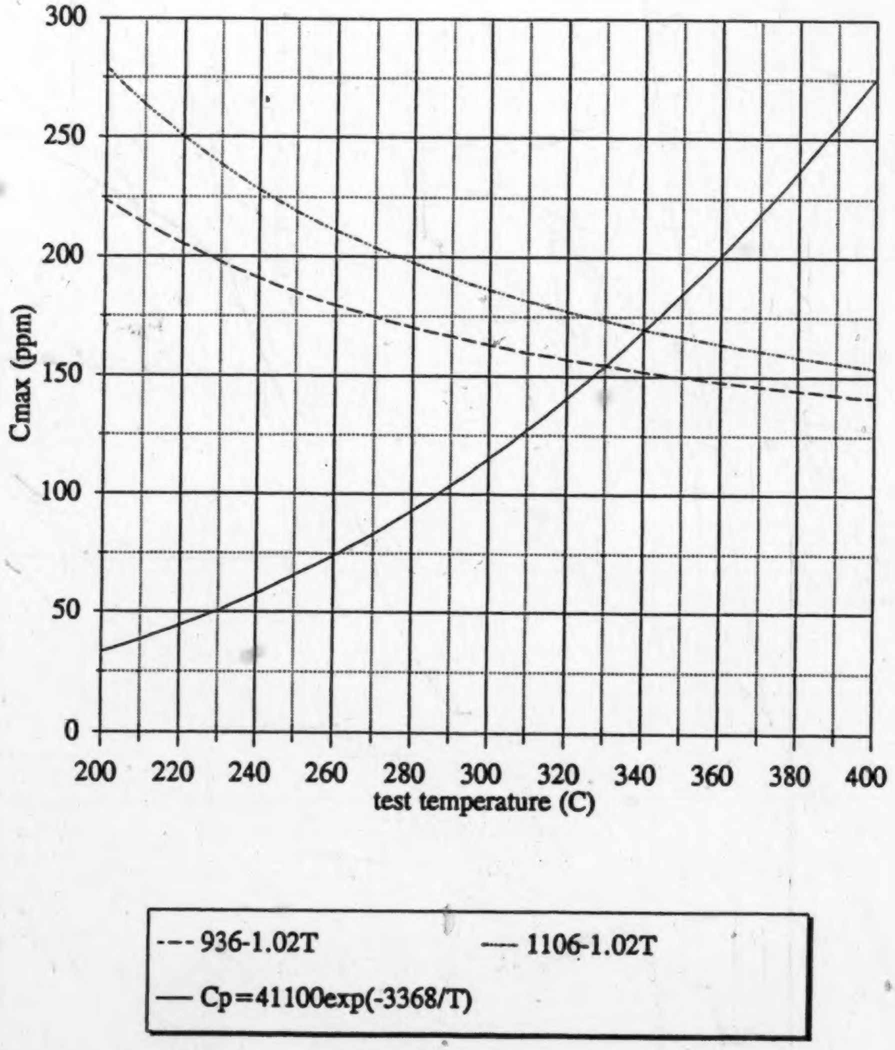

Figure 5-9 Graphical calculation of the highest possible temperature for hydride precipitation (T_p) with a peak temperature of 370°C

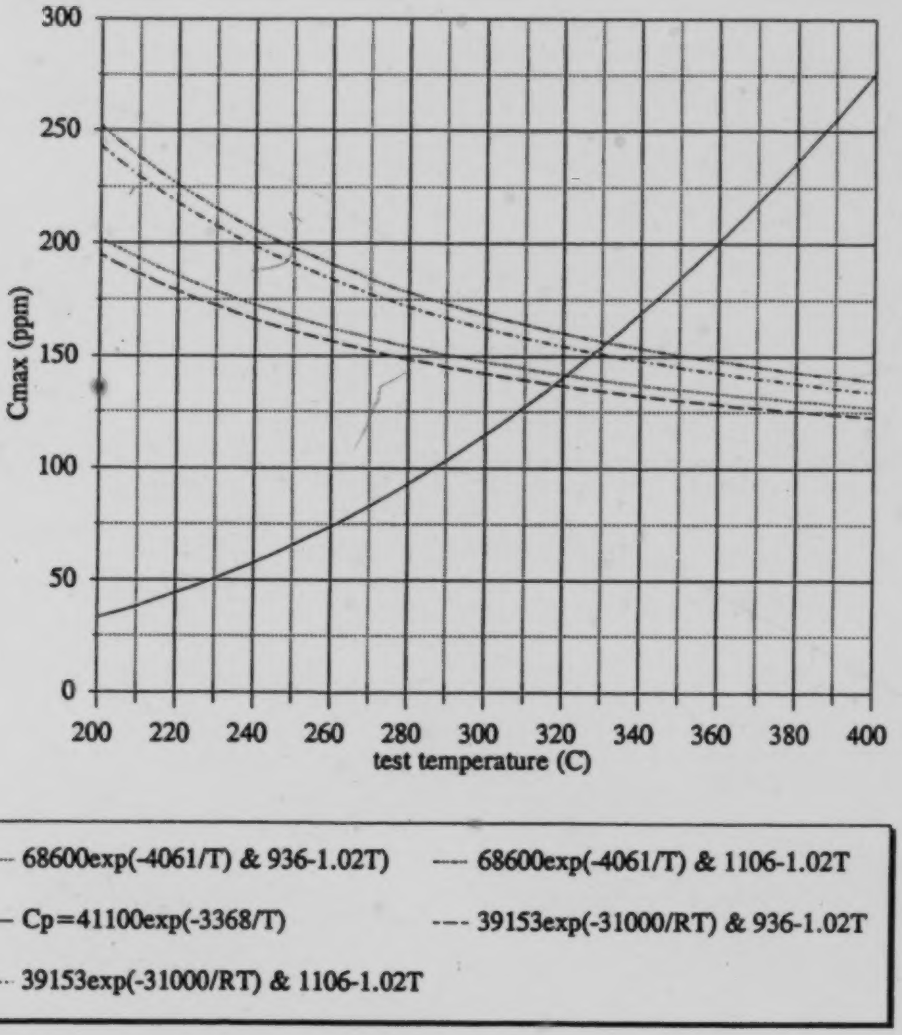

Figure 5-10 Effect of σ_y and C_H^d values on calculating the highest possible temperature for hydride precipitation (T_p)

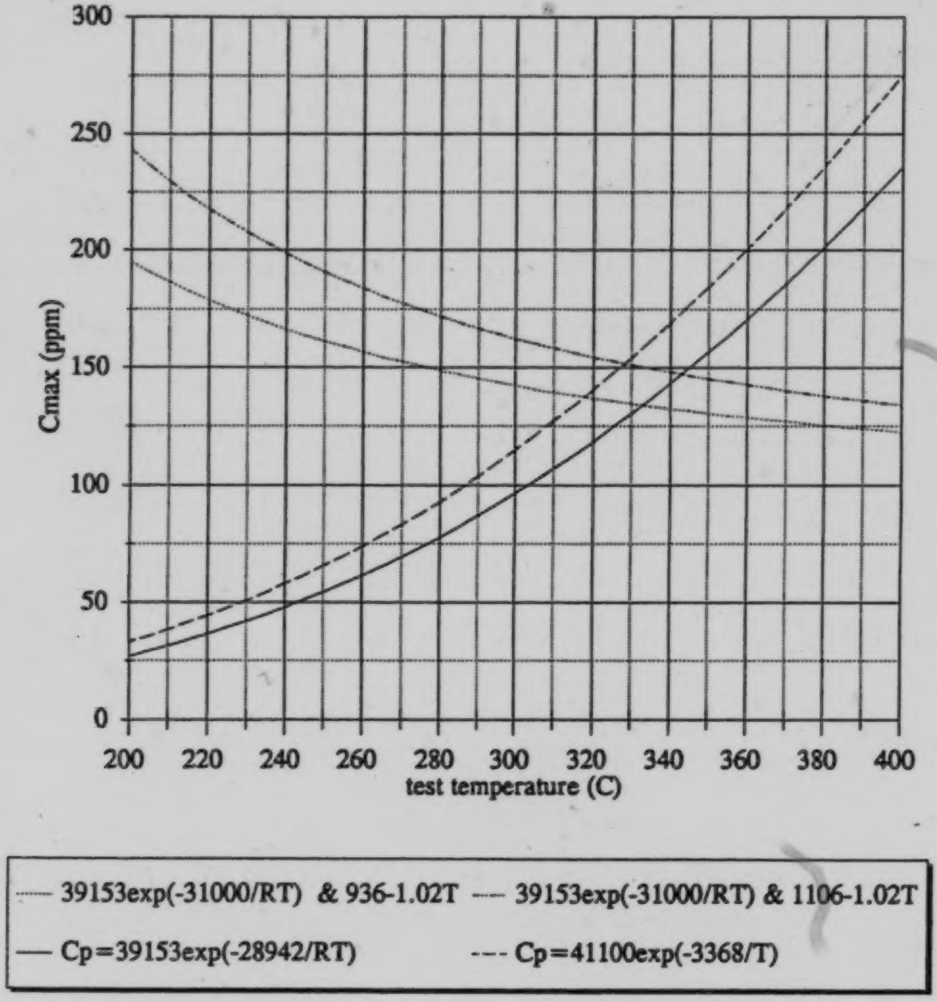

Figure 5-11 Effect of C_H^p values on calculating the highest possible temperature for hydride precipitation (T_p)

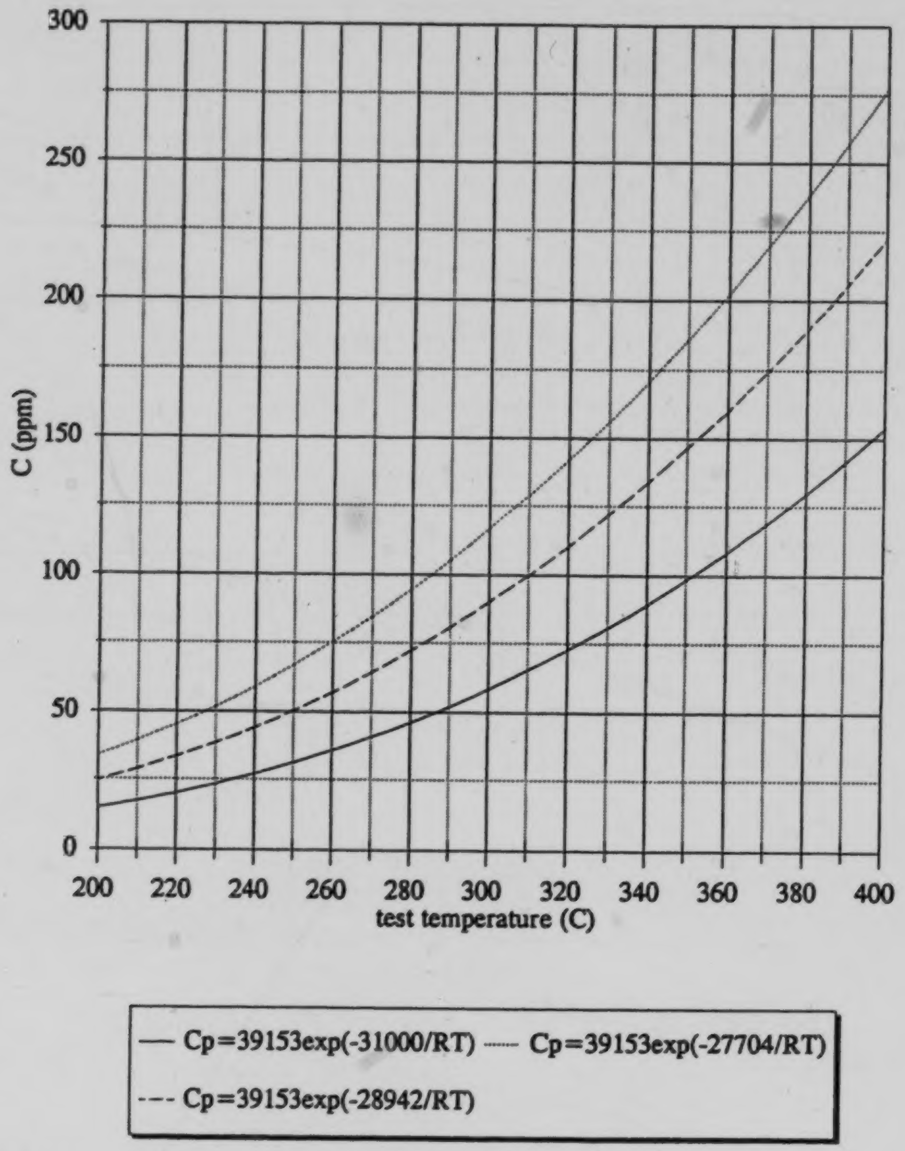

Figure 5-12 The two temperature dependent hydrogen concentration curves from the two C_H^P curves given by Shi [31]

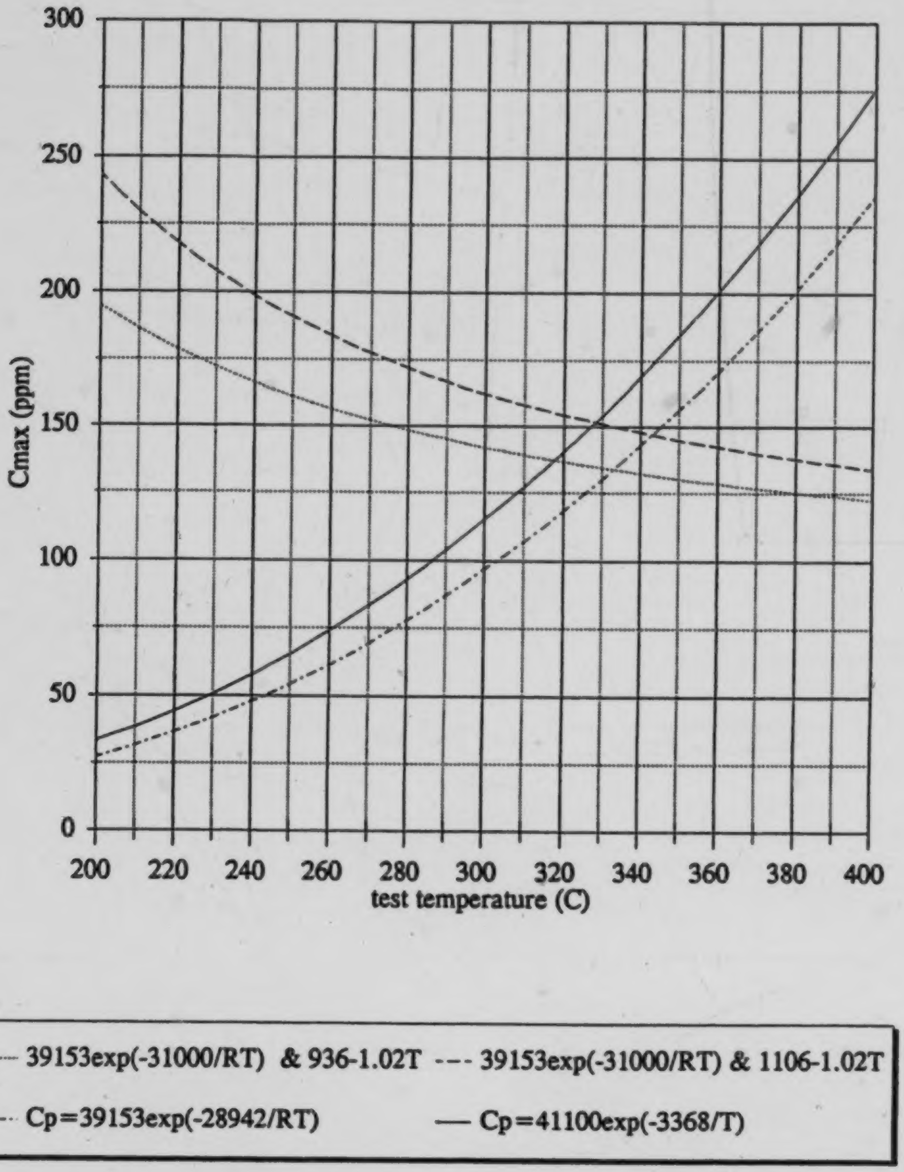

Figure 5-13 Calculated temperature range for the highest possible temperature for hydride precipitation (T_p) with a peak temperature of 360°C

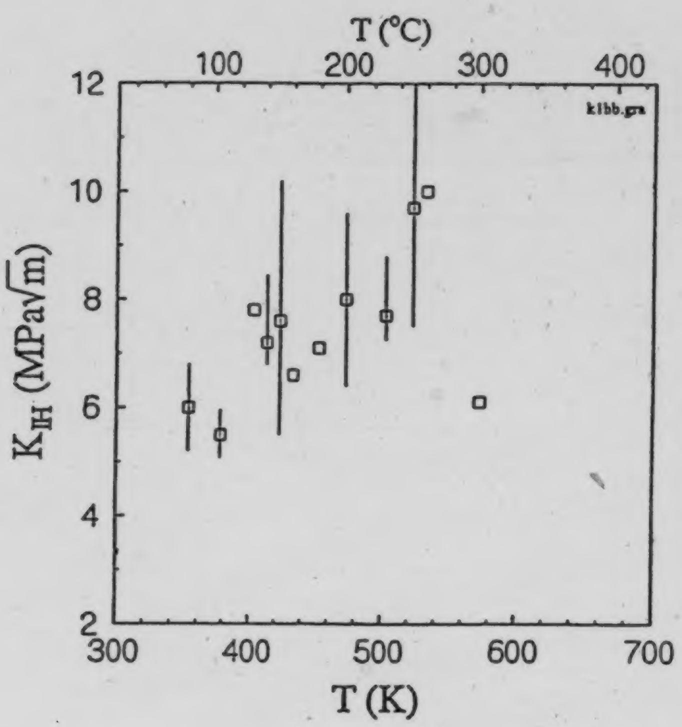

Figure 5-14 Temperature dependence of measured K_{IH} values [31]

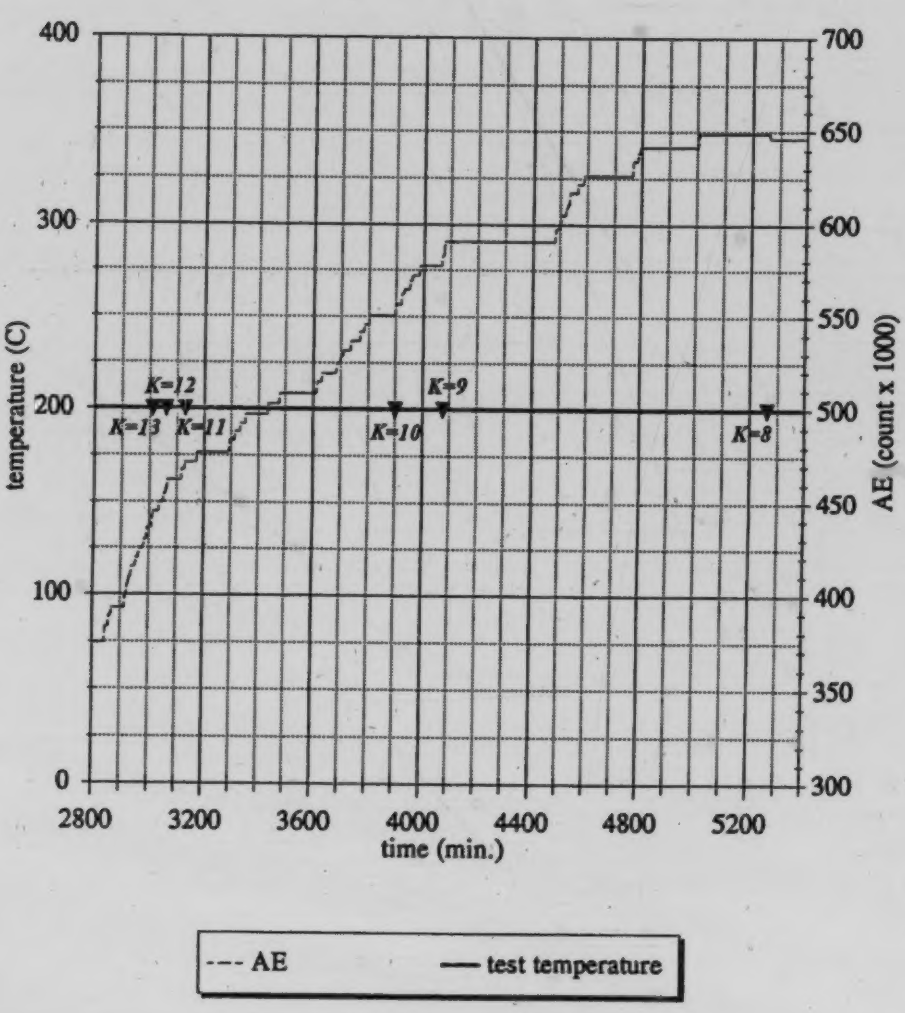

Figure 5-15 Effect of applied stress intensity factor on cracking activity indicated by accumulated AE signals

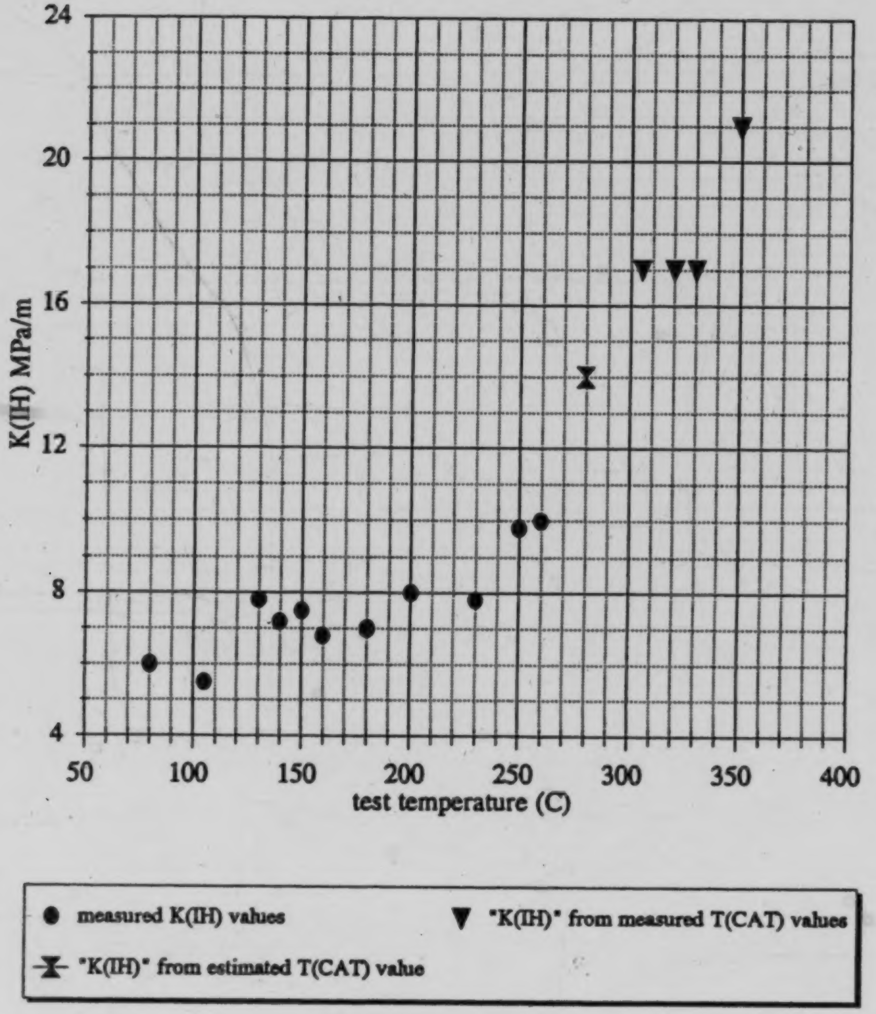

Figure 5-16 Combination of measured K_{IH} and calculated “K_{IH}“ from measured T_{CAT} values

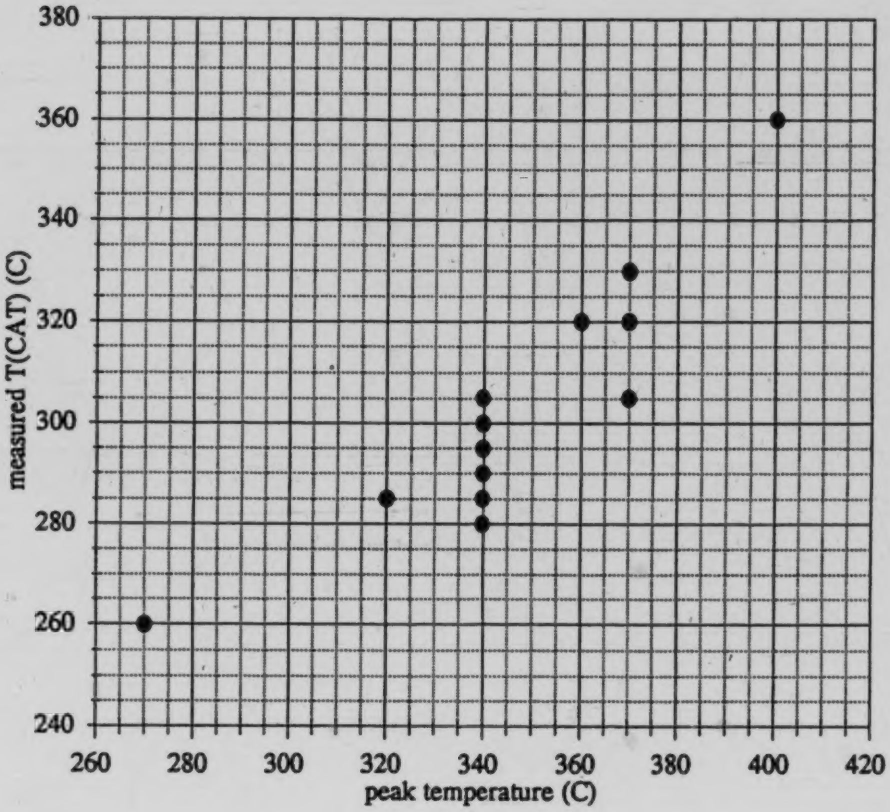

Figure 5-17 Effect of peak temperature on measured T_{CAT} values (The T_{CAT} value for peak temperature=270°C is an estimated one form DHCV measurement)

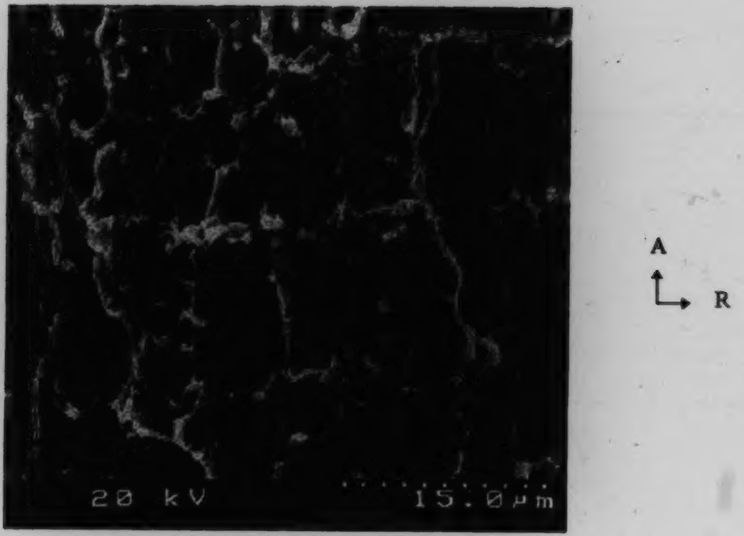
20 kV
15.0μm
A
R

Figure 5-18 SEM image of fractured surface showing a nested structure

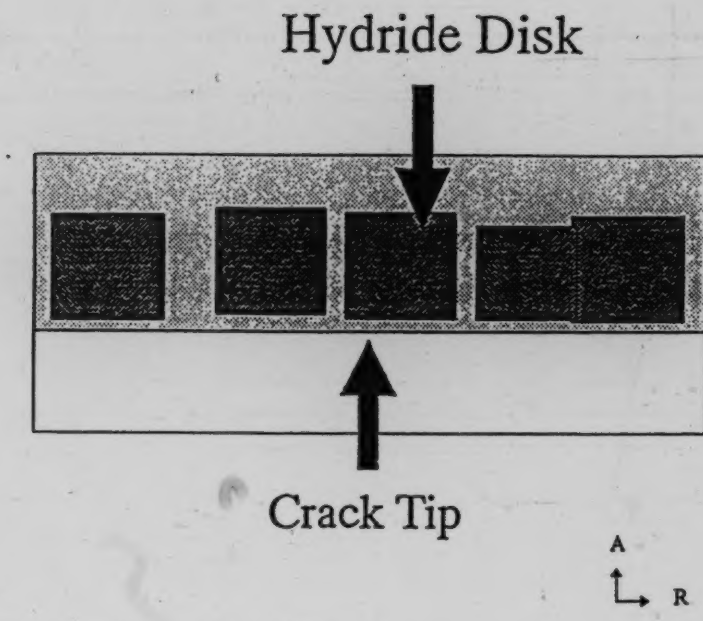
Hydride Disk
Crack Tip
A
R

Figure 5-19 Schematic illustration of a "disk-like" ("cornflake-like") crack tip hydride configuration

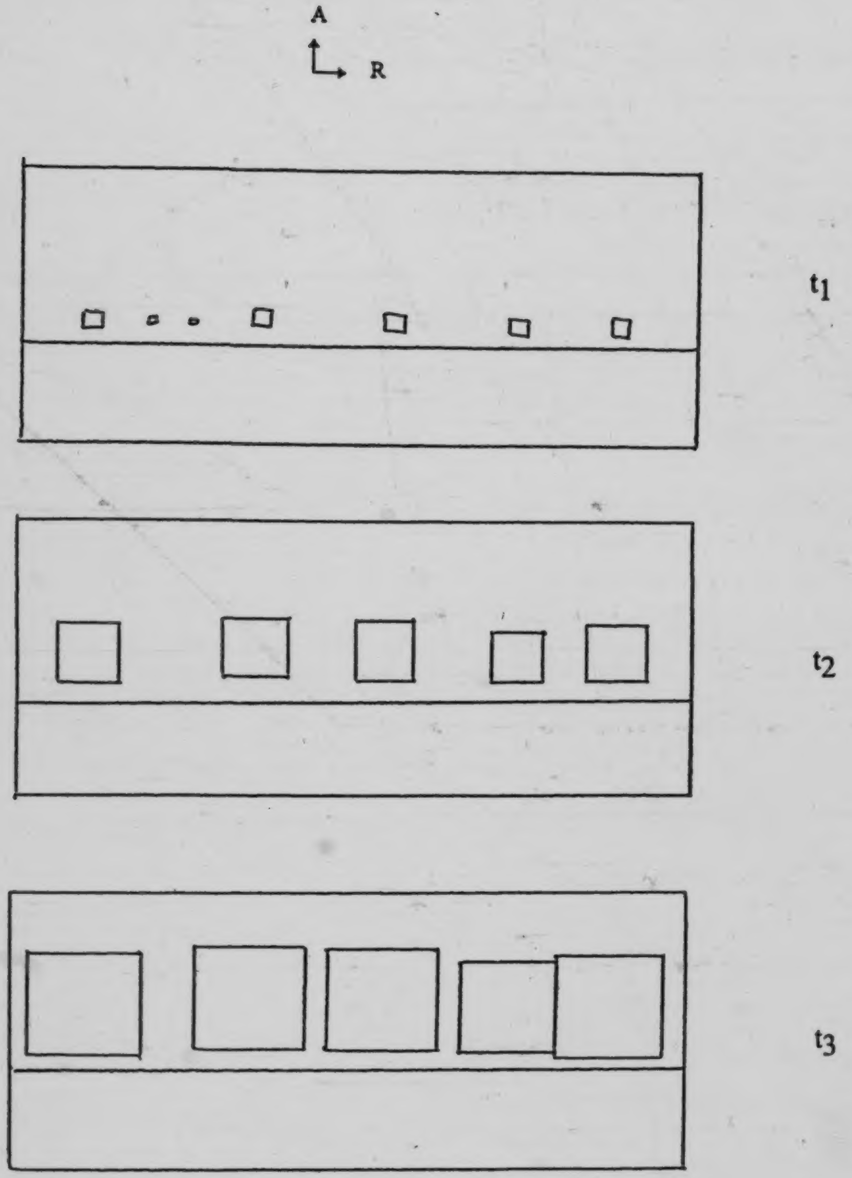

Figure 5-20 Schematic illustration of development of crack tip hydride "disks" ("cornflakes") configuration and its development

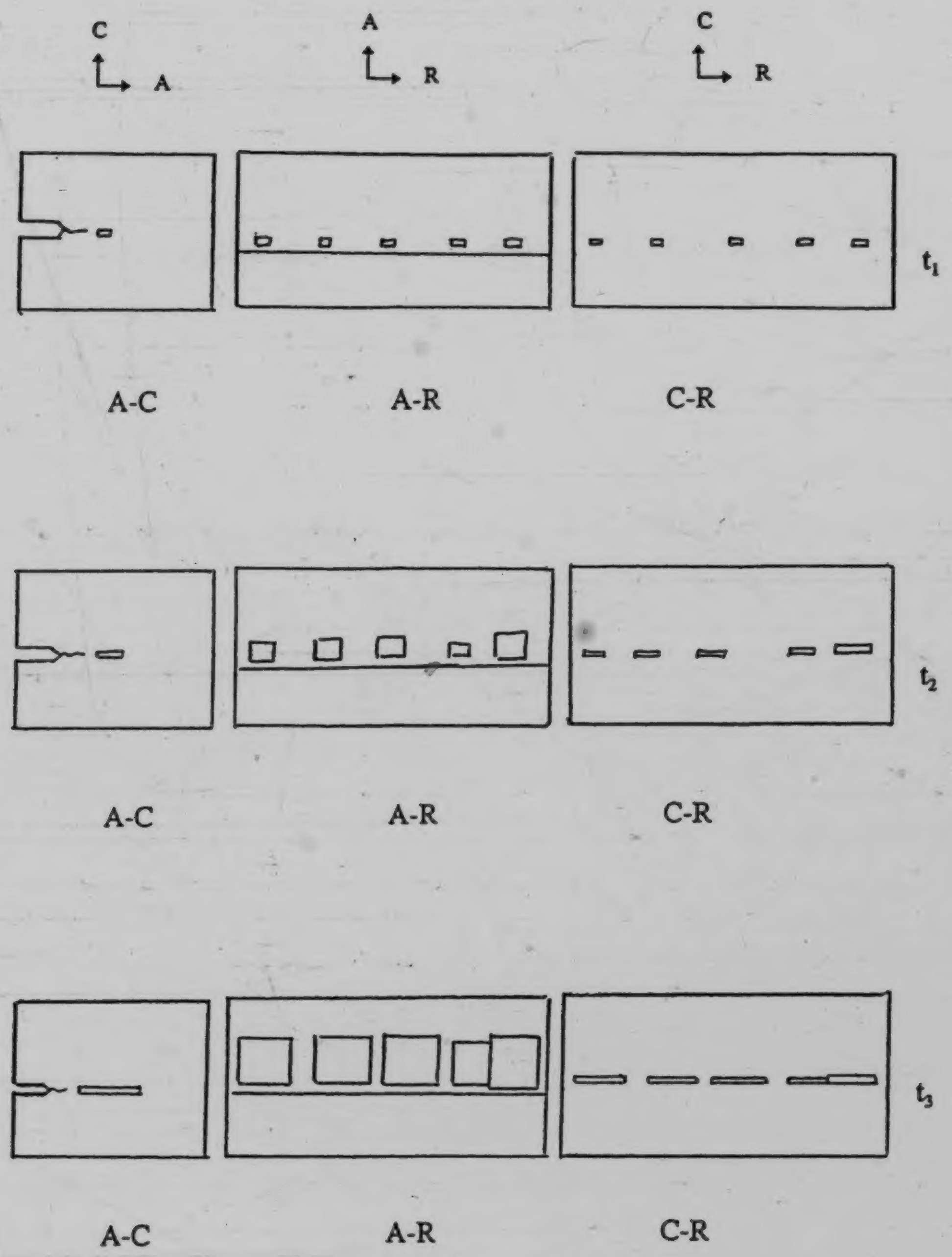
C
A
A
R
C
R
t1
A-C
A-R
C-R
t2
A-C
A-R
C-R
t3
A-C
A-R
C-R

Figure 5-21 Suggested hydride morphologies based on a "disk-like" model

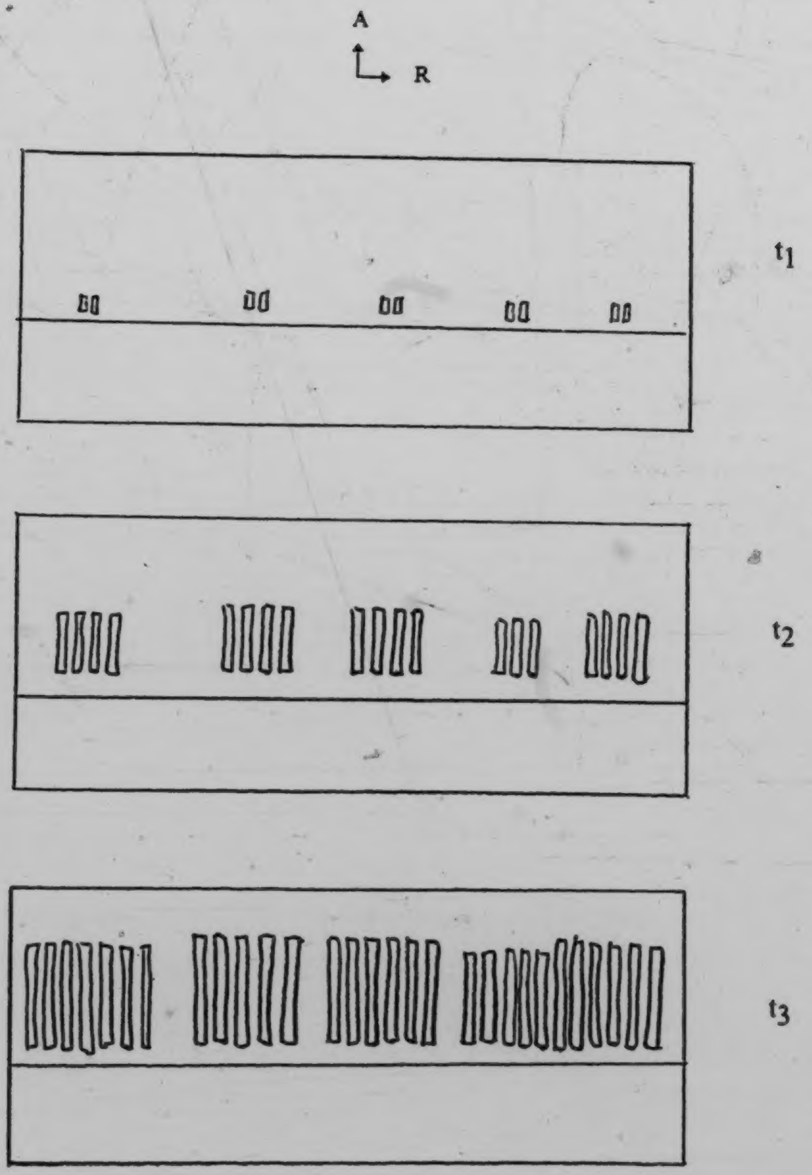

Figure 5-22 Schematic illustration of a "strip-like" crack tip hydride configuration and its development

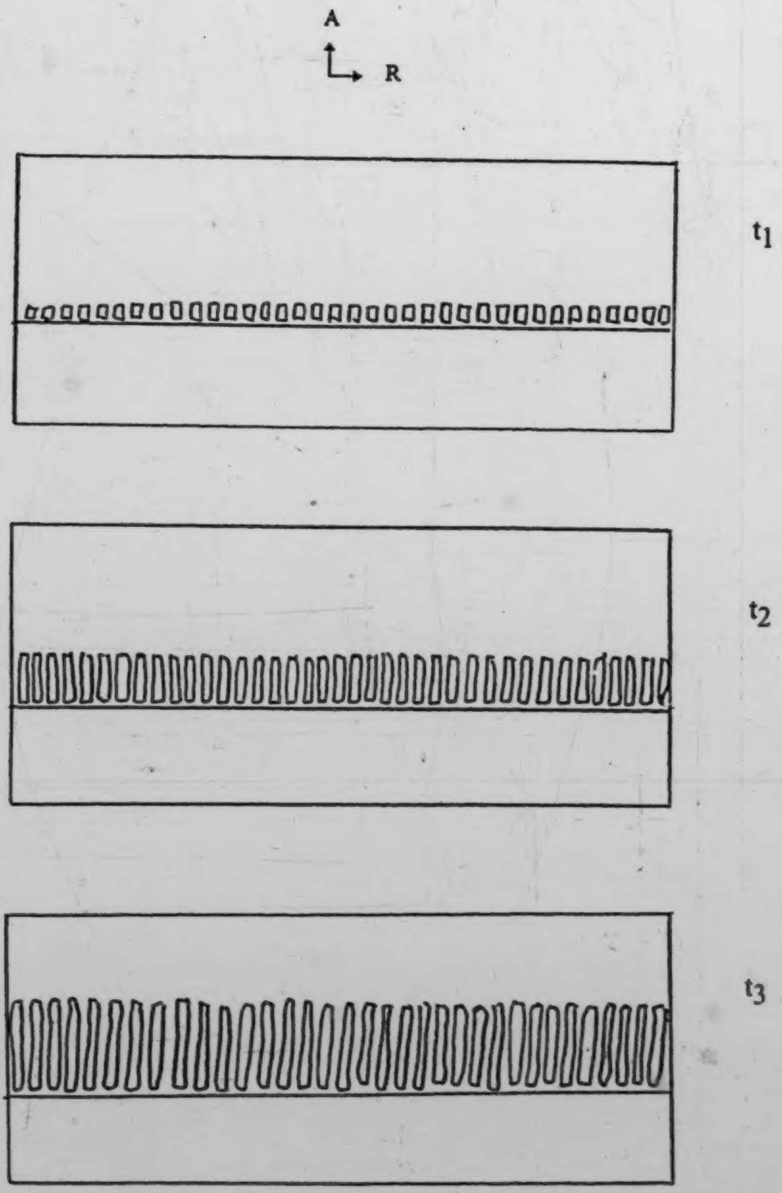

Figure 5-23 Schematic illustration of a uniform "strip-like" crack tip hydride configuration and its development

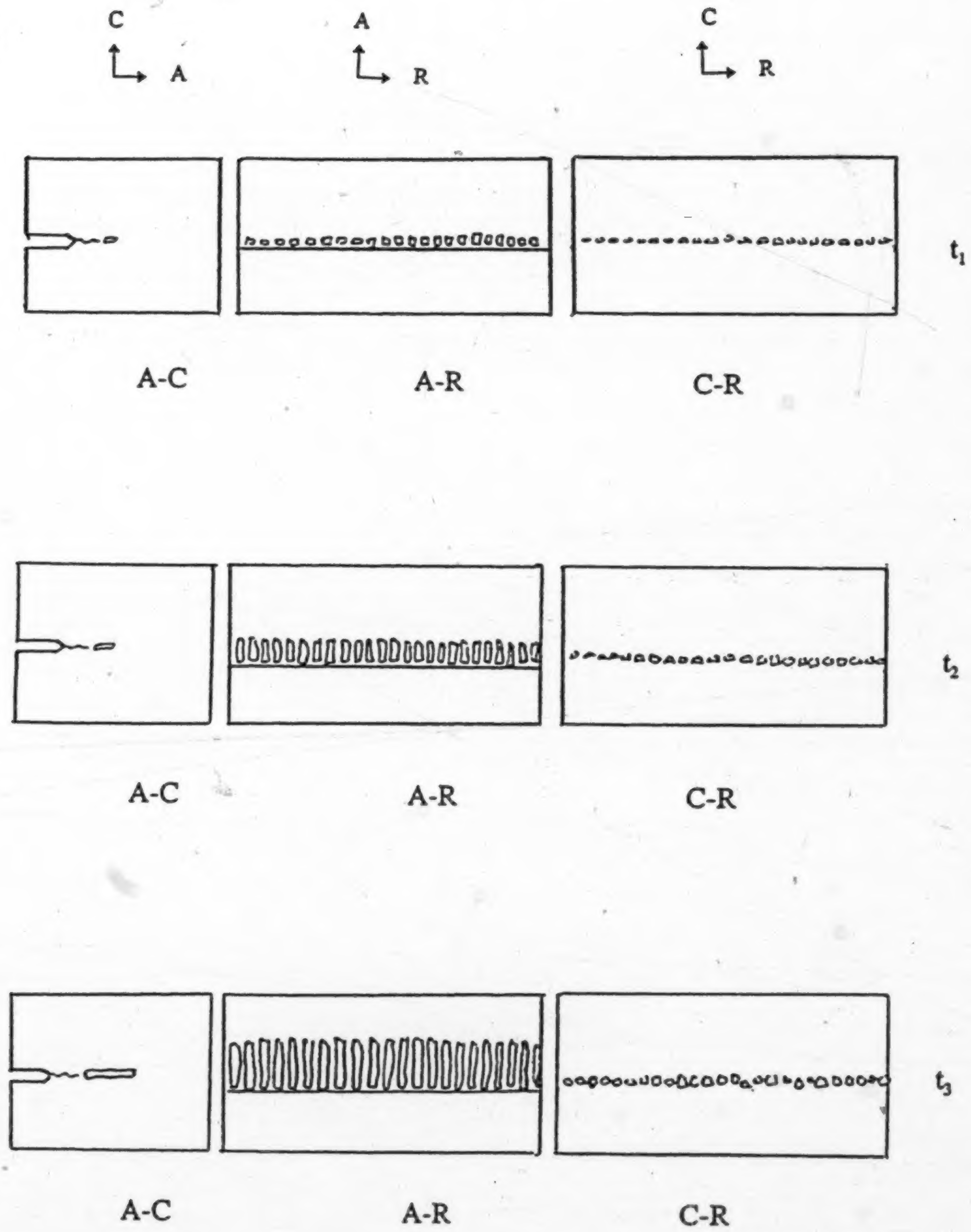
C
A
A
R
C
R
t$_1$
A-C
A-R
C-R
t$_2$
A-C
A-R
C-R
t$_3$
A-C
A-R
C-R

Figure 5-24 Suggested hydride morphologies based on a "strip-like" model

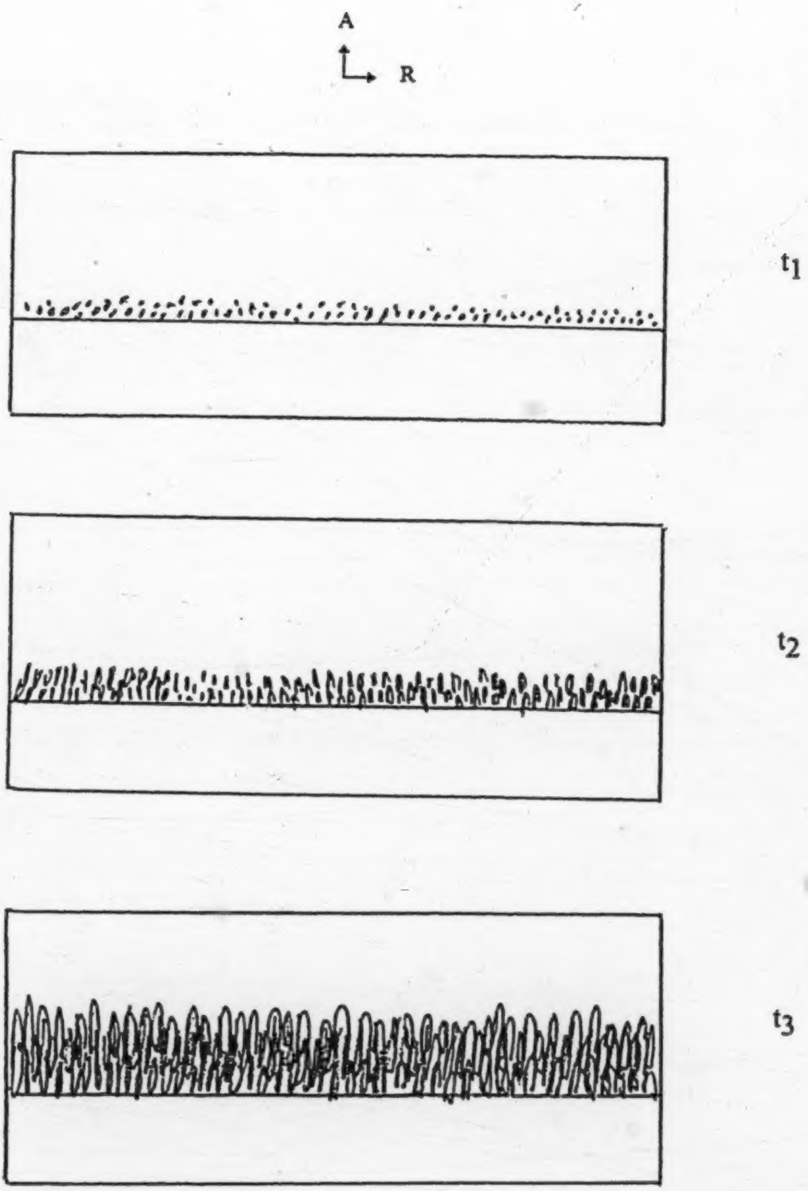

Figure 5-25 Schematic illustration of a "platelet-like" crack tip hydride configuration and its development

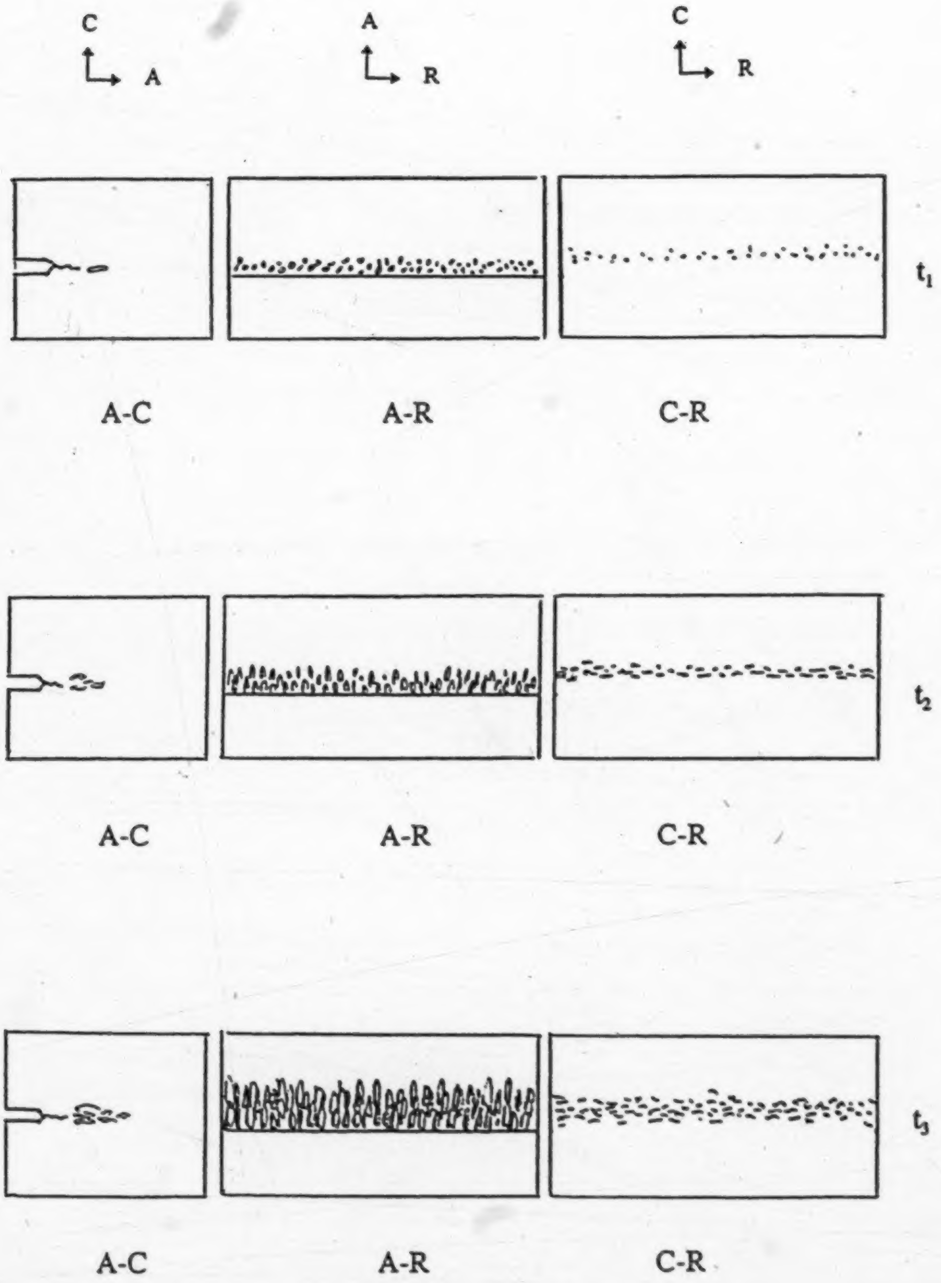
C
A
A
R
C
R
t1
A-C
A-R
C-R
t2
A-C
A-R
C-R
t3
A-C
A-R
C-R

Figure 5-26 Suggested hydride morphologies based on a "platelet-like" model

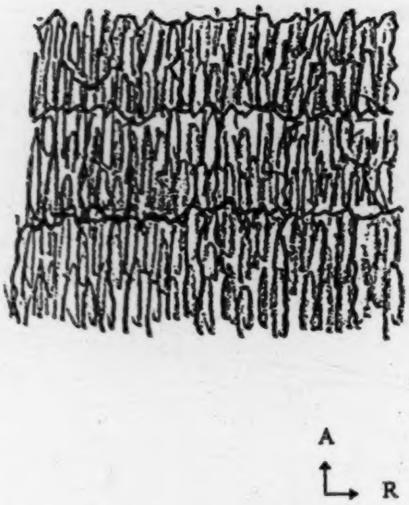

Figure 5-27 Schematic illustration of a featured surface produced by a "platelet-like" crack tip hydride configuration

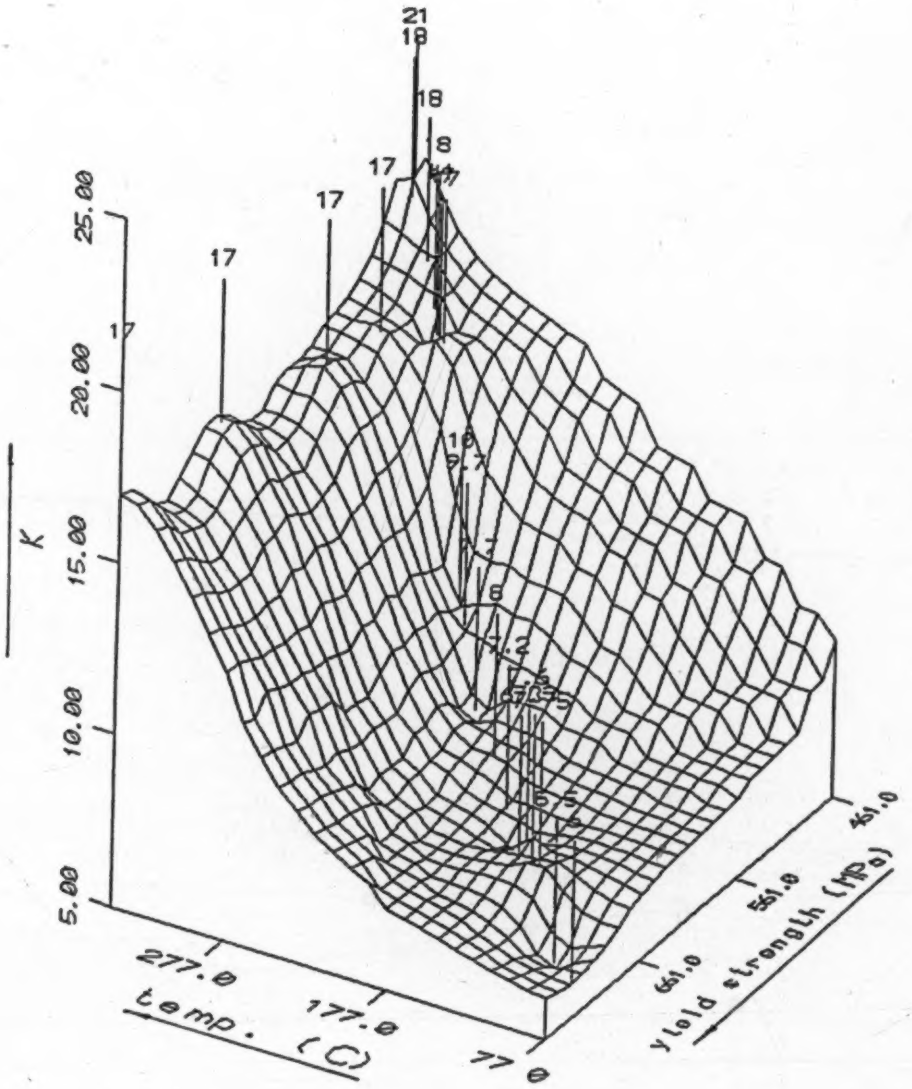

Figure 5-28 A three dimensional presentation of critical conditions for DHC fracture initiation

Table 5-1 The effect of cold work on the preferred orientation of basal plane of hexagonal zirconium in the three directions [75]

	plane A* (%)	plane B* (%)	plane C* (%)
as-manufactured	68	6	~26
25% additional CW	61	7	~32
40% additional CW	54	10	~36

** Planes A, B and C are normal to transverse, axial and radial directions, respectively.*

Table 5-2 Comparison of calculated T_p and measured T_{CAT} values

	T_p (°C)	T_{CAT} (°C)
peak temperature=320°C		
0%CW	289	285
peak temperature=340°C		
0%CW	305	280-305
peak temperature=360°C		
0%CW	321	320
40%CW	332	335
peak temperature=370°C		
0%CW	330	330
40%CW	340	330
peak temperature=400°C		
0%CW	362	360

Chapter 6 Conclusions

- Cracking arrest in Zr-2.5%Nb at high temperature is just a "*PAUSE*" (a temporary arrest) not a "*STOP*" (a permanent arrest) in the DHC process.
- This "*PAUSE*" is caused not by the inability of crack tip hydrides to form but by their inability to crack.
- The reason that these crack tip hydrides can remain uncracked at T_{CAT} is that the hydrides stop growing.
- This "*PAUSE*" is a dynamic equilibrium rather than a static one because cracking activity resumes almost immediately whenever the testing condition is changed.
- The theoretical significance of T_{CAT} lies in the fact that T_{CAT} represents the real upper limit for DHC in Zr-2.5%Nb alloys. Compared to this upper limit represented by T_{CAT}, the limit given by TSSp, as it has been widely accepted, is conservative.
- Despite its theoretical importance, however, precise prediction of T_{CAT} for any given specimen are not possible.

- Due to the instability of the cracking "*PAUSE*" reached at T_{CAT}, the inconsistency in measured T_{CAT} values in nominally identical parts and the impossibility of calculating T_{CAT} values precisely, the chance of developing a practically applicable maneuver procedure based on T_{CAT} for cracking control in nuclear reactors is minimal for cold worked Zr-2.5%Nb.

- Within the scope of this work, the cracking arrest at high temperature is believed to be a conditional phenomenon rather than a material property of Zr-2.5%Nb. Within the peak temperature range up to 400°C, no unconditional independency of T_{CAT} value has been found.

- The importance of cracking arrest phenomenon comes also from the fact that cracking arrest at T_{CAT} provides a great opportunity for the morphological study of crack tip hydrides.

- The semi-quantitative, three dimensional description of crack tip hydrides, which is believed to be the very first and the only one of this kind, is very valuable in providing a basis for constructing a scientific model of the DHC process based on a "multi-hydride" configuration.

- The benefit of studying the cracking arrest phenomenon also comes from its possible contributions to the understanding of other fracture initiation related phenomena including K_{IH} and the incubation period. The study of cracking arrest phenomenon is also beneficial in the development of fracture initiation criteria.

Chapter 7 References

[1] Cheadle, B.A., Blair, J.M., Coleman, C.E., Urbanic, V.F., Dunn, J.T., Price, E.G., Field, G.J. and Jackman, A.H.: "Evaluation of Hydride Cracking in Zr-2.5wt%Nb Pressure Tubes in Pickering Units 3 and 4", CRNL-2415, 1982

[2] Ells, C.E.: "Influence of Hydrogen on the Behaviour of Zirconium alloys in CANDU Reactors", *AECL Report*, 1978, AECL-6504

[3] Perryman, E.C.W.: "Pickering Pressure Tube Cracking Experience", *Nuclear Energy,* Vol.17 [2], 1978, pp.95-105

[4] Dunn, J.T and Jackman, A.H.: "Replacement of a Cracked Pressure Tube in Bruce GS Unit 2", Presented to the Canadian Nuclear Society in Toronto, Ontario, AECL Report, AECL-7537, 1982

[5] Cheadle, B.A., Coleman, C.E. and Ambler, J.F.R.: "Prevention of Delayed Hydride Cracking in Zirconium Alloys", *Zirconium in the Nuclear Industry*: Seventh International Symposium, ASTM STP-939, ASTM, 1987, pp.224-240

[6] Smith, R.R and Eadie, R.L.: "High Temperature Limit for Delayed Hydride Cracking", *Scripta METALLUGICA et MATERIALIA*, Vol.22, 1988, pp.833-836

[7] Simpson, L.A.:" The Critical Propagation Event for Hydrogen-Induced Slow Crack Growth in Zr-2.5%Nb", *Mechanical Behaviour of Materials*, Vol.2, K.J. Miller and R.F. Smith, Eds., JCM3, Cambridge, England, 1979, Pergamon Press, Oxford and New York, pp.445-455

[8] Amouzouvi, K.F. and Clegg, L.J.: "Effect of Heat Treatment on Delayed Hydride Cracking in Zr-2.5 Wt Pct Nb", *Metallurgical Transactions A*, Vol.18A, 1987, pp.1687-1694

[9] Roberson, J.A.L: "Nuclear Power in Canada: The CANDU System", *AECL Report*, AECL-6238, revision 2, 1990

[10] Urbanic, V.F.,Cox, B. & Field, G.J.: "Long Term Corrosion and Deuterium Uptake in CANDU-PHW Pressure Tubes," *Zirconium in the Nuclear Industry: Seventh International Symposium, ASTM SPT 939*, R.B. Adamson and L.F.P. Van Swam, Eds., American Society for Testing and Materials, 1987, pp.189-205

[11] Weinstein, D.G. and Holtz, F.C.: "Susceptibility of Zirconium Alloys to Delayed Failure Hydrogen Embrittlement", *Transactions of American Society for Metals*, Vol.57, 1964, pp.284-293

[12] Östberg, G.: "Some Observations on the Ductility of Zirconium Alloys, with Special Reference to the Effect of Hydrogen", *Journal of the Institute of Metals*, Vol.93, 1965, pp.223-228

[13] Simpson, C.J. and Ells, C.E.: "Delayed Hydrogen Embrittlement in Zr-2.5wt% Nb", *Journal of Nuclear Materials*, Vol.52, 1974, pp.289-295

[14] Ross-Ross, P.A., Dunn, J.T, Mitchell, A.B., Towgood, G.R. and Hunter, T.A.:"Some Engineering Aspects of the Investigation into the Cracking of Pressure Tubes in Pickering Reactors", *AECL Report*, AECL-5261, 1990

[15] Perryman, E.C.W.: "Pickering Pressure Tube Cracking Experience", *Nuclear Energy*, Vol.17 [2], 1978, pp.95-105

[16] Cheadle, B.A. and Williams, G.N.: "Computer Assisted Analysis of Cracking in Zr-2.5wt% Nb Pressure Tubes", The American Society of Mechanical Engineers, New York, NY, ASME Publication, 78-PVP-42, 1978

[17] Rodgers, D.K., Coleman, C.E. and Hosbons, R.R.: "Fracture of a Core Component in a Nuclear Reactor", *Proceedings of the International Conference on Failure Analysis*, ASM International, Montreal, Quebec, 1991

[18] Dutton, R.: "Hydrogen Embrittlement Effects in Hydride-Forming Metals", *Hydrogen in Metals* (Annual Volume), The Metallurgical Society of CIM, 1978, pp.16-25

[19] Dutton, R. and Puls, M.P.: "A Theoretical Model for Hydrogen Induced Sub-Critical Crack Growth", *Effect of Hydrogen on Behavior of Materials*, A.W. Thompson and I.B. Bernstein, Eds., The Metallurgical Society of the AIME, 1975, pp.516-524

[20] Ambler, J. F. R. and Coleman, C. E.: "Acoustic Emission during Delayed Hydrogen Cracking in Zr-2.5 wt% Nb Alloy", *AECL Report, AECL*-5798, 1977

[21] Shalabi, A.F. and Meneley, D.A.: "Initiation of Delayed Hydride Cracking in Zirconium-2.5 wt% Niobium", *Journal of Nuclear Materials*, Vol.173, 1990, pp.313-320

[22] Cheadle, B.A., Coleman, C.E. & Licht, H.: "CANDU-PHW Pressure Tubes: Their Manufacture, Inspection & Properties", *Nuclear Technology*, Vol.57, 1982, pp.413-425

[23] Eadie, R.L., Mok, D., Scarth, D. and Léger, M.: "The Hydrostatic Stress Field Around the Crack Tip in Zirconium-2.5% Niobium and Implications for Delayed Hydride Cracking", *Scripta METALLUGICA et MATERIALIA*, Vol.25, 1991, pp.497-502

[24] Eadie, R.L., Tashiro K., Harrington D. and Léger, M.: "The Determination of the Partial Molar Volume of Hydrogen in Zirconium in a Simple Stress Gradient using Comparative Microcalorimetry", *Scripta METALLUGICA et MATERIALIA*, Vol.26, 1992, pp.231-236

[25] Mueller, v.M., Eds. *Metal Hydrides*, Academic Press, 1968

[26] Simpson, L.A. and Cann, C.D.: "Fracture Toughness of Zirconium Hydride and its Influence on the Crack Resistance of Zirconium Alloys", *Journal of Nuclear Materials*, Vol.87, 1979, pp.303-316

[27] Coleman, C.E., Cheadle, B.A., Ambler, J.F.R, Lichtenberger, P.C. and Eadie, R.L.: "Minimizing Hydride Cracking in Zirconium Alloys", *Canadian Metallurgical Quarterly*, Vol.24 (3), 1985, pp.245-250

[28] Yuan, X.Q. and Tangri, K.: "Metallographic Observations on the Developing Hydride Morphology at the Crack Tip during Hydrogen Induced Delayed Hydride Cracking in a Zr-2.5Nb Alloy", *Journal of Nuclear Materials*, Vol.105, 1982, pp.310-317

[29] Rodgers, D.K.: "Hydride Growth at Crack Tips", unpublished report, 1990

[30] Luo, L.: "Development of a Quantitative Model to Correlate Crack Initiation Toughness with Hydride Structures of Zr-2.5%Nb Pressure Tube Material", unpublished report, 1993

[31] Shi, S.-Q. and Puls, M.P.: "Criteria for Fracture Initiation at Hydrides in Zirconium Alloys, I. Sharp Crack Tip", *Journal of Nuclear Materials*, Vol.208, 1994, pp.232-242

[32] Zheng, X.J., Luo, L., Metzger, D.R. and Sauvé, R.G.: "A United Model of Hydride Cracking Based on Elasto-plastic Energy Release Rate over a Finite Crack Extension", *Journal of Nuclear Materials*, Vol.218, 1995, pp.174-188

[33] McMeeking, R.M.: "Finite Deformation Analysis of Crack-tip Opening in Elastic-plastic Material and Implications for Fracture", *Journal of Mech. Phys.* Solids. Vol.25, 1977, pp.357-381

[34] R.L. Eadie and Ellyin, F.:" The Effect of Hydride Precipitation on the Stresses near the Crack Tip in a Delayed Hydride Crack in Zirconium-2.5%Niobium", *Scripta METALLUGICA et MATERIALIA*, Vol.23, 1989, pp.585-592

[35] MacEwen, S.R., Coleman, C.E., Ells, C.E. and Faber, J. Jr.: "Dilation of h.c.p. Zirconium by Interstitial Deuterium", *Acta Metallurgica*, Vol.33 (5), 1985, pp.753-757

[36] Ellyin, F. and Wu, J.: "Effect of Hydride Precipitation on the Elastoplastic Stress Field near a Crack Tip", *Acta Metallurgica*, Vol.42 (8), 1994, pp. 2709-2717

[37] Metzger, D.R. and Sauve, R.G.: "Interaction of Hydride Expansion with Hydrogen Diffusion at Flaw Tip Stress Peaks", unpublished report, 1995

[38] Coleman, C.E. and Ambler, J.F.R.: "Delayed Hydrogen Cracking in Zr-2.5wt%Nb Alloy", *Reviews on Coatings and Corrosion*, Vol.3, Freund Israel, 1979, pp.105-157

[39] Northwood, D.O. and Kosasih, U.: "Hydrides and Delayed Hydrogen Cracking in Zirconium and its Alloys", *International Metals Reviews*, Vol.28 (2), 1983, pp.92-121

[40] Sagat. S., Coleman, C.E., Griffiths, M. and Wilkins, B.J.S.: "The Effect of Fluence and Irradiation Temperature on delayed Hydride Cracking in Zr-2.5wt%Nb, Draft Report for the *Tenth International Symposium on Zirconium in Nuclear Industry*, Atomic Energy of Canada Limited, 1993

[41] Simpson, L.A. and Cann, C.D.: "The Effect of Microstructure on Rates of Delayed Hydride Cracking in Zirconium-2.5% Niobium Alloy", *Journal of Nuclear Materials*, Vol.126, 1984, pp.70-73

[42] Perovic, V. and Weatherly, G.C.: "The Nucleation of Hydrides in a Zr-2.5 wt%Nb Alloy", *Journal of Nuclear Materials*, Vol.126, 1984, pp.160-169

[43] Simpson, L.A. and Puls, M.P.: "The Effects of Stress, Temperature and Hydrogen Content on Hydride-Induced Crack Growth in Zr-2.5 Pct Nb", *Metallurgical Transactions A*, Vol.10A, 1979, pp.1093-1105

[44] Simpson, L.A. and Nuttall, K.: "Factors Controlling Hydrogen Assisted Subcritical Crack Growth in Zr-2.5Nb Alloys", *Zirconium in the Nuclear Industry*, A.L. Lowe and G.W. Perry, Eds., American Society for Testing and Materials, ASTM STP 663, 1977, pp.608-629

[45] Ambler, J.F.R.: " Effect of Direction of Approach to Temperature on the Delayed Hydrogen Cracking Behavior of Cold-Worked Zr-2.5Nb", *Zirconium in the Nuclear Industry, Sixth International Symposium,* D.G. Franklin and R.B. Adamson, Eds., American Society for Testing and Materials, *ASTM STP 824*, 1984, pp.653-674

[46] Eadie, R.L., Metzger, D.R. and Léger, M.: "The Thermal Ratchetting of Hydrogen In Zirconium-Niobium - an Illustration using Finite Element Modeling", *Scripta METALLUGICA et MATERIALIA*, Vol. 29, 1993, pp.335-340

[47] Shi, S.-Q. and Puls, M.P.: "Dependence of the Threshold Stress Intensity Factor on Hydrogen Concentration During Delayed Hydride Cracking in Zirconium Alloys", *Journal of Nuclear Materials*, Vol.218, 1994, pp.30-36

[48] Shek, G.K. and Seahra, H.: "A Parametric Study on K_{IH}- Effects of Hydrogen Supersaturation", unpublished report, 1993

[49] Shalabi, A.F.: "Initiation of Delayed Hydride Cracking in Zirconium-2.5wt% Niobium Pressure Tubes, Ph.D Thesis, University of New Brunswick, Department of Mechanical Engineering, 1988

[50] Coleman, C.E. and Ambler, J.F.R.: "Susceptibility of Zirconium Alloys to Delayed Hydrogen Cracking", *Zirconium in the Nuclear Industry*, A.L. Lowe and G.W. Perry, Eds., American Society for Testing and Materials, ASTM STP 663, 1977, pp.589-607

[51] Coleman, C. E.: "Acoustic Emission from Zirconium Alloys during Mechanical and Fracture Testing", *AECL Report,* AECL-9111, 1986

[52] Sagat, S., Ambler, J. F. R. and Coleman C. E.: "Application of Acoustic Emission to Hydride Cracking", *AECL Report,* AECL-9258, 1986

[53] Tangri, K. and Yuan, X. Q.: "Acoustic Emission Study of the Various Stages of Hydrogen Induced Cracking in Zr-2.5%Nb Alloy", *Fracture Problems and Solutions in the Energy Industry*, Pergamon Press, Oxford, UK, 1982, pp.27-38

[54] Halliday, M. D. and Beevers, C. J.: "The D.C. Electrical Potential Method for Crack Length Measurement", *The Measurement of Crack Length and Shape During Fracture and Fatigue*, Engineering Materials Advisory Services Ltd, UK, 1980, pp.85-103

[55] Lindley, T. C. and McIntyre, P.: "Application of Acoustic Emission to Crack Detection and Measurement", *The Measurement of Crack Length and Shape During Fracture and Fatigue*, Engineering Materials Advisory Services Ltd, UK, 1980, pp.285-322

[56] Tuikin, O. R. and Ivanov, V. I.: "Factorial Analysis of Stability for Acoustic-Emission Parameters", *Soviet Journal of Nondestructive Testing* (English Translation of *Defektoskopiya*) Vol.21 (8), 1985, pp.554-558

[57] Erminson, A. L. and Zhikhareva, O. V.: "Evaluation of Error for the Digital Method of Measuring Energy in Acoustic-Emission Signals", *Soviet Journal of Nondestructive Testing* (English Translation of *Defektoskopiya*) Vol.23 (11), 1988, pp.784-787

[58] Tushkin, A. P.: "Relationship Between the Number of Acoustic Emission Signals and the Development of the Plastic Zone at the Crack tip", *Soviet Journal of Nondestructive Testing* (English Translation of *Defektoskopiya*) Vol.25 (2), 1989, pp.131-135

[59] Muravin, G. B., Ship, V. V., Lezvinskaya, L. M. and Merman, A. I.: "Energy Aspects of Acoustic Emission Inspection of Crack Development with the Use of Different Types of Waves", *Soviet Journal of Nondestructive Testing* (English Translation of *Defektoskopiya*) Vol.25 (3), 1989, pp.169-176

[60] Kline, R. A.: "The Influence of Attenuation on Acoustic Emission Measurements", *IEEE 1984 Ultrasonic Symposium*, Published by IEEE, New York, NY, USA. Available from IEEE Service Centre (Catalog number 84CH2112-1), Piscataway, NJ, USA, pp.930-932

[61] Ivanov, V. I.: "Acoustic Emission: Some Problems, tasks and solutions", *NDT International*, Vol.17 (6), 1984, pp.323-327

[62] Dietzel, W., and Schwalbe, K.-H.: "Monitoring Stable Crack Growth Using a Combined A.C./D.C Potential Drop Technique", *Materialpruefung*, Vol.28 (11), 1986, pp.368-372

[63] Lugg, M. C.: "The Analysis of Sparse Data in ACPD Crack Growth Monitoring", *NDT International*, Vol.21 (3), 1988, pp.153-158

[64] Joyce, J. A. and Schneider, C. S.: "Crack Length Measurement During Rapid Crack Growth Using Alternating-Current Potential Different Method", *Journal of Testing and Evaluation, JTEVA*, Vol.16 (3), 1988, pp.257-270

[65] Nakai, Y. and Wei, R. P.: "Measurement of Short Crack Lengths By an A.C. Potential Method", *Engineering Fracture Mechanics*, Vol.32 (4), 1989, pp.581-589

[66] Gu, J. and Yu, L. Y., "The Influence of Geometric Factors on Crack Depth Measurement Using the Potential Drop Technique", *NDT International*, Vol.23 (3), June 1990, pp.161-164

[67] Lin, G., Skrzypek, S., Li, D. and Eadie, R.L.: "Monitoring Crack Advance Using Acoustic Emission and Combined Acoustic Emission and Potential Drop in Zr-2.5%Nb", *Journal of Testing and Evaluation, JTEVA*, Vol. 26 (1), January 1998, pp. 15-25

[68] Sawatzky, A.: "Hydriding Zircaloy-2 by Electrolysis", *AECL Report*, AECL-1046, 1960

[69] Davis, P.H. and Stearns, C.P.: "Experimental Compliance Calibration of A Tapered DCB (Constant K_I) Specimen", *OHR Report*, OHR-81-389-K, 1981,

[70] Schrire, D.I. and Pearce, J.H.: "Scanning Electron Microscope Techniques for Studying Zircaloy Corrosion and Hydriding", Tenth International Symposium on Zirconium in Nuclear Industry, 1993

[71] Kiely, G.P.: "Metallographic Preparation of Zirconium and Its Alloys", CRNL-2523 Report, 1983

[72] Shek, G.K. and Graham, D.B.: "Effect of Loading and Thermal Maneuvers on Delayed Hydride Cracking in Zr-2.5Nb Alloys", *Zirconium in the Nuclear Industry: Eight International Symposium, ASTM STP 1023*, L.F.P. Van Swam and C.M. Eucken, Eds., American Society for Testing and Materials, Philadelphia, 1989, pp. 89-110

[73] Eadie, R.L., Li, D. and Shek, G.K.: "Delayed Hydride Cracking During Temperature Transients in As-Manufactured and in Hardened Zr-2.5Nb Pressure Tube Material", unpublished report, 1994

[74] Cheadle, B.A. "Introduction to The Physical Metallurgy of Zirconium Alloys", unpublished report, CRNL-1208

[75] Lee, W.K., unpublished results

[76] Hertzberg, R.W., *Deformation and Fracture Mechanics of Engineering Materials*, John Wiley & Sons, 2nd Ed., 1983

[77] Anderson, M.J.: "Finite Element and Analytical Modeling of Microstructural and Textural Anisotropy of Zr-2.5%Nb Nuclear Reactor Pressure Tube Material", M.Sc. Thesis, 1996

[78] Shek, G.K., Seahra, H. and Metzger,D.R.: "Effects of Hydrogen Supersaturation on K_{IH} - Part II", unpublished report, 1993

[79] Shi, S.-Q., Shek, G.K. and Puls, M.: "Determination of the Solubility Limit to Delayed Hydride Cracking in Zirconium Alloys", to be published in Journal of Nuclear Materials, ???, pp?-?

[80] Smith, E.: "Near Threshold Delayed Crack Growth in Zirconium Alloys", UMIST Materials Science Centre, Manchester University, unpublished report